Life-cycle assessment of 3rd-generation organic photovoltaic systems : developing a framework for studying the benefits and risks of emerging technologies

Michael Tsang

université de BORDEAUX

THÈSE PRÉSENTÉE

POUR OBTENIR LE GRADE DE

DOCTEUR DE

L'UNIVERSITÉ DE BORDEAUX

ÉCOLE DOCTORALE

SPÉCIALITÉ : CHIMIE ANALYTIQUE ET ENVIRONNEMENTALE

Par Michael TSANG

Cycle de vie de systèmes photovoltaïques organiques 3ème génération :

Élaboration d'un cadre pour étudier les avantages et les risques des technologies émergentes

Life-cycle Assessment of 3rd-Generation Organic Photovoltaic Systems:

Developing a Framework for Studying the Benefits and Risks of Emerging Technologies

Sous la direction de : Guido SONNEMANN
(co-directeur : Dario BASSANI)

Soutenue le 07 Décembre 2016

Membres du jury :

M.	Ralph Rosenbaum,	Chaire industrielle ELSA-PACT Irstea Montpellier	Rapporteur
Mme	Lisolette Schebek,	Professeur Université Darmstadt	Rapporteur
M.	Nicola Armaroli,	Directeur de Recherche, CNR	Examinateur
M.	Philippe Garrigues,	Directeur de Recherche, CNRS	Président
M.	Dario M. Bassani,	Directeur de Recherche, CNRS	Co-directeur de thèse
M.	Guido W. Sonnemann,	Professeur Université Bordeaux	Directeur de thèse

Titre : Analyse du cycle de vie de systèmes photovoltaïques organiques de 3ème génération : Élaboration d'un cadre pour étudier les avantages et les risques des technologies émergentes

Résumé : Les systèmes photovoltaïques organiques sont des technologies émergentes présentant de forts potentiels d'économie de ressources et de réduction des impacts sur l'environnement et la santé humaine par rapport aux dispositifs photovoltaïques conventionnels. La méthode de l'analyse du cycle de vie est appliquée afin d'évaluer la façon dont les différents procédés de fabrication, les caractéristiques des dispositifs, la phase d'utilisation et les scénarios de fin de vie des cellules photovoltaïques organiques influent sur ces avantages potentiels. Les impacts de cette technologie émergente sont comparés aux technologies conventionnelles à base de silicium pour établir un référentiel de performance des technologies photovoltaïques. En outre, les effets potentiels sur la santé humaine de l'utilisation de nanomatériaux dans les cellules photovoltaïques organiques ont été spécifiquement étudiés ; et la pertinence de l'analyse du cycle de vie pour évaluer cette catégorie d'impact a été examinée. Ainsi, un nouveau modèle d'évaluation de l'impact sur le cycle de vie est présenté afin de quantifier les dangers potentiels posés par les nanomatériaux. Enfin, ces impacts potentiels sont comparés aux avantages des cellules photovoltaïques organiques sur les cellules à base de silicium.

Mots clés : l'analyse du cycle de vie, photovoltaïques organiques, nanomatériaux fabriqués, l'evaluation des risques, l'exposition, énergie renouvelable

---

Title : Life-cycle Assessment of 3rd-Generation Organic Photovoltaic Systems: Developing a Framework for Studying the Benefits and Risks of Emerging Technologies

Abstract : Organic photovoltaics present an emerging technology with significant potential for increasing the resource efficiencies and reducing the environmental and human health hazards of photovoltaic devices. The discipline of life-cycle assessment is applied to assess how various prospective manufacturing routes, device characteristics, uses and disposal options of organic photovoltaics influences these potential advantages. The results of this assessment are further compared to silicon based photovoltaics as a benchmark for performance. A deeper look is given to the potential human health impacts of the use of engineered nanomaterials in organic photovoltaics and the appropriateness of life-cycle assessment to evaluate this impact criteria. A newly developed life-cycle impact assessment model is presented to demonstrate whether the use of and potential hazards posed by engineered nanomaterials outweighs any of the resource efficiencies and advantages organic photovoltaics possess over silicon photovoltaics.

Keywords : Life-Cycle Assessment, Organic Photovoltaics, Engineered Nanomaterials, Risk Assessment, Characterization Factor, Indoor Occupational Exposure, Monte Carlo Analysis, Sustainable Production, Eco-Design, Renewable Energy, Life-Cycle Impact Assessment, production durable, éco-conception,

---

Institut des Sciences Moléculaires

[CYVI Group, 351 Cours de la Libération 33405 Talence]

Dedication

This work is dedicated to my wife and daughter who are my foundation and to my parents who have continuously encouraged my educational and professional pursuits.

Acknowledgements

A tremendous amount of gratitude is owed to the many people who were involved in and around my Ph.D. I, first, would like to thank my co-advisors Professors Guido W. Sonnemann and Dario M. Bassani for providing me with the opportunity to broaden and strengthen my research and professional pursuits. It cannot be emphasized enough that a successful Ph.D. depends on the relationship a student has with their advisor(s), and I was fortunate to have advisors that were engaged, supportive and productively-challenging throughout my three years of research.

The work presented in this dissertation also involved the partnership and collaboration with several other Universities and research groups. I would like to thank Professor Antonio Marcomini and Danail Hristozov from Ca' Foscari University in Venice, Italy for inviting and hosting me in their research group for 3-months. Additionally, I would like to thank Professor Sangwon Suh from the University of California, Santa Barbara for, similarly, funding and hosting me in his research group for 3-months. These were both indispensable (and memorable) opportunities which were the basis for two critical chapters of this thesis.

I would like to extend my appreciation to Philippe Garrigues, Ralph Rosenbaum, Liselotte Schebek, and Nicola Armaroli for participating in my defense and being a part of this vital aspect of the Ph.D. process.

Many, many thanks are due to Karine Ndiaye for always being so incredibly gracious and generous with her time, particularly during my first months in Bordeaux. Without her assistance, it is doubtful my stay in France would have been a success.

My wife for her support and understanding of the time commitments these last three-years have required. My daughter for defining the word precious.

And to the countless other individuals who have helped and contributed to my Ph.D. along the way: Alex Zabeo (Ca' Foscari), Sara Alba (Ca' Foscari), Stella Stoycheva (Ca' Foscari), Chengfang Pang (Ca' Foscari); Professor Lang Tran and the MODENA (E.U.) COST initiative for funding my research in Venice, Italy; Keld Alstrup Jensen (Technical University of Denmark), Joonas Koivisto (Technical University of Denmark); Arturo Keller (UCSB), Dingsheng Li (UCSB), Kendra Garner (UCSB); Masahiko Hirao (University of Tokyo), Emi Kikuchi (University of Tokyo); Cyril Aymonier (University of Bordeaux), Gilles Philippot (University of Bordeaux), Eskinder Gemechu (University of Bordeaux), Amandine Foulet (University of Bordeaux)

Philippe Loubet (University of Bordeaux), Dieuwetje Schrijvers (University of Bordeaux), Baptiste Pillain (University of Bordeaux), Edis Glogic (University of Bordeaux), Raphaël Brière (University of Bordeaux), Thibaut Maury (University of Bordeaux), Amélie Thevenot (University of Bordeaux), Annie Corrêa Da Costa (University of Bordeaux), Fabrice Forlini (University of Bordeaux) and Pascal Pajot (University of Bordeaux).

Table of Contents

List of Tables

List of Figures

List of Equations

Executive Summary

Solar photovoltaics (PV) are poised to play a predominant role in energy production over the next century given imminent environmental and human health challenges such as climate change. While PV take freely available energy from the sun and convert it into electricity, there are still environmental and human health impacts that can occur along its life-cycle, albeit at lower levels than conventional fossil fuels. A new generation of PV technology is pushing the boundaries of these advantages by using extremely thin, lightweight, flexible materials. One such technology is the 3rd-generation organic photovoltaic (OPV) device that uses organic, engineered nanomaterials (ENM) in its active layer.

The overall objective of this thesis was to demonstrate whether OPV have proven themselves to be a preferable energy supply option compared to silicon PV from an environmental and human health perspective. In turn, the thesis addresses whether life-cycle assessment (LCA) – an environmental management tool that can quantify resource efficiencies and environmental and human health impacts of products across their entire life-cycles, from material extraction to product disposal – is the most appropriate methodology for making such evaluations. Based on the outcomes of an extensive review of the existing OPV-LCA literature, further objectives were to address (i) a comprehensive range of OPV's environmental and human health impacts across (ii) all life-cycle stages, (iii) in comparison to silicon PV and (iv) the limitations to evaluating the human health impacts from ENM used in OPV devices.

Two attributional LCA case-studies were completed from cradle-to-gate and cradle-to-grave. The results of the cradle-to-gate assessment demonstrate that per watt-peak of power production, OPV's resource efficiency was higher while their environmental and human health impacts were up to 93% lower than silicon PV's impacts, on average. While encouraging, OPV have lower efficiencies and shorter working life-times compared with silicon PV. Thus, changes in these outcomes of the LCA might occur after considering OPV's use and end-of-life stages. The results of the cradle-to-grave assessment demonstrated that, per kWh of energy produced over 25-years as a rooftop solar array, OPV's environmental and human health impacts were still 60% lower than silicon. These environmental and human health impact reductions could be pushed to 73%, on average, per 10 Wh of energy produced over 5-years as a portable solar charger.

While the results demonstrated a preference for OPV over silicon PV, there was no specific estimation regarding the toxicological impacts resulting from emissions of ENM across the OPV life-cycle. To address this, a human health risk assessment (HHRA) was performed. In general, LCA and HHRA are often used by

two different sets of decision makers and for different purposes. LCA is often used to address the *resource efficiencies* of a product, while HHRA is used to evaluate the *toxicological risks* of specific substances used in a product. A first-tier, qualitative HHRA identified that occupational scenarios were the life-cycle stages with the greatest risk potential due to interaction with large volumes of loose ENM particulates. Additionally, inhalation posed the most significant exposure route for workers directly handling these materials. A focused, quantitative HHRA demonstrated that industrial-scale handling of nano-TiO_2 where large amounts of power are dumped into open vessels presented airborne nano-TiO_2 concentrations with statistically significant risks of inducing pulmonary inflammation to workers over a lifetime of work.

This *Separate Use* of LCA and HHRA is one possible approach for addressing the resource efficiencies and toxicological risks of emerging technologies such as OPV. Additionally, the results of both tools can be combined into a *Complementary Use* approach using multi-criteria decision analysis, for example. Another approach is *Integration* of these tools at the methodological level. The methods of the HHRA were integrated with life-cycle impact assessment, introducing a novel nano-specific characterization factor (CF_{NS}) and presented as a case-study of nano-TiO_2. After reassessing the OPV-LCA with the newly defined CF_{NS}, there was a less than a 1% contribution of human health impacts resulting from the emissions of nano-TiO_2 during occupational handling of the ENM. These findings suggest that ENM emissions across the life-cycle are marginal, however these results must be met with caution as they only include the impacts resulting from occupational nano-TiO_2 emissions. Further emissions may occur during the use and end-of-life phases or from other ENM in the other layers of the OPV.

The results of the OPV-LCA case-studies and the further evaluation of ENM human health impacts indicate that OPV are a preferable energy production option compared to silicon PV from an environmental and human health standpoint. Outcomes were limited by uncertainties associated with OPV lifetime and efficiencies, which were marginalized when OPV were restricted to products with relatively short lifetimes (i.e. < 5 years) and moderate OPV efficiencies (i.e. > 5%). In terms of the assessment approach, LCA stands as the most comprehensive and appropriate methodology for evaluating the resource efficiencies and potential hazards of energy producing technologies such as OPV. Its broad environmental scope and focus on the entire life-cycle help to avoid burden shifting. While understanding the human health impacts to ENM is necessary, this is not fully achievable using existing life-cycle impact assessment methodologies. An integrated HHRA and life-cycle impact assessment approach would dually ensure that the resource

efficiencies of OPV do not come at the expense of shifting burdens to the occupational human health impacts.

Keywords: Life-Cycle Assessment, Organic Photovoltaics, Engineered Nanomaterials, Risk Assessment, Characterization Factor, Indoor Occupational Exposure, Monte Carlo Analysis, Sustainable Production, Eco-Design, Renewable Energy, Life-Cycle Impact Assessment

List of Abbreviations

AER	Air exchange rate
a-Si	Amorphous silicon
a-Si-NC	Amorphous silicon with no case
BAL	Bronchi-alveolar lavage
BMC	Benchmark concentration
BMC_a	Benchmark concentration based on animal toxicological data
BMC_h	Human equivalent benchmark concentration
BMD	Benchmark dose
BMR	Benchmark response
BOS	Balance of system
C_{60}	Fullerenes
CCE	Cumulative carbon equivalents
CCE_{RER}	Cumulative carbon equivalents for average European energy production mix
CDI	Context-dependent integration
CED	Cumulative energy demand
CF	Characterization factor
CF_{NS}	Engineered nanomaterial-specific characterization factor
$CF_{NS,C}$	Engineered nanomaterial-specific, cancer characterization factor
$CF_{NS,NC}$	Engineered nanomaterial-specific, non-cancer characterization factor
CPBT	Carbon payback time
CTU	Comparative toxic unit
DALY	Disability adjusted life year
DI	Dustiness index of particulate matter
EF_{inter}	Interspecies extrapolation factor
EF_{intra}	Intraspecies extrapolation factor
EF	Effect factor in life-cycle impact assessment
E_g	Energy generated over during the use of a photovoltaic panel
ENM	Engineered nanomaterial or nanoparticle
EPA	U.S. Environmental Protection Agency
EPBT	Energy payback time
ERA	Environmental risk assessment
ES	Exposure scenario
ETL	Electron transport layer
EU	European Union
FF	Fate factor for life-cycle impact assessment
FP7	The Seventh Framework Programme (2007-2013) of the European Commission
FTO	Fluorine-doped tin oxide
GI	Global integration
GM	Geometric mean
GSD	Geometric standard deviation
HHRA	Human health risk assessment
HTL	Hole transport layer
IEA	International energy agency
iF	Intake fraction in life-cycle impact assessment
ISO	International Organization for Standardization
ITO	Indium tin oxide

LCA	Life-cycle assessment
LOAEL	Low observed adverse effect level
MC	Monte-Carlo Analysis
MRL	Minimum required lifetime
m-Si	Multi-crystalline silicon
NF	Near-field workroom volume
NIOSH	U.S. National Institute of Occupational Safety and Health
NMVOC	Non-methane volatile organic compounds
NOAEL	No observed adverse effect level
OPV	Organic photovoltaics
OPV-NC	Organic photovoltaics with no case
P3HT	Poly(3-hexyl)thiophene
PBPK	Physiologically-based pharmacokinetic
PCBM	[6,6]-phenyl C61 butyric acid methyl ester
PCS	Phagocytizing cells
PEDOT:PSS	Poly(3,4-ethylenedioxythiophene) polystyrene sulfonate
PET	Polyethylene terephthalate
POP	Workplace population
PV	Photovoltaic
RA	Risk assessment
REL	Recommended exposure limit
RiF	Retained-intake fraction for use in life-cycle impact assessment
RIVM	Netherland's National Institute for Public Health and the Environment
SSI	Site-specific integration
Wp	Watt-peak
XF	Exposure Factor in life-cycle impact assessment

Chapter 1 Organic Photovoltaics as a Sustainable Technology

Energy is arguably the most important issue confronting society in the 21st century. That is because energy seems to be at the heart of what is considered to be sustainability. Although sustainability means many things to many people, it is often reduced to three core pillars of sustainability development: economics, society and environment.[1] In this way, it is hard to imagine another factor over the previous two and a half centuries that has been so influential on society. The development and use of fossil fuels has spurred tremendous growth in industry and the overall global population as well as technological achievements on a scale never seen before the industrial revolution. Along the way, however, this has come at the expense of certain environmental and public health costs. The world is now, arguably, entering an era of peak-oil,[2] coincidentally while changes to the earth's atmosphere due to anthropogenic sources of greenhouse gases and pollution[3] are producing environmental conditions, such as global climate change, that will test the limit of society's capacity for adaptation and resiliency.[4]

Thus, sustainability is not simply an energy issue but also an environmental and public health issue. The true cost of an energy source cannot be quantified solely as a function of its procurement, refinement and distribution transactions, for example, but it must also account for the "externalities" or indirect costs related to its environmental and human health damage. Taking this comprehensive vantage point is necessary to avoid burden shifting, for instance, as can be the case with biofuels and its issues of adverse land and freshwater use impacts[5–7] and increases in greenhouse gas emissions[8] or in regards to the use of solar photovoltaics (PV) and increases in the use and consumption of metals.[9]

Therefore, research and development into new, sustainable sources of meeting the world's current and future energy demands will, consequently, continue to be an important topic throughout the 21st century. Coupled with the urgent need to address greenhouse gas emissions and climate change, among a host of other environmental and public health challenges, renewable energy sources such as PV are poised to take on a more pronounced role in the world's energy procurement strategy.

Photovoltaic Technology: Background

The photovoltaic effect is the production of electric current under the application of light. Its discovery is attributed to the French physicist Edmond Becquerel who, in 1939, used silver bromide coated platinum electrodes to produce a current when illuminated in solution (Figure 1-1).[10,11]

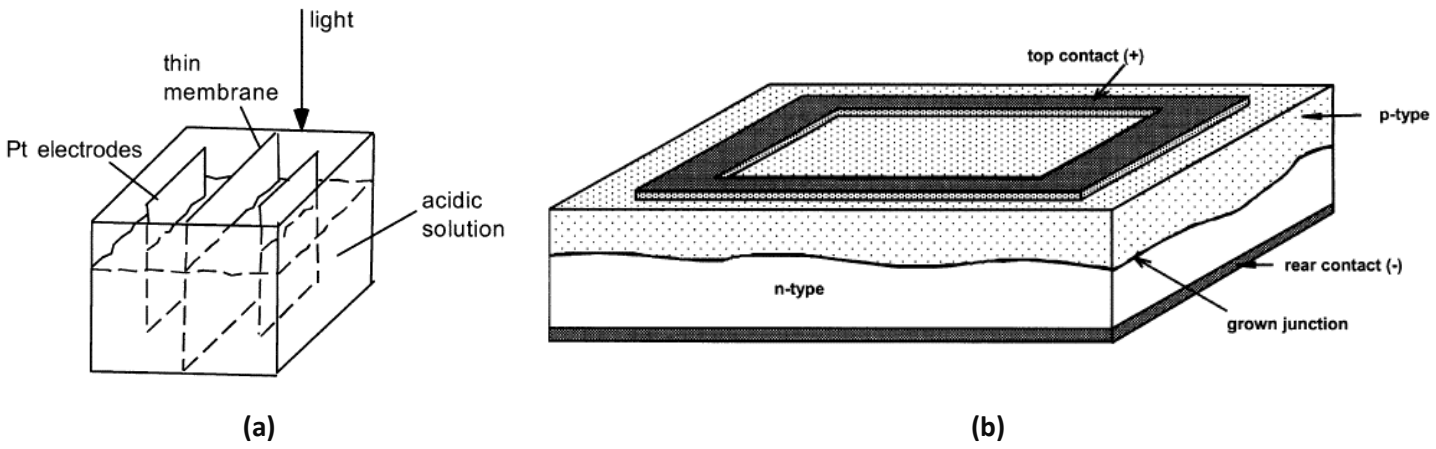

Figure 1-1 Illustrations of (a) the setup described by Becquerel in 1939 to achieve the first known, intentionally produced photovoltaic effect and (b) the oldest contemporary interpretation of the p-n silicon semiconducting cell as it is known today. (Source: Greet 2002)[12]

Mainstream and modern forms of PV technologies began to take shape in the mid-20th century with the introduction of p-n junctions of silicon semiconductors as described by Russel Ohl.[13] The p-n junction exploits the difference in work function between these two materials, thus producing an electric field.[12] Current silicon technologies, for example, artificially "dope" silicon with impurities such that there is a p-type silicon that has an excess of electrons and a n-type silicon that has a reduction of electrons (i.e. an excess of holes). Upon absorption of light, electrons are excited from their valence to conductions bands. Ultimately, electrons will flow from the p-type material to the n-type material and then on to the rear (back) electrode.[12] Simultaneously, the holes left behind by the electron will travel in the opposite direction to the top (front) electrode.[12]

From expensive, relatively low efficient solar panels,[14] silicon-based PV matured quickly achieving efficiencies of 20% by the mid-1980s. Lab-based record efficiencies have increased beyond 25% for most of the silicon-based cells.[15] Lab-based efficiency records have reached upwards of 45% conversion of light to electricity using triple- and quad-junction cells using combinations of gallium, indium and arsenic, for example. Silicon-based PV are still the most widely used PV technology globally, particularly in large scale ground and roof mounted systems, and capture over 90% of the global PV production annually.[16] The use of silicon PV also has tremendous resource efficiency and environmental benefits. Previous studies have shown, for example, that the greenhouse gas emissions per kWh of electricity produced using silicon PV are five-times lower than coal based production and over two-times lower than natural gas based production.[17] Moreover, since 2008 there has been a steady drop in market prices of silicon.[18] This has

put PV technology at close price parity with conventional energy sources as such as coal.[19] Although this is great news for the renewable energy market in general, this trend may stabilize and even reverse in the near-term.[20]

The competitive price of silicon PV may have the unintended consequences of reducing incentives to invest in and develop alternative PV technologies that may not yet be as cost competitive.[21] Nonetheless, the last four decades of PV development are marked by research and development of a wide range of viable technologies, spanning from conventional single-crystal silicon and multi-crystalline silicon (m-Si) PV to second generation technologies such as amorphous silicon (a-Si), cadmium-telluride and cadmium-indium-gallium-selenium cells. Since the mid- to late- 1990s, increasing amounts of research and development have gone into the so-called *third generation* (3rd-generation) PV technologies. This generation of PV are much more diverse from previous generations and include dye-sensitized, perovskite, quantum dot and organic photovoltaic (OPV) cells, among others (Figure 1-2).

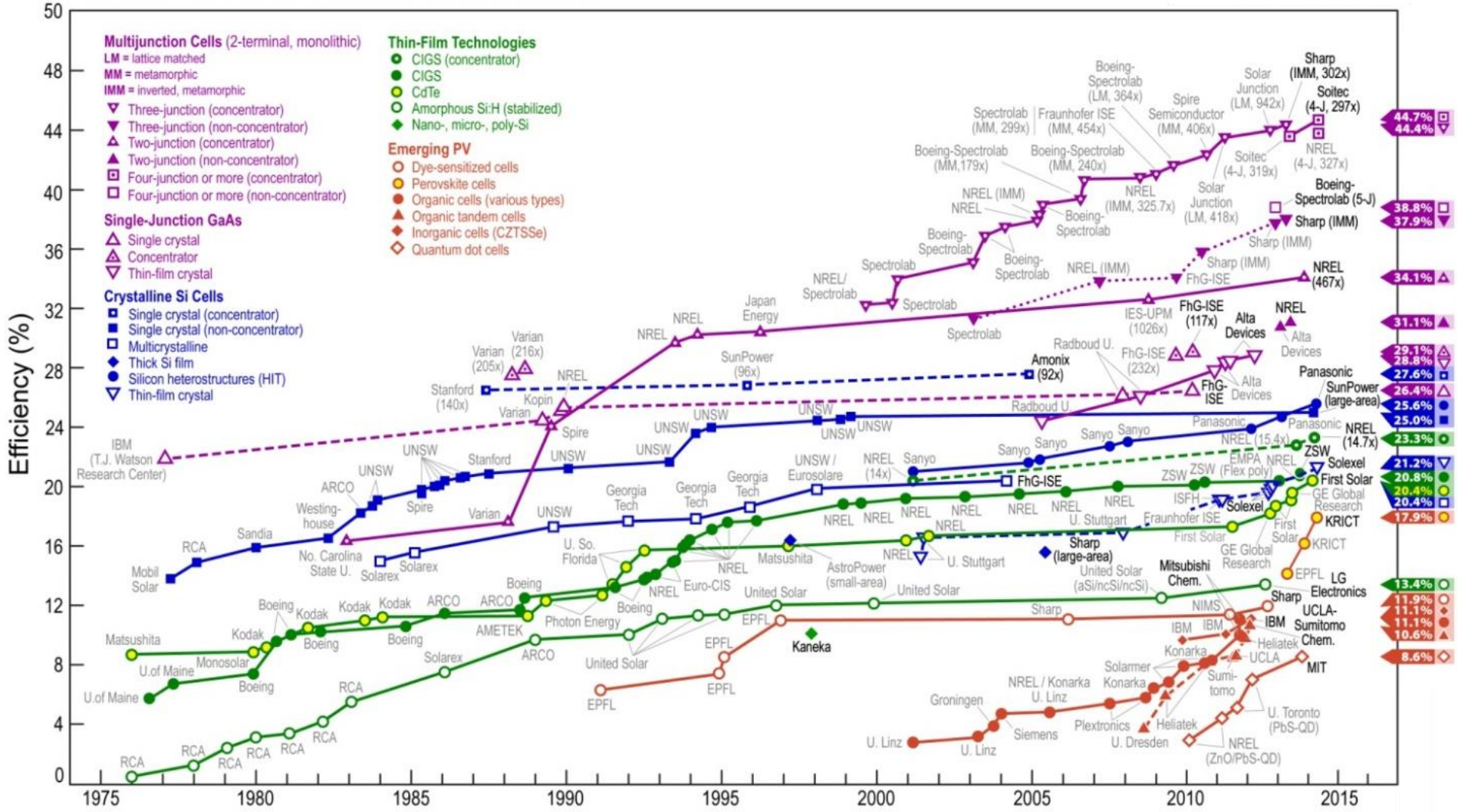

Figure 1-2 Laboratory-based solar cell efficiency records (Source: U.S. National Renewable Energy Laboratory)[22]

Organic Photovoltaics: The Third-Generation of Photovoltaics

The focus of this dissertation rests with the 3rd-generation OPV technologies that utilize organic materials in their active layers instead of inorganics such as silicon. The birth of the first practical OPV technology began with a patent filed by C.W. Tang in 1979 for an organic bulk-heterojunction device.[23] That first device utilized an active layer of copper-phthalocyanine and a derivative of perylene, a 20 carbon, 5-ring, polycyclic hydrocarbon ($C_{20}H_{12}$). Since then, this technology has remained primarily as a lab-based technology, with small pilot-scale projects (www.infinitypv.com) coming online as recently as 2015 and large-scale deployment of OPV solar panels having been deployed on land for demonstrative and research purposes.[24] Conceptually, OPV cells are not much different from conventional PV technologies in that they are composed mainly of the same principal components (Figure 1-3) such as a front electrode, back electrode, active layer (i.e. where charge separation occurs).

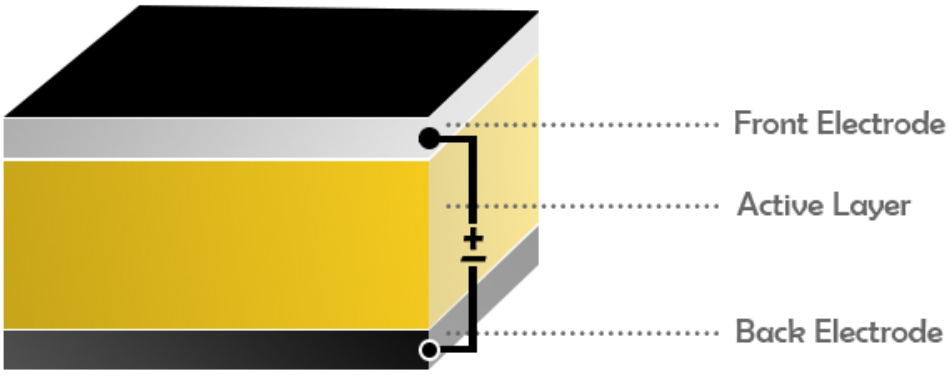

Figure 1-3 Geometry and layout of a generic photovoltaic cell.

Unlike other PV technologies, the active layer of an OPV cell is composed distinctly of organic electron donor (n-type semiconductor) and electron acceptor (p-type semiconductor) material layers, hence the name of this technology. OPV cells may require additional components such as a substrate to which all other components are deposited as well as layers for improved efficiency and charge separation, such as electron transport and hole transport layers, and barrier-coating layers for protection (Figure 1-4). However, there is no one "standard" OPV geometry and device composition due to the fact that OPV are still very much a developing technology.

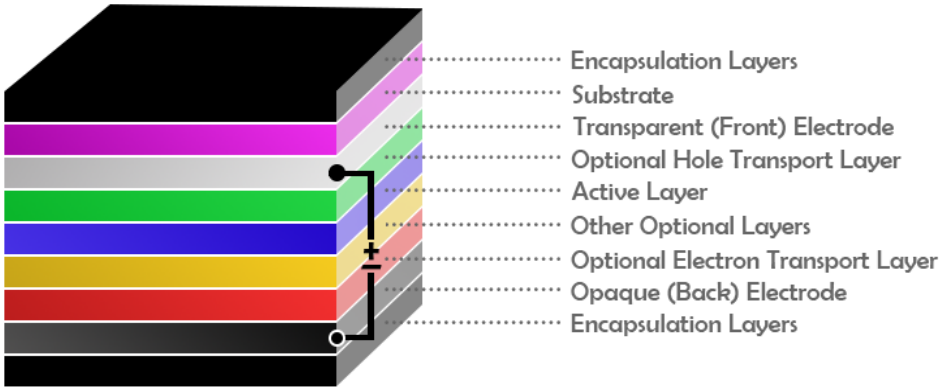

Figure 1-4 Geometry and layout of a generic organic photovoltaic cell.

Overall Objectives of the Thesis

Although PV technologies in effect take freely available solar radiation and convert it into a more useful form of energy (i.e. electricity), there are environmental burdens (e.g. greenhouse gas emissions) that may occur during the production, use or disposal of the PV. Keeping this in mind, OPV have many characteristics that make them a compelling choice for further development in the solar energy field. These characteristics include being extremely thin, flexible (Figure 1-5), requiring small amounts of production materials and less energy intensive manufacturing routes.[25]

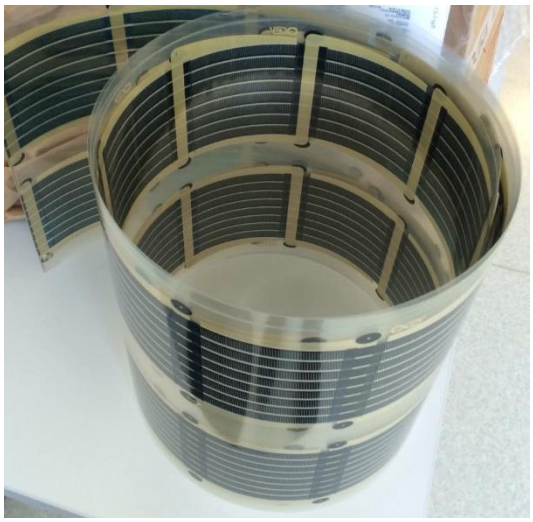

Figure 1-5 Example of printed organic photovoltaic panel

While the large-scale application of silicon PV has been realized and its resource efficiencies and environmental impacts largely proven beneficial, [17,26] the overall objective of this thesis is to demonstrate

whether OPV have proven themselves to be a preferable energy supply option compared to conventional silicon PV from an environmental and human health point of view.

Life-Cycle Assessment: A Primer

Central to the environmental evaluation of energy-related systems has been the use of life-cycle assessment (LCA). LCA is an environmental management tool outlined by ISO 14040:2006 and 14044:2006.[27,28] A very brief introduction is provided here with a more detailed explanation of its use and methods in Chapter 2. It is viewed as a key tool to evaluate energy-related systems because of its ability to track all of the directly consumed and/or embedded energy in each life-cycle stage of the energy-related system. This information can be used to determine how much time it will take for the system, during its use, to generate the energy that was consumed during the production of that same system. This is known as the energy payback time (EPBT).[29–31] Similar metrics such as the carbon payback time (CPBT) can also be calculated since LCA allows for the tracking of other non-energy materials flows such as greenhouse gases along the life-cycle. The EPBT and CPBT are core metrics to which all energy production systems are discriminated against and thus essential for defining the applicability of OPV in the energy sector.

LCA is composed of the (1) goal and scope definition, (2) life-cycle inventory analysis, (3) life-cycle impact assessment and (4) interpretation steps (Figure 1-6).

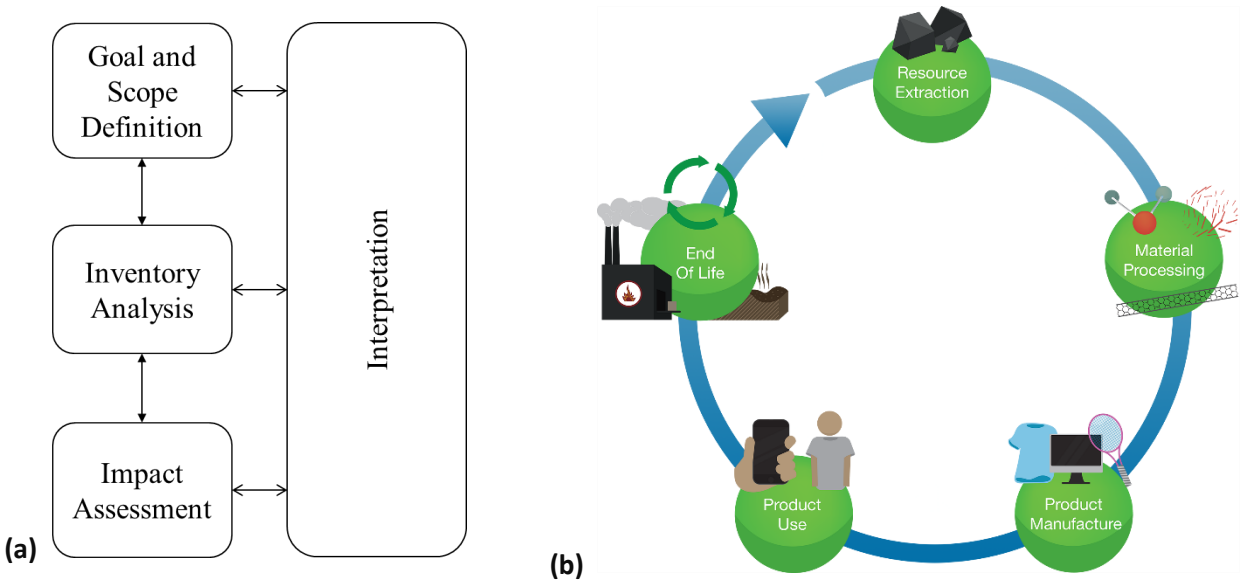

Figure 1-6 The (a) four principle steps of a life-cycle assessment beginning with the goal and scope definition which identifies the problem and the boundaries of the study. The second step is the inventory analysis and corresponds with all relevant data collection requirements. Next the impact assessment stage converts the inventory entries into potential impacts using characterization factors. Lastly, the step of interpretation is conducted throughout the entire study to refine any necessary steps and discuss the significance of the inventory and impact results in context of the original scope of the study. The (b) general life-cycle stages that can be considered in a life-cycle assessment. (Source: Figure (a) adapted from ISO 14040[28])

The goal and scope defines what is being studied in the LCA and includes defining the functional unit and the system boundaries. The functional unit describes a function being fulfilled such as a process (e.g. solvent regeneration), product (e.g. solar panel) or event (e.g. environmental remediation). The functional unit is directly related to the system boundaries, which further clarify which aspects of the functional unit are or are not included in the assessment. An important aspect of the system boundaries is identifying the life-cycle stages contained within the study (Figure 1-6). For example, a LCA study could be classified as gate-to-gate if the assessment only includes one life-cycle stage (e.g. product manufacturing), cradle-to-gate if the assessment includes raw material extraction through product manufacturing, or cradle-to-grave if the assessment includes each life-cycle stage. In addition, identification and choosing the environmental and human health impact criteria for evaluation is to be completed as a part of the goal and scope definition.

The second step of a LCA, the life-cycle inventory, involves the identification, quantification and aggregation of all the material, energy and waste streams contained within the boundaries of the functional unit. Many times, the inventory data can be obtained from pre-existing life-cycle inventory databases such as Ecoinvent (The Ecoinvent Association, Zurich) which is the most widely used database for LCA studies. The life-cycle impact assessment involves the conversion of life-cycle inventory data into environmental and human health impacts, sometimes referred to as life-cycle impacts. These impacts may include, but are not limited to, acidification of land and water, climate change potential, resource depletion potential, ecotoxicity, eutrophication of waterways, human toxicity, ionizing radiation potential, land use changes, ozone layer depletion potential, particulate matter formation, and photochemical oxidant (smog) formation potential. The final step in an LCA, interpretation, is used to (a) understand and make the logical connections between the life-cycle impact assessment results, life-cycle inventory and the goal/scope definition, but also to (b) identify anomalies and errors that may present themselves in each of these LCA steps. Lastly, LCA does not quantify absolute environmental or human health impacts. Instead, LCA uses generalized models that provide a potential, relative impact. This is in contrast to certain other impact analyses such as human health risk assessment (HHRA)[32] and environmental risk assessment (ERA).[33] In those approaches, individual substances contained within a product are identified and assessed for their probability of exposure in a population in distinct and specifically defined environmental conditions. Chapter 5 and Chapter 6 will introduce HHRA and ERA in greater detail.

Photovoltaic Life-Cycle Assessments: A Brief Background

PV-related LCA studies date back to 1995 with a first such study published by Huber and Kolb.[34] That study demonstrated the first known life-cycle inventory for a silicon-based PV system as well as the first life-cycle impact assessment using 15 different environmental and human health criteria. By the time of the International Energy Agency's (IEA) 2011 report on *Life Cycle Inventories and Life Cycle Assessments of Photovoltaic Systems*,[35] there had been many dozens of PV-LCA studies published in the literature. However, acknowledging the steep life-cycle inventory demands and technical nature of this technology, the IEA report aimed to provide further guidance on conducting PV-LCA to assure "consistency, balance, transparency and quality" as well as the "credibility and reliability of [LCA] results." While their report gathered the best-known life-cycle inventory data for crystalline silicon, cadmium telluride, and high-concentration PV, there was no consideration of OPV systems or other 3rd-generation technologies in that report. This exclusion was understandable given the lack of maturity and consistency in the developments of OPV at that time. Consequently, the OPV-LCA literature itself is heterogeneous, representing material

choices, processing routes and device structures as well as varying methods and environmental and human health impact results. The following sections outline the findings from a review of the OPV-LCA literature that was conducted at the start of this thesis and thus considers the published literature up to the end of 2013.

Review of Organic Photovoltaic Life-Cycle Assessments

The first OPV-LCA appeared in 2009 by Roes et al.[29] and between then and the end of 2013 there were a total of ten such studies (Table 1-1).[29–31,36–42] However, an additional eight peer-reviewed case studies, including the two from this thesis, have been published through October 2016.

Material Choices and Device Structures

Between 2009 and 2013, the types of OPV devices represented in the LCA literature have some overall consistency, owing to the fact that eight out of ten of these studies were either (a) from the same group of related authors[30,31,36–38,41] or (b) were based on devices described in a prior LCA study that came before it.[39,40] Nearly all of the studies considered a flexible OPV device that had a plastic substrate, however the very first two published OPV-LCA considered OPV devices on rigid, glass substrates.[29,30] Glass substrates are typical for lab-based experiments and production, but since the time of the first OPV-LCA, it has been shown that the physics and performance of OPV are fully compatible with plastic, flexible substrates such as polyethylene terephthalate (PET).[43]

Table 1-1 Material choices of the life-cycle assessment studies on organic photovoltaic systems existing in the peer-reviewed literature up to December 2013.

Case Study	Year	Substrate	Transparent Electrode	Hole Transport Layer	Active Layer	Electron Transport Layer	Opaque Electrode	Lamination and Additional Components	Deposition
Roes et al.[29]	2009	Glass, PET	ITO	PEDOT:PSS	P3HT PCBM	LiF	Aluminum	PVF, PET, EVA, SiO_2 barrier layer	Sputtering, inkjet and gravure printing
Garcia-Valverde et al.[30]	2010	Glass	ITO	PEDOT:PSS	P3HT PCBM	N/A	Aluminum, Calcium	EVA layer, SiO_2 barrier layer, Aluminum frame	Sputtering in inert atmosphere
Espinosa et al.[31]	2011	PET	Silver	PEDOT:PSS	P3HT PCBM	nano-Zn	ITO	PET Barrier layer	Sputtering of ITO onto PET in a vacuum roll-to-roll process, slot-die coating all other layers
Espinosa et al.[36]	2011	PET	Silver	PEDOT:PSS	P3HT PCBM	N/A	ITO	AMCOR Barrier, MPF Adhesive	Sputtering of ITO onto PET in a vacuum roll-to-roll process, slot-die coating all other layers
Espinosa et al.[37]	2012	Kapton (polyimide)	Silver	PEDOT:PSS	P3HT PCBM	N/A	Aluminum, Chromium	AMCOR Barrier, MPF Adhesive	Sputtering of aluminum and chromium on the Kapton in vacuum, Slot-die coating all other layers
Espinosa et al.[38]	2012	PET	Silver	PEDOT:PSS	P3HT PCBM	nano-Zn	PEDOT:PSS, nano-Ag, Graphite, Graphene	PET Barrier layer	Slot-die coating under ambient conditions for the front electrode, active layer, ETL and HTL. The silver electrode was screen printed.
Yue et al.[39]	2012	PET	Silver	PEDOT:PSS	P3HT PCBM	nano-Zn	PEDOT:PSS, nano-Ag, Graphite, Graphene	PET Barrier layer	Slot-die coating under ambient conditions for the front electrode, active layer, ETL and HTL. The silver electrode was screen printed.
Emmott et al.[40]	2012	PET	Silver	PEDOT:PSS	P3HT PCBM	nano-Zn	PEDOT:PSS, nano-Ag, CNT	PET Barrier layer	Various non-sputtering, normal atmosphere deposition for the transparent electrode, all other layers were slot-die coated.
Espinosa et al.[41]	2013	PET	Silver or Graphite	PEDOT:PSS	P3HT PCBM	nano-Zn	Silver, PEDOT, Graphite	PET Barrier layer	Various non-sputtering, normal atmosphere deposition for the transparent electrode, all other layers were slot-die coated.
Anctil et al.[42]	2013	PET	ITO	PEDOT:PSS, ZnO, MoO_3	Various Polymers and Small Molecules	Various $PC_{60}BM$, $PC_{70}BM$	TiO_2, Bathocuproine, Bathophenanthroline	Silver	PET Barrier layer	Sputtering in inert atmosphere

EVA: ethylvinylacetate | PVF: polyvinylfluoride | MoO_3: Molybdenum Oxide | Lithium Fluoride

In conventional or normal device structures (Figure 1-4), light is incident through the top (front) facing electrode which acts as the anode, to which positive charge carriers pass into. Seven out of the ten studies considered an inverted device structure whereby light is intended to come through the bottom (rear) electrode which acts as an anode. In three of the studies indium tin oxide (ITO) was used as the front facing anode.[29,30,42] In two other studies, ITO was used as the cathode of an inverted device.[31,36] ITO is a commonly used transparent electrode given its high level of optical transparency and electrical conductivity.[44] However, most of these studies acknowledged the limitation ITO poses as a scalable technology due to its availability, cost and to a lesser extent its toxicity.[45–47] Thus, the other five studies investigated the use of various ITO substitutes for use as a cathode in an inverted structure such as other low-work function metals (e.g. aluminum), small molecule organics, nanoparticles and carbon nanotubes.[37–41] In the non-inverted devices that used ITO as the transparent front electrode, two of the studies used aluminum or aluminum with calcium as the back electrode,[29,30] while the third study used silver.[42] In the seven studies that assessed inverted structures, silver was uniformly employed as the anode.[31,36–41] In addition, Espinosa et al. assessed the use of graphite as a non-silver substitute in order to begin to address the limitations silver poses in terms of abundance and cost if this technology were to be scaled to commercial and high volume scales.

Between electrodes and the active layer, optional hole-transport (electron-blocking) and an electron transport (hole-blocking) layers may be employed in order to increase efficiency and avoid premature recombination of the mobile charge carriers at the active layer.[48] In all ten of the OPV-LCA, poly(3,4-ethylenedioxythiophene):poly(styrenesulfonate) (PEDOT:PSS) was used as the hole transport layer. In Anctil et al., both PEDOT:PSS and molybdenum oxide (MoO_3) were individually tested. For the electron transport layer, three of the studies did not include this, one used a layer of lithium fluoride, five used nanoparticles of zinc oxide (nano-ZnO),[31,38–41] and one other study individually assessed titanium dioxide (TiO_2), bathocuproine and lastly bathophenanthroline.[42]

At the heart of any PV device is the active layer, at which charge separation occurs. As described earlier, in a silicon-based device there are n-type and p-type silicon layers that donate and receive electrons, respectively, although in an OPV device these are all organic layers. In all ten of the reviewed OPV-LCA studies, the modified C_{60} fullerene, phenyl-C_{61}-butyric acid methyl ester (PCBM), was used as the electron acceptor (Figure 1-7).

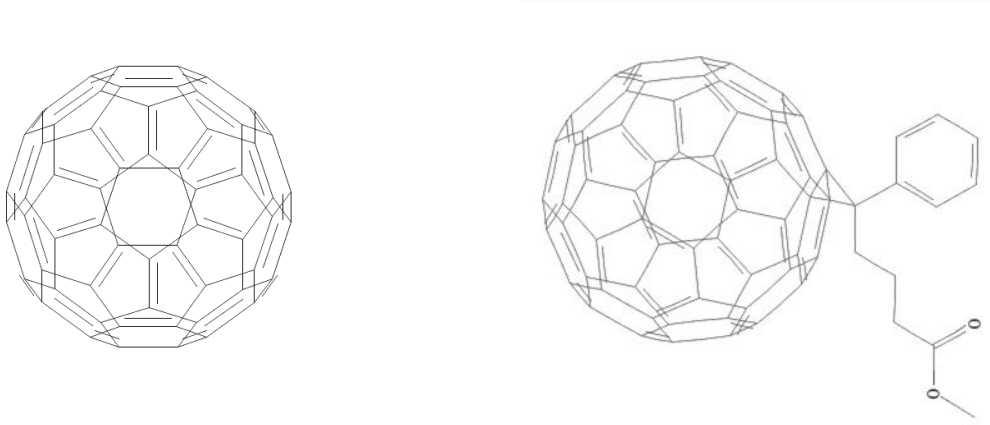

(a) (b)

Figure 1-7 Two-dimensional structures of (a) an unmodified fullerene with 60 carbon atoms and (b) a functionalized 60-carbon ring fullerene (PCBM). (Source: PubChem Open Chemistry Online Database)

Apart from PCBM, Anctil et al. assessed OPV's environmental impacts for devices using non-functionalized C_{60}-fullerene as well as non-C_{60} PCBM alternatives such as $PC_{70}BM$, *bis*-PCBM and the indene-*bis*-adduct.[42] PCBM is an engineered nanomaterial (ENM) and specifically a derivative of the Buckminsterfullerene or fullerene, named after the American engineer and architect Richard Buckminster Fuller. Its structure is a stable, geodesic cluster of carbon atoms that was first discovered by scientists at Rice University in 1985.[49]

Clusters of 60 carbons with an approximate diameter of 0.7 nm is the most accessible forms of the fullerene and is commonly referred to as C_{60}.[50] Market application and large scale use of C_{60}-fullerenes began in the early 2000s, where these materials were used initially for enhancing sporting equipment. However, their research, development and use for other sectors has grown beyond such applications. The principal properties specific to the functionality of C_{60}-fullerenes are closely related to its small size and ability to reversibly accept upwards of six additional electrons, which is partly why they have been heavily researched for their electrochemical applications.[50,51] C_{60}-fullerenes are strongly electronegative and provide high electron mobility and when in conjunction with a co-polymer provide reliable charge separation under illumintation.[43,52–54] Ideally, the use of the so-called low bandgap polymers are most effective p-type materials for use with PCBM (Figure 1-8).

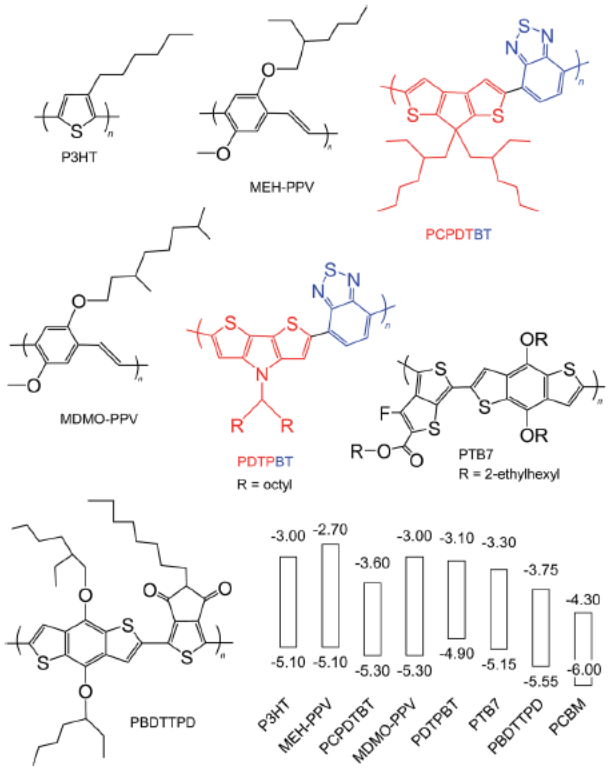

Figure 1-8 Selection of p-type polymers that could be used with PCBM as a basis for the active layer of an organic photovoltaic solar cell. (Source: Yan and Saunders 2014[55])

In all ten of the OPV-LCA studies, poly(3-hexylthiphene) (P3HT) was used as the co-polymer. However, Anctil et al. also assessed OPV environmental impacts using two non-P3HT co-polymers as well as a selection of small molecules such as zinc, copper and aluminum based phthalocyanines, 2,4,-bis[4-N,N-diisobutylamino_2,6-dihydroxyphenyl] squaraine, chloroboron subnaphthalocyanine and chloroboron subphthalocyanine.[42]

For general protection and durability of the device, additional barrier and lamination layers are applied to the OPV panels. In all the OPV-LCA studies that involved flexible substrates, PET was used as the additional barrier and lamination layers. In some cases, silicon dioxide was also used for lamination. In the cases where a glass substrate was used, ethylvinylacetate and polyvinylfluoride served as the lamination and barrier layers.[29,30] All studies used some form of synthetic epoxy resin or acrylic adhesive to bind the barrier layers with the core OPV layers.

Among these ten OPV-LCA studies, there was significant differences in the way that the devices were constructed and how each layer was applied to the substrate of the PV device. Six of the studies, for

example, utilized sputtering of ITO onto the PET using vacuum and/or intern atmospheric conditions.[29–31,36,37,42] In the other four studies, these conditions were avoided altogether and substituted with other solution based deposition processes such as slot-die coating.[38–41] For other layers, various techniques were used such as screen printing, gravure printing and inkjet printing. Besides Garcia-Valverde et al.,[30] all of the studies assumed non-batch processing using continuous roll-to-roll production.

The diversity in the materials, production routes and device structures used in these ten studies resulted in a range of OPV defined by differences in (i) the (photo)-active area of the panel, (ii) conversion efficiency and (iii) lifetime of the device. The active area of the OPV ranged from a low of 45% to a high of 90%. These differences were sometimes actual measurements and in other times forecasted estimations of near-term feasible limits.[29,39,42] The efficiencies of the OPV ranged between 1% to 10%. Again, some of these values were based on actual measurements, while many of the studies engaged in sensitivity analyses to test various near-term changes in device efficiency.[30,37–39,42] These projections are not unheard of, given that lab-scale OPV has reached upwards of 12% as of 2016.[15] Lastly, only seven of the OPV-LCA made any mention of device lifetime, with assumptions ranging from 2-15 year[30,36–41] and in one case as high as 25 years.[29] Up to 2016, maximum reported OPV lifetimes have reached seven years.[56] Thus, the projected lifetimes of some of the reviewed OPV-LCA studies are overestimations and thus underestimate their reported environmental impacts.

Scope and Boundaries

The majority of the OPV-LCA studies were limited to a cradle-to-gate assessment from raw material extraction through the manufacture of the OPV panel (Table 1-2). [29–31,37–42]

Table 1-2 Scope, boundaries and select number of assumptions that were made in the life-cycle assessment studies on organic photovoltaic systems existing in the peer-reviewed literature up to December 2013.

Case Study	Year	Efficiency	Active Area	Lifetime	Functional Unit	Use Phase	End-of-Life
Roes et al.[29]	2009	5%	90%	25 years	25-year production of 1 Wp	Rooftop system including balance of system for the glass, no BOS for the plastic (assumed not producing energy that will be transmitted to grid in AC form, but used directly by personal device, however they do not account for any other use phase systems or change in the functional unit)	N/A
Garcia-Valverde et al.[30]	2010	5% and 10%	90%	15 years	1 m^2 of framed solar module	N/A	N/A
Espinosa et al.[31]	2011	2%-3%	67%	N/A	1 m^2 of framed solar module	N/A	N/A
Espinosa et al.[36]	2011	5%	67%	2 years	104 cm^2 lamp (0.1 Wp of OPV)	BOS: overlay frame, adhesives, spacer, battery, LED, circuits	Landfill
Espinosa et al.[37]	2012	1%-5%	68%	15	1 m^2 of framed solar module	N/A	N/A
Espinosa et al.[38]	2012	1%-5%	45%	15	1 m^2 of framed solar module	N/A	N/A
Yue et al.[39]	2012	3%-8%	45%-85%	15	1 m^2 of framed solar module	N/A	N/A
Emmott et al.[40]	2012	3%	67%	15	1 m^2 of framed solar module	N/A	N/A
Espinosa et al.[41]	2013	3%	46%	15	1 m^2 of framed solar module	N/A	N/A
Anctil et al.[42]	2013	3%-7%	85%	N/A	1 Wp	N/A	N/A

Wp: watt-peak | LED: light emitting diode | BOS: balance of system

Accordingly, the functional units were defined for 1 m^2 of OPV panel. Anctil et al. defined their functional unit as a watt-peak (Wp) of power production. A Wp is defined as the nominal power of a solar cell, where the ability of a device to produce one Wp is tested under standardized conditions. Roes et al. stated that the scope of their study included the use-phase in the form of a rooftop mounted system using a functional unit defined as an average Wp of power produced over 25 years. As mentioned above, these results of their LCA study might be underestimating the environmental impacts given that the assumed lifetime of the OPV in that study was 25 years. Espinosa et al. was the only study that considered a use phase as well as an end-of-life phase.[36] Their use phase included the production of light using an OPV-integrated lamp and the end-of-life phase considered landfilling of the lamp. The functional unit for their study was the production of 0.31 Wp for light production over two years.

Environmental and Human Health Impact Assessment Criteria

All of the ten OPV-LCA studies published between 2009-2013 estimated the impact criteria of cumulative energy demand (CED), EPBT or a combination of both. This makes sense since OPV are an energy producing technology and one of the most obvious questions one can ask is *how much energy is consumed in order to produce energy* and ho*w much time does it take for that technology to reproduce the energy it consumed* (i.e. EPBT). These are useful calculations that also allow for comparisons between different types of energy producing systems (i.e. PV versus wind versus nuclear). In addition, six of the studies calculated the greenhouse gas emissions[29–31,36,37,41] and two of the studies assessed a more comprehensive set of environmental impacts beyond energy or greenhouse gas accounting as were presented in the previous "primer" on LCA.[29,41]

Environmental and Human Health Impact Assessment Results

Because of the differences in the scope and boundaries of each study as well as differences in types of devices investigated and assumptions made on their performance, there was some variation in the results between each of the ten OPV-LCA studies. For example, these differences were reflected in the CED values estimated for each cradle-to-grave OPV study (Figure 1-9).

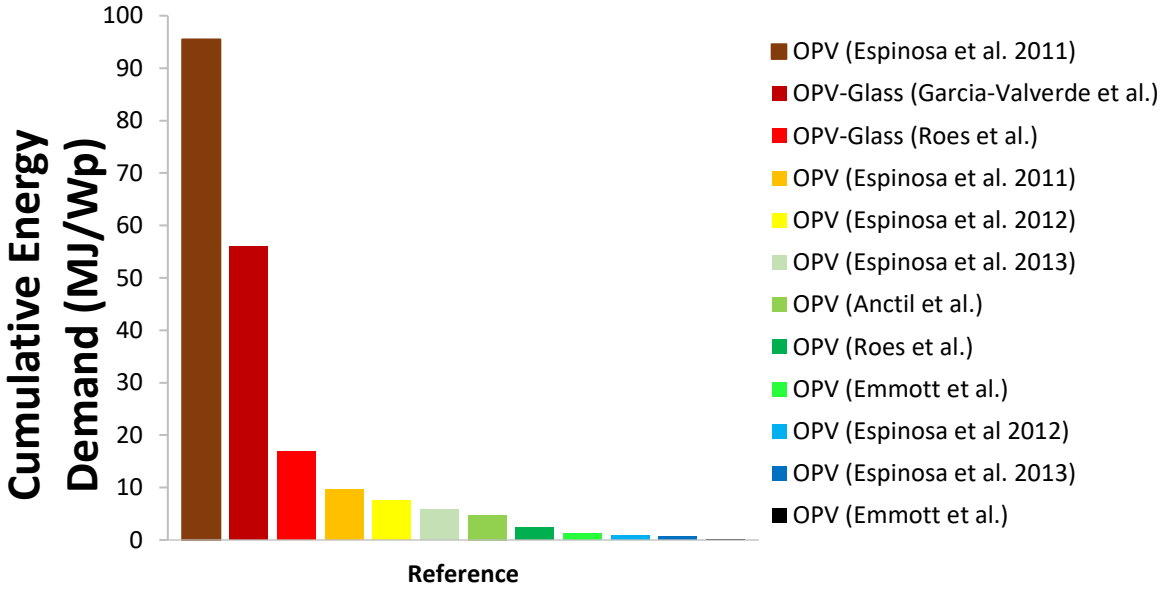

Figure 1-9 Cumulative energy demand for organic photovoltaic cells as reported in the literature up through December 2013 per watt-peak of power production

The results range from a low of 0.11 MJ per Wp to a high of 96 MJ per Wp. These results are specific for the baseline OPV assumptions defined in each study and do not reflect their various sensitivity analyses. The CED value of 96 MJ per Wp reported by Espinosa et al. was much larger than all the other studies due to its greater scope and boundaries of the study, which included the use phase and the end-of-life phases.[36] More importantly, the use-phase included the production of many non-OPV parts that were associated with a functioning lamp such as a protective case, light emitting diode, cables and other circuitry. While Roes et al. also included the use-phase along with non-OPV parts such as the frame, inverter and cables, it is not apparent why exactly their CED is nearly 5-times lower than Espinosa et al. Although, a small portion of this might be explained by the 23% greater active area assumed in Roes et al. The results by Garcia-Valverde et al. report the second highest CED of 56 MJ per Wp. This is mainly a consequence of its use of fully lab-based, batch production methods of a rigid, glass OPV device. One of the main challenges cited by most of the studies with higher CED was reported as the energy demands for

producing and sputtering ITO on the substrate under vacuum or inert atmospheric conditions.[29–31,36,37] In some cases ITO production and deposition account for upwards of 87% of the embodied energy of the entire OPV.[30,31] ITO itself is an energy intensive material to extract, produce and refine, however even if substituted with another material, it was found that the inert atmosphere needed for deposition could still account for nearly 17% of the energy demand.[37] In the cradle-to-grave study by Espinosa et al., the ITO substrate only constituted 35% of the overall CED, while the protective plastic layers, blocking diode, and light emitting diode represented 22%, 16% and 16% of the total demand. Those results again demonstrate the importance of and difference between cradle-to-gate and cradle-to-grave studies. When produced in normal atmosphere conditions, the reported CED values dropped significantly by over one-order of magnitude.[38–41] Under these conditions, the main energy consuming aspects of the OPV shifted to the substrate, hole transport layer and electrodes.

It is curious to note that, since most of the studies were either from the same group of related authors[30,31,36–38,41] or were based on devices described in a prior LCA study that came before it,[39,40] a lot of the life-cycle inventory data originate from a single source. If the data come from a primary, industrial source this could be reliable, however in many cases these data were being reported from lab-based processes, older techniques, expert judgement or stoichiometric calculations. One clear example of this influence on the results was brought to light in a LCA study by Anctil et al.[42] In a previous study, those authors completed an assessment of the CED for the processing and manufacturing of C_{60}-fullerenes and PCBM.[57] They found their results were much higher than previously reported energy demands per kg of fullerene production and reasoned this to be on prior studies' use of older and/or incomplete data of the production route, particularly the purification steps.[57] When they integrated this information back into their OPV-LCA, they found that nearly 20% of the CED was due to the production of PCBM.[42] This is in contrast to the much lower percentages ranging between 0.21%-10% reported in the other OPV-LCA studies reviewed. Thus, whereas most of the other studies pointed to the non-active layer components as the main bottle-necks or targets for environmental improvement, Anctil et al. was the first study to identify the active layer as such.

Correspondingly, the EPBT reported in the OPV-LCA studies range from a low of 0.35 years to a high of 9.9 years. Because the EPBT is determined using the CED, the differences in the EPBT results can be attributed to the same factors driving the CED results. Once again, the highest EPBT of 9.9 years was reported by the cradle-to-grave study by Espinosa et al. that included the non-OPV components utilized during the use

phase and impacts from the end-of-life landfilling process.[36] The glass-substrate OPV devices reported by Garcia-Valverde et al. and Roes et al. had EPBT of 4.0 and 1.3 years, respectively.[29,30] Those two studies also happened to report the highest active areas of 90%. Using Monte-Carlo uncertainty analysis,[58] Yue et al. demonstrated that the active area and efficiency of the OPV devices were the most significant sources of uncertainty in the calculation of the EPBT. Those authors also took into consideration the degradation rate of the OPV, as opposed to the other OPV-LCA studies, and found that it contributes upwards of 9% of the total uncertainty in the results.[39] When OPV manufacturing switched from inert to normal atmosphere conditions, the EPBT decreased by over one-order of magnitude similar to the CED values.[38–41]

The results from the two studies that reported a more comprehensive set of environmental impacts differed quite significantly. Some of the impacts reported by Espinosa et al.[41] were upwards of 3-orders of magnitude lower than Roes et al., for instance, in ozone depletion potential. These differences were most likely a consequence of the manufacturing differences taken by Espinosa et al. which used normal atmosphere conditions compared to Roes et al. who used an inert atmosphere for ITO sputtering onto the substrate.

In regards to conventional silicon PV, only half of the OPV-LCA studies made a comparison between OPV and conventional panels.[29,30,36,39,42] Garcia-Valverde et al. reported that the CED of a 5% efficient OPV panel was 56 MJ/Wp, nearly two-times and over three-times greater than the referenced values of 28.3-29.9 MJ/Wp and 15.9 MJ/Wp for m-Si and a-Si, respectively.[30] This resulted in a 4.0-year EPBT that was 1-2 times longer than the EPBT values of 2.7-4.1 referenced for m-Si as well as 4-times longer than the values referenced for a-Si. Anctil et al. reported CED values ranging between 3-10 MJ/Wp for the 26 different OPV tested in their study. All such values were below the referenced CED of 16-24 MJ/Wp and 29 MJ/Wp for a-Si and m-Si, respectively. Yue et al. reported EPBT < 0.25 years for OPV which were one order of magnitude smaller than the nearly 2.4 years estimated for m-Si. Using two different functional units, Roes et al. compared a glass-substrate OPV and plastic-substrate OPV to both m-Si and a-Si. The EPBT for the glass-substrate OPV was 1.3 years compared with 2.33 years and 1.93 years for m-Si and a-Si PV, respectively. The EPBT for the plastic-substrate OPV was 0.2 years compared with 2.0 and 1.3 years for m-Si and a-Si, respectively. The reason why the EPBT for the silicon-based PV became shorter in the second comparison was due to the change in the functional unit which eliminated certain use-phase components (i.e. fewer physical materials used and thus a lower embodied energy of the entire system). Furthermore,

Roes et al. compared OPV and silicon cells across 6 other impact categories: climate change potential, (abiotic) resource depletion, ozone layer depletion, photochemical oxidant formation, acidification and eutrophication. For the glass-substrate, all impacts were lower for OPV, however the extent of which was not uniform for all impact categories. For instance, whereas ozone layer depletion for OPV was over 1-order of magnitude smaller than m-Si, acidification for OPV was only 13% lower. The reductions over m-Si were more pronounced for the plastic-substrate OPV. For instance, the acidification potential was now 81% lower for OPV compared to silicon. However, the plastic-substrate scenario resulted in a photochemical oxidant formation potential that was 25% greater than m-Si due to the toluene emissions estimated for gravure printing. In comparison, the results presented by Espinosa et al. were unique in the fact that the LCA was cradle-to-grave, as opposed to the cradle-to-gate or cradle-to-use scopes that were applied in the other four studies that made comparisons to silicon-based PV. Espinosa et al. demonstrated that switching from an a-Si PV lamp to an OPV powered lamp can save 0.52 kg of greenhouse gas emissions per Wh of electricity produced and nearly 64 MJ of energy per lamp over a two-year period of use.[36] However, it should be noted that there were differences in the type of battery and other non-OPV components that contribute to this difference. The relative difference between OPV and the silicon PV reported by these five studies were of course influenced by the distinct types of OPV and methods of each study. However, different versions of pre-existing, background life-cycle inventory source data were used as a basis of the silicon-based analysis.[26,59–61]

Summary of the Review

The OPV systems represented in the ten OPV-LCA studies reviewed up to the end of 2013 represented a mix of different material choices and device structures for the OPV as well as a mix of scopes, boundaries, functional units, inventory data and impact assessment categories. Some of these studies were unique in that they happen to be produced at fairly high production volumes akin to pilot-scale setups,[31,36–38] while their technical capacities, since 2013, have also been tested in large-scale outdoor demonstrations.[24,62] Even so, OPV still lack proper industrial scale technology or a market for use and consumption. Therefore, OPV may have the potential to reduce cradle-to-gate carbon emissions and energy consumption by over an order of magnitude compared to silicon (Figure 1-9), but such resource efficiencies may not necessarily remain after considering the use and end-of-life phases.[36] This is because OPV are also known to be less efficient[22,63] and have shorter lifetimes[45] compared to conventional PV. Consequently, environmental benefits seen during OPV manufacturing might be offset by the cumulative use and replacement of exhausted OPV panels over an entire lifetime of its service. In addition, important questions remain

regarding how PV panels can and will be disposed of at their end-of-life.[64] This infrastructure is lacking for conventional PV, with landfilling being a default solution.[65] It is similarly uncertain how OPV panels might be disposed of once they are used at large scales or commercially. Thus, it is important to anticipate the influence a disposal route will have on the environmental impacts of these technologies.

In addition to considering the entire life-cycle, standard OPV-LCA should include impact categories beyond CED or greenhouse gas accounting as was limited to in a majority of the reviewed studies. While those two metrics are important for outlining baseline progress and advantages in this field, energy consumption and greenhouse gas emissions are only a limited selection of other environmental and human health indicators and impacts. A life-cycle approach should accommodate a broad range of environmental criteria in order to expose and reduce any potential environmental burden-shifting.[66] This recommendation is important because although CED may on occasion be a proxy for other potential impacts,[29] this may not always be the case. For example, what would be the correlation between CED and human toxicity? Even when there may be some correlation with CED and other potential impacts, that relationship is not necessarily linearly correlated.[45] Thus, comparing products based on one or two indicators may result in an unintended increase in other environmental impacts that were, as a consequence, not explicitly estimated. To date, only half of the currently published OPV-LCA completed such an assessment.

Furthermore, to demonstrate OPV advantages as an alternative, new source of sustainable energy, LCA studies should ideally compare them with conventional silicon-based PV, which currently dominate the market.[16] However, and as was discussed above, only five of the previously published OPV-LCA literature have done so, and of those, only one study has compared OPV and silicon PV across the entire cradle-to-grave.[62] Thus, a review of OPV-LCA studies that are cradle-to-grave, multi-criterion based, and comparatively assessed with conventional silicon shows there were no such existing studies in the literature through at the start of the research put forth in this dissertation (i.e. the end of 2013) (Table 1-3).

Table 1-3 Life-cycle assessment studies on organic photovoltaic systems existing in the peer-reviewed literature up to the end of 2013. (Adapted from Chatzisideris et al.[67])

Individual Case Studies	Year	Cradle-to-Grave	Full Range of Life-Cycle Impact Criteria	Comparison to Conventional Photovoltaics	Comprehensive Across All Indicators
Roes et al.[29]	2009	○	●	●	○
Garcia-Valverde et al.[30]	2010	○	○	●	○
Espinosa et al.[31]	2011	○	○	○	○
Espinosa et al.[36]	2011	●	○	●	○
Espinosa et al.[37]	2012	○	○	○	○
Espinosa et al.[38]	2012	○	●	○	○
Yue et al.[39]	2012	○	○	●	○
Emmott et al.[40]	2012	○	○	○	○
Espinosa et al.[41]	2013	○	●	○	○
Anctil et al.[42]	2013	○	○	●	○

Overview of Problem Context for the Thesis

The future of energy production is an immediate problem facing the world's population, not only in terms of finding enough energy and at reasonable cost, but finding energy solutions that address pressing major environmental and human health challenges coinciding with our use of fossil fuels and impacting climate change effects. Conventional silicon-based PV technologies offer one means of providing a relatively low environmentally burdensome energy supply. At the beginning of this chapter, an overall objective of this thesis was put forth to answer if it is possible to demonstrate whether OPV have proven themselves to be a preferable energy supply option compared to conventional silicon-based PV from an environmental and human health point of view. While silicon-based PV have already proven themselves both in performance and environmental benefits, the results of preliminary OPV-LCA literature review only hint at OPV's potential greater resource efficiencies and reduced environmental hazards. However, a definitive view was not able to be taken based on those studies. The following chapters of this thesis explores this objective in greater detail based on the following set of hypotheses and research questions.

Hypotheses

1) The resource efficiencies and potential hazards of organic photovoltaics technologies can be adequately demonstrated, even from its current, early developmental stage.

2) The resource efficiencies are greater and potential hazards lower for prospective, near-term organic photovoltaic technology, compared with conventional silicon-based photovoltaics.
3) Life-cycle assessment is the most appropriate methodology for evaluating organic photovoltaics' resource efficiencies and potential hazards (i.e. human health exposure).
4) Human health risk assessment is the most appropriate tool for evaluating the human health impacts of potentially toxic substances used in organic photovoltaic technologies.
5) The approach and methodologies of life-cycle assessment and human health risk assessment are fully compatible for making evaluations of emerging technologies.
6) Life-cycle assessment and human health risk assessment can be used to inform the potential discussions and justifications for supporting the use and adoption of emerging technologies.

These hypotheses are intended to be supported or refuted based on the following set of core research questions posed in this thesis.

Questions Addressed in this Thesis:

1) What are the full range of cradle-to-grave environmental impacts of prospective organic photovoltaic technologies?
2) How do the environmental impacts of organic photovoltaic technologies compare with conventional silicon-based photovoltaics?
3) What are the current limitations of using life-cycle assessment to evaluate organic photovoltaic and other emerging technologies?
4) What tools are available for addressing the human health hazards and risks to engineered nanomaterials?
5) How can these human health impacts of engineered nanomaterials be integrated within life-cycle assessment methodologies?

Structure of the Thesis

The previous portion of this chapter referred to the literature leading up to the development of the objectives of this thesis. Specifically, the review was used to address *to what degree did the state-of-the-literature support the notion that OPV are an environmentally preferable energy supply option compared to conventional silicon-based technologies*. The literature largely demonstrated that the production of

OPV on a watt-for-watt basis have shorter EPBT and lower greenhouse gas emissions compared to silicon. There were also some indications that environmental and human health impacts may remain lower even after considering the use and disposal of OPV products. However, there is further support that needs to be demonstrated to support the claim that OPV are truly an environmentally preferable energy production option compared to conventional silicon.

In Chapter 2, a more detailed account of LCA is presented in order to better understand the environmental criteria and assessment methods that have been largely used to evaluate OPV. Chapter 3 introduces a cradle-to-gate LCA up to the point of the production of a prospective OPV cell. These results are further compared to the life-cycle results for conventional PV cells, discussing the implied advantages and drawbacks of each technology. Chapter 4 is a direct extension on the work of Chapter 3 and expands the LCA to explore the potential uses and end-of-life scenarios for OPV. Chapter 5 takes a further look at the possible issues of burden shifting, specifically examining LCA's limitations in estimating the human health impacts from the production, use and release of ENM across the OPV life-cycle. Chapter 6 then presents a more formal HHRA study to address these potential ENM impacts, and Chapter 7 reintegrates this information into the LCA methodology to reassess the overall environmental performance of the OPV. Chapter 8 takes stock of the results provided by the updated LCA with human health impacts to address whether there is a case to be made regarding the environmental preference of OPV over silicon-based PV. Lastly, ongoing work and future opportunities for developing OPV are presented. Following the main text, in order, are the Bibliography, Appendices and List of Publications.

Table 1-4 Flow diagram of the structure, objectives, hypotheses and research questions put forth in this thesis

Chapter 2 Life-Cycle Assessment and Its Application to Organic Photovoltaics

In Chapter 1 the topic of LCA was briefly introduced as a primer and segue before discussing the OPV-relevant literature on the subject. It is worthwhile to discuss this tool and its methodology in greater detail, not only for providing the appropriate background for non-LCA experts, but also to describe the life-cycle inventory and life-cycle impact assessment methods that were applied in the case studies presented in Chapter 3 and Chapter 4. The latter point will also serve to orient the reader later in Chapter 5 and Chapter 7 during further review and analysis, respectively, of the impact assessment models created in this thesis.

Life-Cycle Assessment: A Brief History

Coinciding with the trends in industrial development and concerns over environmental protection and public health, the ideas of defining a product's resource efficiency date back to the early-mid 20th century. Early in the development of such assessments, energy was the main criteria of focus but soon after started to assess emissions, pollutants and waste generation. This was exemplified in one of the first types of these studies commissioned by the Coca-Cola Company in 1969, studying the effects of using different types of containers for their soda-products.[68] After a period of relative inactivity in this field of science, a formal report published in the mid-1980's by the Swiss Federal Laboratories for Materials Testing and Research (EMPA) outlined the data requirements for producing a life-cycle inventory.[68] Yet, it was not until the beginning of the 1990s until LCA, in its current form, began to take shape. This period of time saw a number of workshops, frameworks, journal articles, codes of practice and standards being officially published and promulgated on an internationally recognized basis.[27,28,69–73] Today, LCA has grown into a core scientific discipline finding its application in a myriad of other subjects which is reflected by the growth of published "life-cycle assessments" over the past two decades (Figure 2-1).

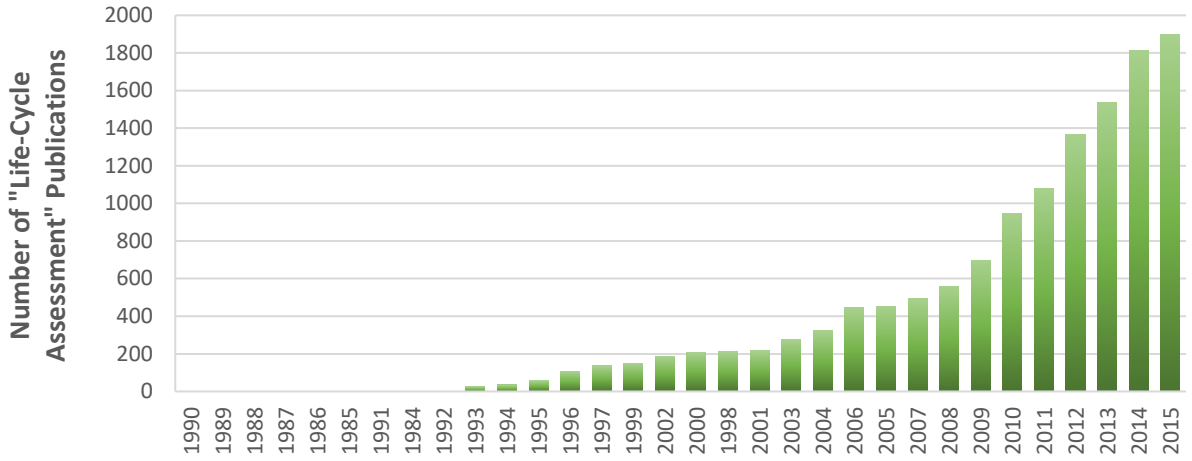

Figure 2-1 Growth in the number of peer reviewed scientific journal articles in the subject area of "life-cycle assessment." Results generated using SCOPUS (www.scopus.com).

As mentioned in Chapter 1, LCA is a broadly scoped environmental management tool outlined by ISO 14040:2006 and 14044:2006.[27,28] These standards are founded on the concept of environmental management for measuring and communicating the relative environmental impacts of a product or process. The strengths of LCA are that it is a comprehensive tool, that models entire product systems, estimating the impacts of multiple environmental and sustainability metrics in response to the entire supply-chain of a product. Hence, it is often used by individuals and organizations promoting the concepts of resource efficiency,[74] eco-design or sustainable consumption and production. The results of an LCA can provide hot-spot analysis and identify burden-shifting, allowing for effective environmental management, guidance during early-stage technology development and environmental product declarations (ISO 14025).[75] More specifically, LCA is composed of the (1) goal and scope definition, (2) life-cycle inventory analysis, (3) life-cycle impact assessment and (4) interpretation steps (Figure 1-6).

Goal and Scope Definition

The goal and scope defines what is being studied in the LCA and what research question is being addressed. This activity includes defining the functional unit and the system boundaries. The functional unit describes the function being fulfilled such as a process (e.g. solvent regeneration), product (e.g. solar panel) or event (e.g. environmental remediation). The functional unit is directly related to the system boundaries, which further clarify which aspects of the functional unit are or are not included in the assessment. An important aspect of the system boundaries is identifying the life-cycle stages contained within the study (Figure 1-6). For example, a LCA study could be classified as gate-to-gate if the assessment

only includes one life-cycle stage (e.g. product manufacturing), cradle-to-gate if the assessment includes raw material extraction through product manufacturing, or cradle-to-grave if the assessment includes each life-cycle stage. The goal and scope definition also involve decisions regarding the appropriate age, geographic relevance, sources, uncertainty and specificity of the life-cycle inventory data. In addition, identification of environmental and human health impact criteria that will be assessed is to be completed as a part of the goal and scope definition.

Attributional and Consequential Life-Cycle Assessment

The inherent flexibility in ISO 14040:2006 and 14044:2006 allow for differences in the design of one's LCA study and the modeling approach taken in terms of the goal and scope definition and life-cycle inventory analysis. In general, two main modeling approaches are acknowledged within the LCA community. One approach is called the *attributional*-LCA approach and is described as an "accounting" or "descriptive" approach, in which the aim is to attribute the share of total, *current* global environmental impacts to a particular product or process.[76] The other approach is entitled *consequential*-LCA and is described as a "change-oriented" approach as is concerned with quantifying how changes in demand for a product *influences* total, global environmental impacts and therefore both direct and indirect environmental impacts of that product. These two approaches are illustrated in **Figure 2-2**.

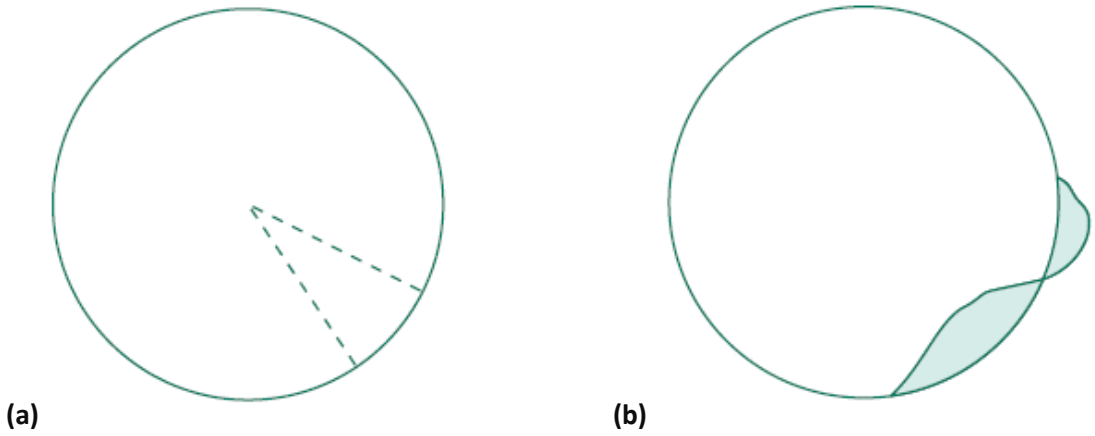

Figure 2-2 The (a) attributional modeling approach in life-cycle assessment depicted as a *share* of total, current global environmental burdens of a product or process as opposed to the (b) consequential modeling approach that is concerned with the *changes* in total, global environmental burdens due to decisions made regarding the product or process. (Source: Weidema 2003[77])

The decision to perform one modeling approach over the other will then determine the type of life-cycle inventory data and analysis that needs to be performed. This means that an attributional life-cycle inventory must be used for attributional-LCA and consequential life-cycle inventories for consequential-LCA. Specifically, an attributional life-cycle inventory is sourced from any typical, average supplier and deals with co-products using an allocation approach (see description in the following section). A consequential-LCA ideally uses data from the marginal supplier (i.e. one that is not constrained and by default responds to the change in demand for that product) and expands the system boundaries of its study to include the life-cycle stages and impacts from co-products (see description in the following section). The concepts of allocation and system expansion are further described in context of the life-cycle inventory in the following section.

Life-Cycle Inventory

Once the functional unit and system boundaries are defined, all material, energy and waste streams are identified, quantified and aggregated into a single inventory. More formally, the life-cycle inventory involves the quantification of all these inventory items per their use defined by each unit process within the boundaries of the functional unit that are initially defined within the goal and scope definition of the LCA. Figure 2-3 shows a generic flow diagram and system boundaries of a single unit-process that is typical in LCA for outlining and tracking the data required of a study.

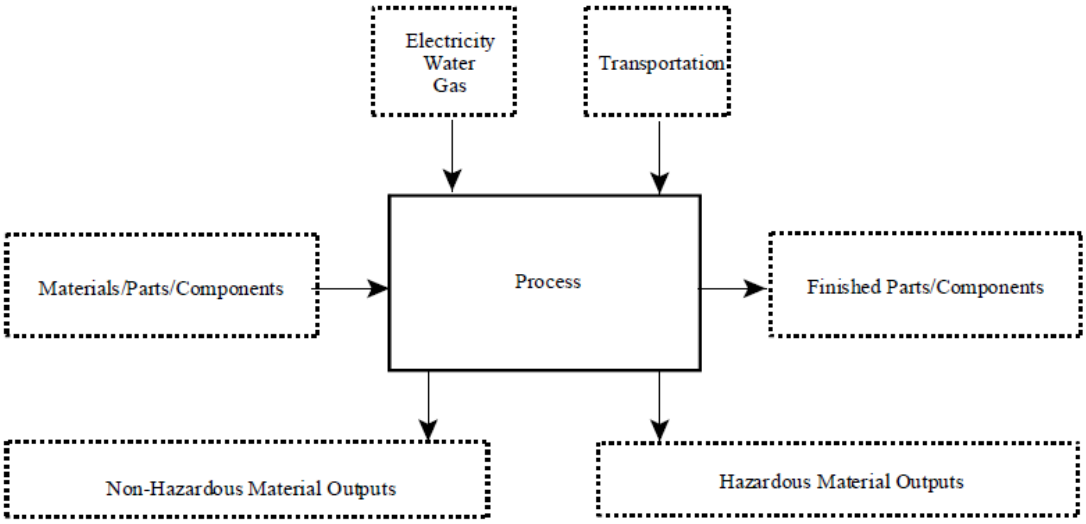

Figure 2-3 General flow diagram created during the life-cycle inventory phase. The flow diagram helps to outline the data requirements for each process and along each step of a life-cycle assessment. (Source: U.S. EPA[78])

Typically, in LCA the inputs themselves are processes with their own set of inputs and outputs, and thus an LCA can be thought of as a series of unit-processes connected in series. The outputs are typically defined as products or elementary flows. Elementary flows represent resources taken from and pollution emitted to the environment, while products represent the technical flows out of the process. Products can be created in isolation or in conjunction with a co-product or by-product. In the latter cases, a formal decision must be made how the inventory is shared between these various product outflows. In attributional-LCA, it is common for these decisions to be made on a basis of "allocation." This means that distinct and separate portions of the total inventory items are ascribed to each co-product. For instance, if a process creates one kg of Product-A and one kg of Product-B, mass-based allocation (i.e. scaling by the fraction of total mass) would result in allocating 50% of the inventory to Product-A and 50% to Product-B. Similar forms of allocation can be made based on economic value or energy content of the products, for example.

In place of allocation, one can use "system expansion," which is a means of expanding the system boundaries to include the substitution of a primary product with the co-product. The result being a reduction of total life-cycle inventory data, because of avoiding primary production of the analogous co-product. However, this approach is the default recommendation of the ISO 14040 and 14044 standards and also most typical of consequential-LCA modeling as opposed to attributional modeling. Besides the

management of co-products, other considerations must be made while building a life-cycle inventory such as the inclusion or exclusion of small material amounts, age-appropriateness of the data, spatial-appropriateness of the data, and uncertainty in the data, for example.[78]

The life-cycle inventory can be consolidated using pre-existing databases such as the previously mentioned Ecoinvent life-cycle database, extracted from scientific literature, professional reports or patents, empirically measured, modeled with detailed engineering and scientific tools, or estimated using expert judgment. As a rule of thumb, data extracted from pre-existing life-cycle databases, published literature or other sources that already pre-define a unit process and its inventory data is considered as background data. Conversely, primary data that is measured, modeled or estimated for the first time to create new life-cycle inventory process are considered as foreground data (Figure 2-4). Foreground data is often associated with the unit processes that are the principal focus of one's LCA study.

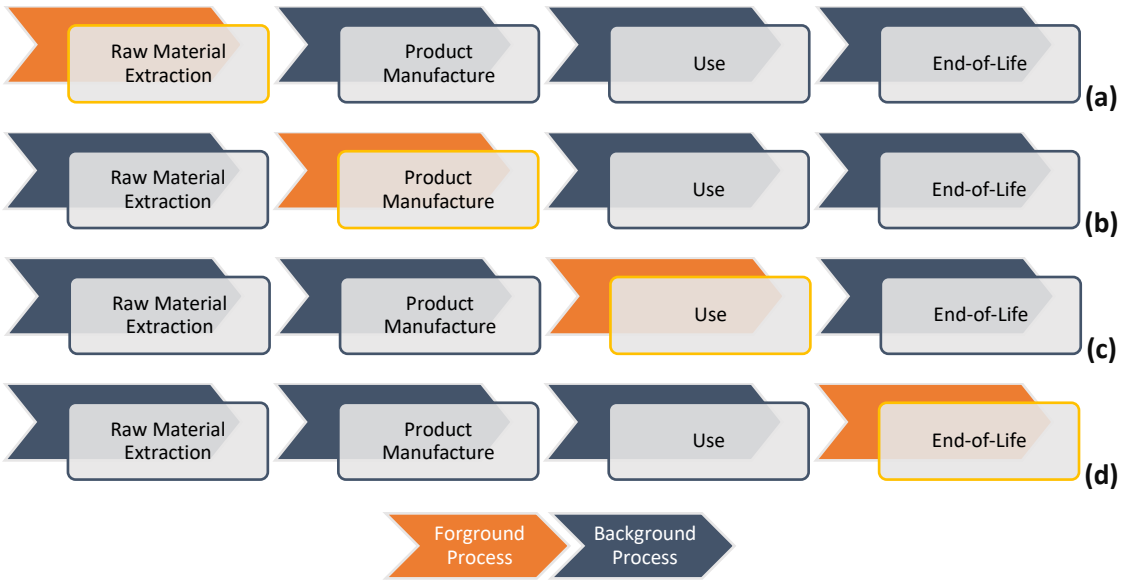

Figure 2-4 Illustration of foreground and background processes within a life-cycle inventory. Foreground processes are defined as the primary processes of concern and/or which the development of new and novel data is used to define those processes. Thus, foreground processes can represent any stage of the life-cycle assessment such as during (a) raw material extraction, (b) product manufacturing, (c) use and/or (d) end-of-life scenarios.

There are several widely available life-cycle inventory databases such Ecoinvent, GaBi (Thinkstep, Leinfelden-Echterdingen), the European Reference Life-Cycle Database (European Commission Joint Research Center) also known as ELCD, and the U.S. Life-Cycle Initiative database (U.S. National Renewable Energy Laboratory, Golden), among others. Ecoinvent and GaBi are perhaps the two most widely used

life-cycle inventory databases globally. While both are quite comprehensive in their amount and types of inventory data collected across a wide range of industrial sectors, business activities and technospheres, GaBi is distinct in that it utilizes inventory data collected from industrial sources. Although such data provides tremendous value and validation to the LCA process, much of this data is "rolled up" into aggregated system processes (i.e. a collection of so-called smaller unit processes) to protect sensitive industrial data and provide insulation to any one company from targeted scrutiny. Ecoinvent on the other hand contains a greater number of unit processes and thus greater resolution at the impact assessment stage, although much of its data come from non-industrially supplied sources. However, many of the Ecoinvent inventories relevant to PV systems such as semiconductor-grade level silicon, production of PV cells, did include non-aggregated, industry-specific data.[79] Since a majority of environmental impacts are heavily influenced by background processes, it is beneficial to have non-aggregated data for understanding the sources of potential hazards related to PV systems.[35]

Life-Cycle Impact Assessment

During the impact assessment step – the environmental and human health impact categories and methodologies are initially chosen in the goal and scope definition but then applied separately – inventory data are converted into potential impacts using their corresponding characterization (i.e. conversion) factors (CF) (equation (2-1)).

$$Impact\ Assessment\ Score = \frac{I_x \cdot CF_{x,i} \cdot W_i}{N_i} \qquad (2\text{-}1)$$

I_x: Inventory value for flow, x

CF_i: Characterization factor for inventory flow, x, and impact category, i

W_i: Weighting factor for impact category, i (optional)

N_i: Normalization value for impact category, i (optional)

The optional steps of normalization and weighting can be employed during the life-cycle impact assessment step. Weighting provides an approach expressing one's preference of concern for some impact categories over other. After weighting, normalization can be applied to harmonize impact category units so that each can be directly and relatively compared. External normalization involves dividing impact results by reference values, such as total global emissions. Internal normalization can be used when there are multiple alternatives fulfilling the same functional unit and division by the alternative with the greatest impact per impact category is used, for example.

There are a wide set of both environmental and human health impacts one can consider in an LCA. Often, these can be chosen from pre-defined impact assessment methodologies such as ReCiPe[80] (www.lcia-recipe.net), ILCD[81] (European Commission), TRACI (U.S. EPA), LC-Impact (www.lc-impact.eu), CML (University of Leiden), Cumulative Energy Demand (CED), or USEtox (www.usetox.org), among others (Table 2-1).

Table 2-1 Commonly applied life-cycle impact assessment methodologies and their commonly defined midpoint impact categories. (Adapted from Acero et al.[82])

Methods	Acid-ification	Climate change	Cumulative Energy Demand‡	Resource depletion	Ecotoxicity	Eutro-phication	Human toxicity	Ionising Radiation	Land use	Odour	Ozone layer depletion	Particulate matter	Photo-chemical oxidation	Water Use†
CML, 2001 (Baseline)	●	●	○	●	●	●	●	○	○	○	●	○	●	○
CML, 2001 (Non-Baseline)	●	●	○	●	●	●	●	●	●	●	●	○	●	○
Ecoinvent	○	○	●	○	○	○	○	○	○	○	○	○	○	○
Eco-Indicator 99	●	●	○	●	●	●	●	●	●	●	●	○	●	○
Eco-Scarcity 2006	○	○	○	●	○	○	○	○	○	○	○	○	○	●
EDIP 2003	●	●	○	○	●	●	●	○	○	○	●	○	●	○
ILCD 2011 (Midpoint)	●	●	○	●	●	●	●	●	●	○	●	●	●	●
IMPACT World+	●	●	○	●	●	●	●	○	●	○	●	●	●	●
LIME	●	○	○	●	●	●	●	○	●	○	●	●	●	●
ReCiPe	●	●	○	●	●	●	●	●	●	○	●	●	●	●
TRACI 2.1	●	●	○	●	●	●	●	○	○	○	●	●	●	○
USEtox	○	○	○	○	●	○	●	○	○	○	○	○	○	○

‡Cumulative energy demand is not an impact category in the strict definition of the term, and instead it represents an approach for calculating an energy based inventory, and it is often reported by life-cycle assessment studies as a proxy-impact indicator.

†Water use methods vary between inventory-based calculations, akin to cumulative energy demand, but can also represent actual impacts estimated across the cause and effect chain.

These life-cycle impact assessment methods differ on the types of impact categories included, the spatial representativeness of the methods, and their modeling choices, among other things. Although Table 2-1 is not a comprehensive account of all possible impact categories, it is representative of 14 very common environmental and human health criteria. Some of these impacts, for instance, represent multiple impact categories such as ecotoxicity which can be sub-divided into freshwater or marine water ecotoxicity. Other impact categories which are nevertheless important, such as impacts from noise pollution, are not commonly included in these methods, lack formal reporting within life-cycle inventory databases and are, thus, not included in the Table 2-1.[83] The majority of the life-cycle impact assessment methodologies are specific for European conditions and impacts. These include CML, Eco-indicator99, EDIP, ILCD and ReCiPe. TRACI was developed specifically for estimating the impacts within North America, while LIME was originally developed for the Japan but has since expanded its focus. Other impact methodologies such as Eco-Scarcity, Ecoinvent and USEtox focus on resource depletion, CED and toxicity, respectively. USEtox, in particular, is a consensus model focused on estimating freshwater ecotoxicity as well as non-cancerous and cancerous human health toxicity.[84] It was developed from authors of formerly and widely used environmental impact models such as CalTOX,[85] IMPACT 2002,[86] BETR,[87] EDIP,[88] WATSON,[89] USES-LCA[90] and EcoSense.[91]

Inventory flows must be classified into specific impact categories. Inventory flows might contribute to more than one impact category (i.e. one compound might influence two separate types of environmental impacts). Thus, formal decisions must be made regarding how to partition the inventory flows, which will in turn affect how the final environmental and human health impacts. Impact assessment modeling can be divided into midpoint- or endpoint-modeling (Figure 2-5).

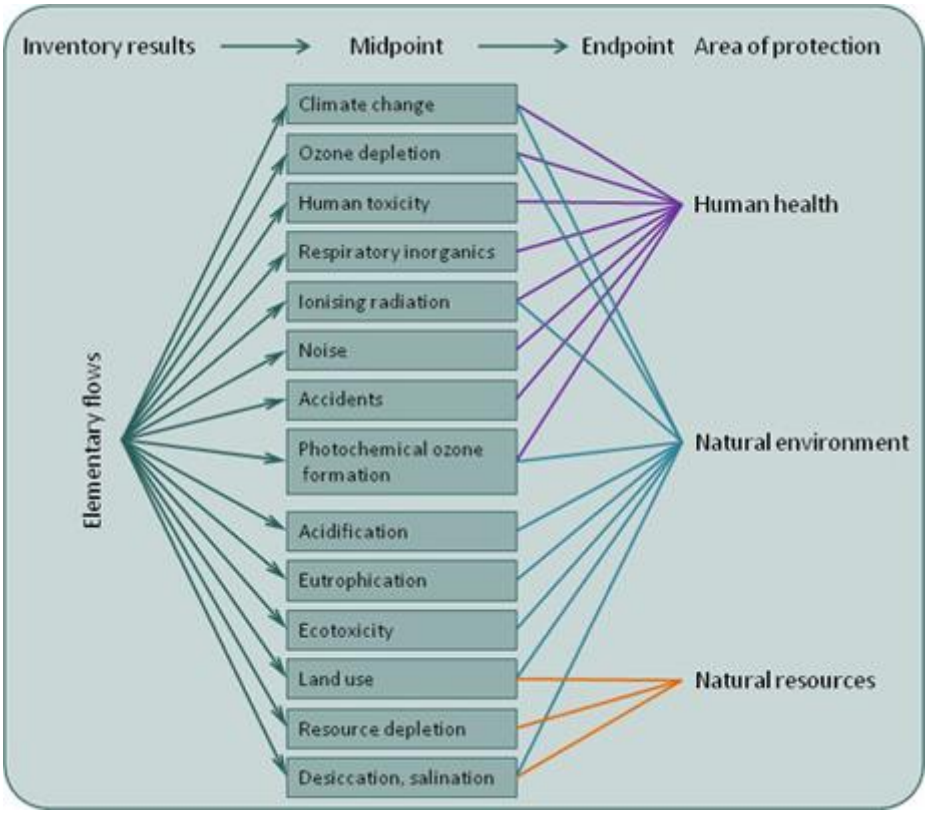

Figure 2-5 A general cause and effect chain considered in life-cycle impact assessment methodologies, following the classification of inventory items into their respective midpoint and/or endpoint levels of impact and converted to impact values using each categories' substance-specific characterization factor. (Source: European Commission Joint Research Centre)

Midpoint impact assessment models consider the "relative" potency of an inventory flow somewhere in the middle of the cause and effect chain, while endpoint-models estimate levels of "damage" all the way through the cause and effect chain to what are known as "areas of protection." In other words, the midpoint can be thought of as an environmental mechanism of action while the endpoint is the ultimate effect. Midpoint impact assessment methods, thus, utilize fewer assumptions and have less uncertainty in their results, while endpoint-modelling has greater uncertainty but more comprehensiveness. Endpoint modeling also facilitates the decision-making processes because it reduces the LCA results into fewer, more manageable categories.

The midpoint indicators used in this thesis were derived mostly from the ReCiPe methodology but supplemented with USEtox for the human health and ecotoxicity impacts as well as the methods for CED outlined by Ecoinvent (Table 2-2).

Table 2-2 Life-cycle impact assessment categories considered in this study. ReCiPe 2008 midpoint (H) impact categories were used, with toxicity estimated using the midpoint USEtox 2.0 indicators and cumulative energy demand estimated based on Hischier et al.[92]

Recipe Impact Category	Abbreviation	Unit
Climate change potential	(CC)	kg (CO_2-equivalents to air)
Ozone depletion	(OD)	kg (CFC-115-equivalents to air)
Terrestrial acidification	(TA)	kg (SO_2-equivalents to air)
Freshwater eutrophication	(FE)	kg (P-equivalents to freshwater)
Marine eutrophication	(ME)	kg (N-equivalents to freshwater)
Human toxicity	(HT)	CTU_h
Photochemical oxidant formation	(POF)	kg (NMVOC6-equivalents to air)
Particulate matter formation	(PMF)	kg (PM_{10}-equivalents to air)
Freshwater ecotoxicity	(FET)	CTU_e
Ionizing radiation	(IR)	kg (U_{235} to air)
Agricultural land occupation	(ALO)	$m^2 \cdot yr$ (agricultural land)
Urban land occupation	(ULO)	$m^2 \cdot yr$ (urban land)
Natural land transformation	(NLT)	m^2 (natural land)
Water depletion†	(WD)	m^3 (water)
Mineral resource depletion	(MRD)	kg (Fe)
Fossil fuel depletion	(FD)	kg (oil)
Cumulative energy demand‡	(CED)	MJ

CFC: chlorofluorocarbon | P: phosphorus | N: nitrogen | NMVOC: non-methane volatile organic carbon compound | U: uranium.
‡Cumulative energy demand is not an impact category in the strict definition of the term, and instead it represents an approach for calculating an energy based inventory, and it is often reported by life-cycle assessment studies as a proxy-impact indicator.
†Water use methods vary between inventory-based calculations, akin to cumulative energy demand, but can also represent actual impacts estimated across the cause and effect chain.

ReCiPe was chosen as the foundation due its focus on European impact modeling as well as it being a more recent update and successor of other European methods such as CML and Eco-Indicator99. While the 2011 ILCD Handbook[81] is a more recent recommendation for conducting European-based life-cycle impact assessments, previous OPV-LCA literature have not used these recommendations and instead have used methods such as CML and ReCiPe. Thus, for consistency it was decided to use ReCiPe as a basis for the impact assessment methodology. The decision to employ USEtox, which does happen to be an ILCD recommended method, was motivated by the problems addressed in Chapter 5-Chapter 7 regarding

compatibility of impact assessment methodologies with emerging technologies and to create consistency with the previous work in this area that had already considered USEtox in their methodological approaches.[93–97]

A brief description of the midpoint impact indicators used in this thesis are included in the following sub-sections. Their descriptions are by no means exhaustive and serve only to provide sufficient information for understanding the fundamental implications of the results reported in this thesis. Additionally, it should be noted that ReCiPe adapts three different impact assessment "perspectives" that represent three different modeling choices and decision makers' perspectives: individualist (*I*), hierarchist (*H*) and egalitarian (*E*).[98] These perspectives only influence a portion of the total impact categories and differ mainly by their time-frames over which environmental and human health impacts to occur. Perspective *I* can be thought of as an optimistic model, Perspective *E* a precautionary model and Perspective *H* as the average model.

Climate Change Potential (Global Warming Potential)

The effects of climate change are in large part driven by the amounts of greenhouse gases contained in the Earth's atmosphere, such as carbon dioxide, methane, nitrous oxide and fluorinated gases. These gases, whose concentrations are growing due to human induced activities, have the capacity to trap and retain heat, raising near-surface temperatures of the planet.[99] Each gas has a different radiative forcing value and lifetime in the lower atmosphere (e.g. troposphere), meaning each has a distinct and relative "strength" for influencing climate change.[100] CO_2 is considered the standard reference greenhouse gas to which all other substances are given CO_2-equivalent values. These CO_2-equivalent values represent the midpoint CF, while endpoint CF consider the relative temperature increase as well as the specific effect on the areas of protection due to that increase (e.g. extinction of species).[101]

Ozone Layer Depletion

The ozone layer is defined as a portion of the stratosphere that contains an essential layer of ozone molecules (i.e. O_3) that is effective at absorbing and thus blocking incoming radiation from the sun. Some of this radiation, such as ultra-violet B or UVB, is known to have both negative human health and environmental consequences such as contributing to skin cancer. By the 1970s it was identified that many man-made substances such as chlorofluorocarbons can react and deplete the ozone layer.[102] Similar to the effects of climate change with greenhouse gases, ozone depleting substances have different, relevant

strengths and lifetimes in the atmosphere. One of these substances CFC_{11}, a refrigerant, is used as the standard reference ozone depleting substance to which all others are defined by their CFC_{11}-equivalent values. These values represent the midpoint CF, while endpoint CF are concerned with estimating the amount of increased radiation that results from the release of these substances and the corresponding influence on certain types of skin cancers as a result.[101]

Photochemical Oxidation Formation (Smog) Potential

Like climate change potential, photochemical oxidation potential concerns itself with releases of pollutants in the lower troposphere that form photo-oxidants. Photo-oxidants form when nitrogen oxides (NO_x) react with hydrocarbons in the presence of sunlight.[103] This reaction leads to the creation of "ground-level" ozone, as opposed to stratospheric ozone that comprises the protective ozone layer. Ground level ozone can be dangerous to humans, causing various adverse pulmonary effects.[104] It can also have adverse impacts on terrestrial species, resulting in the loss of vegetation and plant life.[105] Midpoint CF are expressed as equivalents of non-methane volatile organic compounds (NMVOC-equivalents), expressing the marginal change in ground-level ozone per emission of a substance, x.[101] Endpoint CF are further defined by their level of exposure either by humans or terrestrial systems (e.g. plants) and their corresponding adverse effects per kg of ozone uptake.[101]

Resource (Minerals) Depletion

This impact category represents multiple types of resources, often categorized by minerals and fossil fuels. At the midpoint level, resource depletion represents the quantity of resources used in comparison to their known quantity of obtainable reserves existing in nature. These midpoints are reported in terms of kg of iron-equivalents (kg Fe-eq.) and kg of oil-equivalents (kg Oil-eq.) for mineral and fossil fuel depletion, respectively.[101] At the endpoint level, resource depletion includes the consideration of decreasing ore grades as a function of depletion and is reported in terms of monetary costs (e.g. USD) per mass of extracted resource.[101]

Land Use, Land Occupation and Land Transformation

Specific types of activities (e.g. mining) and structures (e.g. warehouses) require land either through which they directly use as a raw material or as a place to physically occupy. At the midpoint level, the impacts of land use are defined by the area (e.g. m^2) of physical land occupied or transformed as well as the timeframe (e.g. years) for these activities.[101] The endpoint impact may be defined by species-land

relationships whereby an increase in the area of available natural land, or a decrease in time of occupied/transformed land, implies an increase in the number of vegetative-species present in that same space.[101] Furthermore, the time of restoration is assumed to be linearly linked to the overall impact. Of course, this approach implies that the impacts of land use will be heavily dependent on the geographical location, considering that default species abundances and resiliency of the land to restore itself will be closely linked to the type of "natural" landscape present in a region.

Energy Use (Cumulative Energy Demand)

Although energy use is not a true impact category,[106] the concept of CED is important to energy related systems because it facilitates the calculation of how much time it will take for a device, during its use, to generate the energy that was consumed during the production of that same device (i.e. EPBT). The CED quantifies all the directly consumed energy across the entire life-cycle of a system as well as the indirect, embodied energy of materials consumed, created and discarded along the way. So far, there is no standardized approach for quantifying the CED in life-cycle impact assessment methodologies. The approach most commonly used in life-cycle impact assessment methods is the Ecoinvent approach that applies the upper heating value (e.g. MJ-energy per kg-material) for estimating the indirect energy consumed in a system. Other sources of non-combustible energy such as nuclear, hydro, wind and solar power are also included in the calculation and can be reported with or without the non-renewable sources of energy.

Water Depletion

The reporting of a water-based impact category has not been fully harmonized in impact assessment methodologies either. Some methods may report water use impacts similar to resource depletion impacts in terms of an overall summation of water use, potentially comparing it with known obtainable amounts for that resource. However, this is largely an inventory based statistic, similar to CED, and does not estimate any particular impact from water use specifically. Such values are typical of midpoint water use impact categories and are reported as m^3 of water used.[101]

Acidification

There are a number of pollutants that have the capacity to increase the number of hydrogen (H^+) ions in the environment, including sulfur dioxide, nitrous oxides, hydrogen chloride and ammonia, for example.[107] The release or formation of H^+ can decrease the pH in both soil and water systems. Such changes can

cause imbalances in local ecosystems and ultimately result in the loss of species.[107] The fate and transport of these pollutants are defined by their behavior in the atmosphere as well as their behavior in the soil using steady-state and dynamic models, respectively. The midpoint CF are defined in equivalents of sulfur dioxide (SO_2-equivalents) and represent the ratio of the fate for substance, x, with the fate of SO_2.[101] Endpoint CF are defined by for a potentially disappeared fraction of plant species impacted by the change in pH of the media.[101]

Eutrophication

Eutrophication is a phenomenon that occurs in fresh and marine water systems whereby an excess of nutrients, namely phosphorous and nitrogen, can cause unfavorable ecological conditions for living organisms. Specifically, excess phosphorous and nitrogen can promote the exponential growth of algae and other organisms.[108] In the long run, if growth is excessive, it can result in low oxygen conditions in the water, due to interference with photosynthesis-cycles of sub-surface plant life and the aerobic breakdown of the algae by bacteria. The lack of oxygen can ultimately cause stress and death in certain organisms within the hypoxic zones.[108] The midpoints for eutrophication are defined in terms of phosphorous- (P-equivalents) and nitrogen-equivalent (N-equivalents) mass emissions for freshwater and marine water environments, respectively.[101] Eutrophication endpoints are defined by a linear effect factor describing the number of disappeared species based on the change in phosphorous- or nitrogen-equivalent emissions in the environment.[101]

Ionizing Radiation

The effects of radioactive isotopes may occur if humans encounter these substances either by directly working with them or after they are released into the environment. Although *naturally* occurring radioactive isotopes are the most abundant form of these substances, anthropogenic sources contribute to these levels through combustion of coal, production of nuclear fuel and use of military weapons, for example.[109] When these substances decay they release high amounts of ionizing radiation that can induce alterations in one's DNA and other organ systems.[110] The midpoint CF is defined by the internally absorbed dose, expressed using the mass of U_{235}-equivalents and interpreted from the commonly applied unit Sievert (Sv), while the endpoint takes into consideration the incidence and severity of corresponding diseases (e.g. cancer) for this amount of internal dose.[101]

Particulate Matter Formation

In ReCiPe, particulate matter is defined as substances with diameters less than 10 μm (PM_{10}). This type of particulate matter can form from emissions of sulfur dioxide, ammonia and nitrogen oxides, for example.[111] Particulate matter is specifically important for human health impacts, where they are associated with pulmonary diseases such as inflammation and/or cancer.[111] The fate of and exposure to particulate matter is calculated using steady-state models, while the resulting intake fraction is estimated directly from the number of persons exposed and their respective breathing rates.[101] The midpoint CF is then expressed in equivalents of the intake for PM_{10} (PM_{10}-equivalents).[101] Endpoint CF are then defined based on the corresponding effect at that particular exposure dose, estimated from a corresponding dose-response relationship.[101]

Ecotoxicity

The life-cycle impact assessment methodology embodied by USEtox considers the potential eco-toxicological impacts that result from the exposure to organic chemicals and certain non-organic metals in freshwater. USEtox is a consensus model that came out of the Life-Cycle Initiative jointly partnered by the United National Environment Programme (UNEP) and the Society for Environmental Toxicology and Chemistry (SETAC). The goal of the initiative was to produce recommended ecotoxicity (and human health) CF for LCA. Multi-compartmental models are used to trace the fate and transport of a chemical from the source of its emission in one medium to the final concentration of another medium. Steady-state, equilibrium models are employed, largely dependent on partition (equilibrium) coefficients for characterizing these behaviors.[84] Exposure is estimated using steady-state bioaccumulation models using the same types of partition coefficients mentioned above.[84] This estimated level of exposure (e.g. bioavailable mass) is then combined with an estimation of the concentration at which 50% of the population has the observed impact, referred to as the effective concentration at 50% (EC50).[84] The EC50 value is calculated from *in vivo* toxicological studies for at least three different species/trophic levels.[84] The midpoint impact is defined here as a non-reference unit expressed as the comparative toxic unit for ecosystems (CTU_e).[84] The endpoint may be combined with a damage factor that estimates the number of potentially disappeared fraction of species.

Human Toxicity

The life-cycle impact assessment methodology embodied by USEtox considers the potential human health impacts that result from the exposure to organic chemicals and certain non-organic metals. Multi-

compartmental models are used to trace the fate and transport of a chemical from the source of its emission in one medium to the final concentration of another medium. Steady-state, equilibrium models are employed, largely dependent on partition (equilibrium) coefficients for characterizing these behaviors (equation (2-2)).[84]

$$CF_{i,j} = FF_i \cdot XF_i \cdot EF_{i,j} = (iF_i) \cdot EF_{i,j} \qquad (2\text{-}2)$$

FF_i: fate factor (days) for substance i

XF_i: exposure factor ($days^{-1}$) for substance i

iF_i: intake fraction for substance i

EF_i: effect factor (cases/kg) for substance i and pathology j

The FF represents the various transformation and removal mechanisms from one compartment to another and is reported in days. Exposure is limited to inhalation and ingestion, without consideration of dermal exposure and is expressed as the XF in units of 1/days. It is assessed on a population-based level as opposed to an individual level, the latter being more conventional for HHRA methods. The results of the fate and exposure calculations provide a lifetime intake fraction (iF), which is defined as the ingested or inhaled amount per mass of emitted substance. This intake fraction is then combined with an estimation of the human-equivalent dose at which 50% of the population has the observed impact. This is referred to as the effective dose at 50% (ED50) and represented as the EF with units of cases of cancerous or non-cancerous disease per kg of emitted substance.[84] This dose is generally quantified using *in vivo*, animal dose-response toxicological data at which 50% of the test subjects gave a response. Both carcinogenic and non-carcinogenic doses may be defined depending. Midpoint impacts are expressed in non-equivalent unit defined as the comparative toxic unit for humans (CTU_h).[84] Endpoints may be presented in terms of the disability-adjusted life years (DALY), where one DALY is defined as one year of lost life (YLL) due to mortality and/or due to disease and disabilities (YLD).[112]

Interpretation

The interpretation stage is a process that is involved along each of the three other steps of the LCA (i.e. the goal/scope definition, the life-cycle inventory analysis and the life-cycle impact assessment). LCA is commonly described as an iterative process, one in which the development of the objective, methods and result calculations are repeated and refined based on the previous set of outcomes. Interpretation should be used to (a) understand and make the logical connections between the life-cycle impact assessment

results, life-cycle inventory and the goal/scope definition, but also to (b) identify anomalies and errors that may present themselves in each of these LCA steps. Because LCA is involved with copious amounts of data, it is often best to use systematic approaches to the interpretation phase such as (i) contribution analysis (i.e. analyzing each impact category per life-cycle stage, unit-process and/or elemental flow), (ii) uncertainty analysis (e.g. defining the inventory data with distributions based on their inherent uncertainty and variability as opposed to deterministic values), and (iii) sensitivity analysis (e.g. modifying the life-cycle inventory to reflect specific technology decisions at the early development and design stages).[78]

It should be noted that inventory items and their resulting impacts are aggregated over time and broad environmental landscapes/compartments. Consequently, LCA results do not communicate absolute values, as briefly mentioned in Chapter 1. Thus, the environmental impact results of an LCA derived for one product are best utilized when they are compared to the impacts of another product instead of being used to measure its definitive, absolute impact on human health or the environment, as is done in HHRA or ERA. Both HHRA and ERA will be presented in greater detail in Chapter 5 and Chapter 6.

Chapter 3 Cradle-to-Gate Life-Cycle Assessment of Organic Photovoltaics

From a material and device structure perspective, there are a variety of OPV that have been studied using LCA (Chapter 1). While there are some general consistencies across the devices such as the use of a PCBM:P3HT active layer, there are some noticeable differences in such choices as the electrodes, for example. The results of those studies identified hot-spots that could be addressed for improving the environmental performance of OPV devices. Additionally, there were points raised about technical and functional aspects of material choices that should be addressed such as the assumptions regarding their lifetimes as well as their efficiencies. Furthermore, only three of the ten previous OPV-LCA studies looked beyond CED or greenhouse gas accounting. Of those that did, only one study compared those impact categories to conventional silicon PV. Illustrating the differences between OPV and silicon PV across a greater range of LCA impact categories, can help provide meaningful motivation for the development of this technology. Therefore, the objective of this chapter is to define a near-term, prospective OPV life-cycle inventory based on the recommendations and lessons from the review in Chapter 1 and complete a life-cycle impact assessment comparing OPV and silicon-based PV across a comprehensive set of LCA impact categories.

Organic Photovoltaic Device Structure and Material Choices in this Thesis

As was discussed in Chapter 1, all the previously reviewed LCA literature was completed on devices that exploit the functionality of ENM such as C_{60}-fullerenes and their derivatives. C_{60}-fullerenes have garnered the most interest in OPV research as an organic “n-type” (i.e. electron acceptor) semiconductor because of its strong electronegativity and high electron mobility. Specifically, the fullerene derivative PCBM is widely employed, often in conjunction with the common “p-type” (i.e. electron donor) polymer P3HT.[43,52–54] During charge separation in the active layer, there is the creation of both a negative and positive charge carrier, the latter referred to as a “hole” or absence of an electron in an atom. Current is created when the negative charge is allowed to move through the PCBM and through to the (back) cathode while the holes simultaneously propagate through the P3HT and on to the transparent anode.[48]

Substrates of early OPV devices were originally rigid structures such as glass, however it has become common and technologically feasible to print the components of an OPV cell directly onto a flexible substrate.[25,43] The substrate used in this work was polyethylene terephthalate (PET), which has proved to

be an effective material particularly for large-volume roll-to-roll printing of OPV panels.[43] Immediately adjacent to the substrate is the transparent (front) anode layer (Figure 3-1), towards which the positive charge carriers (i.e. holes) travel.

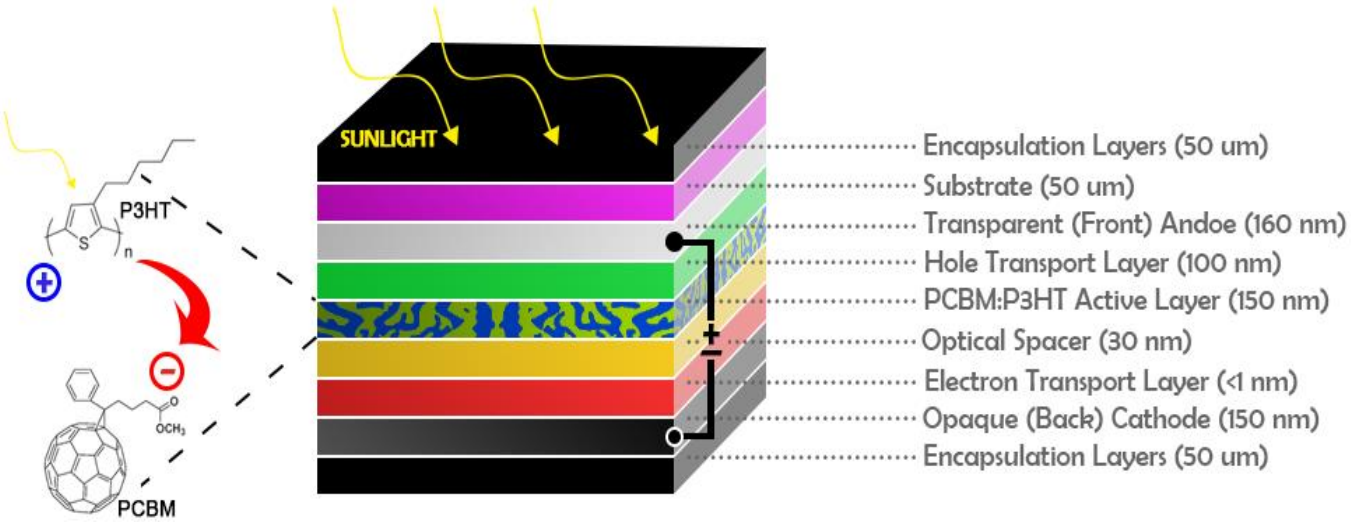

Figure 3-1 General depiction of the bulk heterojunction organic photovoltaic cell considered in this chapter, incorporating (the skeletal formulas of) (a) phenyl-C_{61}-butyric acid methyl ester (PCBM) which acts as the electron acceptor and (b) poly(3-hexylthiphene) (P3HT) which acts as the electron donor in the active layer.

Commonly used transparent anodes are ITO, given its high level of optical transparency and electrical conductivity.[44] However, due to cost, scarcity and to a lesser extent toxicity,[45–47] fluorine doped tin oxide (FTO) was used. FTO was a suitable replacement due to favorable qualities such as high availability, lower market prices and relative effectiveness as a transparent conductive oxide compared to ITO.[44,113,114] FTO also has the potential to be printed[47] onto a flexible substrate.[115] While these assumptions were made in this work, this has yet to be effectively proven on a roll-to-roll basis using a plastic substrate.

As previously stated, the active layer of OPV cells consists of organic donor and acceptor materials. The bulk heterojunction is an interlacing morphology of donor:acceptor materials which maximizes the opportunity for charge separation. To avoid recombination of the mobile charge carriers at the active layer and increase efficiency, OPV cells are often given a hole-transport layer and an electron transport layer. PEDOT:PSS is a common hole transport layer used in OPV cells, but this material has been shown to have low stability in ambient conditions.[116,117] Instead, MoO_3 was chosen as the hole transport layer due to good stability, non-interference with the active layer's light absorption profile (i.e. no interference with

the 350-700 nm light absorption profile of the active layer) and compatibility with solution-based deposition and processing.[118]

An additional layer of nano-TiO_2 was modeled in-between the active layer and the cathode to increase absorption of light. In many cases, the reflection of light off the (back) cathode redirects light towards the active layer for a second pass, and depending on the thickness of the overall cell, this can interfere with absorption. This is particularly true when the thickness of the active layer is on the tens-of-nanometers.[119,120] Optical spacers can avoid this problem and increase the spectrum of absorbed light (Figure 3-2).

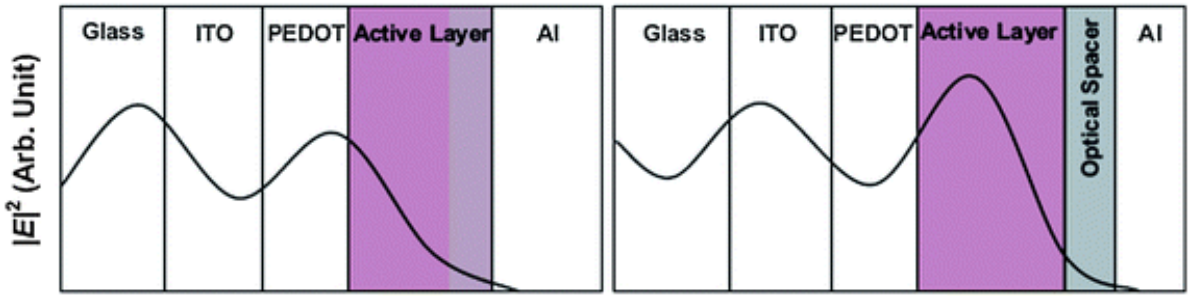

Figure 3-2 Generic schematic of the field strength of light at the active layer for an OPV device without an optical spacer (left) and with an optical spacer (right). (Source: Kim et al.[121])

The optical spacer has the added benefit of acting as a hole-blocking layer and electron transport layer.[122] Even so, a lithium fluoride layer was modeled for increasing the efficiency and mobility of negative charge carriers to the (back) cathode.[123,124] Besides being an effective electron transport layer, lithium fluoride can also protect against pinhole damage during roll-to-roll processes, which leads to shorts and degradation of the device. [123]

Lastly, a low work function (back) cathode is important for collecting the negative charge carriers.[125] A layer of aluminum was modeled as the cathode. Low work function metals can be relatively reactive, leading to potential oxidation and degradation of the device. [125] Thus, to inhibit these problems, the OPV was modeled with additional lamination layers (i.e. encapsulation and barrier layers).

Life-Cycle Assessment Methods

Goal and Scope Definition

The work in this chapter followed ISO 14040:2006 and 14044:2006 guidelines for conducting a LCA study and the recommendations of the IEA's 2011 guidelines and best practices for implementing an LCA for PV.[27,28,35] A cradle-to-gate LCA on the production of OPV cells in comparison to conventional technologies such as silicon is presented in this chapter. This work aims to define a baseline understanding of the life-cycle inventory and corresponding environmental and human health impacts for a prospective device with the most potential for real-world applications but also reduced environmental impacts.[45]

The life-cycle inventory is built for the production of a *default* OPV cell produced as a bulk heterojunction cell of PCBM:P3HT as the active layer. The functional unit considered was one Wp. The OPV cell was assumed to require 200 cm² of surface area per Wp power produced at a module efficiency of 5%.[29] Efficiencies in the range of 2-3% were historically reported for lab-based PCBM-based cells without much improvement.[30,38,63] However, a large-scale deployment of OPV cells on land have already reported efficiencies near 2%.[24] Moreover, lab-scale efficiencies as high as 15% (Figure 1-2) have been reported in the literature for PCBM-based devices similar to what will be considered in this thesis.[126] Generally, as PV technologies mature, their lab-to-industrial scale efficiencies might decrease from 20%-50%.[127] Thus, the efficiency assumption in this work represents an optimistic yet realistic near-term objective.

The OPV cells were subsequently compared with conventional m-Si and a-Si PV. For each technology option, environmental flows were tracked across raw material extraction, material processing, manufacture, and transportation requirements for each solar cell design. Figure 3-3 depicts these life-cycle stages for the OPV cell.

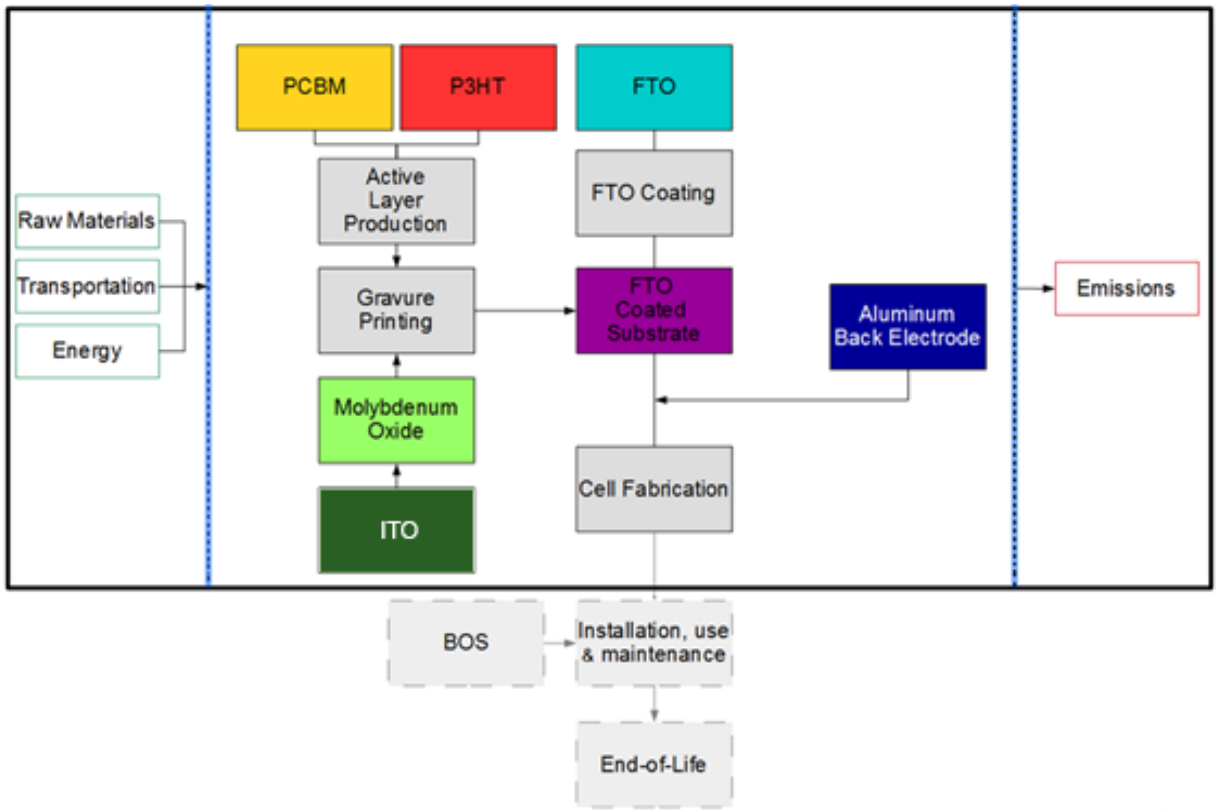

Figure 3-3 System boundaries of the cradle-to-gate life-cycle assessment illustrating the main components for the production of a prospective organic photovoltaic panel. All relevant processes, materials, and waste-streams up to the production of the solar cell are considered, thus excluding any consideration of the use-phase or end-of-life considerations.

Because the use phase was not considered in this LCA, the lifetime of the modules and any additional accessory components such as mounts, cables and invertors that PV panels may be required were not considered.[35] Additionally, capital equipment were also excluded from the assessment as such impacts are often negligible when considering the entire life-cycle and life-time of a product.[78] OPV are not currently manufactured on an industrial scale, therefore the foreground inventory data (Chapter 2) developed for this LCA represented a mixture of lab and pilot scale processes,[29–31,37,39,42,44,57,128] patents, other professional materials,[129–131] stoichiometric calculations, and/or expert judgment. Background inventory data were taken from the Ecoinvent v.2.2 attributional inventory,[132] including an average European electricity mix and transportation processes. An attributional inventory was chosen to determine baseline environmental and human health impacts of OPV, as opposed to assessing the consequential impacts that arise from changes in the PV market and energy market due to OPV production and use, which are currently unknown. Therefore, where it was applicable, co-products were allocated.

Mass allocation, as opposed to economic allocation, was generally applied given that the industrial-scale, price information on specialty chemicals and substances was not available. All transportation requirements for incoming foreground chemicals and materials were taken into account using 100 km truck and 600 km rail transport, while outbound waste materials were estimated using ten km truck transport.[132] The LCA was conducted in OpenLCA v1.4 (GreenDelta, Berlin). The life-cycle impact categories (Table 2-2) were chosen as ReCiPe[80] v1.0.5 midpoint (*H*) impact categories with the substitution of USEtox 2.0 for the human health and freshwater ecotoxicity indicators as well as the addition of the CED.[92] A detailed account of the foreground inventory data collected and calculated in this chapter are explained in greater detail in Appendix: Chapter 3.

Life Cycle Inventory

Substrate

To produce one m² OPV panel, 0.074 kg of PET was used.[29] PET substrate production was modeled using the Ecoinvent process for "extrusion, plastic film" using the input "polyethylene terephthalate, granulate, amorphous, at plant" as the substrate source material.

Transparent (Front) Anode

The FTO anode was modeled as a solution produced from tin tetrachloride pentahydrate, ammonium fluoride, ethanol and water and heated to 60°C.[47,133] It was assumed that the only energy consuming step was for raising the temperature of water and ethanol from room temperature. The materials and energy to produce tin tetrachloride pentahydrate were based on stoichiometric calculations.[131] Wastes generated from these processes were not estimated. The amount of FTO solution applied was 0.042 liters per m² and was calculated as an average of the values reported for ITO in Garcia-Valverde et al.[30] and Roes et al.[29] FTO deposition in the *default* OPV cell was modeled via sputtering in a roll-to-roll process.

Hole Transporter

MoO_3 was modeled as the hole transport layer.[116,117] Oxides of molybdenum do not occur in large amounts in nature, but rather as sulfides (e.g. molybdenite). Production of MoO_3 was modeled by roasting molybdenite at high temperatures in the presence of oxygen.[134] The amount of MoO_3 was estimated as 0.24g per m^2 of OPV.[30,31,128] Deposition of MoO_3 was modeled via gravure printing in a roll-to-roll process as has been demonstrated for PEDOT:PSS.[43,135,136]

Active Layer

The active layer consisted of a bulk heterojunction of PCBM and P3HT. PCBM can be produced in different ways including plasma and pyrolysis techniques.[57] Although plasma techniques can produce a more discrete distribution of C_{60}-fullerenes, this technique also produces smaller quantities of C_{60}-fullerenes, while pyrolysis can produce large quantities of various sized C_{60}-fullerenes.[128] PCBM production was modeled via the pyrolysis technique using toluene as a feedstock.[57] P3HT is a region-regular polymer derived from 3-bromothiophene and bromohexane.[30] Data for bromothiophene production was taken from the inventory presented in Garcia-Valverde et al., [30] while thiophene production was calculated based on stoichiometric calculations.[130] The energy input for annealing the active layer was estimated from Espinosa et al.[38] as 5.07 MJ per m^2 and includes the energy for drying the electron transport and hole transport layers. Per m^2 of OPV, 0.21 g of PCBM and 0.235 g of P3HT were required.[30,31,128] Additionally, a 30 nm (0.13 g per m^2 of panel) optical spacer composed of nano-TiO_2 particles was modeled on the back-side of the active layer.[120,121,137,138] Deposition of P3HT:PCBM plus the optical spacer was modeled via gravure printing in a roll-to-roll process[135,136] using chlorobenzene as the solvent.[30]

Cathode

Per m^2 of OPV, 0.3 g of aluminum was modeled for the (back) cathode.[29,42] A layer of lithium fluoride was deposited along with aluminum to act as an electron transport layer.[29] Deposition of both layers was modeled via gravure printing.[11]

Encapsulation and Lamination

Framing of the polymer solar cell is not considered in this inventory. Instead, several additional barrier layers were modeled. Per m^2 of OPV, 133 g PET, 0.44 g silica (SiO_2), 0.99 g of an epoxy-silica ENM-composite, and 9.25 g of an epoxy resin was used per the description in Roes et al.[29] Deposition of all layers was modeled as gravure printing.[11]

Sensitivity Analysis

Alternative production and manufacturing options were assessed and compared with the *default* OPV production route as described above. The first alternative, labeled FTOinkjet, involved a change in the deposition method of the transparent electrode (i.e. FTO), using inkjet printing in place of sputtering.[44] Samad et al.[47] demonstrate the application of FTO solutions onto glass substrates using inkjet printing. As a prospective analysis, the approach presented by Samad et al. was assumed to be compatible with

printing onto a flexible PET substrate and roll-to-roll compatible.[139] Electricity usage for inkjet printing was estimated as 21.3 kJ per m² substrate.[29] The second alternative, labeled PCBMdcb, was based on changes to the solvent used during PCBM manufacturing. Anctil et al. previously identified PCBM as a notable contributor to the total CED of OPV panel production.[57] PCBM requires large amounts of solvent, particularly toluene, during production.[57] Instead, another common industrial solvent, dichlorobenzene, was substituted for toluene as the solvent in PCBM production.

Additionally, a second OPV technology (OPV-PP) was considered as an all-polymer (i.e. polymer accepter-polymer donor) panel.[140] C_{60}-fullerenes can represent nearly a quarter of an OPV's total material and production cost. They also require relatively large amounts of energy input for production, processing steps and purification to achieve electronic grade materials. Thus, some developments of alternative OPV devices such as those that utilize non-fullerene acceptors in the active layer are currently being researched and developed. The company Polyera reported a laboratory-based record of 6.4% with such an all polymer cell. Although, their materials are proprietary, these records have been verified by the National Renewable Energy Laboratory (NREL).[141] Others have demonstrated advancements upwards of 7% and 10% efficiency by using small molecule acceptors and non-bulk-heterojunction active layers.[142–144] However, average efficiencies for these devices are still low (i.e. circa 2%) and particularly lower than fullerene-based cells.[140] That being said, the effectiveness of this technology seems probable and the adaptation of existing PCBM:P3HT production routes to accommodate an all polymer active layer is extremely feasible. Thus, an additional consideration in this work was to evaluate the environmental impacts to produce an all polymer active layer. The alternative tested in this study exchanged PCBM with a *n-type* polymer. The inventory for the *n-type* polymer was based on the P3HT polymer as a proxy. For the sake of demonstration, an OPV-PP panel was modeled with the same 5% efficiency as the OPV-D panel outlined above and an identical geometry apart from the polymer substitution in place of PCBM.

Comparison to Conventional Silicon-Based Photovoltaics

The OPV devices described above were further compared to two conventional silicon-based PV: m-Si and a-Si. m-Si technology has the largest share of global PV production at 70% of the market.[16] a-Si is 2nd-generation thin film technology that once has nearly 10% market share in early 2000 but has since receded due to the influence of other 2nd-generation technologies such as cadmium-telluride and copper-indium-gallium-selenium PV.[16] The inventories for the silicon modules were taken from Ecoinvent 2.2.[132] To appropriately compare the silicon-based PV to OPV, the silicon inventories excluded glass encapsulation.

The m-Si cell was assumed to require 75 cm² of surface area per Wp power with an efficiency of 13.2%, and the a-Si cell was assumed to require 154 cm² of surface area per Wp power with an efficiency of 6.5%.[145]

Energy Payback Time

The EPBT took into consideration how much energy was consumed across each life-cycle stage to produce the PV cell (i.e. CED) and how much would be generated (E_g) by the panel over its use (equation (3-1)).

$$\mathrm{EPBT} = \frac{CED}{E_\mathrm{g}} \qquad (3\text{-}1)$$

EPBT: Energy payback time
CED: Cumulative energy demand
E_g: Energy generated by the PV device

E_g is defined by equation (3-2):

$$E_\mathrm{g} = \frac{I \cdot S \cdot C \cdot A}{X} \qquad (3\text{-}2)$$

I: Solar insolation
S: System performance ratio
C: Cell power conversion efficiency,
A: Active area of the cell,
X: Electrical conversion efficiency

The values of the parameters used to quantify the EPBT are listed in Table 3-1.

Table 3-1 Estimated parameters used to calculate the energy-payback times for each solar cell considered. Insolation is based on an average European insolation of 1300 kWh per m^2.

	Cell Power Conversion Efficiency (%)	**System Performance Ratio (%)**	**Insolation (MJ/m²/year)**	**Active Area of Cell (%)**	**Electrical Conversion Efficiency (%)**
Default	5.00E-02	7.50E-01	4.68E+03	100	3.60E-01
FTOinkjet	5.00E-02	7.50E-01	4.68E+03	100	3.60E-01
PCBMdcb	5.00E-02	7.50E-01	4.68E+03	100	3.60E-01
OPV-PP	5.00E-02	7.50E-01	4.68E+03	100	3.60E-01
m-Si	1.32E-01	7.50E-01	4.68E+03	95	3.60E-01
a-Si	6.50E-02	7.50E-01	4.68E+03	100	3.60E-01

Carbon Payback Time

To calculate the carbon payback time (CPBT), the cumulative, cradle-to-gate CO_2-equivalent emissions (CCE) of each PV panel was compared to the CCE avoided from a European average electricity production mix (CCE_{RER}) for the same Wp produced by the PV panel per year of operation (equation (3-3)).

$$CPBT = \frac{CCE}{(\mathrm{E_g} \cdot \mathrm{CCE_{RER}})} \quad (3\text{-}3)$$

CPBT: Carbon payback time
CCE: Cradle-to-gate CO2-eq. emissions generated for the PV device
CCERER: CO2-eq. emissions avoided from an average European electricity mix per kWh of energy produced
E_g: The amount of energy (kWh) produced by the PV device over one year

CCE_{RER} was estimated as 4.9E-04 kg per Wp of the Ecoinvent process "electricity, medium voltage, production RER, at grid."

Minimum Required Lifetime

The concept of a minimum required lifetime was used to communicate how long the OPV should be operational such that its environmental impacts are no greater than conventional PV (equation (3-4)):

$$MRL = \frac{\mathrm{T_{o,n}}}{\mathrm{T_{i,n}}} \cdot L_{\mathrm{i}} \quad (3\text{-}4)$$

MRL: Minimum required lifetime
$T_{o,n}$: Environmental and human health impact criteria (n) for OPV (o)
$T_{i,n}$: Environmental and human health impact criteria (n) for the silicon PV (i)
L_i: Lifetime of the ith technology

The minimum required lifetime was estimated using a-Si as the *i*th technology.

Results and Discussion

The greatest contribution to the overall environmental and human health impacts of the *default* OPV arose from the production and deposition (i.e. sputtering) of the FTO anode onto the substrate. FTO substrate production had an average contribution of 62% across all impact categories, with a high of 95% for metal depletion and low of 57% for fossil fuel depletion (Figure 3-4).

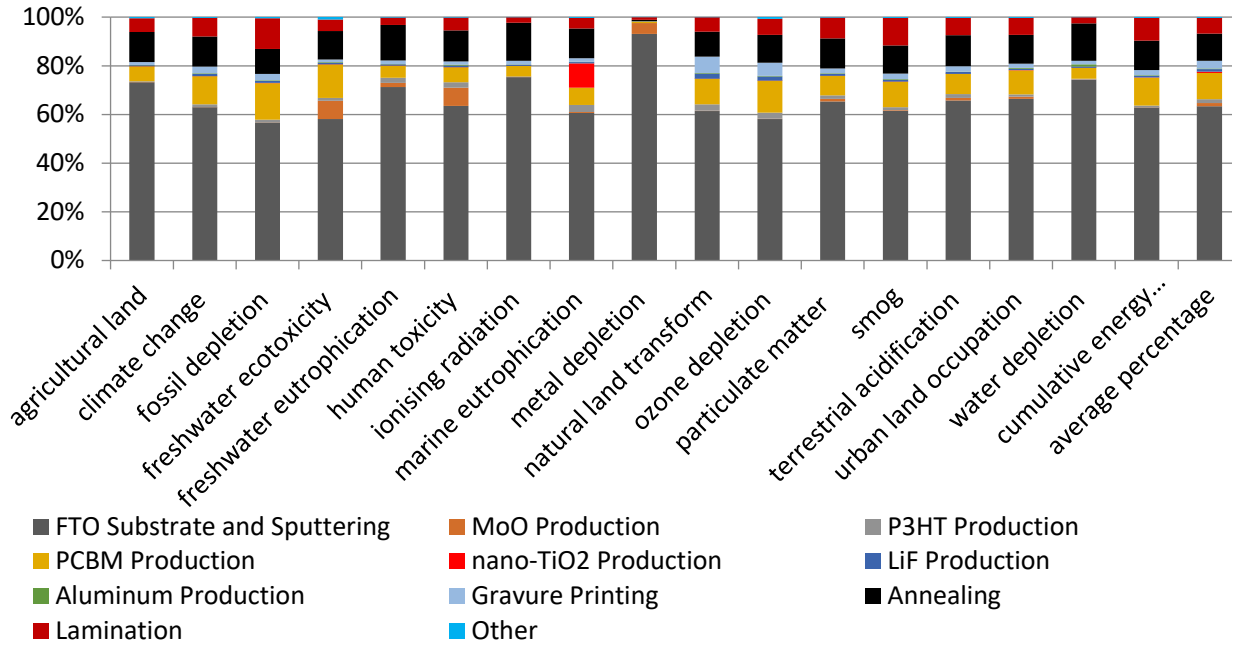

Figure 3-4 The contributions of life-cycle stages and production processes to the overall impacts of the default organic photovoltaic cell considered in this study.

In general, contributions from production of the FTO were on the order of a few percentage points, except for the metal depletion potential where upstream impacts from tin production accounted for roughly 90% of that impact. The high average contributions from FTO-substrate production was driven by the sputtering process, something also seen in previous OPV-LCA for ITO-based substrates.[45] Contributions from manufacturing PCBM, annealing of the active layer, and lamination of the solar cell also result in sizable average contributions of 11%, 11% and 6%, respectively. Contributions from PCBM production varied greatly and ranged from a high of 13% for ozone depletion to a low of 4% for water depletion. For PCBM production, the impacts were influenced heavily by both the production of C_{60}-fullerene and subsequent modification and purification into PCBM. This was in part due to upstream impacts of producing toluene, *ortho*-dichlorobenzene and pyridine compounds. Previous estimations of CED per kg of PCBM ranged between 64-125 GJ amongst the studies reviewed (Chapter 1). Impacts from production of the nano-TiO_2 optical spacer ranged from a high of 10% for marine eutrophication to a low of 0.01% for water depletion. Its overall contribution to all environmental and human health impacts were marginal and averaged 0.55%.

The annealing contribution of 11% was slightly higher compared to previously published literature which report estimations between roughly 0.2-10%.[30,37] However, in some studies the energy consumed during

annealing of the active layer is not explicitly demonstrated,[128] or it is simply left out of the assessment altogether.[29] For lamination, the greatest influences were due to PET production and the epoxy resin. Previously reported literature on the contribution of lamination to CED, for example, varies significantly from as little as 0.1% to as much as 37%.[29,30,38] In regards to the co-polymer P3HT, there was a smaller contribution of 2% on average across all impact categories. Previous studies demonstrated that P3HT can contribute between 0.1-0.8% of the CED, which is in line with the results of this thesis which show a 0.7% contribution to CED from P3HT production. Although this is a fairly moderate contribution to the overall environmental and human health impacts, the literature reports a trend moving away from P3HT for alternate low-bandgap polymers.[42] While these have the potential to increase OPV efficiency, it may come at the expense of increasing the environmental and human health impacts of the total device.[42]

Sensitivity Analysis

For the FTOinkjet alternative, sputtering was removed from the production route and replaced with inkjet printing. Sputtering was previously identified as a highly energy intensive process and, when avoided, decreases the overall CED.[29,38,128] The results of this thesis confirmed this, but also demonstrate that the other life-cycle impact categories do not necessarily respond in-step with CED. For instance, whereas CED had an approximate 56% decrease, impact reductions ranged from 2% for metal depletion to 72% for ionizing radiation in other impacts (Figure 3-5).

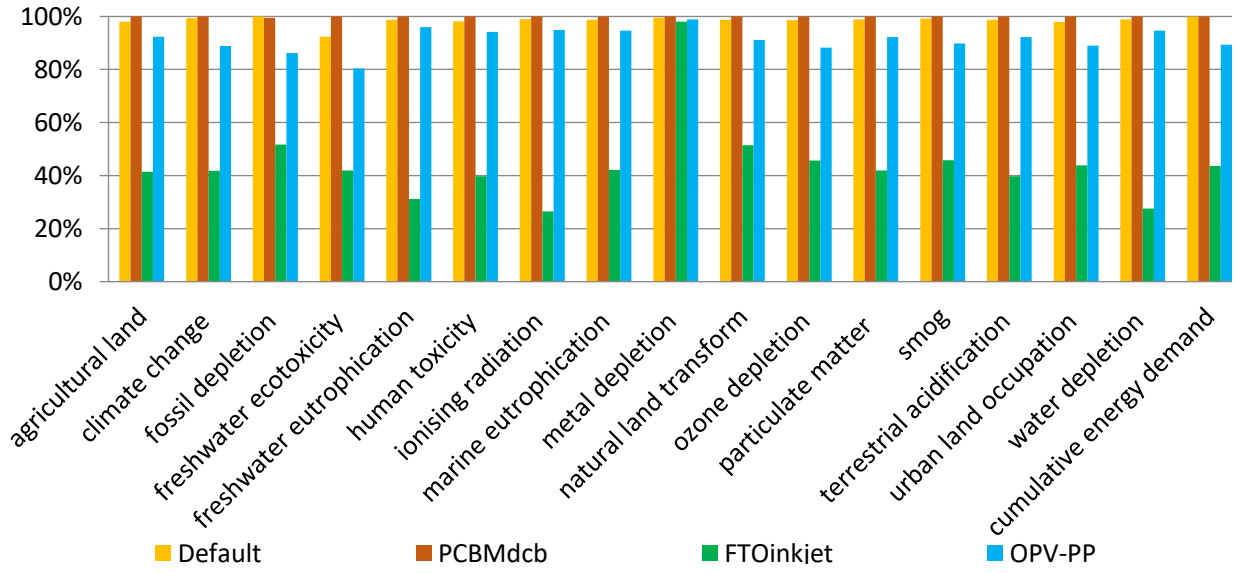

Figure 3-5 Life-cycle impact results for the three alternative and one default organic photovoltaic cells considered in this life-cycle assessment. The impact results are internally normalized using division by the maximum impact value per impact category.

Replacement of the PCBM with an additional polymer in the OPV-PP alternative resulted in an average decrease of 10% across all impact categories. Whereas PCBM has previously been identified as a low to moderate factor in the environmental and human health impacts of OPV production,[29,45,128,146] quite significant impact reductions from the polymer replacement were seen for ecotoxicity, where impacts were reduced by 20%. In general, polymers such as P3HT have shown much lower contributions to the environmental impacts of OPV production, however polymers are quite heterogeneous and their CED, for example, can differ by up to an order of magnitude.[42]

In the PCBMdcb alternative, PCBM production was modeled with dichlorobenzene as the solvent instead of toluene. Impacts for this alternative resulted in an average increase of 2% in all categories except for fossil fuel depletion, which was only a fraction of a percent lower than the default case. Notably the human health impacts for dichlorobenzene were 10% higher than the default case using toluene. In contrast, ecotoxicity impacts were only 2% higher for the dichlorobenzene alternative. Nonetheless, production of C_{60}-fullerenes requires large amounts of solvent for purification and separation,[45] thus solvent use could still be targeted as one way to further reduce OPV impacts. Dichlorobenzene is a widely used solvent in industry, and although the environmental impacts for this alternative were only slightly greater than the default case, concerns over potential human health impacts would be a limiting factor for its use.

Comparison to Conventional Silicon-Based Photovoltaics

The results show that all environmental and human health impacts were higher for both of the silicon-based PV compared with OPV (Figure 3-6).

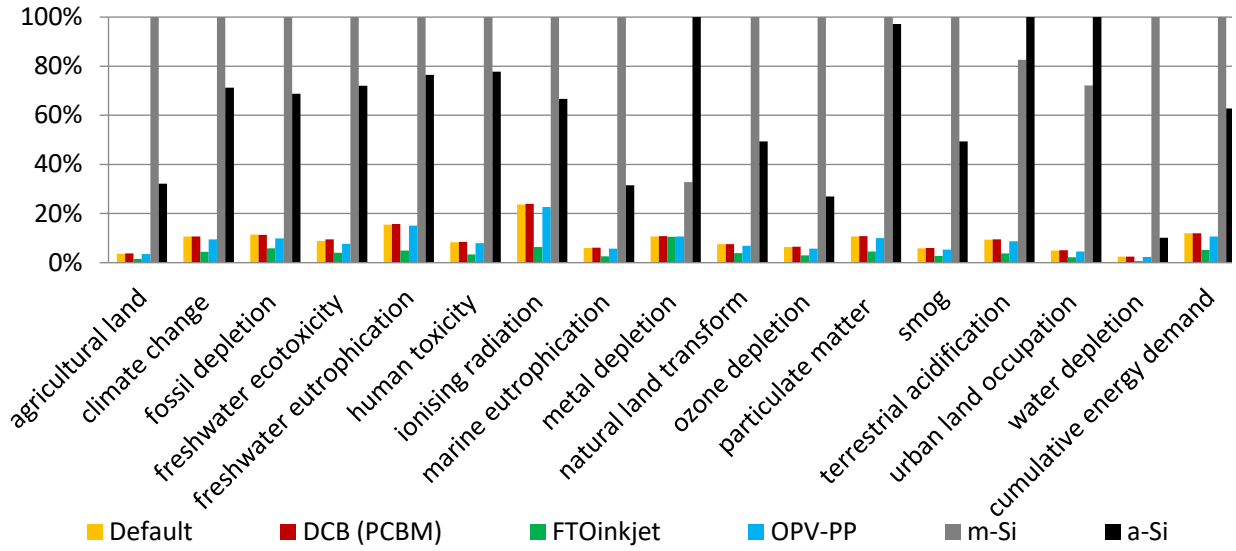

Figure 3-6 Comparison of life-cycle impacts for the organic photovoltaic cells and two conventional silicon cells. The impact results are internally normalized using division by the maximum impact value per impact category.

Particularly, m-Si cells had the greatest impacts for 14 of the 17 impact categories except for metal depletion, particulate matter formation, terrestrial acidification, and urban land occupation which were greatest for a-Si cells. The *default* OPV impacts were on average 93% lower when compared to the worst performing silicon cell. The impacts of the OPV cells that used inkjet printing for FTO deposition, OPV-PP and dichlorobenzene during PCBM production were on average 97%, 93% and 92% lower than the silicon-based cells, respectively.

Energy and Carbon Payback Times

The CED for the *default* OPV was 2.6 MJ/Wp. This decreased to 1.1 MJ/Wp, 2.6 MJ/Wp, and 2.3 MJ/Wp for the FTOinkjet, PCBMdcb and OPV-PP alternatives, respectively. Because OPV cells can be produced any number of ways (i.e. various materials and manufacturing routes), embodied energy for such systems has varied widely in the literature and ranges between 0.89-27 MJ/Wp (Chapter 1).[29–31,38,42,128] As is shown in Figure 3-7, the CED for the default case is in line with previously published values for similar PCBM:P3HT 5% efficient solar cells.

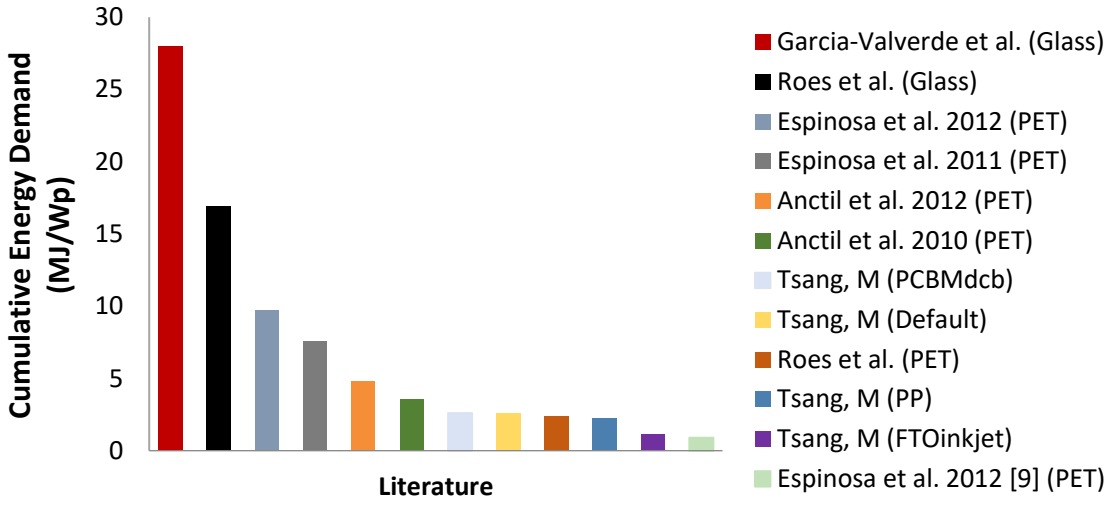

Figure 3-7 Comparison of cumulative energy demand per watt-peak for organic photovoltaic cells reported in the literature as well as from this thesis.

Per m^2, the EPBT for the default OPV cell was 0.27 years (97 days) compared with m-Si and a-Si's 3.6 and 2.8 years, respectively (Table 3-2). For the OPV alternatives, EPBT decreased to 0.12 years (42 days) and 0.24 years (87 days), for the FTOinkjet and OPV-PP cells, respectively. These results are of importance given that the OPV cells only generate between 40% and 80% of the energy produced by m-Si and a-Si, respectively (Table 3-2).

Table 3-2 Power generation, embodied energy, energy payback time, embodied carbon, and carbon payback time for each solar cell considered in this chapter, assuming an average European insolation value of 1300 kWh per m^2.

	Wp/m²	CED (MJ/m²)	CED (MJ/Wp)	CO2(kg)/Wp	Energy Generated (MJ/m²/year)	EPBT (yrs)	CPBT (yrs)
Default	50	130.0	2.6	0.115	4.88E+02	0.27	0.088
FTOinkjet	50	57.1	1.1	0.049	4.88E+02	0.12	0.037
PCBMdcb	50	130.0	2.6	0.116	4.88E+02	0.24	0.088
OPV-PP	50	116.0	2.3	0.103	4.88E+02	0.27	0.078
m-Si	210	4,580	21.8	1.088	1.29E+03	3.60	1.31
a-Si	128	1,750	13.7	0.775	6.34E+02	2.81	1.16

The results in this thesis show that OPV still recover their embodied energy one-order of magnitude quicker than their silicon-based counterparts. These results were in the range of previously reported literature, with reported EPBT between 52 days to 2 years.[29,30,38,128] It should be noted that EPBT calculations depend on the regions with which it operates and thus higher insolation values produce quicker payback-times. In terms of the CPBT, these were much shorter for OPV compared to conventional

silicon. The default OPV CPBT was 32 days and decreased to 13 days for the FTOinkjet alternative and 29 days for the OPV-PP alternative. CPBT for m-Si and a-Si were 1.31 years and 1.16 years, respectively.

Minimum Required Lifetime

Compared to a-Si cells, the minimum required lifetimes of the default OPV cell ranged from 1.2-8.9 years and averaged 4.1 years (Table 3-3).

Table 3-3 Minimum lifetimes required of organic photovoltaic to achieve environmental and human health parity with amorphous silicon cells having 25-year lifetimes. Categories are displayed in descending order of results for the *Default* OPV.

Impacts	***Default* (yrs)**	**FTOinkjet (yrs)**	**PCBMdcb (yrs)**	**OPV-PP (yrs)**
ionizing radiation	8.9	2.4	9.0	8.5
water depletion	6.1	1.7	6.1	5.8
ozone depletion	5.9	2.7	6.0	5.3
freshwater eutrophication	5.1	1.6	5.1	4.9
marine eutrophication	4.8	2.0	4.8	4.6
cumulative energy demand	4.7	2.1	4.7	4.2
fossil depletion	4.1	2.1	4.1	3.6
average	***4.0***	***1.8***	***4.1***	***0.2***
natural land transform	3.8	2.0	3.8	3.5
climate change	3.7	1.6	3.7	3.3
freshwater ecotoxicity	3.1	1.4	3.3	2.7
smog	3.0	1.4	3.0	2.7
agricultural land	2.9	1.2	2.9	2.7
particulate matter	2.8	1.2	2.8	2.6
metal depletion	2.7	2.6	2.7	2.7
human toxicity	2.7	1.1	2.7	2.5
terrestrial acidification	2.3	0.9	2.4	2.2
urban land occupation	1.2	0.6	1.3	1.1

For climate change potential and CED, the minimum lifetimes were 3.7 and 4.7 years, respectively. These results demonstrate that even for the worst performing environmental indicator, ionizing radiation, OPV cells only need to have a theoretical lifetime of 8.9 years such that its replacement over 25 years is not any worse than an analogous a-Si cell. This is both reasonable and encouraging given current maximum lifetimes of OPV have reached circa 7 years.[45] The OPV cells that used inkjet printing of the FTO layer, dichlorobenzene in PCBM production or an all polymer active layer resulted in minimum lifetime ranges of 0.6 years to 2.7 years, 1.3 years to 9.0 years, and 1.1 years to 8.5 years, respectively. In the case of the FTOinjet alternative, minimum required lifetimes ranged from 0.6 years for urban land occupation to a

high of 2.7 years for ozone depletion. The average values for this alternative was only 1.8 years which is an even more promising result for the future of this technology.

Conclusion

The results from this LCA forecast a rather optimistic place for OPV as an energy producing technology, where all environmental and human health impact results indicate a much more favorable option for OPV on a watt-per-watt basis compared with conventional silicon cells. Although, the results of this LCA are applicable to the OPV described in this chapter, the materials used and modeling assumptions which were all chosen based on reasonable expectations that such a device could enter the market in the near-term. As was demonstrated in this LCA, researchers in this field should be encouraged to consider a broader range of environmental and human health impacts for assessing the benefits of OPV over conventional technologies. As was presented, estimations of OPV minimum lifetimes to reach parity with a 25-year lifetime a-Si solar cell ranged from 1.2-8.9 years in the default case and as short as 0.6-2.7 in the FTOinkjet case. These represent moving targets for stakeholders, researchers and regulators in the field. More specifically and from an LCA perspective, the higher reported minimum required lifetimes reported for the default OPV demonstrate that OPV may be most advantageous in niche and short-term use scenarios compared to traditional long-term solar arrays. Although, the results for the FTOinkjet OPV point to potential justifications for using them in such traditional settings. However, these results were simplified theoretical calculations based on power production for just the PV cell (i.e. just the cradle-to-gate consideration up to the point of PV cell production were considered). The results implicitly imply that the PV would need no other components to be fully operational and would also have no impacts from the use-phase and/or end-of-life phases. Thus, this is an over simplified set of assumptions and no definitive determination can be given as to whether OPV are a preferred technology option over silicon-based PV from an environmental and human health perspective. Further research in this area should focus on how the use phase and end-of-life considerations will influence potential OPV deployment. For instance, recycling of precious metals has the potential to reduce the EPBT by 13% for OPV cells.[147] However, collection and the ultimate recovery rate of both the solar cells and materials with value will depend on where and how the OPV cells are employed.[148,149] The focus of Chapter 4 begins to address these questions by extending the system boundaries to include potential uses and end-of-life scenarios for OPV panels.

Chapter 4 Cradle-to-Grave Life-Cycle Assessment of Organic Photovoltaics

In Chapter 1, a review of the OPV-LCA literature through the end of 2013 demonstrated that only two of the ten studies had considered the use phase, with one of those two studies also considering an end-of-life phase of the OPV. Of the two use phases considered, one was a rooftop glass-substrate system[29] while the other was a flexible-substrate OPV-powered street lamp.[36] The latter study also included the impacts from landfilling the OPV device, however as far as can be told, there does not seem to be any reporting of those end-of-life impacts in the results or mention of how this life-cycle stage influenced the overall LCA profile of the OPV. It should be noted that between the end of 2013 and the time this chapter was being prepared for submission, there were three other OPV-LCA studies published that contained use and/or end-of-life phases. In 2014, Espinosa et al. completed a cradle-to-use LCA for ground-installed solar arrays as well as three non-conventional onshore, offshore and balloon arrays.[24] In 2015, Espinosa et al. completed a cradle-to-grave LCA for a ground-installed solar array with the additional consideration of either recycling or incinerating the entire solar-array.[62] Lastly, in 2014 Sondergaard et al. completed a LCA that considered the cradle-to-gate production of the OPV plus the additional consideration of recycling the silver content at its end-of-life (i.e. without the consideration of the use-phase).[147] The results of those studies are presented later in the results and discussion of and in context with the results of this chapter.

Methods

Goal and Scope

This LCA was conducted according to ISO 14040:2006[28] and 14044:2006[27] guidelines and the IEA's recommendations for implementing LCA for PV technology.[35] All life-cycle stages and impacts from raw materials extraction, materials processing, PV manufacturing, use, end-of-life considerations were included (Figure 4-1).

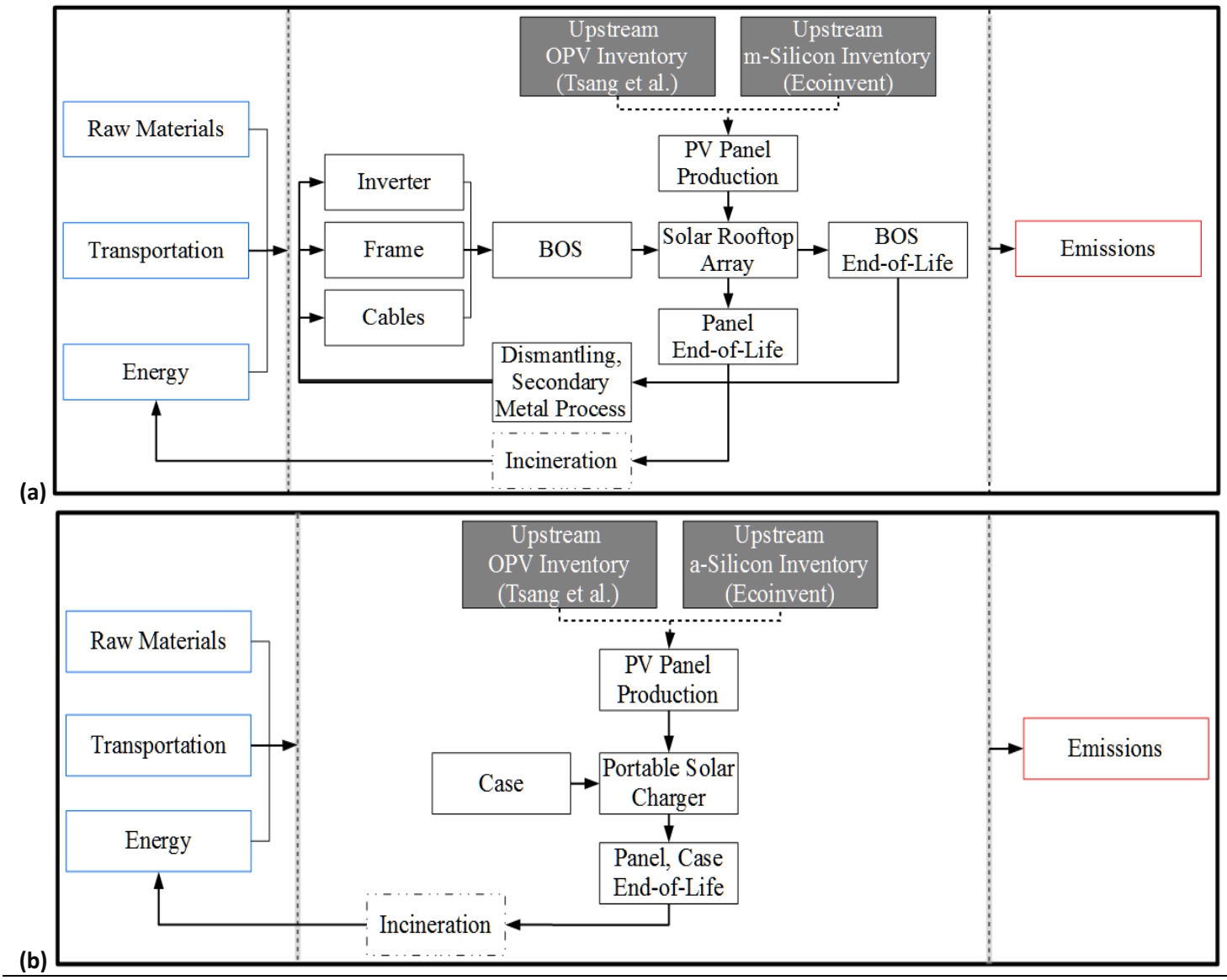

Figure 4-1 System boundaries for (a) System 1 (rooftop array) and (b) System 2 (portable charger). Incineration was just one of the end-of-life scenarios modeled in the life-cycle assessment and is shown for clarification of how the energy recovery was considered in the life-cycle inventory.

OPV are not currently produced at industrial scale or used for commercial purposes. Therefore, two different systems (i.e. uses of the PV) were considered to better inform the potential role OPV could play for energy production and consumer product sectors. System 1 (S1) was defined by a functional unit of an average kWh of electricity generation over 25 years using a solar rooftop array (Figure 4-2), while System 2 (S2) was defined by a functional unit of an average ten Wh of electricity generation over five years via a portable charging-device (Figure 4-2).

Source: novato.org

Source: instapark.com

Figure 4-2 Examples of the two different systems (i.e. functional units) studied in this chapter

All foreground inventory data are explained in the following sections, while relevant background data were taken from the Ecoinvent v2.2 attributional life-cycle inventory.[132] All transportation requirements for incoming foreground chemicals and materials were taken into account using 100 km truck and 600 km rail transport, while outbound waste materials were estimated using ten km truck transport.[132] Capital equipment (e.g. buildings for solar panel production) were excluded from the OPV inventory as such environmental burdens are often negligible when considering the entire life-cycle and life-time of a product.[78] Where applicable, co-products resulting from the end-of-life treatment option of the solar panels (e.g. electricity from incineration) were handled as avoided products. Energy production from incineration was assumed to replace an average European medium-voltage electricity production mix (RER) defined by Ecoinvent v2.2. Only electrical energy, as opposed to thermal energy was considered. Using an energy conversion efficiency half that of thermal energy, all potential thermal energy was converted to electrical energy. The LCA was conducted within openLCA v1.4.2 (GreenDelta, Berlin). The impact assessment was completed using ReCiPe[80] v1.0.5 midpoint (*H*) impact categories (*Table 2-2*) with the substitution of USEtox (www.usetox.org) for the human health and freshwater ecotoxicity indicators and the addition of CED.[92] Detailed inventories for each foreground data entry and stoichiometric estimation are supplied in Appendix: Chapter 4.

Life-Cycle Inventory: System 1 (Rooftop Solar Array)

Organic Photovoltaic Technology Description

The *default* technology (OPV-D) was based on a typical polymer-based bulk heterojunction that employed aPCBM:P3HT active layer as described in Chapter 3 for the FTOinkjet OPV.[52] The general geometry of the solar cell is depicted in Figure 1-3 and the main material and energy requirements are listed in Table 4-1.

Table 4-1 Generalized account of material components and energy requirements for producing one m^2 of an OPV-D panel based on the description in Chapter 3 for the FTOinkjet OPV. Indirect, upstream or auxiliary material and energy requirements as well as emissions are not reported here.

Materials	**Amounts**	**Notes**	**References**
Aluminum	0.3 g	Back electrode	52,140
PET	74.0 g	Substrate	52
FTO	1.80 g	Applied as an FTO solution	42,52,126
PET	133 g	Lamination	52
Lithium Fluoride	6.00E-5 g	Back electrode	52
Molybdenum oxide	0.240 g	Hole transport layer	42,52,56,140
Chlorobenzene	7.66 g	Solvent for active layer application	56
P3HT	0.235 g	Active layer	42,52,56,140
PCBM	0.205 g	Active layer	42,52,56,140
Nano-TiO_2	0.127 g	Optical Spacer	121
Energy	**Amounts**	**Notes**	**References**
Electricity	5.13 MJ	Annealing	145
Electricity	2.56 MJ	For printing of panel components	29
Electricity	0.0850 MJ	For lamination of the panel	29

All layers of the panel were roll-to-roll printed under normal atmosphere conditions on a flexible substrate made from PET, using a transparent FTO electrode on the light-collecting face, an active layer composed of PCBM:P3HT, a hole transport layer made of MoO_3, a back electrode made from aluminum with a thin layer of lithium fluoride, a nano-TiO_2 optical spacer, encapsulation and lamination layers composed of PET, silica and various epoxy resins.

The device efficiencies of OPV panels have been on a slight upward trend since the early 2000s, with lab-scale devices that are similar to what is considered in this current LCA reaching 15% in some cases.[150] Additionally, as PV technologies mature, their lab-to-industrial scale efficiencies might decrease from 20%-50%.[127] Given these considerations, a conservative 5% efficiency was assumed, requiring 200 cm^2 of panel per Wp of power produced. To fulfill the one kWh functional unit, 20 m^2 of OPV panel were required. Historically, OPV lifetimes have been shorter than conventional silicon PV. More recently, maximum lifetimes for OPV reached seven years.[56] For any practical and mainstream use of OPV devices, typical lifetimes should start to approach these upper boundaries. Therefore, this LCA assumed a 5-year lifetime for the OPV. Given this estimation, the OPV panels needed to be replaced four times (five installations total) during the 25-year timeframe of S1, resulting in the total use of 100 m^2 of OPV panels.

Silicon-Based Photovoltaic Technology Description

For S1, the OPV panels were further compared to m-Si, which was chosen due to its 70% share of global annual production and high uptake in roof-mounted solar installations.[16] The inventory for m-Si panels was taken from the Ecoinvent process for "photovoltaic panel, multi-Si, at plant" and included the production and connection of individual panels plus the frame.[39] The m-Si panel was assumed to have an efficiency of 13.2%, requiring 75 cm² of surface area per Wp and a 25-year lifetime.[39] To fulfill the functional unit, 7.6 m^2 of silicon panels were used.

Balance of System

For each technology option, the rooftop installation included an estimation of a balance of system (BOS): mounting-structure, an inverter and cables for electrical installation (Table 4-2).

Table 4-2 Inventory for an average kWh of installed OPV solar roofing array, mounted with support (S1)

Flow	Notes	Unit	Amount
OPV panel, at plant	This inventory amount represents a total of 5 kWh of paneling in order to account for the subsequent replacement over 25 years of the use-phase while assuming an OPV lifetime of 5 years.	m^2	20.0
Cabling, rooftop, solar installation	Appendix: Chapter 4	m^2	20.0
Slanted-roof construction, OPV solar, mounted, on roof	Appendix: Chapter 4	m^2	20.0
Inverter, 2500W, at plant (with disposal)	Appendix: Chapter 4	# Items	1.0
Transport, lorry 16-32t, Euro3 – RER		tkm	0.74
Transport, freight, rail – RER		tkm	4.44
Inventory for the disposal of cabling per m^2 of PV capacity			
Disposal, OPV solar cell, incineration	Appendix: Chapter 4	kg	22.0
OR			
Disposal, OPV solar cell, landfill	Appendix: Chapter 4	kg	22.0

The inventory for the mounting-structure was based on Ecoinvent's "slanted-roof construction, mounted, on roof" process.[79] For the OPV-specific inventory, the mounting-structure was based on a modified version of this process (Appendix: Chapter 4), taking into account an aluminum-backing that the OPV panels would sit on. The aluminum backing was defined as a two mm thick panel with the exact dimensions of the OPV panel (20 m^2), requiring 3.9 kg of aluminum per functional unit. The backing panel was not completely solid (100% filled) but was modeled with repeating holes within it in since it was not foreseen that a filled structure would be necessary for support. For the m-Si inventory, the original Ecoinvent slanted-roof inventory was also used with the additional considerations of recycling the steel and aluminum components (Appendix: Chapter 4). In all cases, the mounting-structure was assumed to

last 25 years and was recycled after use. Recycling estimations were made assuming 100% collection of the mounting components and entrance into the recycling waste stream, whereby aluminum and steel were used as scrap to produce secondary aluminum at conversion rates of 97% and 90%, respectively. As described above and at any single time during the use-phase, 20 m^2 of OPV panels were needed to fulfill the one kWh functional unit, requiring the installation of a 20 m^2-equivalent OPV-specific mounting structure. Similarly, 7.6 m^2-equivalent of the m-Si-specific mounting structure were installed for the m-Si panels.

The inventory for the inverter was based on a modified version the Ecoinvent "inverter, 2500W, at plant" process whereby recycling of the inverter was estimated using a mix of manual and mechanical dismantling processes and material transfer coefficients to recover aluminum, copper and steel (Appendix: Chapter 4). All three metals were assumed to be used as scrap in the secondary metals market with conversion rates of 97%, 76% and 90%, respectively, while the remaining waste was incinerated to generate electricity at 2.97 MJ/kg of waste. It was assumed that a single inverter was used throughout the duration of the functional unit.

Cabling requirements[151] included the recovery of copper used in secondary metal production at a 76% conversion rate. The remainder of the plastics was assumed incinerated, ultimately producing four MJ of electricity per kg of plastics waste. Twenty m^2-equivalent of cabling and 7.6 m^2-equivalent of cabling were required for both OPV panels and the m-Si panels, respectively.

End-of-Life Considerations

Assumptions were made that 100% of all PV devices were collected and directed to the appropriate waste stream, with 100% of the m-Si aluminum frame (19.99 kg) being dismantled and recycled along with the aluminum BOS mounting-structure components. No further energy or material inputs were considered for dismantling these components. Two end-of-life scenarios were considered: (a) incineration and (b) landfilling. Currently, the core infrastructure, economics, regulatory frameworks and the size of the waste stream indicate that most PV panels fall into these conventional disposal options as opposed to recycling.[64,65,152] Both disposal-process inventories were calculated using Ecoinvent's waste disposal modeling tools.[150] The tool was used to create a waste-inventory (Appendix: Chapter 4) based partially on the elemental composition of the waste as well as an assumed set of non-waste-specific technosphere and disposal related processes. The composition of the waste for each panel was based on the panel

composition at the time of manufacture (i.e. not considering losses or degradation of components over the lifetime of the PV device). For incineration, lower heating values for the major components were used to determine potential energy recovery from the system. Because the majority of the OPV panel is PET, its lower heating value of 22.9 was used, resulting in 4.95 MJ of electricity generated per kg of OPV panel incinerated. m-Si panels are composed almost entirely of materials that have insignificant lower heating values (i.e. silicon and glass) and thus it was assumed that incineration of m-Si panels generated no electricity. OPV panels weigh 0.22 kg per m^2, resulting in the disposal of 22 kg of OPV panels. m-Si panels weigh 11.6 kg/m^2, resulting in a total disposal of 88 kg of silicon panels.

Life-Cycle Inventory: System 2 (Portable Solar Charger)

OPV Technology Description

The same OPV-D panels described above were considered in S2. To fulfill the ten Wh functional unit, 0.2 m^2 of OPV panels were needed (Table 4-3). The solar panels were used as portable chargers and were assumed to require a one mm thick PET-polyester case for protection, requiring 0.27 kg of PET and polyester each per charging unit.

Table 4-3 Inventory for an average ten watt-hours of an organic photovoltaic portable solar charger (S2)

Flow	Notes	Unit	Amount
OPV panel, at plant	This inventory amount represents a total of 5 kWh of paneling to account for the subsequent replacement over 25 years of the use-phase while assuming an OPV lifetime of 5 years.	cm^2	2000.0
Plastic film, pet, at plant	Used for the casing; based on Ecoinvent process for extrusion of plastic film for packaging	g	273.7
Polyester resin, unsaturated, at plant	Used for the casing	g	273.7
Transport, lorry 16-32t, Euro3 – RER		tkm	0.010
Transport, freight, rail – RER		tkm	0.063
Inventory for the disposal of cabling per m^2 of PV capacity			
Disposal, OPV solar cell with casing, incineration	Appendix: Chapter 4	kg	0.59
OR			
Disposal, OPV solar cell with casing, landfill	Appendix: Chapter 4	kg	0.59

Silicon-Based Photovoltaic Technology Description

The OPV portable chargers were compared to a-Si ones, which were chosen due to its thinness, flexibility and lighter weight, providing a conventional product mirroring some similarities to OPV. The inventory for a-Si panel was taken from the Ecoinvent process for “photovoltaic panel, a-Si, at plant” and includes the

production and connection of a triple-junction silicon laminate that is roll-to-roll processed on a stainless steel substrate with the frame.[39] The a-Si panel was assumed to have an efficiency of 6.5%, requiring 159 cm^2 of surface area per Wp.[39] To fulfill the functional unit, 0.16 m^2 of a-Si panels were needed. The a-Si portable charger was assumed to require a one mm thick PET-polyester case for protection, requiring 0.22 kg of PET and polyester each per charging unit.

End-of-Life Considerations

The portable chargers were assumed to be collected at a rate of 100%, entering their appropriate waste streams without further consideration of dismantling. Incineration and landfilling were considered as the two end-of-life options. The lack of literature on the subject and low amounts of silicon in a-Si solar cells provides little support for recycling as a plausible disposal scenario, compared with m-Si.[152] A total of 0.044 kg of OPV-D panels were disposed, along with the 0.27 kg of PET and polyester in the casing. A total of 0.41 kg of a-Si panels were disposed of along with the 0.44 kg of casing. An average 4.95 MJ, 1.25 MJ, and 6.99 MJ of electricity production was estimated per kg of OPV incineration, a-Si incineration and plastic-casing incineration, respectively.

Energy Payback Time

To calculate the EPBT, the total CED, representing total energy consumption across the entire life-cycle of the PV device, was compared to the panel's E_g during that same time (equation (3-1)). EPBT was estimated using an average European insolation value of 1,300 kWh/m^2/year (Appendix: Chapter 4) and the model parameters listed in Table 4-4.[153]

Table 4-4 Estimated parameters used to calculate the energy and carbon payback times

	Power Conversion Efficiency (%)	System Performance Ratio (%)	Insolation (MJ/m^2/year)*	Active Area of Panel (%)	Electrical Conversion Efficiency (%)
OPV-D	5.00E-02	7.50E-01	4.68E+03	0.95E+00	3.60E-01
m-Si	1.32E-01	7.50E-01	4.68E+03	100E+00	3.60E-01
a-Si	6.50E-02	7.50E-01	4.68E+03	100E+00	3.60E-01

*Converted from the average European insolation of 1300 kWh

Carbon Payback Time

To calculate the CPBT, the CCE of each PV panel was compared to CCE_{RER} generated from a European average electricity production mix for the same Wh produced by the PV panel (equation (3-3)). CCE_{RER} was

estimated as 0.49 kg per kWh of the Ecoinvent process "electricity, medium voltage, production RER, at grid."

Minimum Required Lifetime of Organic Photovoltaics

The minimum lifetime afforded by or required of OPV determined the lifetime of the panel which theoretically would result in the same environmental impacts compared to silico-based PV. It was calculated using equation (4-1):

$$MRL = \frac{(A \cdot Z)}{(C - B)} \qquad (4\text{-}1)$$

MRL: Minimum required lifetime
A: OPV_i panel-specific[1] impacts (i)
B: all other (OPV) impacts
C: total silicon impact
Z: default OPV lifetime

Sensitivity Analysis

Although the default analysis rests on interpreting and estimating realistic efficiencies and lifetimes from their experimental maximums,[56] there is still considerable uncertainty in whether industrial production of such cells could achieve these estimates in the near-term. For instance, when transitioning from the lab to large-scale development, device efficiencies decline roughly by a factor of two, which could lead to situations where the default assumptions are potentially overly optimistic, particularly given the range of probable OPV devices in development and their corresponding range of lifetimes and efficiencies. The assumptions were tested assuming (a) lifetimes of one, three, five, seven and nine years with a constant efficiency of one percent and (b) assuming efficiencies of one, three, five, seven and nine percent with a constant lifetime of one year. The constants of one percent and one year were chosen in order to reflect more actual immediate-term scenarios which in effect act as a baseline set of characteristics from which industrial-level characteristics could be targeted.

[1] Referring to the impacts that result from the production and disposal of the panel as opposed to the BOS components

Results and Discussion

Results for the Default Organic Photovoltaic Technologies in Scenario 1 and Scenario 2

The relative impact differences between OPV-D and the silicon-based PV for S1 and S2 are shown in Figure 4-3.

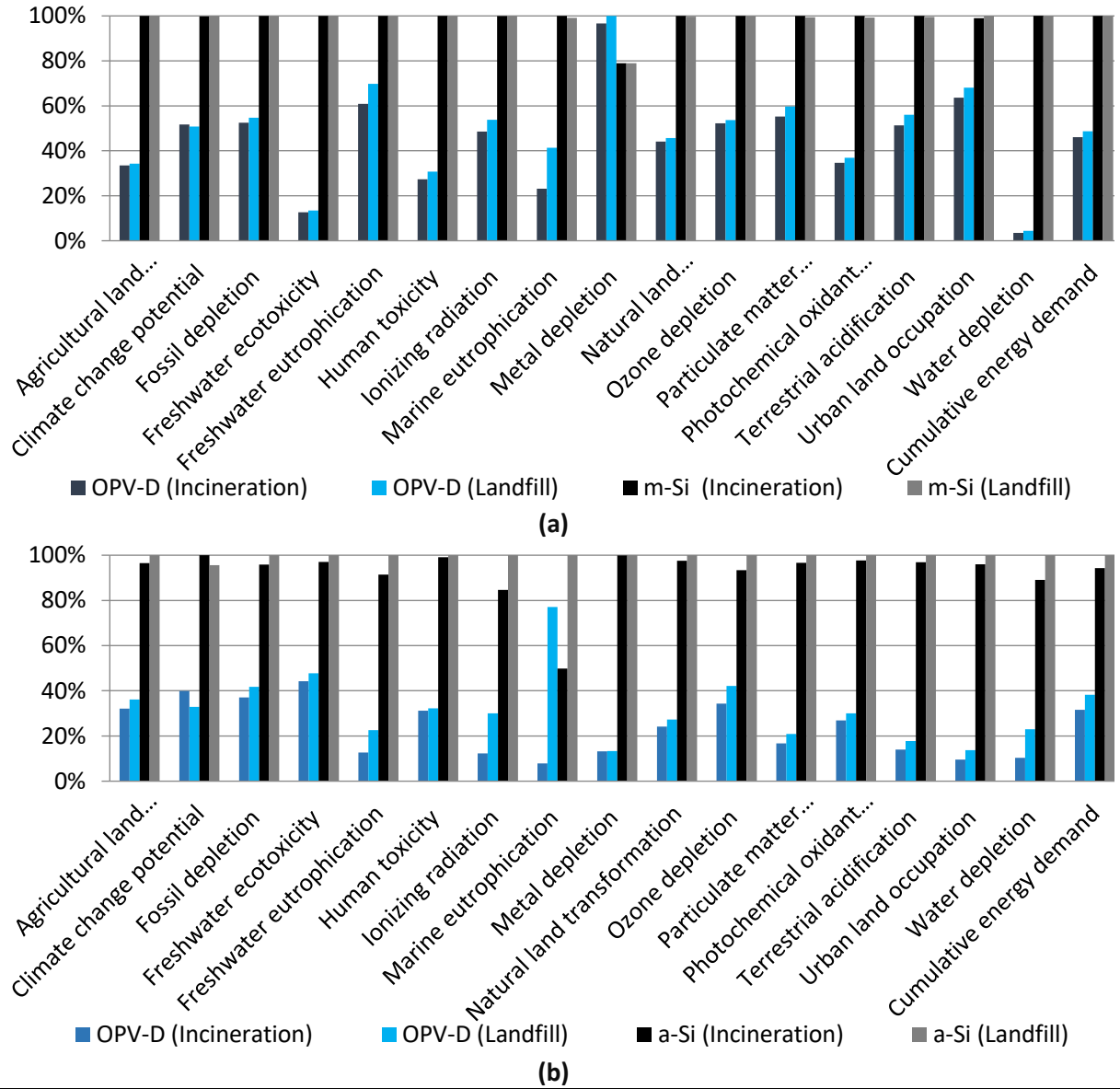

Figure 4-3 Relative default impacts of (a) System 1 (rooftop array) comparing the default OPV-D scenario with m-Si panels and (b) System 2 (portable charger) comparing the default OPV-D with a-Si panels. Two separate disposal processes are additionally shown for each system. The impact results are internally normalized using division by the maximum impact value per impact category.

In both S1 and S2, the OPV panels have lower environmental and human health impacts compared to their silicon counterparts. In S1, OPV-D (with incineration) impacts ranged from 96% lower for water depletion to 40% lower for freshwater eutrophication, with the exception that metal depletion was approximately 21% greater for OPV-D mainly due to upstream demands of producing tin for the FTO electrode (Appendix: Chapter 4).

The OPV-D impact in S2 ranged from 92% lower for marine eutrophication to 56% lower for freshwater ecotoxicity compared with a-Si. In S2, the relative decrease between OPV and the silicon-based PV was more pronounced than in S1. The reason for the differences in OPV's relative impacts between S1 and S2 are in part explained by the different use phases. The use phase of S1 is 5-times longer than S2 (i.e. 25 years versus 5 years). Therefore, given the assumed 5-year OPV lifetime, there was a need to replace "exhausted" OPV panels many times over during the 25-year use-phase of S1. This contrasts with S2 which did not require replacements over the 5-year use-phase and thus the environmental and human health impacts were comparatively much lower for the portable charger compared with the rooftop setting. This is similar to the findings of Espinosa et al. where, on average, the majority of the cradle-to-grave impacts from their "solar-park" (duration 35 years) were due to the production and disposal of the panels themselves.[62] In that study, OPV-specific contributions were, for example, more than 90% for resource depletion, non-cancerous human toxicity and freshwater toxicity. However, in some cases the OPV-specific contributions were less than 50%, as was seen with particulate matter formation and ionizing radiation. Those authors ultimately attribute many of these high OPV-specific impacts to the production of silver electrode and its associated upstream processing and production. On the contrary, a 2014 study by Espinosa et al. reported that various on-land and offshore solar-array configurations contained support structures that were roughly 50% of the total CED. In the case of a balloon system, over 75% of the CED was due to components other than the OPV panel. Thus, use phase contributions to overall environmental and human health impacts over the OPV life-cycle should not be underestimated.

The results of this current chapter were mostly uniform regardless of the disposal route (i.e. incineration versus landfill). This was particularly true for S1 but not for S2, which had more noticeable impact reductions for incineration due to the added value of incinerating the plastic casing along with the OPV panel. It should be noted that climate change impacts for OPV-D were 3% (S1) and 16% (S2) greater when they are incinerated compared with when they are landfilled. This is a necessary consequence of combustion of the plastic components which were converted wholly into CO_2 during the process.

Specifically looking at CED results, OPV-D saw reductions of 53% (S1, incineration) and 51% (S2, incineration) over their silicon-based counterparts. Previous studies have demonstrated that cradle-to-gate energy consumption savings for OPV panels can be nearly one-sixth and one-fourth the demand of m-Si and a-Si panels.[140] Roes et al. completed a cradle-to-gate LCA of a flexible OPV cell compared to a m-Si cell and estimated an average decrease of 73% in environmental impacts.[29] Similarly, the findings in Chapter 3 demonstrated average reductions in cradle-to-gate OPV impacts up to 97% and 92% over m-Si and a-Si cells, respectively. The results of the current cradle-to-grave LCA highlight that cradle-to-gate impacts were only part of the picture and that some amount of resource efficiency will be reduced when including the use and end-of-life phases for OPV.

Although the end-of-life options tested in this LCA were only marginally influential on the environmental and human health impacts, this analysis did not include potential effects from recycling of the PV panels. Silicon-based PV may stand to gain the most from recycling since silicon-wafer and panel production were dominant influences on the overall impacts for both m-Si and a-Si (Appendix: Chapter 4). Müller et al., previously reported a nearly 57% reduction in energy consumption for m-Si modules made with recycled silicon wafers.[154] In the context of S1, the reduced cradle-to-gate energy demands reported by Müller et al. could lead to potential CED reductions of 49% for m-Si panels (Appendix: Chapter 4), resulting in a CED of 12,520 MJ. This estimate is just slightly higher than the CED estimate of 11,634 MJ for OPV-D, thus highlighting the potential importance of this end-of-life option. Although CED is not linearly related to the other impact categories,[146] a reasonable assumption would be that many of the other impact categories will also decrease, although at an unknown magnitude. This brings about some uncertainty surrounding the environmental benefits of OPV over conventional panels. Unlike m-Si, no relevant information on potential recycling options for a-Si is found in the literature, and due to its much lower silicon content the feasibility of recycling a-Si is not certain.[152]

Recycling of OPV panels may also provide some environmental and human health benefits, albeit with lower yields compared to silicon PV. Sondergaard et al. demonstrated that use and subsequent recycling of silver for both front and back OPV electrodes may provide a decrease in cradle-to-grave CED for OPV panels by 12%.[147] They estimated a theoretical yield of 95% recycling rate of the original silver content used in the OPV panel. In almost all cases and as should be expected, recycling resulted in lower impacts across all impact categories they reported. This was not the case for climate change potential, however, which was higher than the non-recycling case. This increase in CO_2-equivalent emissions was due to the

energy and nitric acid requirements for isolating and recycling the silver back to an electronic grade state. Furthermore, Espinosa et al. demonstrated the recyclability of both the PET laminate and silver electrodes in OPV panels used in their solar-parks, which led to a 57% average reduction in environmental and human health impacts compared with incineration of the panels.[62] However, these reductions were mainly linked to the recycling of their material choice using silver as an electrode, which in the end is arguably not a material that allows for the scalability OPV technologies.

Using the approach from Espinosa et al.,[62] an estimated 1.7% reduction in the CED for S1 was calculated after inclusion of recycling the PET laminate. Thus, these results contrast with the findings of Espinosa et al. Ultimately, the potential motivation to recycle OPV technologies will depend on the geometry and material selection of the panel, particularly whether they include high valuable materials such as silver electrodes.[62,147]

Energy and Carbon Payback Times

In S1, the EPBT (Table 4-5) for OPV-D panels were 436 days (incineration) and 449 days (landfill).

Table 4-5 Power generation, cumulative energy demand and energy payback time for System 1 (rooftop array) and System 2 (portable charger)

Scenario	Alternative	Wp/m²	Eg (MJ/m²/year)	CED (MJ/m²)	EPBT (Days)	CCE (kg CO_2-eq. /m²)	CPBT (Days)
S1	OPV-D (Incineration)	50	4.88E+02	1.22E+02	436	6.60E+00	192
S1	OPV-D (Landfill)	50	4.88E+02	1.25E+02	449	6.34E+00	185
S1	OPV-D (Incineration, No mount)	50	4.88E+02	9.67E+01	362	5.30E+00	157
S1	OPV-D (Landfill, No mount)	50	4.88E+02	1.00E+02	376	5.05E+00	150
S1	m-Si	210	1.29E+03	3.24E+03	919	1.68E+02	362
S1	m-Si	210	1.29E+03	3.24E+03	918	1.68E+02	363
S2	OPV-D (Incineration)	50	4.88E+02	2.93E+02	220	2.14E+01	118
S2	OPV-D (Landfill)	50	4.88E+02	3.54E+02	265	1.76E+01	97
S2	OPV-NC (Incineration)	50	4.88E+02	5.62E+01	209	2.86E+00	115
S2	OPV-NC (Landfill)	50	4.88E+02	5.98E+01	255	2.61E+00	94
S2	a-Si (Incineration)	128	6.34E+02	1.09E+03	627	6.68E+01	284
S2	a-Si (Landfill)	128	6.34E+02	1.16E+03	666	6.39E+01	271
S2	a-Si-NC (Incineration)	128	6.34E+02	8.55E+02	492	4.85E+01	206
S2	a-Si-NC (Landfill)	128	6.34E+02	8.64E+02	498	4.90E+01	209

Wp: watt-peak | E_g: energy generated | CED: cumulative energy demand | EPBT: energy payback time | CCE: cumulative CO_2-equivalent emissions | CPBT: carbon payback time

These EPBT were approximately 53% and 51% shorter than the m-Si panels. In S2, the EPBT for OPV-D panels were noticeably much shorter at 220 days (incineration) and 265 days (landfill). These EPBT were approximately 65% (incineration) and 60% (landfill) shorter than the a-Si panels. As previously explained for other impacts in this chapter, it is likely that the EPBT for S1 were much higher due to the influence of having to replace the OPV-D panels every five years over 25 years. Additionally, a negative consequence of the energy production from incineration of the (mostly) plastic OPV-D panels could be seen by the shortened EPBT compared with landfilling. This effect was also slightly more influential in S2 due to the added amount of incinerated plastic from the casing materials, since those were assumed to follow the same end-of-life options as the panels. Although the results demonstrate that default OPV-D panels resulted in a 50%-65% reduction in EPBT compared to silicon panels, they were much higher than the payback-times previously seen for cradle-to-gate production of the panel alone which are on the order of days to weeks (Chapter 3).[29,38,128,146,149] This is in part due to the greater scope of this current chapter which evaluates the use and end-of-life phases, but also that previous studies calculated the EPBT and CPBT for regions with higher insolation values (e.g. Southern European conditions).

In S1, the CPBT for OPV-D panels were 192 days (incineration) and 185 days (landfill), approximately 47% and 50% shorter than the m-Si panels, respectively (Table 4-5). Similar to the EPBT, the CPBTs for S2 were also shorter at 118 days (incineration) and 98 days (landfill). These CPBT were approximately 59% and 64% shorter than the a-Si panels. It should be noted that the CPBT rose slightly for incineration of OPV panels due to direct releases of CO_2 from combustion of the plastic components of the panel as discussed previously for the results of the climate change potential.

It should be noted that payback times calculated for S2 were purely theoretical measurements assuming chargers were consistently exposed to the sun under typical 24-hour patterns of light/dark 365 days per year. However, products like solar chargers are not intended to be an alternative energy supply but instead are a commodity. In reality, these chargers will be much less utilized by a consumer (i.e. compared with solar rooftop arrays) and in actuality EPBT will depend on the individual pattern of use by the consumer. To demonstrate this trade-off, a hypothetical example is presented whereby each PV was used to charge a typical 1.2 amps, 5-volt cell phone battery. It was assumed that the consumer used the portable charger five times (full-charging cycle) per week and that the charging cycle had a duration of two hours. Given these technical specifications and usage patterns, OPV-D consumer-adjusted EPBT of 5.3 years (incineration) and 6.3 years (landfill) would be expected, an increase of nearly 850% over the

default OPV scenario (Appendix: Chapter 4). This was still 68% and 63% shorter than a-Si's 15.4-year (incineration) and 16.3-year (landfill) consumer-adjusted EPBT, respectively. Similarly, the OPV-D CPBT increased to 2.82 (incineration) and 2.3 (landfill) years compared to the default scenario (Appendix: Chapter 4). The CPBT of a-Si increased to 7.02 (incineration) and 6.68 (landfill).

Minimum Required Lifetime of Organic Photovoltaics

The minimum required lifetimes for S1 are listed in Table 4-6.

Table 4-6 Minimum required lifetimes (in years) of the default organic photovoltaic scenario for System 1 (rooftop array) and System 2 (portable charger) compared to their respective silicon-based photovoltaic counterparts

	Scenario 1				**Scenario 2**			
	OPV-D (Incineration)	**OPV-D (Landfill)**	**OPV-D (Incineration, No Mount)**	**OPV-D (Landfill, No Mount)**	**OPV-D (Incineration)**	**OPV-D (Landfill)**	**OPV-NC (Incineration)**	**OPV-NC (Landfill)**
Agricultural land occupation	0.3	0.3	0.3	0.4	0.26	0.29	0.24	0.26
Climate change potential	1.6	1.5	1.5	1.3	0.41	0.36	0.37	0.33
Fossil depletion	1.7	1.8	1.6	1.6	0.47	0.51	0.43	0.45
Freshwater ecotoxicity	0.2	0.2	0.2	0.2	0.95	0.97	0.85	0.86
Freshwater eutrophication	1.9	2.1	1.7	1.9	0.45	0.50	0.44	0.47
Human toxicity	0.4	0.4	0.3	0.3	0.58	0.60	0.54	0.55
Ionizing radiation	1.5	1.8	1.5	1.7	0.46	0.54	0.45	0.51
Marine eutrophication	0.5	1.6	0.4	1.5	0.08	1.18	0.24	0.79
Metal depletion	11.4	11.4	6.0	6.0	0.58	0.59	0.58	0.58
Natural land transformation	1.2	1.2	1.0	1.1	0.43	0.44	0.41	0.42
Ozone depletion	1.0	1.0	0.6	0.7	0.60	0.67	0.55	0.58
Particulate matter formation	1.7	1.8	1.5	1.6	0.27	0.29	0.26	0.27
Photochemical oxidant formation	0.9	0.9	0.8	0.8	0.16	0.34	0.31	0.31
Terrestrial acidification	1.6	1.7	1.4	1.5	0.22	0.24	0.21	0.22
Urban land occupation	1.3	1.5	0.9	1.0	0.15	0.27	0.15	0.16
Water depletion	0.2	0.2	0.2	0.2	0.34	0.39	0.34	0.38
Cumulative energy demand	1.5	1.6	1.4	1.5	0.39	0.44	0.41	0.43
Average	*1.5*	*1.6*	*1.1*	*1.2*	*0.46*	*0.55*	*0.44*	*0.48*

Minimum required lifetimes ranged from a low of 0.01 years (freshwater ecotoxicity) to 11.4 years (metal depletion), with an average 1.4 years when considering incineration. These results indicate that in order for metal depletion OPV-D impacts to not exceed the impacts of m-Si, the OPV-D panels should have a lifetime of 9.8 years. Results of landfilling the panels were nearly identical, with an average minimum

required lifetime of 1.6 years. The lifetime values for S2 averaged 0.46 years (incineration) and 0.55 years (landfill), while specifically for incineration they were as low as 0.08 years (marine eutrophication) and as high as of 0.9 years (freshwater ecotoxicity). For landfilling, the minimum required lifetime was lowest for terrestrial acidification at 0.24 years, however it was highest at 1.18 years for marine eutrophication due to associated landfilling activities and processes leading to nitrate releases in the environment. The impacts of marine eutrophication were landfill-specific impacts that would have occurred irrespective of the type of material discarded.

These overall minimum require lifetimes are encouraging for OPV development given that experimental maximum lifetimes for this technology have surpassed all the results reported for S2 and have started to approach the upper bound minimum required lifetime values for S1.[56] However, it should be noted that these results are based on the assumed OPV efficiency of 5%. In the next section, this assumption is challenged against a range of different efficiencies as well as different lifetimes to better understand the influences these assumptions have on the overall environmental and human health impacts of OPV systems.

Influence of Lifetimes and Efficiencies on LCA Results

The influence from assumed OPV panel lifetimes ranging between one to nine years is shown in Figure 4-4.

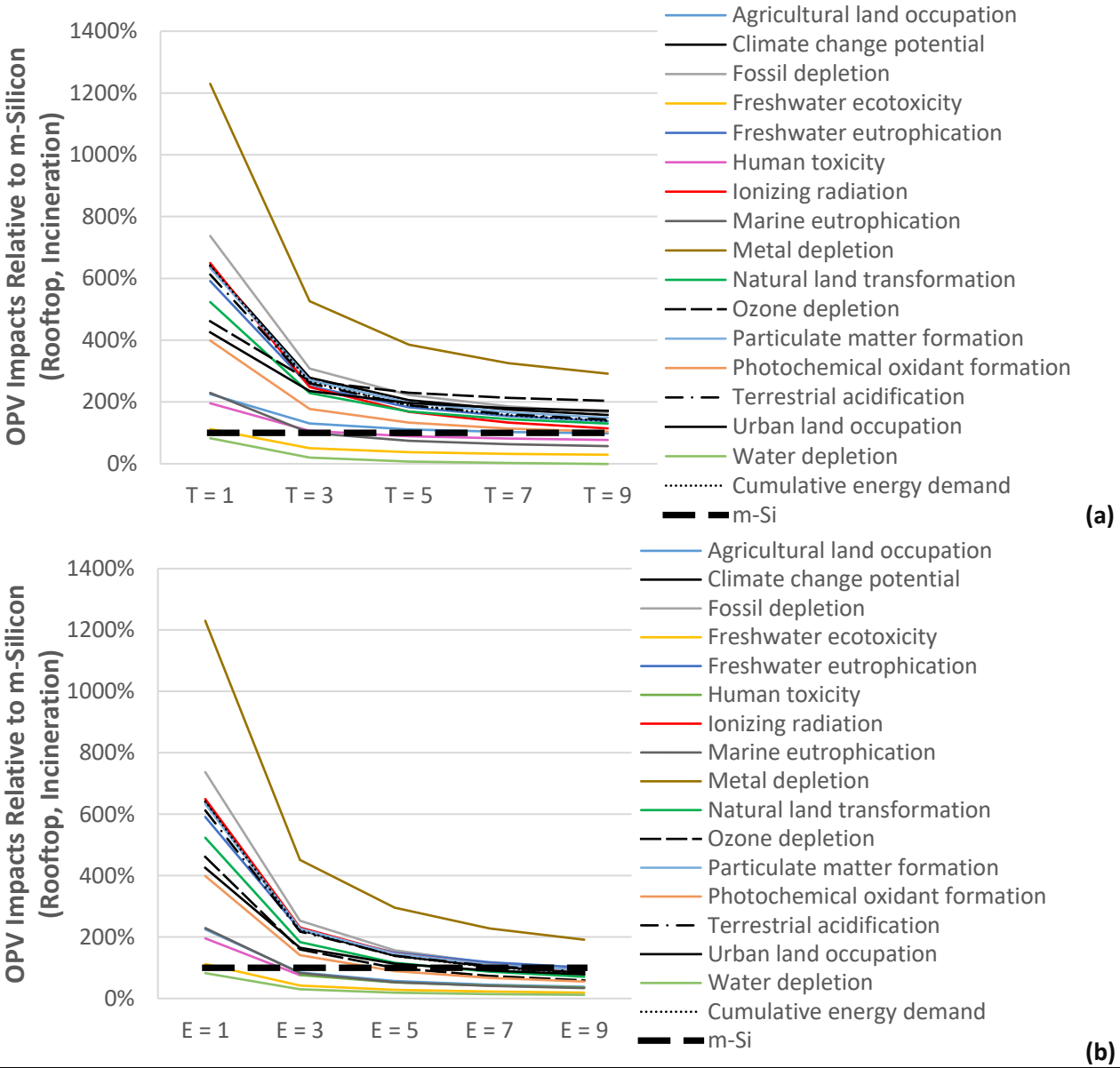

Figure 4-4 Changes in life-cycle impacts for S1 (rooftop, incineration) according to forecasts in (a) lifetime of organic photovoltaic panels (with a 1% efficiency) and (b) efficiencies of organic photovoltaic panels (with a 1-year lifetime). The impact results are internally normalized to the impact values of m-Si (i.e. m-Si's impacts are set at 100%). See Appendix: Chapter 4 for the sensitivity analysis for S1 with landfilling as the end-of-life option.

The time-sensitivity was calculated for an OPV device with a 1% efficiency. The increase in lifetime from one to three years resulted in an initial, sharp decrease in environmental and human health impacts which then leveled off beyond three years. At the maximum lifetime tested of nine years, nine of 17 OPD-D

impacts, including climate change potential and CED remained proportionally higher than m-Si. Accordingly, the EPBT and CPBT never fell below that of m-Si. The EPBT ranged from a high of 16 years for panel lifetimes of one year to a low of 3.5 years for lifetimes of nine years, while the CPBT ranged from a high of 6.4 years to a low of 1.6 years, respectively. The results of increasing the efficiencies against a constant lifetime of one year were additionally tested. A similar trend was observed where increases in the efficiency from 1-3% was correlated with an initial sharp decrease in environmental and human health impacts (Figure 4-4). Beyond 3%, the impact reductions began to level off but not as sharply as in the case of the lifetime sensitivity. Thus, at efficiencies of 9% only metal depletion remained proportionally higher than m-Si. In particular, the CED and climate change potential were 18% and 16% lower than m-Si, with an EPBT and CPBT of 2.1 years and 305 days, respectively.

The trends in S2 were similar to S1 (Figure 4-5).

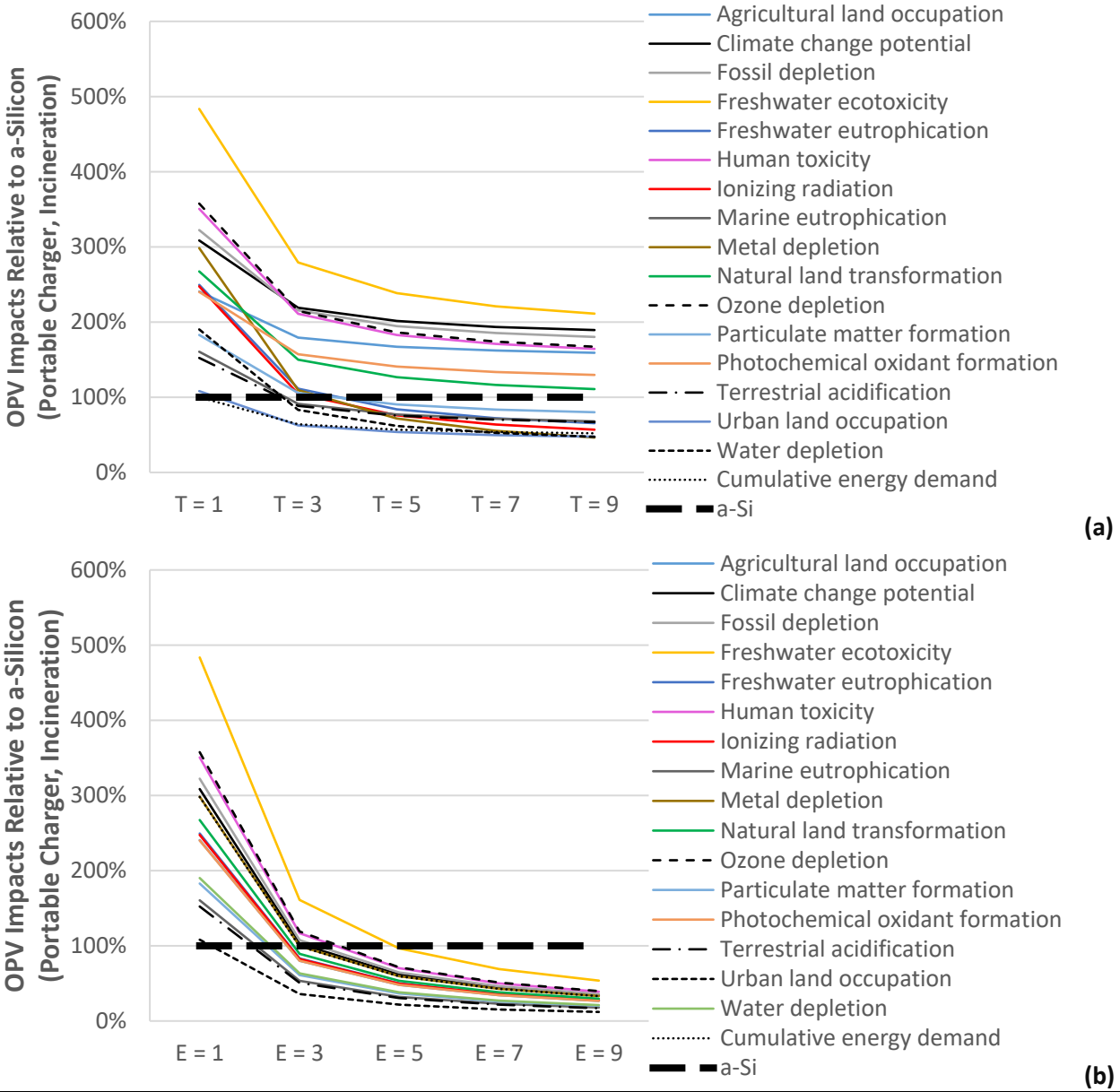

Figure 4-5 Changes in life-cycle impacts for System 2 (portable charger, incineration) according to forecasts in (a) lifetime of organic photovoltaic panels (with a 1% efficiency) and (b) efficiencies of organic photovoltaic panels (with a 1-year lifetime). The impact results are internally normalized to the impact values of a-Si (i.e. a-Si's impacts are set at 100%). See Appendix: Chapter 4 for the sensitivity analysis for System 2 with landfilling as the end-of-life option.

The increase in lifetime from one to three years also resulted in an initial, sharp decrease which then leveled off beyond 3 years. At the maximum lifetime tested of nine years, seven of the 17 impacts, including CED and climate change potential remained higher than a-Si. This resulted in EPBT and CPBT of

2.8 years and 1.5 years, respectively, which remained higher than a-Si. In contrast, the effects of increasing the efficiency resulted in a sharper and slightly more sustained decrease when moving from 1-9% efficiency (Figure 4-5). By 3% efficiency, over half of the OPV-D environmental and human health impacts were less than a-Si and by 5% all impacts were lower than a-Si. This means that by an efficiency of 5% the EPBT and CPBT were lower than that of a-Si. At an efficiency of 9% the EPBT and CPBT were 215 days and 101 days, respectively.

These results indicate that there might be more value in trying to achieve greater efficiencies than greater lifetimes. This is because with greater efficiencies, the PV panels become smaller in size per power output and thus require smaller amounts of materials for producing the framing structure (S1) or casing materials (S2). However, the same is not true for increasing the lifetime (i.e. the same amount of framing structure or casing materials are always needed). Moreover, due to the additional components in S1 that are not influenced by efficiency (e.g. inverter), there will be points at which further efforts to increase lifetimes and/or efficiencies level off without further improvement even with increasing effort to increase these characteristics. It should be noted that these results only test the *assumption* of the lifetime and efficiency of the currently envisioned OPV panels and do not attempt to account for material changes and/or production manufacturing differences. For example, reductions in the EPBT based on forecasted OPV efficiency gains may not always prove to have a direct relationship as moderate gains in efficiency may come at the expense of significant changes in embodied energy, materials consumed and pollutants emitted during production.[149,151]

Impacts by Life-Cycle Stage

For S1, there was a general trend that the BOS components such as the mounting structure and inverter where the major contributing factors to the environmental and human health impacts. For the scenario including incineration, the BOS contributed from 15% of the water depletion impacts up to 87% of the agricultural land occupation. In particular, the BOS accounted for 54% and 57% of the CED and climate change potential, respectively (Appendix: Chapter 4). Specifically, the mounting structure and inverter contributed 61% and 12% of the CED, while they contributed 63% and 13% of the climate change potential, respectively. Unlike an inverter that is always required for the use-phase of S1, a mounting structure is arguably questionable. Conceivably the OPV panels could themselves be directly placed on the roofing's surface.

Figure 4-6 displays the results for S1 when no mounting structure was used during the use phase. Impacts were reduced overall, with reductions over the default scenario ranging from 13% for metal depletion to 93% for water depletion.

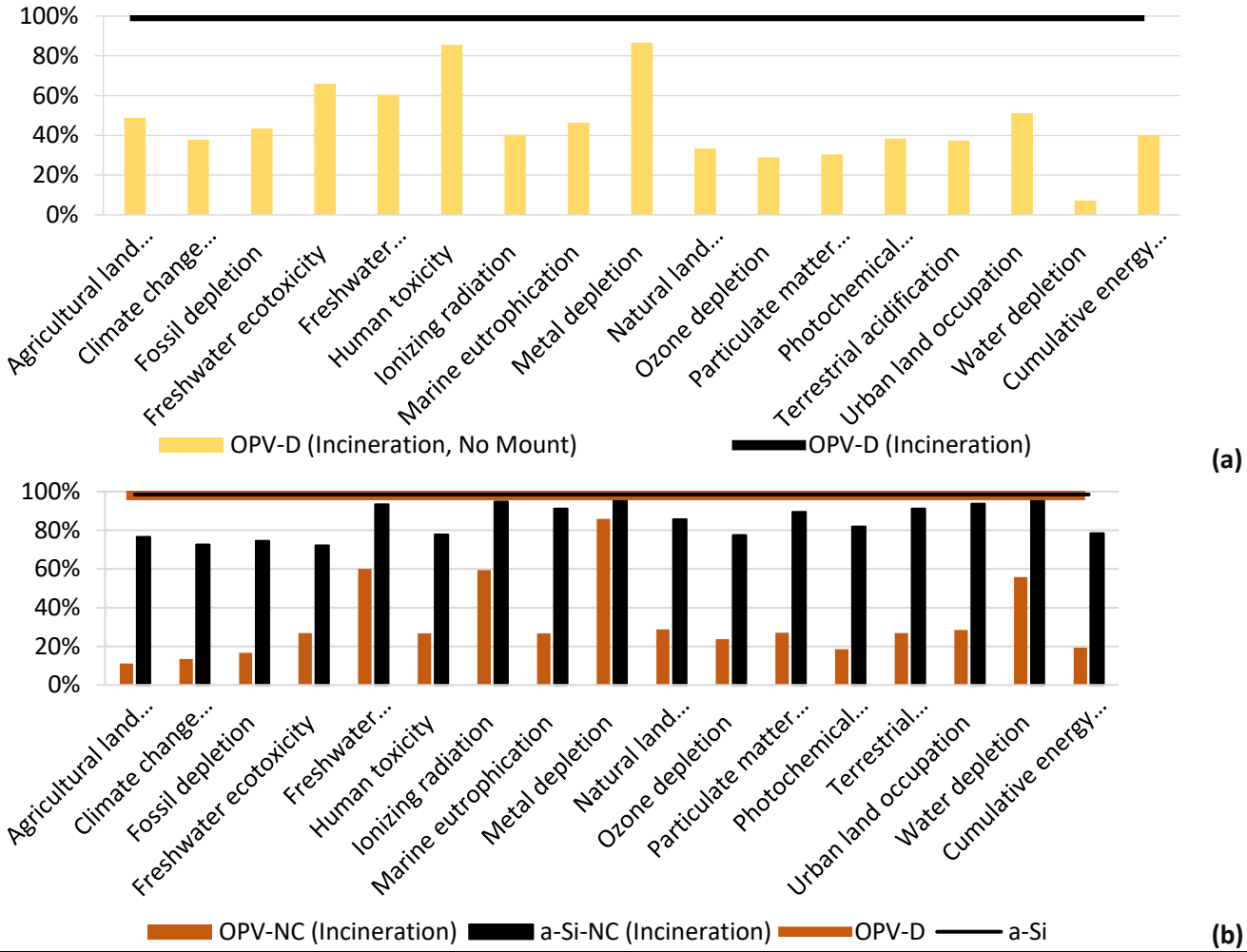

Figure 4-6 Comparison of organic photovoltaic alternatives for (a) System 1 that involved removing the mounting structure (No Mount) and (b) System 2 based on portable chargers without casing (NC). The impact results in System 1 are all internally normalized to OPV-D as the maximum value (i.e. 100%). The impact results in System 2 are internally normalized by technology-type (i.e. OPV-NC is normalized by OPV-D and a-Si-NC is normalized by a-Si). See Appendix: Chapter 4 for the results of the landfilling options.

The greater decreases in ozone depletion potential, for example, were a consequence of eliminating the energy demand and aluminum oxide production (including aluminum mining) that would be consumed for the aluminum components. Furthermore, removing the mounting structure resulted in a 17% decrease in EPBT to 362 (incineration) and 376 days (landfill) over the default OPV-D scenario. Similarly, the CPBT decreased by 18% to 157 days (incineration) and 150 days (landfill).

For S2, a similar trend was seen where the casing material heavily dominated the impacts for the OPV-D panels. Overall, the casing contributed from 21% of the metal depletion up to 91% of the photochemical oxidant formation potential in the incineration scenario. Alternatively, S2 could be envisioned without the need for external casing to protect the portable charger, for both the OPV-D and a-Si panels. Direct comparisons of the OPV (OPV-NC) and a-Si panels without casing (a-Si-NC) showed more pronounced decreases for the OPV-NC panels compared to a-Si-NC in contrast to the relative decreases found when both panels had casing. This is because a-Si impacts depend more on the contribution from the panel itself as opposed to the casing. A highly noticeable finding was the EPBT for OPV-NC panels that were on the order of 42 days (incineration) and 45 days (landfill) in total. Similarly, the CPBT for this technology decreased to 16 days and 14 days, respectively.

The high impact contribution from the BOS for OPV-D panels contrasts with the m-Si panels, whose environmental and human health impacts were most heavily influenced by production of the solar cell itself (Appendix: Chapter 4). This was somewhat expected knowing that the production of OPV-D panels is much less impactful on a watt-per-watt basis, compared with m-Si panels.[146] However, these results were also dependent on the expected lifetime of the OPV-D panels. For instance, Epsinosa et al. found that the majority of the environmental and human health impacts from their OPV "solar-park" resulted from the production of the panels themselves,[62] whose lifetimes were estimated at one year compared to the default scenario of five years in this chapter. In contrast, S2 saw a decrease in the contribution arising from the production of the OPV-D panel itself. As discussed previously, S1 required that the OPV-D panels be replaced every five years, leading to a greater contribution of the panels themselves to the overall results. The shorter use-phase of S2 resulted in a situation where such replacements were not necessary and thus the impacts from the panels had diminished.

Conclusion

As was demonstrated in Chapter 3, the production of OPV panels (i.e. cradle-to-gate analysis) have shown greater resource efficiencies and lower environmental hazards compared to conventional silicon-based PV. The findings of the current chapter demonstrate that these potential advantages remain after including the use and end-of-life stages, albeit at a lower relative value. Obvious uncertainties remain regarding the assumed lifetimes and efficiencies that will be achieved at the industrial scale. Increasing both are necessary to reducing the environmental and human health impacts of this technology, however there is a non-linear relationship between lifetimes or efficiencies and impacts changes across the life-

cycle. This is a consequence of the use-phase application setting which dictates what other contributing factors (i.e. auxiliary components other than the panel itself) will exist in the production, use and end-of-life phases.

The current results suggest that OPV are a preferred energy producing technology compared with silicon-based PV from an environmental and human health perspective, particularly for uses where the product lifetime is relatively short (i.e. < 5 years) or where product systems are extremely simplified. This latter point was reflected in the LCA results for the solar rooftop array (S1) that had no mounting structure and the portable charger (S2) that had no case. This was also noticeable based on the quicker EPBT and CPBT for S2 compared with S1. Additionally, there may be important sources of uncertainty for the silicon panels as well. Although m-Si and a-Si are much more mature technologies, advances in silicon-cell technology at the lab-scale still continue.[15] However, their influence on the average market silicon-module efficiency is not yet apparent.[22] Moreover, as more 1st-generation silicon panels come to their end of serviceable life, the switch to full-scale silicon recycling could have a greater impact on the environmental profile of that technology compared with incremental adjustments to the efficiencies and lifetimes.

Chapter 5 Options for Assessing the Toxicological Impacts from Engineered Nanomaterials Use in Organic Photovoltaics

Toxicological Hazards of Organic Photovoltaics

An element missing from the LCA results presented in Chapter 3 and Chapter 4 was any estimation of ENM emissions and calculation of their human- and/or eco-toxicological impacts. There are only a few principle components of most PV, and for OPV these are generally the front electrode, back electrode, active layer, and the substrate. Additional components might include a hole transport layer, electron transport layer, UV-blockers, coatings, barriers and/or optical spacers, for example. To achieve the thinness that is characteristic of OPV, these layers must contain very little material in extremely thin layers on the orders of tens to hundreds of nanometers. Consequently, the materials used often will be on the nanometer size range. In the OPV device considered throughout this thesis, PCBM nanoparticles were used in the active layer and TiO_2 nanoparticles used as the optical spacer (Figure 3-1). While the previously reviewed OPV-LCA studies discussed in Chapter 1 have calculated the material and energy consumption during ENM production and OPV manufacturing, there was no estimation of any ENM emissions during their production, manufacture of the OPV panel, use nor end-of-life (Table 5-1).

Table 5-1 Consideration of nanomaterial-specific emissions and impacts across the previously published life-cycle assessments on organic photovoltaics

Individual Case Studies	Year	Energy and Material Flows During ENM Production	ENM Emissions	ENM Human- or Eco-tox Impacts
Roes et al.[29]	2009	●	○	○
Garcia-Valverde et al.[30]	2010	●	○	○
Espinosa et al.[31]	2011	●	○	○
Espinosa et al.[36]	2011	●	○	○
Espinosa et al.[37]	2012	●	○	○
Espinosa et al.[38]s	2012	●	○	○
Yue et al.[39]	2012	●	○	○
Emmott et al.[40]	2012	●	○	○
Espinosa et al.[41]	2013	●	○	○
Anctil et al.[42]	2013	●	○	○
Espinosa and Krebs[155]	2014	●	○	○
Espinosa et al.[24]	2014	●	○	○
Sondergaard et al.[147]	2014	●	○	○
Espinosa et al.[62]	2015	●	○	○
Sandwell et al.[156]	2016	●	○	○
Hengevoss et al.[157]	2016	●	○	○

Since the initial review up to the end of 2013, six additional OPV-LCA have been published, each without any estimation of ENM release along the life-cycle. Thus, toxicological hazards[158–162] resulting from ENM emissions have not been adequately assessed in the OPV-LCA literature nor in the prior case studies presented in Chapter 3 and Chapter 4. To avoid burden shifting and possible false assumptions about the human health impacts of OPV technologies, data and methodological adaptations in LCA are currently needed or other tools need to be used to address these issues.

Engineered Nanomaterials: Resource Efficiencies and Hazards

ENM are loosely defined as materials having a single dimension at or below 100 nanometers (nm) and generally in the range of 1-100 nm.[163] In the regulatory context, the European Commission defines ENM as intentionally produced materials in which at least 50% of the primary particles, aggregates and/or agglomerates have one or more external dimensions between 1-100 nm.[164] To put this in perspective, a human hair is roughly 100,000 nm in diameter, a single bacterium can be 2,500 nm in length, and DNA has a diameter of 2.5 nm. At the nanometer size range, there are new possible applications ranging from use in pharmaceuticals and agriculture to textile and energy sectors.[165] Use and production of ENM is also expected to assist in environmental protections, produce jobs and increase economic growth.[166,167] Apart from being manufactured at size ranges that are much smaller than their bulk counterparts, ENM can take on distinct shapes (e.g. fibers) and embodiments (e.g. coated materials). ENM are not only defined physically but by their distinct properties and behaviors. For instance, as materials decrease in size, their surface area to volume ratio increases to the point where surface-dominated properties are enhanced and potentially new physico-chemical properties may appear compared with micro-scale materials.[168] Thus, materials that are assumed to be inert or unreactive in their bulk-sizes, such as carbon, may take on greater abilities, such as C_{60}-fullerenes acting as a semi-conductor. ENM are also foreseen to lead to more efficient chemical reactions and industrial processes, reducing energy consumption and avoiding waste production.[74,169] Thus, many 3rd-generation PV have been exploiting ENM properties to achieve smaller, more efficient PV devices than were previously possible.

Coincidentally, the same physico-chemical characteristics leading to enhanced material properties, technological advantages and resource efficiencies may also introduce environmental and human health hazards[170–173] resulting from intentional and/or unintentional releases of ENM across the OPV life-cycle.[174,175] In the last two decades there has been tremendous growth in ‘nanotoxicology’ publications (Figure 5-1), driven by concerns that ENM may present new toxicological challenges compared to their

bulk or non-particulate counterparts.[158–161,170,176–178] At the same time, regulatory frameworks may require that companies collect and submit health and safety data to governmental bodies if their products fall under the definition of an ENM.[179–181]

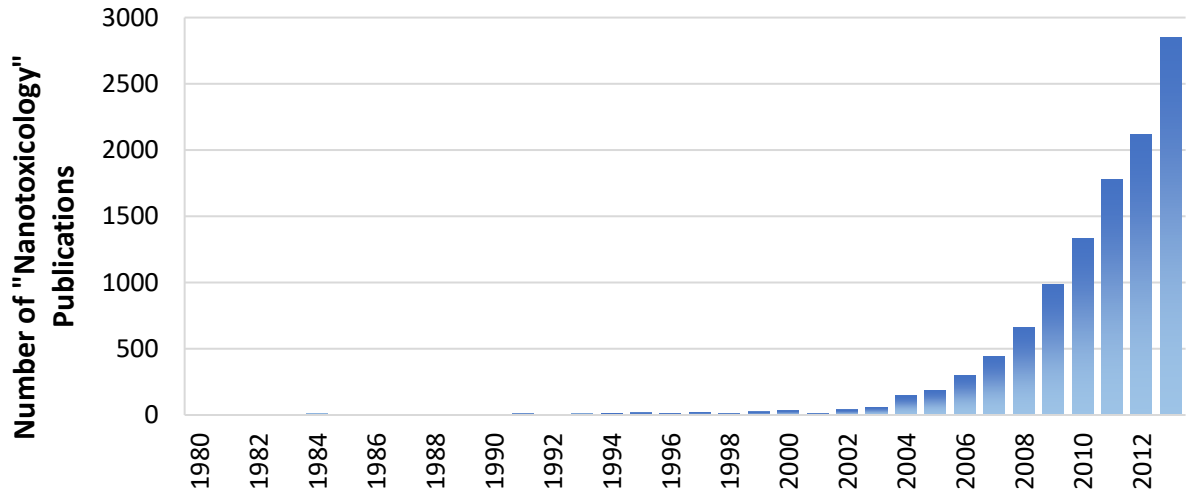

Figure 5-1 Number of publications between 1980-2013 that match the search criteria of "nanotoxicology" (Adapted from H. F. Krug 2014.[182]).

Life-Cycle Impact Assessment: Hazards and Impacts

LCA, in theory, can be applied to ENM-related products The first formal promulgation of using LCA for ENM-related technologies came during a 2006 workshop titled *Nanotechnology and Life Cycle Assessment*,[183] where it was acknowledged that "[LCA] is fully suitable to nanomaterials and [ENM]-products." In practice however, few *complete* ENM-related LCA studies, including those listed in Table 1-1, have been published, particularly those whose system boundaries are cradle-to-grave such as is depicted in Figure 5-2.[184]

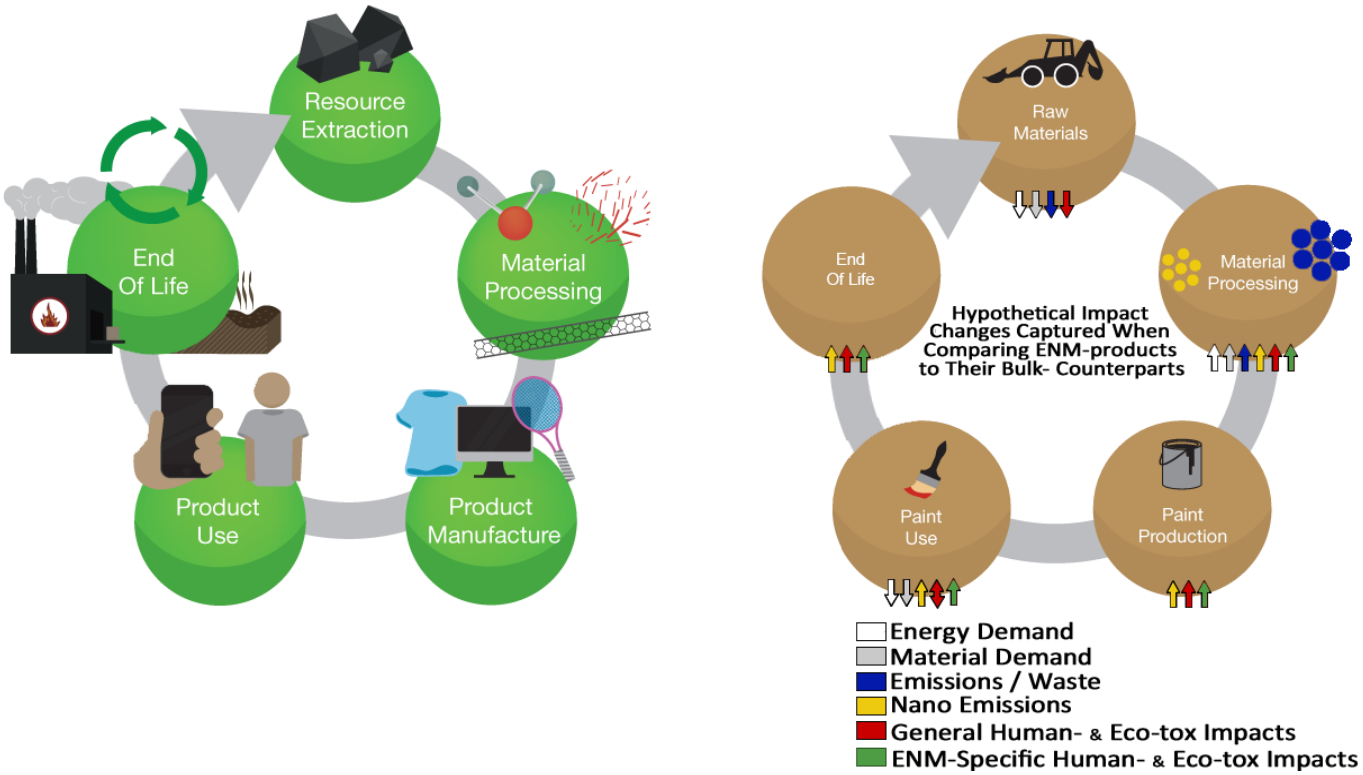

Figure 5-2 Consideration of life-cycle resource consumption and waste emissions using a generic nanotechnology example. The left side of the figure (a) provides a generalization about the considerations during life-cycle assessments of ENM-enabled products. Resource extraction and material processing would involve all relevant materials to the intended product but also those that are ENM-specific (i.e. extraction of the ENM precursor and processing it into the nanometer size range). Product manufacturing will outline the production of a single type of product (e.g. sporting equipment with carbon nanotubes) leading to its related use and potential end-of-life options (e.g. incineration). The right side of the figure (b) represents a hypothetical example of a ENM-enabled versus non-ENM (bulk) product applied in the function of wall-protection (i.e. a paint with a conventional pigment versus a paint using ENM-based pigments). In this example, it is assumed that the two pigments (i) are of the same chemical composition but different sizes, (ii) ENM- versus bulk-manufacturing differ by the energy and materials (e.g. solvents) required to mechanically grind bulk material to ENM-sizes, (iii) due to its higher efficiency, less ENM-enabled material is required during the use-phase and thus less upstream raw material extraction is required and (iv) although less active ingredient is emitted during the use phase, it is distinct that it is being emitted in the ENM form as opposed to bulk emissions. The difference in energy consumption, material use, waste generation and emissions depicted by up/down arrows represent the relative life-cycle inventory of the ENM-enabled product (with up designating the ENM-enabled amounts are higher and vice versa but without any indication of the magnitude of change). Aggregation of all inventory values would then relate to their potential environmental impacts via its material specific characterization factor.

The gap in published literature is due to a lack of databases that contain ENM-specific life-cycle inventories for describing the material and energy inputs and waste outputs during production, but also due to the lack of life-cycle impact assessment methodologies that are able to characterize ENM-specific fate, exposure and human health impacts.[184–188]

In regards to the emissions, there have been some attempts to model and calculate major environmental ENM flows leading from the production[189–191] but also the use[192–194] and disposal of these materials.[195] These approaches and models can be used to estimate average, global ENM emissions that might be used to create foreground life-cycle inventory emissions data of ENM-related products and processes. To be useful in LCA, each ENM emission must contain a corresponding characterization factor (CF_{NS}) that converts its emission into a potential environmental or human health impact.

There are a handful of published papers that have made first approximations to model ENM fate, exposure and toxicity within LCA.[93–96] Those first approximations include one for human health[93] and three[ii] for ecotoxicity CF for nanomaterials.[94–96] In each case, the authors modified existing CF in USEtox to make them ENM-specific. Currently existing life-cycle impact assessment methods, such as USEtox, take advantage of a number of assumptions that conveniently describe the fate and transport of small organic molecules and metals quite well, but these methods are not appropriate for ENM or similarly described colloidal materials.[196] The major assumptions utilized in life-cycle impact assessment methods are that conditions are at steady-state and systems have reached thermodynamic equilibrium.[101,197] Consequently, these models assume that there are no changes in concentration of the pollutant over time and that the fate of these pollutants can be estimated using (equilibrium) partition coefficients (e.g. octanol-water partition coefficient, K_{ow}). These coefficients are defined by the ratio of the resulting pollutant concentration in one medium versus another (e.g. octanol versus water), once the system involving both mediums has achieved equilibrium.

However, when released into a specific medium, ENM exist in their own phase and do not form uniform phases with the surrounding medium unlike organics. Therefore, and by definition, ENM are not thermodynamically stable, even if certain ENM may be *kinetically* stable for long periods of time.[196] In other words, an ENM concentration ratio between two mediums cannot be predicted from a previously measured partition coefficient if conditions were not exactly the same between the two scenarios.[196] This is because the behavior of ENM in the environment are heavily concentration dependent (i.e. the initial conditions of , the amount of ENM in, and the time at which the system is measured will produce different results).[95,196] Thus, in place of equilibrium partition coefficients, ENM should be described kinetically using dynamic fate and exposure models. For example, such models might employ the use of first-order rate

[ii]Walser et al indirectly calculated the impacts from nanosilver by using experimentally derived bioavailable fraction values to estimate the amount of ionic silver released during use and disposal. The applied characterization factor was thus, technically not specific for nanosilver but for ionic silver.

constants to describe the dissolution of ENM into ions in the water column.[198] Furthermore, steady-state models are also not in agreement with the fact that ENM emissions rates are not typically constant events. This is particularly true for indoor, occupational scenarios.[199,200] Instead, ENM emissions are likely to be episodic, further influencing the concentration in the environment and the concentration-dependent transformations specific to that material. Lastly, the exposure to ENM, and specifically inhalation of ENM, will present concentration-dependent mechanisms for deposition, clearance and retention in the lung. That is, inhalation of ENM is not only dependent on the inhalation rate of the individual who is exposed[201] but also the ENM characteristics, biological mechanisms and time at which exposure is measured.[202] It has been proposed to use a ENM-specific retention factor, *R*, for such purposes, calculated using human airway lung deposition and clearance models such as the Multiple-Path Particle Dosimetry (MPPD) model .[97] The MPPD model is a tool typically used in HHRA for determining the internal lung dose from exposure to airborne concentrations of chemicals and particulates. However, the current MPPD model does not allow for estimating deposition or clearance while using exposure conditions that change over time.

Review of Previously Published Characterization Factors for Engineered Nanomaterials

In previously published CF_{NS}, Eckelman et al.[94] estimated the fate and exposure of carbon nanotubes in the environment using empirically derived values for the partition coefficients already used in USEtox such as the octanol-water partition coefficient, Henry's law coefficient, and bioaccumulation factor in fish, for example. In addition, they added a parameter for aggregation and sedimentation that was reported as a deterministic fraction of the carbon nanotubes that are removed from the freshwater. Eckelman et al. report a worst-case and realistic set of results, in which the worst-case fate calculation resulted in a residence time of carbon nanotubes in water of 143 days. Under more "realistic" conditions in which aggregation and sedimentation are considered, the residence time decreased to several days. Their estimation of the exposure calculated as a percentage of the total concentration of carbon nanotubes in water according to the USEtox procedure, resulted in 100% exposure in the worst-case scenario and 98% in the realistic scenario. The resulting CF_{NS} were 29,000 and 3,700 potentially affected fraction of species per kg of emitted carbon nanotubes in the worst- and realistic-case scenarios, respectively.

Miseljik and Olsen[96] presented a simplified USEtox fate calculation by artificially defining the residence time of nanoparticles of silver (nano-Ag) and TiO_2 as one day. This was conceived on a quasi-kinetic basis representing the residence time given aggregation and sedimentation of these materials in freshwater systems. However, this kinetic parameter was ultimately used inside of a steady-state model, as was done

in Eckelman et al.[96] These authors assumed an exposure factor of one in lieu of considering differences between external concentrations and uptake by the species. The resulting CF_{NS} for nano-Ag and TiO_2 were 8,573 and 26.2 potentially affected fraction of species per kg of emitted nanomaterial, respectively. Given the fate and exposure calculations were identical for both silver and TiO_2, the differences in the CF_{NS} resulted from their respective eco-toxicity dose-response relationships, whereby nano-Ag were found to be much more toxic than nano-TiO_2.

Salieri et al.[95] defined their fate factor for nano-TiO_2 using properly defined kinetic descriptors of fate and transport, unlike the two previous studies. Although, the fate factor was employed inside of a steady-state model like the two previous studies. Specifically, Salieri et al. considered the ENM-specific transformation processes of dissolution, homo-aggregation and hetero-aggregation, and sedimentation velocity inside of a freshwater and sediment compartmental model. The results of their fate calculations showed that the residence time for nano-TiO_2 in freshwater was quite short, ranging from 0.1 days for 8 nm diameter particles to 0.001 days for 400 nm diameter particles. Such residence times are much shorter than the previously reported values of Eckelman et al. and Miseljik and Olsen, showing the potential importance of ENM-specific kinetic parameters in the calculation of fate and transport in life-cycle impact assessment models. Their reported fate and transport calculations were combined with a worst-case exposure factor of 1, citing no known knowledge about describing the bioaccumulation and bioavailability of ENM by freshwater species.[95] After creating a weighted-average residence time for nano-TiO_2, the resulting CF_{NS} was reported as 0.28 potentially affected fraction of species per kg of emitted nano-TiO_2. This value is two-orders of magnitude smaller than what was reported by Miseljik and Olsen for nano-TiO_2. While this difference can be partially explained by the difference in residence times calculated between the two studies, there were also differences in the reported eco-toxicity dose-response relationships. Salieri et al. reported an effective concentration at which 50% of species were effected between 0.013-0.018 kg/m^3, while that of Mislejic and Olsen was reported as 0.019 kg/m^3.

In regards to human health, Pini et al.[93] published a human health CF_{NS} based on the framework of Walser et al.[97] The latter framework introduces the potential use of ENM-specific transformations such as aggregation, agglomeration and gravitational settling for calculating the fate of ENM in the indoor air setting.[97] In the end, the CF_{NS} published by Pini et al. estimated the fate of nano-TiO_2 as a function of advective air flow between the indoor and outdoor air, without the consideration of ENM-specific transformations that were outlined in Walser et al.[93] Pini et al. estimated exposure using a retention factor

in order to account for the fact that particle deposition should not assumed to be 100%. Deposition of particles in the human airway may occur in the upper airway (i.e. nasal and mouth cavities), tracheobronchial region, air-exchange regions and/or the interstitial space, for example. The deposition and ultimate retention is a function of both bulk air movement through the airways but also a function of biological and chemical mechanisms that are responsible for sequestering, relocating and eliminating particles from the body. The retention factor calculated using the MPPD model in Pini et al. was specific for deposition, clearance and final retention under constant, steady-state exposure conditions.[97] However, the exposure to ENM, and specifically inhalation of ENM, will present concentration-dependent mechanisms for deposition, clearance and retention in the lung. That is, inhalation of ENM is not only dependent on the inhalation rate of the individual who is exposed[201] but also the ENM characteristics, biological mechanisms and time at which exposure is measured.[202] Since the current version of the MPPD model does not allow for estimating deposition or clearance while using variable exposure conditions, an alternate approach would need to be used to adapt steady-state models for handling these estimations of exposure.

To summarize, while it is possible – even if challenging – to build life-cycle inventories that estimate and quantify ENM emissions along the OPV life-cycle,[190,192,203,204] currently available life-cycle impact assessment software and methodologies do not contain CF_{NS} that are necessary for quantifying the fate of, exposure to and impacts from those ENM.[187]

Risk Assessment: Hazards and Risks

Risk, in the context of environmental and public health disciplines, is defined as the probability that adverse ecological or human health impact results from exposure to an environmental stressor, which may be any physical, biological or chemical entity. To quantify substance-related risks, a HHRA or ERA must be conducted. In contrast to LCA, the aim of these other tools is to quantify *absolute* values of risk. The National Research Council outlined the basic tenants to a generalized account of risk assessment in their 1983 publication on the subject and which was directly interpreted in this chapter to mean HHRA.[205] The main framework of a HHRA contains four steps: (1) hazard identification, (2) dose-response assessment, (3) exposure assessment, and (4) risk characterization (Figure 5-3).

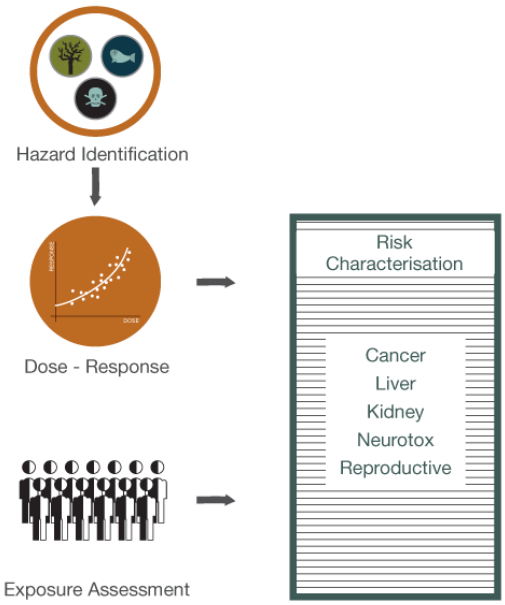

Figure 5-3 Illustration for carrying out a human health risk assessment to determine issues of chemical and substance-specific toxicity. Human health risk assessment involves identifying relevant health hazards, quantifying the critical dose of concern by evaluating the relationship between dose to the substance and toxicological response, estimating the measure of exposure of the receptor (i.e. the individual human) to the substance and calculating the risk involved by comparing the exposure value to the critical dose.

In brief, the hazard assessment involves an observation and determination of substance-specific adverse effects (i.e. hazards), while a dose-response analysis quantitatively characterizes the relationship between the dose or concentration of a substance and the level of adverse effect. The exposure assessment defines exposure scenarios that describe conditions in which a substance (on its own, in a mixture or embedded in an article) is manufactured, handled or used across its life-cycle. The magnitude of exposure is assessed for specified intake routes (e.g. inhalation), either through direct measurements or using models. In risk characterization, estimated exposure doses or concentrations are then compared to a recommended exposure limit (REL) to evaluate potential risk to calculate a risk characterization ratio (RCR) where values greater than or equal to one signify the existence of risk from exposure of to that substance (equation ((5-1)).

$$RCR = \frac{EXP}{REL} \qquad (5\text{-}1)$$

RCR: Risk characterization ratio
EXP: Exposure dose or concentration
REL: Recommended exposure limit

Lastly, an uncertainty analysis is conducted to analyze the level of ambiguity in each step of the HHRA process, pertaining to the quality and/or quantity of the input data and/or the applied models.

Due to the existing regulatory framework governing high-volume, industrial-scale chemicals in commerce, HHRA and ERA are default tools used by scientists, regulators and commercial enterprises that need to ensure the safety of specific chemicals and substances used in their products.[206–208]

In theory, ERA[33] and HHRA[32] could be used on a case-by-case basis to identify whether ENM also pose ecological or human health risks, similar to what is done for regular chemicals (Figure 5-4).[176]

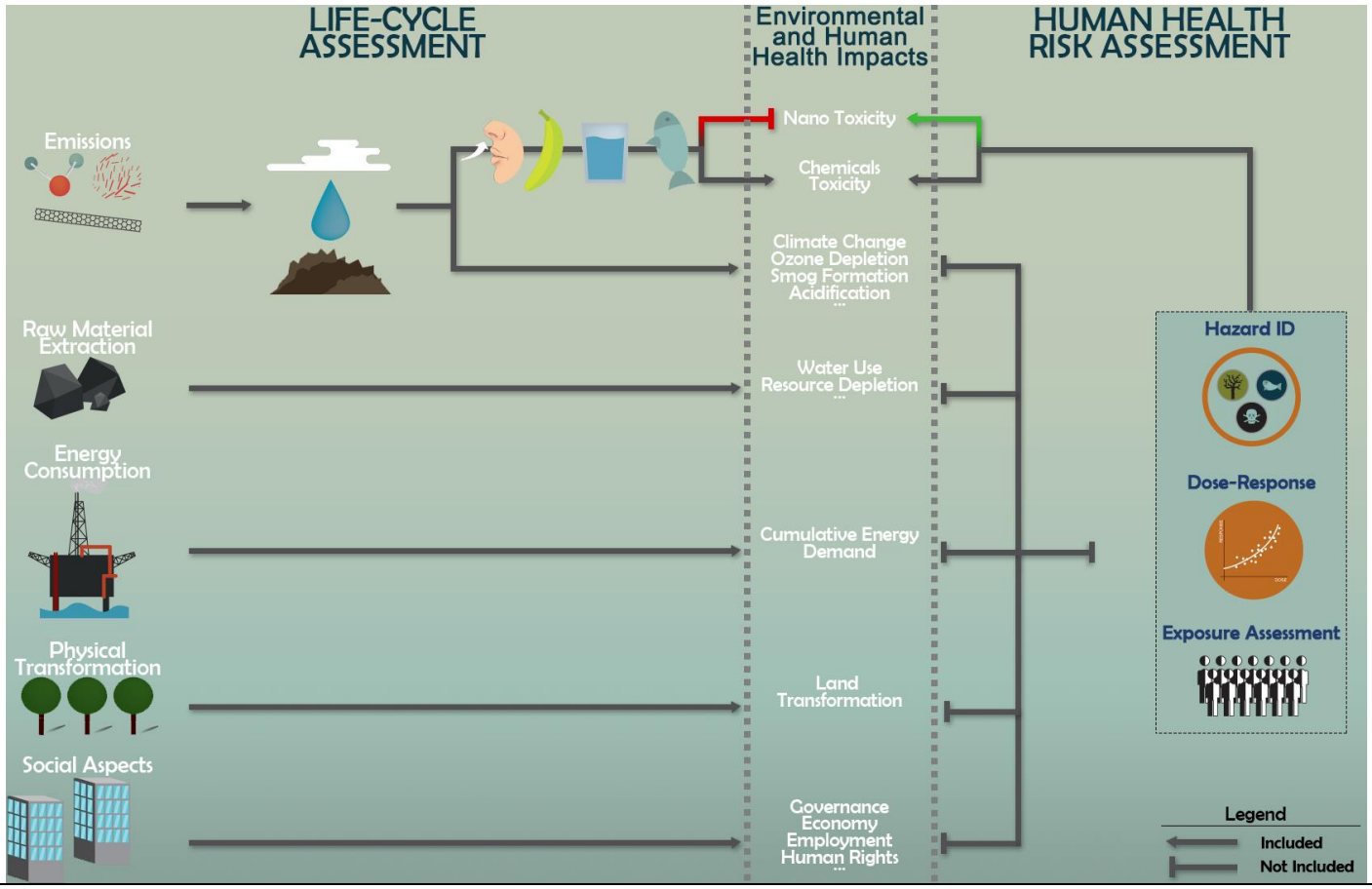

Figure 5-4 Broad overview of the scope of life-cycle assessment (left) and of human health risk assessment (right). The former consisting of emissions, along with their fate and exposure, as well as elementary and techno-sphere flows, all of which are connected to various environmental and sustainability metrics used to measure levels of resource efficiency between products and processes. Human health risk assessment is depicted by its discreet scope that focuses on the toxicological risks. While both can evaluate issues of chemical toxicity, they do so with different methods, and in the case of life-cycle assessment, application of methods to determine ENM-toxicity are not currently employed in practice, they are for human health risk assessment.

However, HHRA is not immune to the same data and methodological gaps that have presented themselves for LCA, and thus HHRA may not necessarily serve as a panacea to the question of human health impacts for ENM-containing products such as OPV. For example, current HHRA efforts for ENM have not kept pace with their production and use in industry. To date, the U.S. Environmental Protection Agency (U.S. EPA) has released just one ENM-HHRA,[209] while the U.S. National Institute of Occupational Safety and Health (U.S. NIOSH) has released two ENM-specific occupational safety exposure levels.[161,210] Data gaps in toxicity and exposure assessments largely hinder the HHRA process from moving forward at sufficient speed.[174,211,212] While the U.S.[213] and E.U.,[181] for example, can demand and gather data to assist in the HHRA procedure for ENM, an assessment of all registered ENM has not been completed. Although, some data and modeling efforts can be bypassed in HHRA, for example, by directly measuring the exposure doses or concentrations that one is subjected to. More commonly, however, *qualitative* HHRA[214–217] approaches have been put forth for *prioritizing* research efforts, environmental management and regulatory activities in the case of ENM. Nonetheless, many ENM-specific models, from those qualitative control banding approaches[218] to more sophisticated, dynamic approaches[219,220] have been or are currently being developed for ENM. Such tools are, thus, one option for addressing the human health impacts of ENM used in OPV.

Complementary and Integrated Approaches for Life-Cycle Assessment and Risk Assessment

Developing nanotechnologies in a responsible and sustainable way should require that the net value to society is considered by considering their resource efficiencies as well as their potential human health and environmental risks. The general tendency is for different stakeholders to focus on these issues as distinct endpoints that must use distinct tools (e.g. LCA, HHRA, ERA), either out of familiarity or opinion, ultimately excepting the exclusion of a more comprehensive viewpoint.[74,221] Together, aspects from both LCA and HHRA may provide an adequate understanding of this information.[185,222–225] However, their use as separate, distinct tools is only one potential option for doing so. In the remainder of this chapter, other options for achieving this objective are presented and discussed in greater detail. These options will be presented in a decision-depend context, exploring the application of ENM as an emerging technology and the corresponding evaluation objectives that may present themselves at different stages of product maturity. In total, five different options for using and combining LCA and HHRA for the environmental evaluation of ENM-related technologies are discussed: one *separate*, one *complementary*, and three *integrative* approaches.

Separate Use of LCA and RA for Nanotechnologies

LCA and HHRA are two separate tools that have distinct methodologies and report different results. While LCA allows the calculation of potential human health impacts from many competing sources of emissions along the life-cycle, decision makers might find it useful to employ this tool at all stages of technology development and eco-design purposes. However, for ENM-containing technologies, if evaluation of ENM is not possible, decision makers may choose to simply use HHRA instead, particularly once product development has increased to relatively large volumes, full-scale development or product adaption by society requires that human health risks are avoided. This is because full scale development will require registration with the appropriate regulatory agencies who may require HHRA knowledge as part of the registration or compliance with agencies tasked with ensuring occupational and consumer protections. While having the ability to provide definitive estimates of ENM human health risk, a critical drawback of this option is the level of detail involved, which is not necessary in the case of early stage development of products containing ENM. Consequently, these tools are often utilized separately by different types of stakeholders who have distinctly different needs. Thus, the separate use of LCA or HHRA (i.e. without the use of the other) for emerging technologies will be limited to one set of results but not the other as well as limited by when along the development of the technology to use these tools.

Complementary Use of LCA and RA for Nanotechnologies

However, *Complementary Use*, defined by using both tools separately and then combining their results, is an obvious approach when the evaluation of both the resource efficiencies and the human health effects of ENM needs to be considered. This option thus necessarily involves a detailed assessment of the exposure to and risk from ENM. Therefore, much like the Separate Use HHRA option discussed above, *Complementary Use* will be most appropriate during full-scale technology development (Figure 5-5) or when it is necessary to ensure human health safety.[214,226,227]

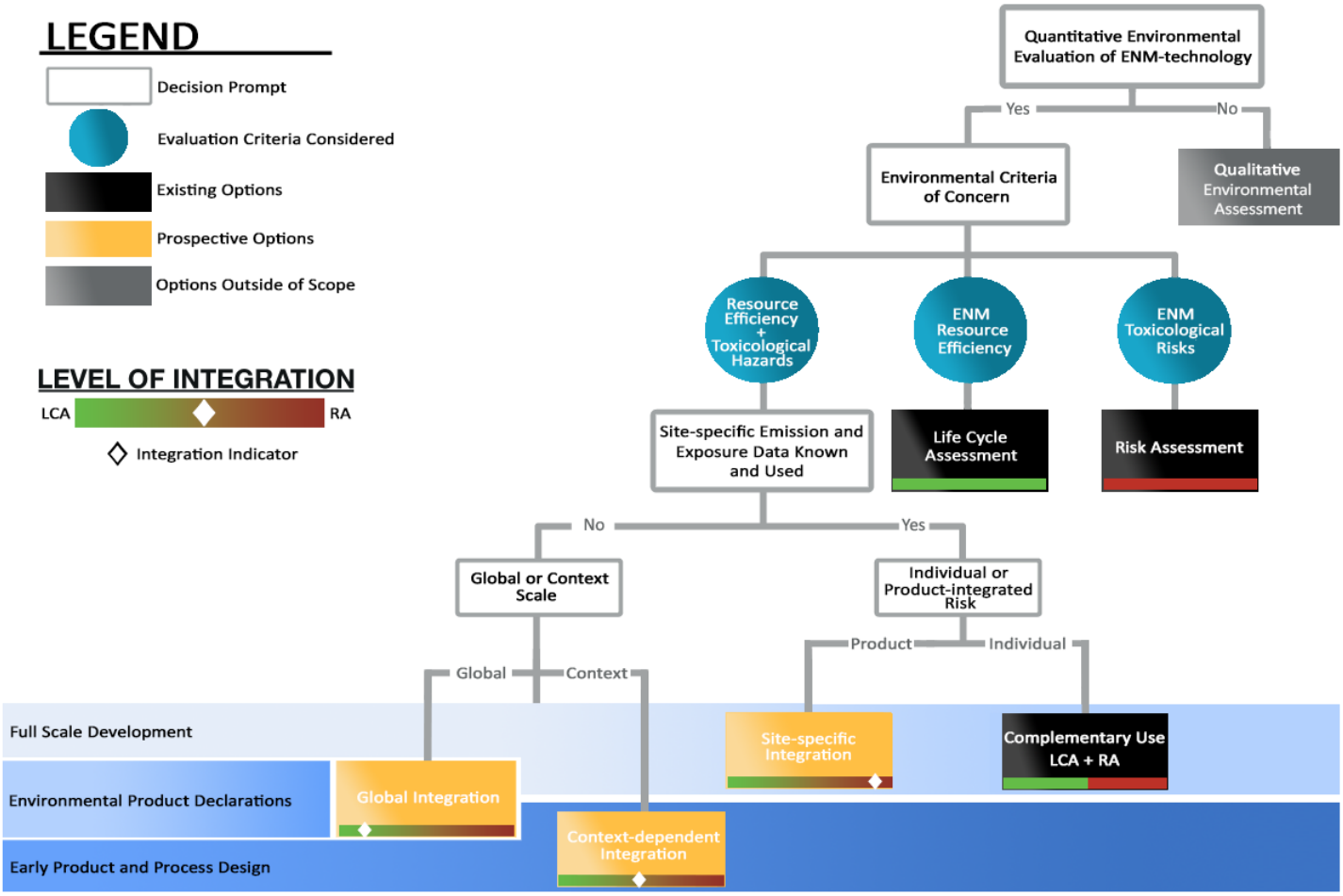

Figure 5-5 One separate, one complementary and three integrated options for using of life-cycle assessment and risk assessment to evaluate products containing engineered nanomaterials. Choices are presented from the perspective of different particular stakeholders and their objectives. Decision makers, for example, may be concerned by both resource efficiency (e.g. changes in energy consumption for a ENM-enabled product) and toxicological impacts and risks of a nanotechnology or only a single dimension of these impacts.

Complementary Use also require that the different scopes or the results of the two tools be reconciled. To clarify, LCA scales its results to a service or 'functional' unit (e.g. production of an average kWh of energy), while HHRA is defined by a relevant exposure scenario (e.g. the human health risk posed by nano-TiO_2 emissions in an industrial plant). Thus, their results would require careful conversion (i.e. normalizing the results of each tool such that they can be compared on relative units, such as the conversion to damages) before useful comparisons of the results could be made.[222] Even then, the comparison essentially is likely to remain an apples-to-oranges scenario as opposed to apples-to-apples, unless the scopes of each tool were defined strategically and sufficiently to the point that they were in agreement

with one another. That is to say, the *Complementary Use* option will likely not be able to express how proportionate the resulting ENM-risk is in context of the toxicological hazards defined by LCA (Figure 5-6).

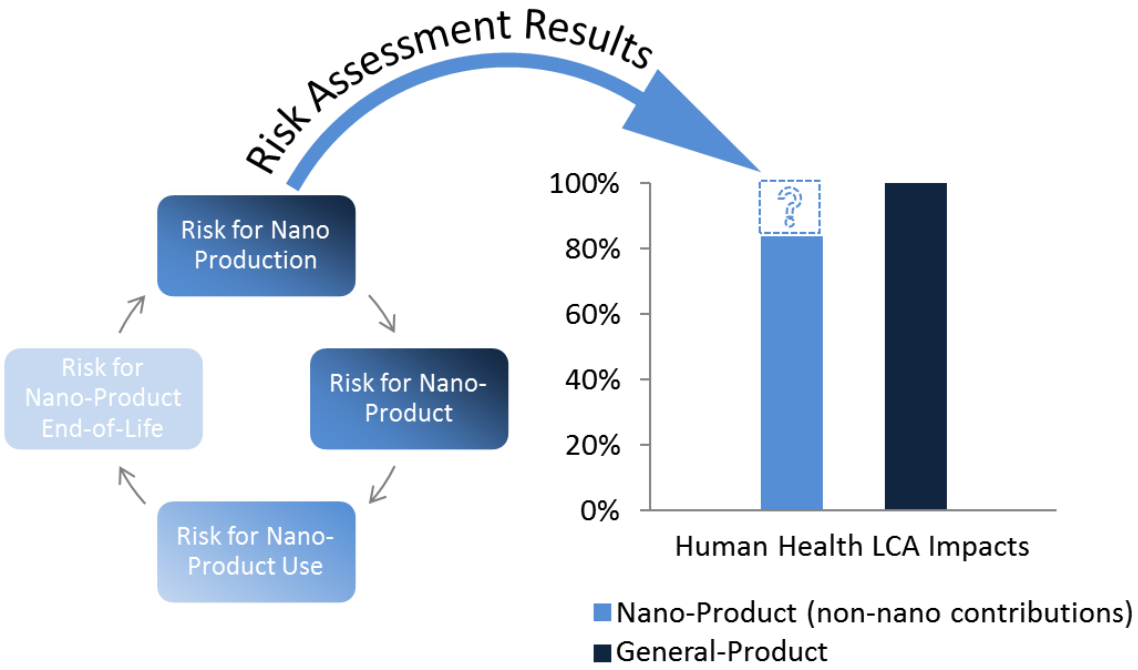

Figure 5-6 Illustration demonstrating that the results of a human health risk assessment (left side of figure) may not always be congruent with life-cycle assessment human health results, since they are calculated using different methods, most important of which is the scope by which these two tools are defined.

In such a situation, one must choose whether they find apples or oranges more important, introducing explicit subjectivity into the decision making process. However, whether this is a true drawback of *Complementary Use* depends on the objectives of the decision maker. For instance, this could very well be a valid option for those looking to use LCA as an early stage eco-design tool while also looking to ensure occupational safety at an early stage of research, development and production.

Integration of LCA and RA for Nanotechnologies

As opposed to *Complementary Use*, *Integration* here refers to combining the methods of each tool instead of combining their results.[228] This approach utilizes methods generally attributed to HHRA to modify the approach for estimating the fate of, exposure to and/or effects from ENM. Because integration allows for (a) the interpretation of ENM toxicological hazards in the context of the intended product (i.e. functional unit) and (b) the direct comparison of ENM hazards to all other chemical-based hazards estimated across

the life-cycle, this approach helps to ensure that 'burden shifting' does not occur.[94] Integration can, therefore, be used as an alternative to existing uses of *Separate* or *Complementary Use* but it can be uniquely used for evaluation at early-stage product development, life-cycle eco-design or environmental product declarations, for example.[229]

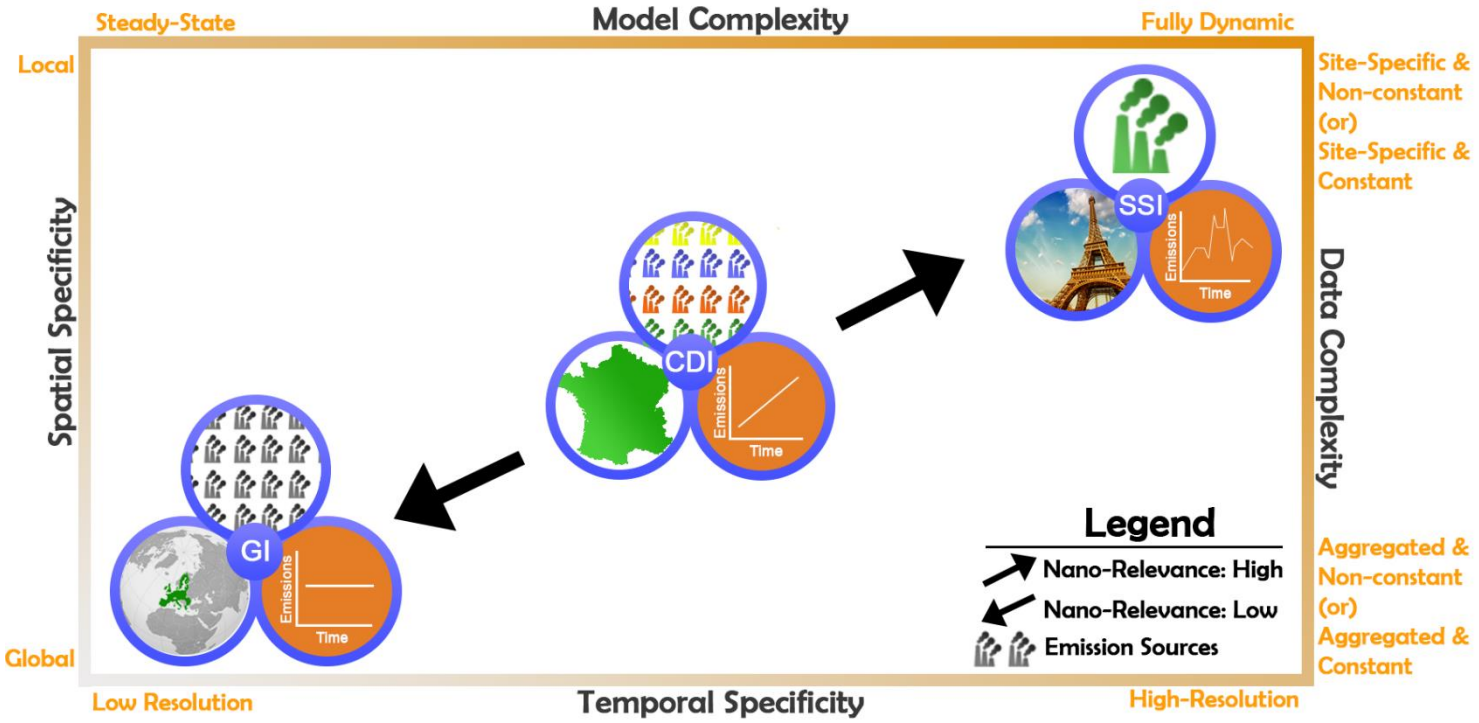

Figure 5-7 Key aspects of life-cycle and risk assessment integration at the methodological level. Integration is replaced on its level of spatial and temporal specificity as well as model and data complexity. For example, low temporal resolution (i.e. no changes in emissions over time) with a global spatial scope will result in a steady-state model that uses constant (i.e. non-variable) and highly aggregated data, respectively, similar to what is used in current life-cycle assessment methods such as USEtox. This is the case labeled as "GI" or Global Integration, and represents one of the three levels of integration set forth in this thesis, however the degree of integration is dynamic for each axis, independent of one another. For instance, low temporal resolution with a local spatial scope (i.e. high spatial resolution) will similarly result in a steady-state model using constant, but, *non-aggregated* (i.e. site-specific) data. To illustrate these points further, ENM emissions modeling is shown in the figure as a practical representation. Global Integration, thus, results in the use of non-changing, aggregated emissions data that is averaged for a large continental region in a steady-state model. In terms of its relevancy to ENM, this approach has less predictive power than the other two options shown in the figure. For example, Site-specific Integration (SSI), uses the empirically determined changes in single-source emissions data measured over an unconditional timeframe in a fully-dynamic model. Context-dependent Integration (CDI) models emissions using a generalized time-dependent assumption (e.g. positive, linear correlation) for classes of sources averaged at the country level in a partially-dynamic model.

Three different approaches which differ by their extent of methodological integration are presented in Figure 5-7. The first degree integration, referred to as *Global Integration* (GI), is based on the general LCA

framework but supplemented with ENM-specific estimations of toxicity, for example, using the USEtox life-cycle impact assessment approach.[93–96,197] *Global Integration*, represents a feasible, first-tier tool that covers the scope of both resource efficiency and toxicological hazards. It is particularly well-suited for supporting eco-design or environmental product declarations which must be evaluated using current LCA standards. However, this approach relies on the predominant tools available, which ignore spatial and temporal acuity in both the life-cycle inventory and also the estimations of fate, exposure and hazard. Models that do not possess sufficient spatial or temporal resolution cannot incorporate specific environmental details and exposure conditions necessary for appropriately estimating the fate of, and exposure to ENM, as discussed earlier in this chapter.[97] ENM are also influenced by both physical and molecular forces akin to colloidal materials, leading to an array of transformations (e.g. aggregation) that are important in determining their fate and exposure.[174,198,211,230] The context setting (e.g. indoor versus outdoor emissions) and their local landscape parameters (e.g. ventilation rates) will also influence these behaviors in important ways.

Thus, emission, fate and exposure models that incorporate more spatial and temporal detail would be more appropriate for and increase the predictive power of ENM evaluation. Therefore, two further degrees of integration are considered: *Context-dependent Integration* (CDI) and *Site-specific Integration* (SSI) that represent models with greater levels of time and spatial resolution compared to *Global Integration* (Figure 5-7). *Context-dependent Integration* relies on models whose underlying parameters (e.g. emission magnitude, ENM size) are estimated per 'group' or 'class'. Groupings can be applied, but not limited, to emission sources (e.g. workplace activity), emission pattern (e.g. constant), emission time-frame, ENM-type (e.g. size), and conditions of the receiving compartment (e.g. ventilation rates).[231] Classes should be defined by statistically significant generalizations such that impact results differ from class to class but not within each class.[232] For example, statistically determined environmental conditions (e.g. meteorological data), operating parameters (e.g. stack height of emissions source) and receptor densities of the air pollution emissions were determined for waste treatment sites across Spain.[232] In this way, the spatial distribution around an emission point could be considered for estimating the concentration increment per receptor in geographically distinguishable environments. Indoor air ENM emissions and exposure scenarios could prove an extremely practical first case-study of the *Context-dependent Integration* approach, given that indoor environmental conditions are more constrained than ambient ones. Indoor, occupational scenarios may even present conditions whereby ENM fate and transport are more dependent on workplace conditions rather than ENM characteristics.[97,233] These

conditions, together, could allow for the relatively simplified grouping of indoor, occupational model parameters, similar to what has been done for regular chemicals in residential indoor air,[234,235] industrial processes[232] and consumer products.[236–238]

Site-specific Integration is the third-degree of the most ideal form of integration, whereby complete spatial and temporal resolution is known and incorporated into a fully-dynamic set of emission, fate and exposure models (Figure 5-7). This approach also assumes that all ENM emissions are known and quantifiable across the life-cycle of the ENM-containing product. *Site-specific Integration* would provide the most accurate results (e.g. absolute impact values), however it can only be applied on a case-by-case approach because of how inclusive the data and model requirements would be. The latter point most fitting for full-scale development and/or the need to ensure human health or ecological safety. Mature nanotechnology market products, such as certain paints and pigments, have well-established manufacturing routes, production volumes and intended uses that pose potential exposures across the life-cycle. In such real-world scenarios, absolute damage and evaluations of risk are necessary to ensure human health safety, local ecosystem integrity and ensure regulatory compliance. While Complementary Use would essentially allow an analogous evaluation of both the environmental resource efficiencies and risks of products containing ENM, as was discussed in the section above, this assessment option lacks harmony in the scopes of the two tools, leading to greater difficulty in interpreting the distinct LCA and RA results. Furthermore, it should be noted that as the number of ENM-emitting processes along the life-cycle become large (e.g. > 20), data collection may become untenable and the option of *Site-specific Integration* impractical.[232] As an alternative in such a situation, a special case of the Complementary Use approach might involve using *Global Integration or Context-dependent Integration* to identify the ENM emission hot-spots of greatest concern, which could then be followed by RA where it is warranted (e.g. where ENM emissions contribute to a noticeably large fraction of the total human health impact across the life-cycle).

On the contrary, the level of data and model detail that is required of *Site-specific Integration* or *Complementary Use* would be unnecessary in cases of early product and process design of nanotechnologies since localized (i.e. site-specific) environmental conditions and operating parameters would not be known. To illustrate more clearly in context of this thesis, 3rd-generation PV devices are a mostly lab-scale technology that exploit the photoelectric properties of ENM for their functionality. In Chapter 3 and Chapter 4, use of LCA as a single tool demonstrated the resource efficiency of these devices

such as potential to reduce embodied energy and carbon of PV. However, those results lack any estimation of the direct toxicological hazards ENM pose to humans across the life-cycle. According to Figure 5-5 a decision-maker at early-stage development (e.g. lab- or pilot-scale) concerned with addressing both the resource efficiency and the toxicological hazards would find *Global Integration* and/or *Context-dependent Integration* most suits their needs (i.e. effective hot-spot analysis to identify where in the life-cycle toxicological impacts and eventually risks may occur). This is because at the current scale of OPV development, there is too much uncertainty in production volumes or operating conditions, for example, and thus spending resources to determine the absolute damages (i.e. using *Site-specific Integration*) or risks (i.e. using *Complementary Use*) posed by ENM in such scenarios would have little to no basis.

Conclusion

LCA and HHRA offer decision makers the ability to evaluate the resource efficiencies and human health risks of their products and substances within their products, respectively, such as OPV. Specifically, LCA was used in Chapter 3 and Chapter 4 to compare the environmental and human health impacts of OPV with silicon-based PV. The results of those chapters demonstrate that OPV benefit from greater resource efficiency and have lower relative impacts overall. However, the results did not include the potential human health impacts from ENM.

The separate or complementary use of HHRA could potentially provide a solution to this assessment gap. Making use of the HHRA makes most sense at the point of full-scale development or ensuring human health safety is required. Conversely, the detailed data needs required to complete a HHRA at early-stage product development would be highly uncertain and largely unwarranted. Instead, integrating HHRA approaches into LCA could provide an alternative option that is more appropriate for early-stage development and eco-design purposes, for example. Unfortunately, a lack of relevant data for most types of ENM remains a barrier for conducting both HHRA as well as LCA, and without such data neither approach will be feasible, let alone present opportunities for integration. For example, without known ENM emissions a life-cycle inventory cannot be calculated nor can an exposure assessment in HHRA be made. The same is true for ENM-specific data that is required for building fate and exposure models and determining dose-response relationship for both life-cycle impact assessment as well as HHRA.

While data is currently limited for ENM, materials such as certain metals, metal oxides and carbon based ENM have relatively more reported data in the literature compared with others and can serve as starting points for establishing HHRA or integrated, dynamic life-cycle impact assessment models similar to what has been done for steady-state models.[93–96] This is quite relevant for the case of OPV who use both carbon and metal-oxide ENM in their material layers and thus could be used to make further evaluations of the potential human health impacts resulting from the use of ENM in OPV. In terms of the three integrative approaches presented in this chapter, the previous steady-state adaptations made for these materials are what is referred to as *Global Integration* in this chapter. Given its use of existing steady-state models, this could serve as an immediate and near-term (i.e. circa 5 years) objective for most ENM evaluations. However, as described previously, this approach also has less relevance for certain fate and exposure processes and, thus, less predictive power for estimating ENM human health impacts. *Context-dependent Integration*, on the other hand, can introduce a more dynamic process to the modeling approach and, hence, more relevant estimations of fate, exposure and impacts. This integration option will require greater coordination among the scientific community to identify the relevant data and appropriate emission, fate and exposure 'classes' that will be relevant to ENM development and uses.

In view of these potential options, Chapter 6 presents a more focused HHRA for the carbon and metal oxide ENM used in OPV. Chapter 7 then uses the approach and lessons learned from the HHRA to construct a *Context-dependent Integration life-cycl*e impact assessment approach for estimating human health impacts of ENM.

Chapter 6 Human Health Risk Assessments: Quantitative Assessment of Titanium Dioxide and Qualitative Assessment of C_{60} Fullerene Nanoparticles

Chapter 3 and Chapter 4 explored the environmental and human health impacts of OPV technologies, their uses and their end-of-life considerations. The results of those assessments demonstrate that OPV have greater resource efficiencies and lower relative environmental and human health hazards compared with their silicon-based counterparts. Chapter 5 highlighted the absence of ENM-specific life-cycle inventory flows to the environment as well as the absence of their corresponding potential human health impacts in those LCA studies. A further analysis was provided in Chapter 5 regarding life-cycle impact assessment methodologies and HHRA, specifically what opportunities exist to use these tools in a complementary or integrative way in order to provide a comprehensive evaluation of the environmental and human health impacts of OPV technologies that use ENM. In this current chapter, HHRA is used as a preliminary tool to evaluate the human health risks of those ENM, and then key methodological HHRA aspects are identified that can be integrated within life-cycle impact assessment methods.

Qualitative (Screening Level) Human Health Risk Assessment

Qualitative Exposure Assessment

As was discussed in Chapter 5, data and methodological gaps for HHRA present challenges to fully implementing this tool across the entire life-cycle of OPV devices. Thus, it was out of the scope of this thesis to focus *quantitatively* on all exposure scenarios (Figure 6-1) nor the risk therein posed by both PCBM and nano-TiO_2.

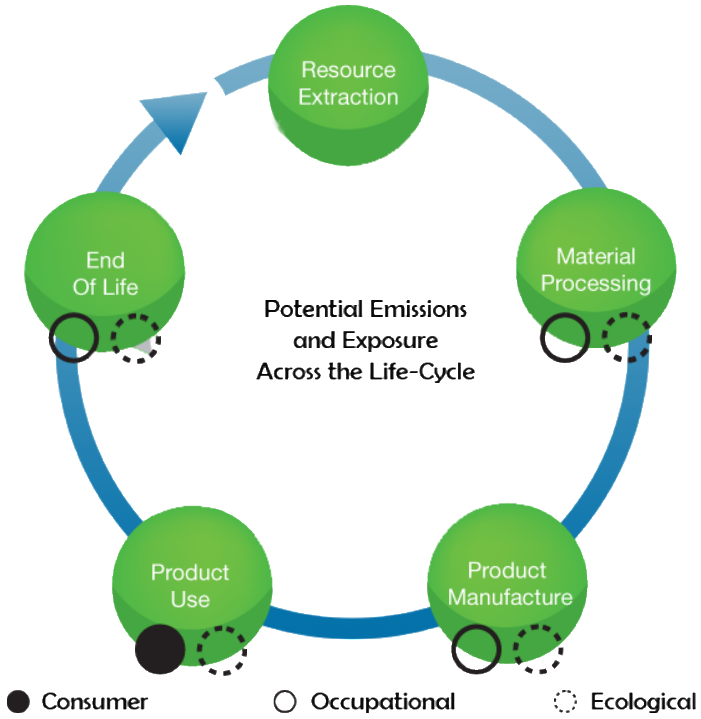

Figure 6-1 Potential exposure to engineered nanomaterials across the life-cycle for a generic ENM-containing product. Exposure along the life-cycle of a ENM-enabled product can result from emissions of engineered nanomaterials at any stage, introducing potential for occupational, consumer and ecological exposures and corresponding toxicological impacts or risks.

Instead, a *qualitative* exposure assessment was first completed in order to identify the life-cycle stage(s) of greatest exposure potential. This assessment was based on a number of basic assumptions and qualitative descriptions of the potential exposure. These main assumptions were whether (a) there was direct interaction with an ENM (i.e. as direct contact of the ENM or in contact with ENM-containing media), (b) the ENM volume was relatively large or small, (c) use of personal protective equipment, (d) tendency for ENM to enter into the environment and (e) the potential pathway of exposure, without specific consideration of the fate and transport of the ENM (Figure 6-2).

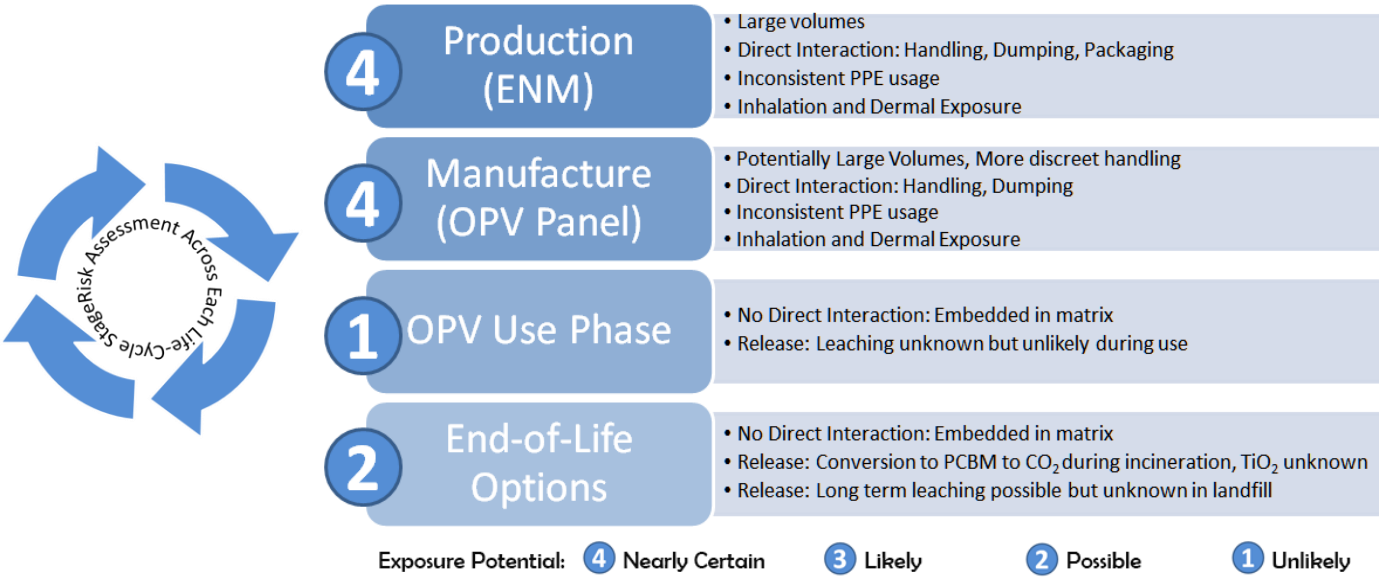

Figure 6-2 Qualitative exposure assessment of PCBM and nano-TiO_2 across the life-cycle of the OPV panels

Occupational settings involve the manufacturing, handling and storage of ENM where workers are in close proximity to crude amounts of ENM.[159,239–243] Additionally, these situations may present ENM at uniquely elevated concentrations, small uniform sizes, with distinct shapes and structures not normally found in the environment.[244] Although the actual synthesis of ENM may occur in closed reaction chambers, exposure during handling, transporting, and post-treatment are all viable possibilities.[245–248] Industrial-scale development will lead to large volumes of ENM being produced and utilized during OPV production. Proper emissions controls such as personal protective equipment may theoretically be in place, actual uptake of such equipment has been shown to be inconsistent and often low.[249]

Downstream of ENM and OPV manufacturing, consumer hazards are hypothetically possible. Due to the fact that both PCBM and nano-TiO_2 are embedded in a polymer matrix, it was assumed the use phase would not pose sufficient conditions to allow leaching of the ENM from the product. During the use-phases explored in Chapter 4, exposure to naturally occurring weather including sun exposure and rainfall will occur. This is particularly true for the case where OPV are installed on rooftops for primary energy production, while portable chargers would likely have much less utilization, they would be subject to potentially greater amounts of physical stress from direct handling of the device. Rooftop systems would thus be hypothetically susceptible to leaching from acid rain or other extreme conditions, while portable chargers' physical integrity could be compromised (e.g. delaminated). There are no studies in the literature reporting any estimation of ENM leaching from OPV panels, although leaching of other

components from intentionally damaged (e.g. shredding) OPV devices has been shown.[250] At their end-of-life, it is assumed that PCBM will be converted to CO_2 during incineration. Based on previously reported results for cerium oxide nanoparticles that remained intact after incineration (i.e. in the bottom-ash),[195] there is a possible exposure scenario for nano-TiO_2 during incineration for the OPV, particularly if the incineration residues are deposited in landfills. Similarly, depositing intact, whole OPV panels into a landfill was assumed to have possible leaching potential due to long term exposures of acidic, leachates typically found in such conditions. In these cases, the polymer matrix could breakdown, exposing the individual layers and leach certain materials over time. Given these considerations, it was found that occupational exposure scenarios involving production of either the ENM themselves or the OPV panel resulted in the greatest potential exposure (Figure 6-2).

Hazard Identification of C_{60}-fullerenes and PCBM

The principal properties specific to the functionality of C_{60}-fullerenes, and thus PCBM, are closely related to its ability to reversibly accept upwards of six additional electrons.[50,51] C_{60}-fullerenes are also nearly insoluble, however functionalization can produce variants of this molecule such as PCBM that are, in effect, soluble.[251] Due to their very small size and classification as an ENM, there is an initial assumption that some of the toxicological trends seen with other spherical ENM may be relevant for C_{60}-fullerenes.[252] On the contrary, and as a consequence of their electrophilic nature, C_{60}-fullerenes have been shown to act as free-radical sponges and have anti-inflammatory effects.[253–260] This may be the reason why some inhalation *in vivo* toxicity studies have found minimal inflammation,[261] no inflammation[262,263] or even anti-inflammatory[259] effects upon exposure to particles of C_{60}-fullerenes. Several *in vivo* studies do, however, demonstrate the pro-inflammatory nature of C_{60}-fullerenes as they have been associated with enhanced reactive oxygen species production, damage to cell membrane integrity and lipid peroxidation, for example.[264,265] Very few studies on dermal exposure have been carried out, demonstrating limited to no uptake by the skin and a lack of evidence that C_{60}-fullerenes could result in skin irritation.[266,267] Upon oral administration, limited uptake by the digestive track has been demonstrated[268] with no obvious toxicological effects taking place either in the gut or systemically.[269,270]

Hazard Identification of Titanium Dioxide Nanoparticles

Titanium dioxide is an important inorganic metal oxide used in industry. Industrial-scale production of TiO_2 began in the early 20th century and has steadily increased since then. Industrial use of TiO_2 is generally in the rutile or anatase forms (Figure 6-3), although the rutile form has found greater commercial use.

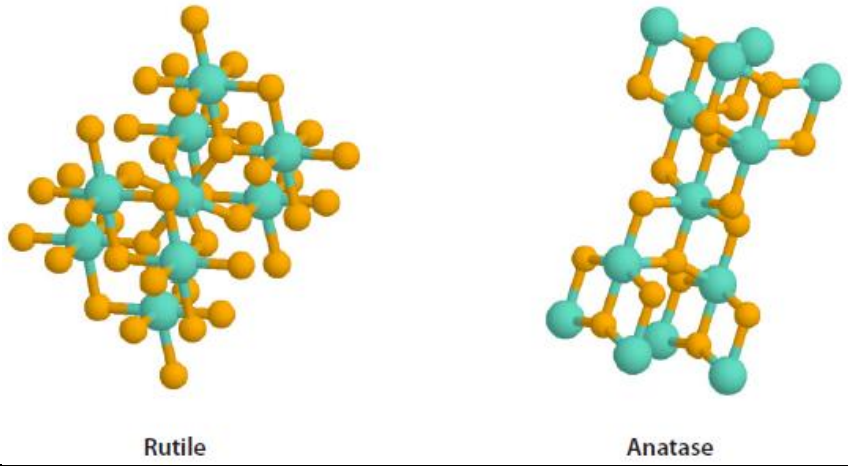

Figure 6-3 Two-dimensional structure of titanium dioxide in its two most commonly found forms: rutile and anatase. (Source: U.S. National Institute of Occupational Safety and Health)

Global TiO_2 production reached 6.6 million metric-tons in 2012,[271] with ENM-forms increasingly dominating both the legacy[272–274] and emerging TiO_2 markets.[275,276] Legacy markets were dominated by fine particle sizes of TiO_2, mostly for use as pigments and coatings. This fine particulate form of TiO_2 is generally considered thermodynamically stable and relatively inert.[161] For this reason, TiO_2 was historically categorized as a nuisance dust in the occupational workplace. However, this is not necessarily true for nano-TiO_2. Because of their large production volume and long historical use, there have been many more toxicological studies performed on TiO_2 compared with PCBM, particularly those for inhalation exposure studies.[277–282]

The range of nano-TiO_2 induced *in vivo* toxicological responses in the respiratory system spans from inflammation, histopathology (e.g. endothelial or epithelial changes), cytotoxicity, oxidative stress, oncogenic effects (e.g. increase rates of carcinoma) and other genotoxic-related events.[160,161,272,277–286] In certain cases, these effects were found to be more pronounced for nano-TiO_2 compared to its bulk counterpart.[273] In their 2011 report, NIOSH specifically addressed concerns over nano-TiO_2, acknowledging a potentially higher hazard potential in terms of inflammation and carcinogenicity of corresponding nanoparticles of this material as compared to bulk sizes.[161] For dermal exposure, there is limited to no evidence from *in vivo* animal studies showing nano-TiO_2 is able to penetrate the (intact) skin.[287–291] Penetration often remains to the superficial layers of the epidermis[288] however dermal[292] and hypodermal penetration, such as in the hair follicles,[293,294] has been observed. Potential toxicological

effects from dermal exposure range from limited to no skin irritation[295] to oxidative stress[296] and lesions in certain organ systems.[292] Oral administration to animals has demonstrated their uptake particularly to the liver but also other organs such as the kidney, brain and testes.[297] Potential toxicological effects from oral exposure range from oxidative stress and neorinflammation[298] to necropathy,[297,299,300] for example.

Relevance of the Qualitative Exposure Assessment and Hazard Data Availability

The limitations to conducting a quantitative HHRA rest on the data availability and/or appropriate models available. For example, toxicological data with multiple dosing groups is required to complete a dose-response analysis. Such data should also involve relevant exposure routes (e.g. inhalation as opposed to instillation) and preferably as long-term studies (e.g. chronic). Thus, the lack sufficient positively correlated toxicological data on C_{60}-fullerenes or PCBM, particularly for *in vivo* long-term, multi-dose studies precludes its further analysis from the HHRA. This decision not to carry out a quantitative HHRA on C_{60}-fullerenes should not be seen as a formal determination that these materials pose no human health risk across the life-cycle of OPV, since as the qualitative exposure assessment discussed, there is a high likelihood that emissions will occur along the OPV life-cycle. On the other hand, current human health relevant toxicological literature does not point to clear and consistent adverse responses nor is there sufficient data to carry out a quantitative assessment. There is, however, sufficient evidence in the literature points to both adverse non-cancerous and cancerous, chronic and sub-chronic human relevant toxicity of nano-TiO_2. Sufficient data also exist to carry out an appropriate dose-response analysis of this material. The remainder of this chapter focuses on the quantitative HHRA of nano-TiO_2 in occupational exposure scenarios in the OPV life-cycle.

Quantitative Risk Assessment

Methods

As described in Chapter 5, the four principle steps of HHRA involve (1) hazard identification, (2) dose-response assessment, (3) exposure assessment, and (4) risk characterization (Figure 5-3). Hazard identification and the background on PCBM and nano-TiO_2's toxicological concerns were addressed in the previous section of this chapter as a part of the *qualitative* HHRA. The methods sections below will describe steps (2), (3) and (4) in greater detail.

Dose-Response Assessment

The benchmark dose (BMD) method was used to quantify the exposure concentration at which the adverse health effect occurs (i.e. dose-response relationship). This concentration was estimated from the corresponding, pre-defined benchmark response (BMR). The BMD is an alternative to the no-observed-adverse-effect-level (NOAEL) and lowest-observed-adverse-effect-level (LOAEL). In this chapter, the terminology benchmark concentration (BMC) is used to clarify that the dose-response modeling used data correlating to exposure concentrations from whole body animal studies. Calculation of the BMC was completed using the Netherland's National Institute for Public Health and the Environment's (RIVM) PROAST software (www.rivm.nl). PROAST was used to first calculate a BMC_{animal} (BMC_a) based on the *in vivo* animal data. This value was converted to a distribution using PROAST's parametric bootstrap option (i.e. sampling with replacement) over 10,000 simulations. The BMC_a was extrapolated to a human effect threshold referred to as the BMC_{human} (BMC_h), by applying the appropriate extrapolation factors[301] using equation (6-1):

$$BMC_h = \frac{BMC_a}{EF_{inter} \cdot EF_{intra} \cdot UF_i} \qquad (6\text{-}1)$$

BMC_h: *Human equivalent benchmark concentration*
BMC_a: *Benchmark concentration based on animal toxicological data*
EF_{inter}: *Interspecies extrapolation factor*
EF_{intra}: *Intraspecies extrapolation factor*
UF_i: *sources of uncertainty (i)*

Extrapolation factors represent differences between and among species according to anatomical differences (e.g. body size) and physiological functions (e.g. metabolism). Values are scaled with the extrapolation factors according the allocation scaling principle. The difference (i.e. increase) in breathing rates for persons exposed in the occupational setting are assumed to be elevated compared to persons at rest or not working and are captured within the EF_{intra}. Log-normal distributions for these factors were defined using similar approaches presented by Slob et al.[302] A brief rationale follows. Biological mechanisms in a population (e.g. survival times after disease onset) are generally asymmetrical as opposed to being described by normal "bell-shape" curves.[303] In deterministic HHRA procedures, it is typical to use factors of ten to extrapolate to conservative yet acceptable human equivalent doses. Although extrapolation factors of ten are supposed to be conservative protective values, it is understood that this does not always provide protection. However, for transparency, demonstration of the approach, and ease of interpretation the log-normal distributions were defined such that a value of ten was one-

order of magnitude greater than the mean and lies at the 99th-percentile. In this regard, the selection of ten as a conservative extrapolation factor remains.[304] The geometric mean (GM) and geometric standard deviation (GSD) were 1 and 2.7, respectively (Figure 6-4).

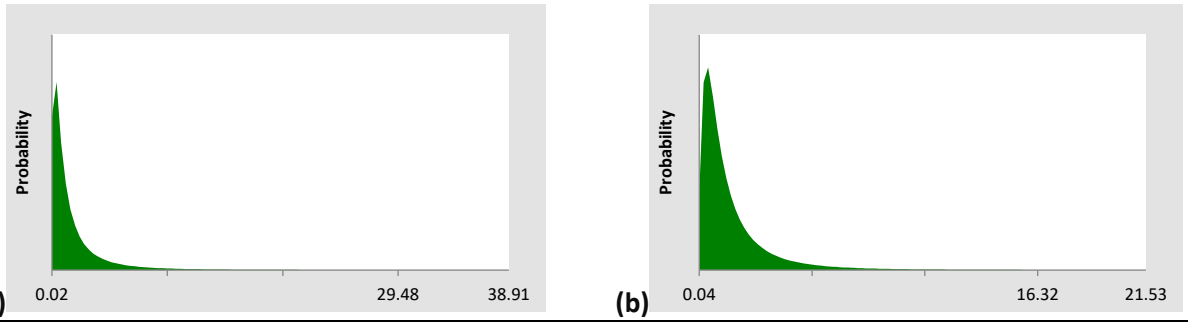

Figure 6-4 Log-normal distributions of (a) the interspecies toxico-dynamic extrapolation factor with a geometric mean of 1 and geometric standard deviation of 3.27 and (b) the intraspecies extrapolation factor with a geometric mean of 1 and geometric standard deviation of 2.7. The x-axis is without units.

10,000 Monte-Carlo (MC) simulations were conducted using Crystal Ball (Oracle Corporation, USA) to complete the extrapolation of BMC_a to BMC_h distributions.

No relevant chronic *in vivo* multi-dose studies were found in the literature, although there was one such sub-chronic study[283] (i.e. 90-day exposure duration) whole body inhalation exposure to nano-TiO_2. Bermudez et al. exposed rats, mice and hamsters to uncoated, nano-TiO_2 obtained from Evonik (formerly DeGussa) with a nominal particle diameter of 21 nm as supplied by the manufacturer.[283] Each species group was exposed to nano-TiO_2 at concentrations of 0.0 mg/m^3 (control), 0.5 mg/m^3, 2.0 mg/m^3 and 10 mg/m^3 for 6 hours/day, 5 days/week, for 13 weeks, while the control group received filtered air only (Table 6-1).

Table 6-1 Summary of the study[283] and select dose-response data used to characterize the inflammatory response upon inhalation exposure to nano-TiO_2

Nanomaterial	Species	Exposure Type	Concentration (mg/m^3)	Effects	BMR
21 nm P25 Degussa (Evonik)	Rat, Mice	13 weeks (6 h/day; 5 days/wk) whole-body inhalation	Control, 0.5, 2.0, 10	Pulmonary inflammation	20% increase in neutrophil cell counts

Control: Filtered air with corresponding concentration of 0.0 mg/m^3
BMR: Benchmark response

Bronchoalveolar lavage (BAL) was completed on the lungs of the sacrificed animals at varying post-exposure times to measure the counts of macrophages, neutrophils, eosinophils and lymphocytes. Only the effects at post exposure time zero (i.e. immediately following completion of exposure) were considered in the dose-response assessment. Bermudez et al.[283] reported that statistically significant changes in the BAL results were limited to the macrophages, neutrophil and lymphocyte cell types in the highest dose-groups. Furthermore, only data from the mice and rats were found to have statistically significant changes in percent cell counts over the control and thus the hamster data was not considered in the dose-response assessment.

Exposure Assessment

Measurements for occupational exposure to ENM are not abundant and the literature generally focuses on airborne concentrations as opposed to internal lung, internal oral, or dermal loading doses.[305,306] There are currently no models to estimate dermal or oral exposure from airborne concentrations. Thus, this HHRA focuses on the inhalation exposure to nano-TiO_2 in the occupational setting. All exposure assessments were made with the near-field–far-field exposure assessment model in NanoSafer v.1.1.[219,220,307] The three exposure scenarios (ES) considered in this chapter (Table 6-2) were based on prompts taken from the MARINA (www.marina-fp7.eu) and NANEX (www.nanex-project.eu) databases.

Table 6-2 Description of the exposure scenarios used for the human health risk assessment of inhalation exposure to nanoparticles of titanium dioxide in the occupational workplace. H_i: handling energy factor.

ES1	Transfer (dumping) of powder from a 10 kg bag into a mixing tank over 10-minute work cycles with 10-minute pauses in-between over an 8-hour workday. Work is performed in a room with high ventilation rate. The process is assumed to be of high energy with the pouring height assumed to be 0.3 m - 1 m corresponding to H_i = 0.8.
ES2	Transfer (dumping) of powder from a 560 kg containers into a larger holding vessel over 10-minute work cycles with 20-minute pauses in-between over an 8-hour workday. Work is performed in a hall with low ventilation rate. The process is assumed to be of high energy with the pouring height assumed to be 0.3 m - 1 m corresponding to H_i = 0.8.
ES3	Continuous filling (pouring) of bag bin with a total 250 kg of powder for 8 hours. Work is performed in a room with low ventilation rate. The process is assumed to be of high energy with the pouring height assumed to be 0.3 m - 1 m corresponding to H_i = 0.8.

MARINA was an EU FP7 project aimed at developing risk management methods for ENM, including development of occupational release and ES. NANEX was also an EU FP7 project which aimed to catalogue potential exposure to EMN across the life-cycle including their manufacturing and industrial use. These scenarios correlated with workplace activities that take place during the production of nano-TiO_2. However, it was assumed that similar workplace scenarios would present themselves during OPV manufacturing activities.

The NanoSafer v.1.1 model parameters used for describing the emissions and estimation of exposure concentration are given in Table 6-3.

Table 6-3 Parameters used in the NanoSafer v1.1 exposure assessment model where H_i = handling energy factor, t_{wc} is work cycle time, p_{wc} is pause between work cycles, n_{wc} is number of work cycles, $A_{transfer}$ is amount of material transferred per transfer event within each work cycle, V_{tot} is the total volume of the work room, and AER is the general air exchange ratio in the work-room.

No.	**Exposure scenario**	**E_i, [mg/min]**	**H_i**	**t_{wc}, [min]**	**p_{wc}, [min]**	**n_{wc}**	**$A_{transfer}$, [kg]**	**V_{tot} [m³]**	**AER [h⁻¹]**
ES1	Manufacturer Dumping into Mixing Tank	1.20E+01	0.8	10	10	24	10	100	8
ES2	Dumping Large Amount of Powder in Vessel	6.72E+02	0.8	10	20	16	560	75	4
ES3	Bag Bin Filling	6.26E+00	0.8	480	0	1	250	70	4

The near-field (NF) was defined as a box with a fixed volume of 2.3 m^3 that surrounds the ENM emission source. The far-field (FF) was defined as a box equal to the total volume of the work room (V_{tot}, m^3) minus the NF volume. Emissions (E_i, mg/min) were quantified (equation (6-2)) as a function of the respirable powder dustiness index (DI_{resp}, mg/kg), determined using the rotating drum system.[308]

$$E_i = \left[\frac{A_{transfer}}{t_{transfer}}\right] \cdot [(DI_{resp}) \cdot (H_i)] \qquad (6\text{-}2)$$

E_i: Emissions
$A_{transfer}$: Amount of nano-TiO_2 handled during work-cycle
$t_{transfer}$: Time length of work-cycle
DI_{resp}: Dustiness index of nano-TiO_2
H_i: Handling energy factor of work-type

$A_{transfer}$ (kg) is the amount of powder transferred during a work cycle, of given time-length $t_{transfer}$ (min), and H_i is the handling energy factor (unit-less). H_i is based on a scale of zero to one, whereby zero is a no-energy event (e.g. no handling of the material) and one is a high energy event (e.g. crushing, dropping from greater than 2 m height).[309] In addition to those parameters used to derive source-term E_i, NanoSafer v.1.1 includes the duration of the activities and work cycle (t_{wc}), the number of work cycles (n_{wc}), the volume of work room (V_{tot}), and the general air-exchange rate (h^{-1}) in the work-room to estimate the NF and FF concentrations. Daily (8-hour) exposure potentials were calculated in both the NF and FF.[220] Uncertainty in the exposure estimations were correlated with the DI_{resp} since the emission potential was found to be the most sensitive and strongest determinant input parameter in the model.[307] This uncertainty (R^2=65.8; $p<0.001$) is given by equation (6-3):

$$\log(\sigma_{DI}) = 0.871 \cdot \log(DI_{resp}) - 0.625 \qquad (6\text{-}3)$$

σ_{DI}: *standard deviation of the* DI_{resp}.

This equation was derived based on statistical analysis (Minitab® version 17.2.1) of the experimental standard deviation related to the dustiness indices of 59 powder samples available from the Danish National Research Centre for the Working Environment (Figure 6-5).

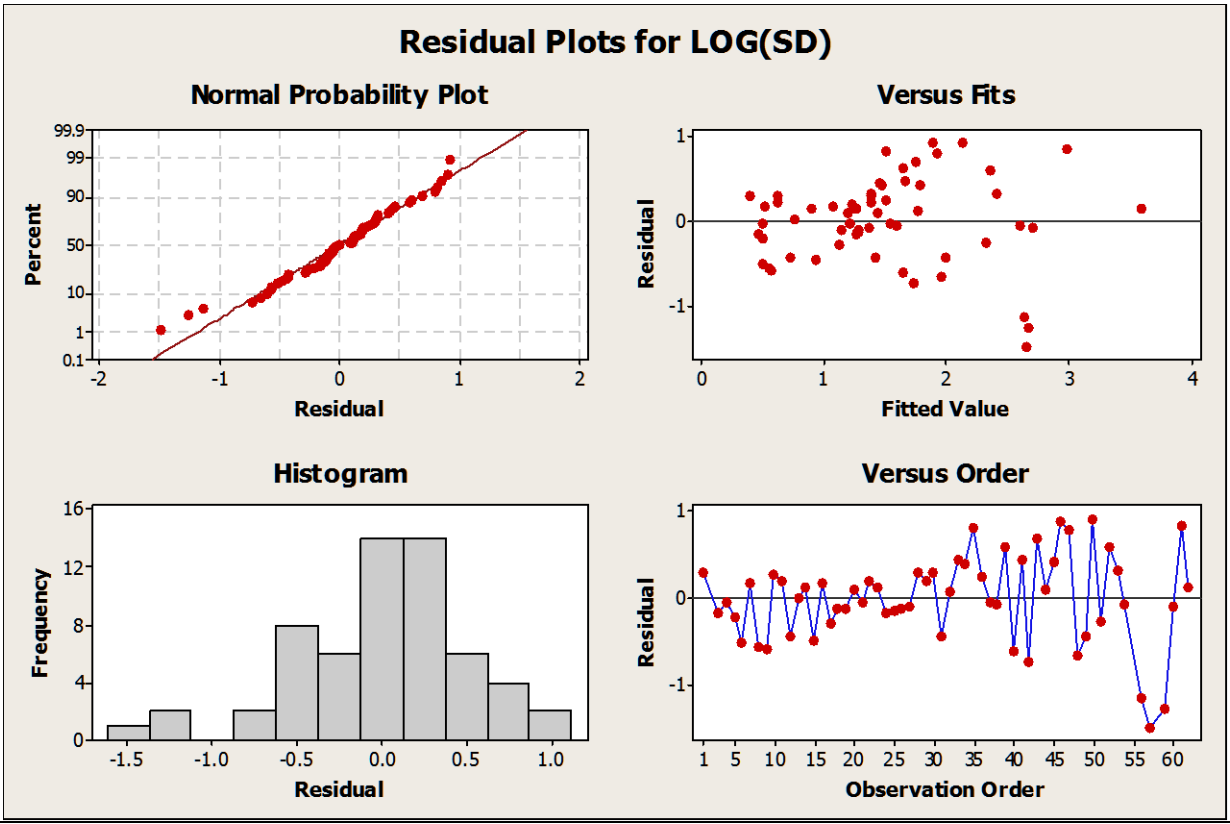

Figure 6-5 Interpretations of the residual values of the log-transformed standard deviations for 59 particulate powder tests (Note: three tests included missing values). The upper and lower left graphs indicate that the assumption of normality for the error terms is valid, as there is no significant deviation from the central trend line and the highest frequency is for values equal to zero. The upper right graph plots the error terms against their fitted values, indicating whether that the mean value of zero holds true.

The equation shows that the standard deviation increased with larger DI_{resp} values. This should be expected given that a larger DI_{resp} generally results in a greater absolute standard deviation resulting from the higher release of particulates and thus uncertainty in fate and transport of this material. The DI_{resp} for the TiO_2 as considered in this chapter was 15 mg/kg, resulting in a standard deviation of 2.5 mg/kg. The

standard deviation was then applied to E_i for quantifying the exposure distribution of each ES. The final airborne exposure concentrations are reported as average 8-hour time weighted averages.

Risk Characterization

Risk was calculated as a RCR (equation (6-4)).

$$\mathrm{RCR} = \frac{\mathrm{EXP_i}}{\mathrm{BMC_h}} \qquad (6\text{-}4)$$

RCR: Risk characterization ratio

EXP_i random sample from the exposure concentration distribution for scenario i

A risky scenario was defined as RCR values ≥ 1.0 (i.e. exposure levels higher than the BMC_h) and represents the lifetime risk of a worker exposed to the 8-hour time weighted indoor air nano-TiO_2 concentrations over 45-years, 50 weeks/year, 5 days/week. The RCR distributions were calculated by sampling the BMC_h distributions and the three NF and three FF exposure distributions over 10,000 Monte-Carlo simulations per exposure scenario.

Results

Dose-Response Analysis

In general, a BMR (i.e. the relevant toxicological response of concern or safety) should approach a lower limit of reasonably measurable effects. For changes in total white blood cell counts relevant to inflammation, increases in 10% over the background response are often found to be significant.[310] However, due to uncertainty in measuring percent changes as opposed to total cell count, significant macrophage, neutrophil and lymphocyte percent changes were determined using a BMR of 20%. For both mice and rats, neutrophil and lymphocyte percent changes increased whereas macrophage changes decreased. Ultimately, the dose-response analysis was completed using the neutrophil rat data since (i) the decrease in macrophage percent change was directly correlated with the measured change in neutrophils and lymphocytes (Appendix: Chapter 6), (ii) neutrophil percent increases were much stronger and dominant compared to lymphocyte percent changes (Appendix: Chapter 6) and lastly (iii) rats showed inflammatory responses at lower concentrations than did mice (Figure 6-6).

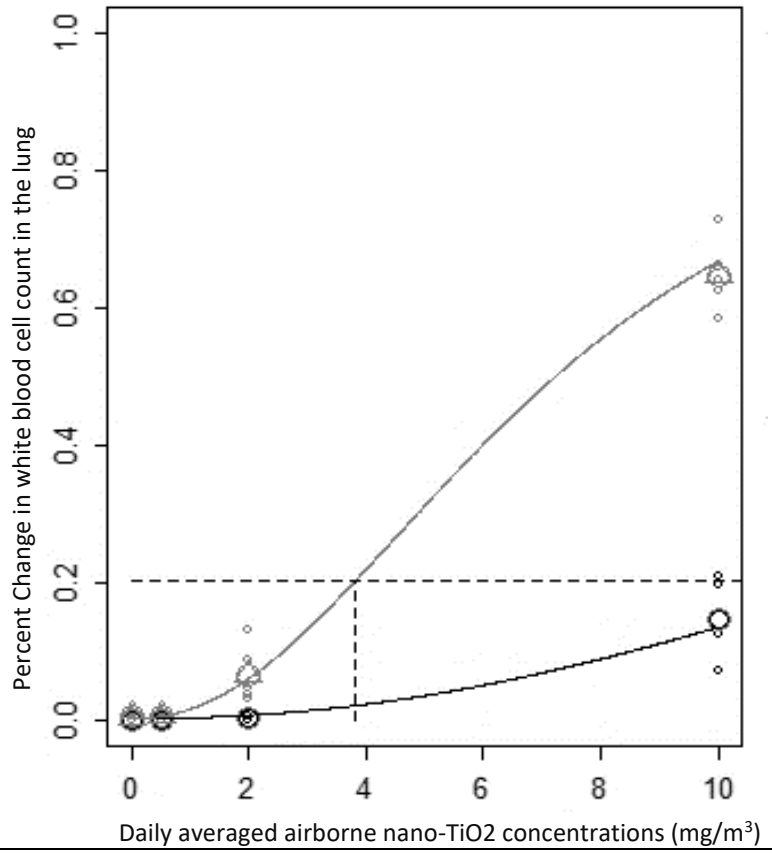

Figure 6-6 Fitted log-logistic models using PROAST software with reported confidence intervals to the mice and rat neutrophil percent changes upon inhalation of nano-TiO_2. The dose-response results demonstrate differences in the slope of the lines per species, with a much more sensitive response for rats. The does-response curve shown in this example was fitted with a log-likelihood of -1374. The benchmark dose for rats is shown by the lower curve corresponding to data with large circles, while the benchmark dose for mice is shown for the upper curve using corresponding triangular data points. (see Appendix: Chapter 6 for full set of models fit to the dose-response data)

For rats, seven valid models were fitted to the neutrophil data (Table 6-4). The models were aggregated into an overall daily averaged inhalation concentration (i.e. BMC_a) distribution that was normally distributed with a mean of 3.71 ± 0.56 mg/m^3.

Table 6-4 Daily averaged, inhalation benchmark concentrations (mg/m^3) for *in vivo* animal studies and corresponding models fit for a 20% increase in neutrophil count in mice.

Model	Two-Stage	Log-logistic	Weibull	Log-probabilistic	Gamma	Exponential	Hill	Aggregation of Models
Median	12.76	12.54	13.04	12.39	12.77	11.44	11.61	**12.32**
Mean	12.84	12.62	13.15	12.47	12.87	11.48	11.66	**12.44**
Standard Deviation	1.15	1.05	1.24	1.06	1.11	0.64	0.99	**1.20**
Minimum	9.25	9.58	9.60	9.37	9.66	9.57	8.82	**8.82**
Maximum	18.20	19.54	21.01	18.39	18.85	14.66	17.78	**21.01**

After applying EF_{inter} and EF_{intra} over 10,000 Monte-Carlo simulations, the BMC_h results followed a lognormal distribution with a geometric mean of 0.91 mg/m^3 and geometric standard deviation of 4.72 mg/m^3 (Figure 6-7). Approximately 59% and 40% of the distribution was explained by uncertainty in the values of EF_{inter} and EF_{intra}, respectively, while little variation was a consequence of the dose-response data used in the analysis (Figure 6-7).

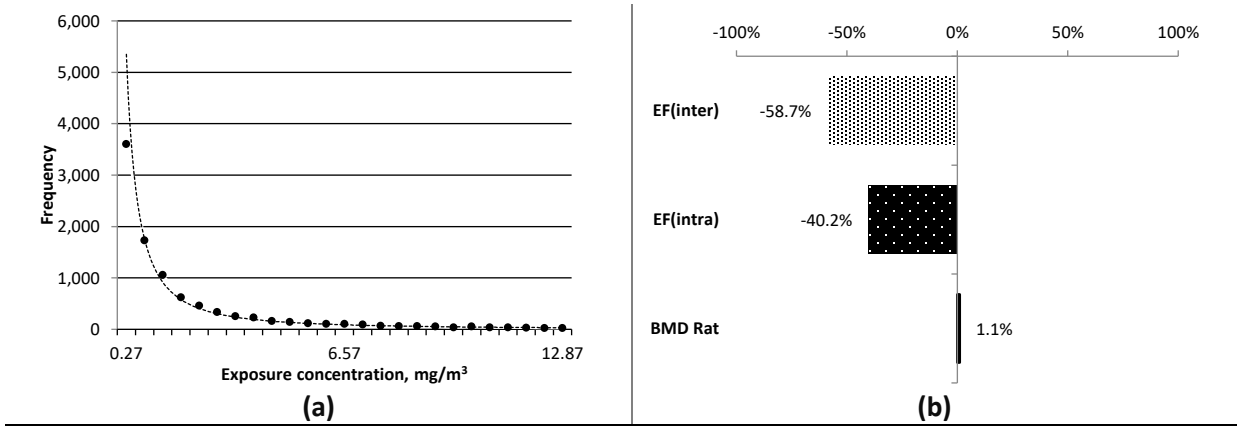

Figure 6-7 Results of (a) the 10,000 Monte-Carlo simulations used to estimate the benchmark concentration for humans (BMC_h) and (b) the contribution of each parameter used to estimate the benchmark concentrations for humans.

Exposure assessment

The daily NF and FF indoor air concentrations of nano-TiO2 were calculated for three different exposure scenarios that ultimately involved three different amounts of nano-TiO_2 throughout the 8-hour workday. The applied emission rates ranged from a low of 6.26 mg/min (ES3) to a high of 672 mg/min (ES2), while the value for ES1 was 12.0 mg/min. Figure 6-8 shows the time-integrated exposure concentrations in each of the exposure scenario.

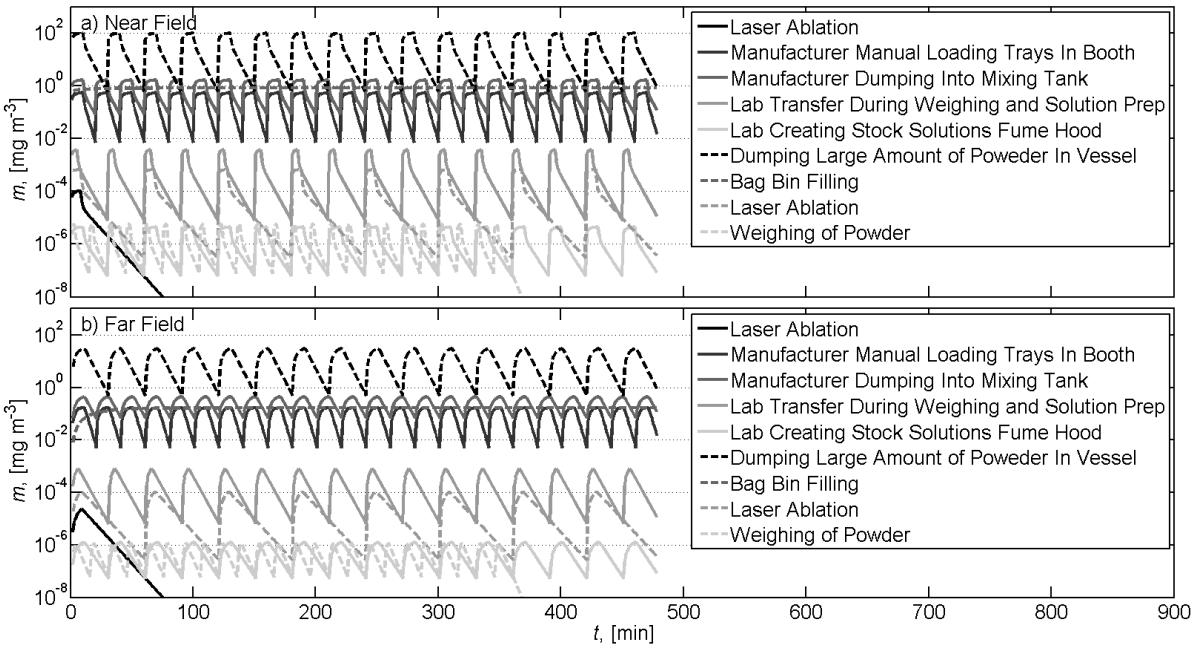

Figure 6-8 Potential exposure time-series in the (a) near field and (b) far field. Note: This figure shows the results for a larger range of exposure scenarios than presented in this chapter. These additional scenarios were completed as a part of a larger publication out of direct context of this chapter. Additional information for the other scenarios can be found in Appendix: Chapter 6.

Geometric means representing 8-hour time weighted averages for NF airborne concentrations of nano-TiO_2 ranged from a low of 0.825 mg/m^3 for ES3 and a high of 36.2 mg/m^3 for ES2, while the NF concentration for ES1 was 0.93 mg/m^3 (Table 6-5).

Table 6-5 Calculated near-field and far-field airborne concentrations of nano-TiO_2 for the three separate exposure scenarios considered in the human health risk assessment

No.	**Exposure scenario**	C_{NF}, [mg m^{-3}]	C_{FF}, [mg m^{-3}]
ES1	Manufacturer Dumping into Mixing Tank	8.93E-01	2.59E-01
ES2	Dumping Large Amount of Powder in Vessel	3.62E+01	1.18E+01
ES3	Bag Bin Filling	8.25E-01	1.60E-01

C: exposure concentration. (Note: These are the geometric means 8-hour time weighted averages that were all defined as having a geometric standard deviation of 2.5)

The daily NF and FF indoor air concentrations were lognormally distributed in all exposure scenarios based on the geometric standard deviation of the DI_{resp} of nano-TiO_2 (Appendix: Chapter 6). Large variations in the NF and FF concentrations observed between the exposure scenarios were due to differences in the time-integrated substance emission, the dilution by room size, and the air exchange rate. As expected, the resulting exposure potentials varied directly with the scenario-specific integrated emission levels

given by the emission rate and duration of the process resulting in a higher exposure potential for ES2 than in the other scenarios. In the case of ES2, the high emissions and small workroom volume were coupled with a high handling energy factor (i.e. dumping powder into a vessel) and lower air exchange rate (4 h^{-1}) as compared to the conditions in the other scenarios. Compared to the NF, the FF exposure concentrations were consistently lower but generally less than an order of magnitude lower. As was the case for the NF exposure scenarios, geometric means for FF exposure concentrations ranged from a low of 0.16 mg/m^3 for ES3 and a high of 11.8 mg/m^3 for ES2, while the value for ES1 was 0.259 mg/m^3.

Risk Characterization and Uncertainty

Table 6-6 displays the results of the risk characterization for the NF and FF exposure scenario, respectively, representing the lifetimes risk of a worker exposed to an 8-hour time weighted indoor air nano-TiO_2 concentrations over 45-years, 50 weeks/year, 5 days/week.

Table 6-6 Summary of the risk characterization (reported as risk characterization ratios) distributions for each near- and far-field exposure scenarios. Results represent 10,000 Monte-Carlo simulations.

Exposure (Near Field)	**ES1**	**ES2**	**ES3**
Risk characterization ratio (geometric mean)	9.91E-02	3.99E+00	9.05E-02
Risk characterization ratio (geometric standard deviation)	6.07	5.96	6.04
Probability risk characterization ratio ≥ 1	9.99%	78.06%	9.08%
Exposure (Far Field)	**ES1**	**ES2**	**ES3**
Risk characterization ratio (geometric mean)	2.83E-02	1.29E+00	1.77E-02
Risk characterization ratio (geometric standard deviation)	6.21	6.10	6.27
Probability risk characterization ratio ≥ 1	2.55%	55.68%	1.39%

The RCR values for each exposure scenario were log-normally distributed (Appendix: Chapter 6). The risk characterization ratio distributions for ES1, ES2 and ES3 all contained some probability of risk to inflammation of the lung (i.e. RCR values ≥ 1). Scenario ES2 had a particularly high probability of risk compared to the other scenarios (Figure 6-9), with nearly 78% of the Monte-Carlo simulation results ≥ 1 (i.e. 22% of the results resulted in no risk to the exposed workers). ES1 and ES3 resulted in 10% and 9% of their RCR ≥ 1 (Appendix: Chapter 6). For all of the exposure scenarios, roughly 75% of the variation in the RCR distributions was influenced by uncertainty in the dose-response analysis (i.e. EF_{inter} and EF_{intra}), while the remaining 25% was the result of uncertainty in the exposure estimations (Appendix: Chapter 6). In accordance with the lower airborne nano-TiO_2 concentrations found in the FF, the probability of individual FF RCR values ≥ 1 were much lower than compared with the NF. In total, approximately 56% of the results

for FF ES2 were ≥ 1 (Figure 6-9). Only 3% and 1% of ES1 and ES2 FF scenarios were likely to result a RCR ≥ 1 (Appendix: Chapter 6).

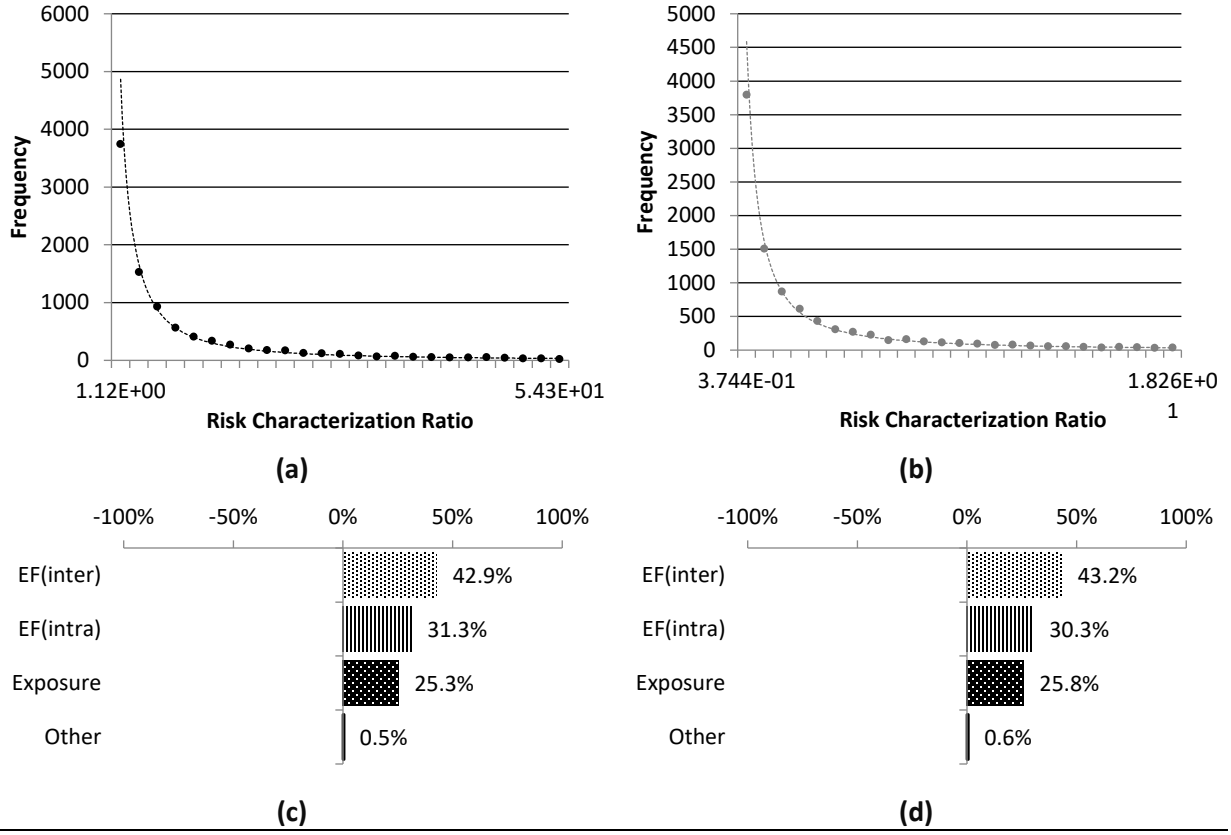

Figure 6-9 Results of 10,000 Monte-Carlo risk characterization ratio simulations for exposure scenario 2 in the (a) near-field and (b) far-field. Note that right-end tails of the distribution are artificially truncated for presentation. Contributions to the uncertainty and variation are displayed in (c) for the near-field and in (d) for the far-field.

Discussion

Risk Relevance to Engineered Nanomaterials Use in Production of Organic Photovoltaics

The results of the occupational HHRA presented in this chapter demonstrate a probability as high as 78% for the lifetime risk of lung inflammation to workers handling nano-TiO_2 during ENM production or OPV panel manufacturing. This risk was particularly relevant for ES2 where large-scale handling and use of high volume nano-TiO_2 powders occurred over 8-hour workdays. The risk to lung inflammation was calculated as a 20% increase in certain white blood cells over background levels, however this response level only indicates the onset of inflammation as opposed to the degree and/or severity of the pathology. OPV are not produced at the industrial scale and thus the exposure scenarios presented in this thesis do not represent a specific OPV industrial profile. Instead, potential and realistic exposure scenarios that involve

the production and handling of nano-TiO_2 were presented and therefore provide a first-tier assessment for OPV. For example, if OPV devices utilizing PCBM and/or TiO_2 come to full industrial scale and uptake to the marketplace, large volumes of these substances will be handled, loaded and dispensed either into other containers, holding tanks or vessels for mixing and/or application to the OPV panel. ES1 and ES3 involved exposure scenarios handling over an order of magnitude less nano-TiO_2 powder compared with ES2. Thus, these represent production volumes that are much more moderate than ES2. Nevertheless, there remained a 10% lifetime probability of lung inflammation to workers handling these lower amounts of powders over an 8-hour workday.

Uncertainties within the Risk Assessment Procedure

The dose-response assessment was completed specifically from nano-TiO_2 *in vivo* toxicological data, in accordance with the scientific literature that demonstrates the toxicological responses upon exposure to ENM and bulk substances can differ. Additionally, the emissions calculation was defined by a distribution that was defined by the standard deviation of nano-TiO_2's dustiness index. While the dustiness index was material specific, its mass-based measurement does not provide detailed information about the size-distributions in the dustiness tests. Overestimations for emissions and exposures from powder handling may be a result, whereas calculations for spray or fugitive-type releases might be closer to reality. Airborne concentrations were further calculated using a two-zone near- and far-field model, which is particularly relevant for single source, non-fugitive emissions[311] that are very relevant for ENM. For instance, the persistence of uniformly small airborne ENM may quickly decline due to aggregation and agglomeration,[199,312,313] meaning that exposure to primary or small "nano" aggregates might be most relevant close to the emission source.[314–316]

It should be noted that the fate and exposure model, NanoSafer, used in this work largely relied on advection and bulk air flow to estimate the concentration of nano-TiO_2 in the workplace. The exposure also is based on external airborne concentrations as opposed to internal doses. Particle sizes are an important characteristic influencing the effectiveness of ventilation control, personal protective equipment and ultimately where ENM retention will occur in the lung. For example, ENM might lodge deeper and more uniformly in the lung (i.e. alveoli) as compared to larger-size materials.[314] Modifying factors (e.g. use of personal protective equipment) were not considered and should be considered for future assessments. For example, Fransman et al.[317] provides protection factors for common localized controls and personal protective equipment, although these can deviate significantly from applied

protection factors for ENM.[318] Additionally, a few occupational exposure studies have shown that particle size distributions in some cases may be similar for both ENM and conventional powders.[199,312] Such considerations could be included in models that utilize size-resolved concentration data (e.g. mass median aerodynamic diameters) in their models.[283,284,319] Given these relative uncertainties, the exposure assessments and corresponding risk calculations in this HHRA can be considered as worst-case scenarios.

The uncertainty arising from the use of a mass-based dose-metric was not addressed in this chapter. Ideally, HHRA of ENM should use a dose-metric that is the best indication of toxicity as well as exposure.[246] For example, this might be indicated by mass concentration, particle number, or lung-deposited surface area. Although mass may not necessarily be the most suitable dose-metric to describe ENM dose-response relationships,[320–323] it is the metric most easily and reliably determined for measuring and managing occupational exposures as management of particle numbers or surface area is not yet achievable.[161] The extrapolation of one dose-metric to another may be possible using specific uncertainty factors. For instance, the surface area can be estimated from a particle concentration size distribution of spherical ENM. However, there are considerable challenges in reliable measurements and, therefore, data conversion between these metrics for ENM with non-spherical morphologies[45] and their agglomerates and aggregates.[324,325]

Conclusions

These findings presented in this chapter suggest that the potential human health impacts from ENM used in OPV cannot, by default, be assumed to be negligible and may in fact be highly probable. This issue may not necessarily be relevant to the current technology and production level of OPV but should be considered for future scale-ups of these devices. It is important to note that the HHRA results are not scaled to the functional units defined by the LCA in Chapter 3 and Chapter 4. The difference in scopes means that the risk pertains to the handling a mass of the ENM that is independent of exact amounts of nano-TiO_2 required to fulfill the functional unit (e.g. production of 1 Wp of OPV). Therefore, the risk cannot be directly interpreted in terms of its overall relevance to the OPV life-cycle, particularly any prospective analysis of future, large scale production of this technology. Of course, the exact exposure to these ENM used at current lab- and small-scale production per functional unit could, in some cases, be determined for the HHRA. While these results might be beneficial from a health and safety perspective for laboratory managers, for example, it may ultimately provide little relevance from an eco-design perspective where material choices and occupational workplace conditions at the industrial scale are being extrapolated

from lab- or research-based scenarios and where uncertainty is thus high. Instead, potential human health impacts calculated within LCA, as opposed to absolute values of risk, might prove more useful for early design and development of emerging technologies. The next chapter presents the methods and results of calculating the potential human health impacts for ENM within the context of life-cycle impact assessment and the OPV-LCA case studies presented in earlier chapters.

Chapter 7 Life-Cycle Impact Assessment Nanomaterial Characterization Factors: Titanium Dioxide Case Study

In the previous chapter, a HHRA was conducted to calculate the human health risk associated with handling and working with moderate to large amounts of nano-TiO_2. The results demonstrate that there are high probabilities of lifetime risk to lung inflammation for workers handling these materials based on the 8-hour time weighted average exposures calculated with the NanoSafer fate and exposure model. The HHRA results will be particularly important and relevant for industries where workplace conditions particularly match the descriptions of the exposure scenarios tested in Chapter 6 (i.e. that represent large or industrial-scale production). It would be of benefit to be able to integrate these methods with life-cycle impact assessment methods. The advantages would allow the simultaneous analysis for other similarly related metal oxide ENM, with the potential to modify the approach for non-metal oxide ENM that are both found in OPV. Additionally, integration facilitates the comparison of ENM-specific human health impacts with non-ENM sources of human health impacts by directly converting all such impacts to the functional units used in Chapter 3 and Chapter 4. Such results could be used to identify if ENM is a driving influence in human health impacts over the OPV life-cycle and, thus, more appropriately prioritize eco-design and product development efforts.

A handful of studies have made first approximations to incorporate the ecotoxicity or human health impacts from ENM into their LCA studies,[93–96] but otherwise these impacts have been conspicuously missing from the majority of published ENM-related LCA studies.[96,184] In those studies that addressed these issues, mainly ambient emissions of and ecotoxicity relevant CF_{NS} have been published. Other studies show that pollutant emissions, including ENM, in occupational and indoor settings can be very important contributors to overall LCA results.[227,326,327,235,328] Occupational settings present unique scenarios where production[329] of pristine particles with small size distributions and thus exposure may occur. Neglecting such occupational, indoor ENM emissions in a LCA may result in burden shifting from the environment to workers. Currently, there is only one such CF_{NS} relevant to indoor emissions of these ENM.

These previously reported CF_{NS} have made use of existing life-cycle impact assessment methods such as USEtox. This approach takes advantage of a number of assumptions that conveniently describe the fate and transport of small organic molecules and metals quite well, but these methods are not appropriate

for ENM.[196] The major assumptions utilized in human health life-cycle impact assessment methods are that conditions are at steady-state and systems have reached thermodynamic equilibrium.[101,197] However, ENM behave, in effect, like colloidal substances that, when released into a specific medium, exist in their own phase and will not form uniform phases with the surrounding medium unlike organics. Therefore and by definition, ENM are not thermodynamically stable, even if certain ENM may be kinetically stable for long periods of time.[196] Previous adaptations to current life-cycle impact assessment methodologies such as USEtox have been made to estimate the ecological[94–96] and human health impacts[93] of ENM. In all previous cases, steady-state conditions were kept in the model, and as was previously discussed in Chapter 5. Thus, the aim of this chapter is to present a dynamic life-cycle impact assessment fate and exposure model for estimating the human health impacts from indoor, occupational ENM air emissions. The approach presented in this chapter integrates part of the HHRA methodology proposes in Chapter 6 with life-cycle impact assessment. The results of the integration are applied for nano-TiO_2.

Methods

The calculation of a CF_{NS} for use in LCA is further presented in this chapter, where CF is defined in an analogous fashion to equation (2-2).[234,330] However, unlike the that equation, the iF is not estimated using (equilibrium) partition coefficients inside of steady-state models. Instead, a dynamic fate and exposure model using kinetically defined fate and exposure parameters is used to define a newly introduced Retained-intake Fraction (RiF).

Emissions of and Exposure Scenarios for Nano-TiO_2 in the Occupational Indoor Setting

ENM emissions can be directly measured, estimated from published literature or calculated using models. In many cases, means for measuring emissions or the primary data needed may not exist. Therefore, it can be useful and often necessary to model such emissions. A total of six exposure scenarios (ES1-ES6) (Table 7-1) were modeled and identified from the previous HHRA in Chapter 6.

Table 7-1 Parameters used in the fate-transport model describing the exposure scenarios involved with "dumping large amounts of powder in a vessel" per the description in Chapter 6, *Table 6-2*. The exposure scenarios differ based on the magnitude of the emission, *e*, per minute and the frequency of the work-cycle activity, *f*. H_i = handling energy factor, t_{wc} is work cycle time, p_{wc} is pause between work cycles, n_{wc} is number of work cycles, $A_{handled}$ is amount of material transferred per transfer event within each work cycle, V_{tot} is the total volume of the work room, and *AER* is the general air exchange ratio in the work-room

No.	**Exposure scenario**	E_i, **[mg/min]**	H_i	t_{wc}, **[min]**	p_{wc}, **[min]**	n_{wc}	$A_{handled}$, **[kg]**	V_{tot} **[m³]**	**AER [h⁻¹]**
ES1	e-high, *f-short*	6.72E+02	0.80	10	20	16	5.60E+02	100	8
ES2	e-high, *f-long*	6.72E+02	0.80	60	60	4	3.36E+03	100	8
ES3	e-high, *f-daily*	6.72E+02	0.80	480	0	1	2.69E+04	100	8
ES4	e-high, *f-single pulse*	6.72E+02	0.80	1	0	1	5.60E+01	100	8
ES5	e-medium, *f-short*	6.72E+00	0.80	10	20	16	5.60E+00	100	8
ES6	e-low, *f-short*	6.72E-02	0.80	10	20	16	5.60E-02	100	8

These scenarios were more precisely six variations of a single representative workplace-activity that involved the handling of nano-TiO_2. The description of this workplace activity was adapted from the NANEX (www.nanex-project.eu) database, an EU FP7 project which aimed to catalogue potential EMN exposure across the life-cycle including their manufacturing and industrial use. The emission scenarios in this case study represented occupational settings where pre-fabricated ENM were *handled* as opposed to scenarios that estimate exposure *during* the production of raw-ENM. The latter scenarios were not included due to the assumption that production of raw-ENM is more likely to occur under automated, enclosed settings where fugitive (i.e. accidents) exposures were assumed to be near zero.

ES1 represents a large (mass) emission event, involving the dumping of large amounts of nano-TiO_2 powder into an open vessel over work-cycles lasting ten minutes and with 20-minute pauses in-between over an 8-hour workday. The magnitude of emission per minute was estimated as a function of the total amount (kg) of nano-TiO_2 handled per minute, the dustiness index of the nanoparticles and the handling energy factor of the work-related activity as previously described in equation (6-2).[219]

ES1 was characterized with a high handling energy factor and which took place in a modestly sized hall with moderately low ventilation (i.e. air exchange rate). ES2-ES6 (Table 7-1) represent variations of ES1 based on differences in (a) the magnitude of the emission, *e*, per minute and (b) the frequency of the work-cycle activity, *f* (i.e. a function of both duration and pattern of occurrence). ES2, ES3 and ES4 all had the same emission rate but at frequencies of 60 min, 480 min and one min, respectively. Compared to ES1 whose frequency of ten min was defined as short, ES2, ES3 and ES4 represent long, all-day (i.e. non-interrupted) and single-pulse frequencies, respectively. Conversely, ES5 and ES 1.6 had the same, short

frequencies as ES1 but contained modified emission rates that were 2-orders and 4-orders of magnitude smaller than ES1, respectively. Compared to ES1 whose emission rate was considered high, ES5 and ES6 were considered medium and low rates, respectively.

Fate and Transport Model for Airborne Emissions of Nano-TiO_2 in Occupational Indoor Air

Similar to what was presented in Chapter 6, a two-zone, dynamic fate and transport model is presented for use with indoor, occupational ENM airborne emissions. The model assumes that there was only one emission source fully located inside a near-field zone. The NF is where exposure was assumed to take place exclusively. The remaining indoor air room volume was defined as the FF and is not to be confused with outdoor air compartments. The NF is defined as the volume of a hemisphere with a radius of 0.8 m. This radius corresponds with being an arm's length away from the source of emission.[309] Both NF and FF zones were modeled as well-mixed compartments, thus the model can be thought of as two well-mixed one-box compartments linked by the airflow between them.[311] Existing LCA indoor air impact assessment methodologies utilize a one-box model under the assumption that there is only one emission source in a well-mixed room[331] (equation (7-1)).

$$V \cdot \frac{dC_{\mathrm{i}}}{\mathrm{d}t} = S - (C_{\mathrm{i\text{-}1}} \cdot Q) \qquad (7\text{-}1)$$

V: the volume of the compartment (m^3)
C_{i}: the concentration at a given time-step (mg/m^3)
$C_{\mathrm{i\text{-}1}}$: concentration at the previous time-step (mg/m^3)
S: the emissions rate (mg/hr)
Q: ventilation rate (m^3/hr)

In the case of indoor air emissions from single point sources, it can be anticipated that large concentration gradients will exist between the point of emission and points further away from the source.[332] Uses of two-box models have thus shown that exposure near the source term can be 1.5-2 times greater than estimates for a one-box model.[332] To accommodate for imperfect mixing, life-cycle impact assessment methods conventionally use a mixing factor, *m* (equation (7-2)).[97,235,234,331]

$$V \cdot \frac{dC_{\mathrm{i}}}{\mathrm{d}t} = S - (C_{\mathrm{i\text{-}1}} \cdot Q \cdot m) \qquad (7\text{-}2)$$

m: mixing factor for an incompletely mixed one-compartment model

However, the use of *m* can still result in underestimations of NF exposure upwards of 50% compared to the results of a two-zone model, depending on the assumptions of the inter-zonal air flow, β, between the NF and FF as well as the ratio of the NF and FF volumes.[311]

β was defined as the volume of air that was exchanged between the NF and FF, equally entering and leaving through half of the curved surface area of a hemisphere (equation (7-3)).[311]

$$\beta = s \cdot \pi \cdot r^2 \qquad (7\text{-}3)$$

s: average air speed between the near- and far-fields (m/s)
r: radius of the near-field (m^3)

Thus, in this chapter a two-zone, dynamic model (equations (7-4) and (7-5)) was used to address the difference between NF and FF exposures.

$$V \cdot \frac{dC_{NF}}{dt} = S + (\beta \cdot C_{FF\text{-}1}) - (C_{NF\text{-}1} \cdot Q \cdot m) - (\beta \cdot C_{NF\text{-}1}) \qquad (7\text{-}4)$$

C_{NF}: near-field concentration at a given time-step (mg/m^3)
$C_{NF\text{-}1}$: near-field concentration at the previous time-step
$C_{FF\text{-}1}$: far field concentration at the previous time-step
β: Inter-zonal air flow between the near- and far-fields

$$V \cdot \frac{dC_{FF}}{dt} = (\beta \cdot C_{NF\text{-}1}) - (C_{FF\text{-}1} \cdot Q \cdot m) - ((\beta + Q) \cdot C_{FF\text{-}1}) \qquad (7\text{-}5)$$

C_{FF}: near-field concentration at a given time-step (mg/m^3)

ENM settling velocities are relatively slow,[333] thus when indoor ENM emissions are sufficiently low and ventilation rates are high, steady-state ventilation models may adequately describe particle loss and estimate indoor ENM concentrations.[97] However, these conditions may not always be met, as has been demonstrated for regular chemicals.[330] For ENM, this would mean contributions from non-ventilation sources of particle loss such as homo-aggregation and gravitational settling.[97] The introduction of non-ventilation sources of particle loss (*k*) in a two-zone, dynamic model is represented by mass balance equations (7-6) and (7-7).

$$V \cdot \frac{dC_{NF}}{dt} = S + (\beta \cdot C_{FF\text{-}1}) - (C_{NF\text{-}1} \cdot V_{NF} \cdot k) - (\beta \cdot C_{NF\text{-}1}) \quad (7\text{-}6)$$

V_{NF}: Volume of the near-field

k: non-ventilation sources of particle loss

$$V \cdot \frac{dC_{FF}}{dt} = (\beta \cdot C_{NF\text{-}1}) - (C_{FF\text{-}1} \cdot V_{FF} \cdot k) - ((\beta + Q) \cdot C_{FF\text{-}1}) \quad (7\text{-}7)$$

V_{FF}: Volume of the far-field

where k_i is any source (i) of non-ventilation removal, V_{NF} is the NF volume and V_{FF} is the FF volume. The V_{NF} equaled 1.07 m3 and was defined as the volume of a hemisphere with (near-field) radius of 0.8 m. The V_{FF} was equal to the total volume of 100 m^3 less the V_{NF}. All the values used in the fate and transport model are listed in Table 7-2.

Table 7-2 Parameters and their values used in the fate and transport model

Parameter	Description	Value	Units	Additional Information
r	Radius of near-field	0.8	m	An average arm's length from the emission source[309]
V_{NF}	Volume of the near-field	1.07	m^3	Defined as the volume of a hemisphere with radius, r
V_{FF}	Volume of the far-field	98.93	m^3	Defined as V_{tot}-V_{NF}, where V_{tot} is 100 m^3
β	Inter-zonal air flow	21.94	m^3/min	Equation (7-3)
s	Air flow between near- and far-fields	0.18	m/s	Calculated from reported (measured) indoor air speeds at occupational workplaces dealing with powder mixers and packers, excluding the outlier (Appendix: Chapter 7)[334]
k_h	Homo-aggregation rate constant	3.19E-4	m^3/kg-s	
v_{set}	Gravitational settling based on Stoke's law	N/A	N/A	Equation (7-8)
ρ_p	ENM particle density	3900	kg/m^3	
d_e	Diameter of ENM	21	nm	Equivalent volume diameter
g	Gravity	9.8	m/s^2	
C_s	Cunningham slip correction factor	1	Unit-less	(Appendix: Chapter 7)[335]
n	Viscosity of air	0.00111	kg/m-min	
x	Dynamic shape factor	1	Unit-less	Values of 1 correspond with perfectly spherical particles
h_w	Height of the workplace	4	m	
h_e	Height of the emission source	1.5	m	
T	Time scale	10,080	min	Number of minutes in a week
t	Time-step	1	min	Time resolution at which the model was integrated
Q (k_{ex})	Air-exchange rate	8	hr^{-1}	In a two-zone model, this represents the air exchange rate of the far-field room volume

The sources of non-ventilation particle loss considered in this model were (i) homo-aggregation and (ii) gravitational settling. Homo-aggregation was estimated using a rate constant (k_h) of 3.19E-4 m^3/kg-s. The removal, k_{set}, due to gravitational settling and interpreted through Stoke's Law[97] was defined by equation(7-8):

$$k_{\text{set}} = \frac{v_{\text{set}}}{h} = \left[\frac{\rho_{\text{p}} \cdot d_e^2 \cdot g \cdot C_s}{18 \cdot n \cdot x}\right] \cdot \left[\frac{1}{h}\right] \qquad (7\text{-}8)$$

v_{set}: Stoke's Law
ρ_{p}: particle density
d_e : the equivalent volume diameter
g: gravity
C_s: Cunningham slip correction factor
n: viscosity of the medium
x: dynamic shape factor (i.e. perfectly spherical materials have a value of 1)
h: height of the emission source

Gravitational settling is likely to be more important for ENM that are ≥ 100 nm while Brownian motion might be more important for ENM below 100 nm, although this distinction is not absolute and may differ based on the type of ENM under consideration.[97,201,336]

The model was constructed in MatLab 9.0 (MathWorks, USA) across time-steps of one-minute and initially ran at iterative, increasing total durations starting with one-day, until pseudo-steady state concentrations, if any, were observed.

Exposure to Nano-TiO_2 in Occupational Indoor Air

A physiologically-based pharmacokinetic (PBPK) model was adapted from Li et al.[337] to establish the deposition and retention of nano-TiO_2 in the lung as a function of time. This PBPK model, which was originally built for estimating the fate and bio-distribution of inhaled nanoparticles of cerium oxide in rats, was adapted for human physiologically based pharmacokinetic modeling upon inhalation of nano-TiO_2 using parameter values from published literature.[338–343] The reader is referred to Li et al. [337] for complete details on the model, but a brief explanation of the component parts and the adaptations made in this chapter follows. The model estimated bio-distribution in the lung after considering (i) mucociliary clearance, (ii) phagocytosis and (iii) entry of nano-TiO_2 into the interstitium of lungs and subsequent systemic circulation via penetration of the alveolar cell walls.[337] In the lungs, the model estimated

deposition in three airway regions: (i) the head or upper airways, (ii) the tracheobronchial region, and (iii) the pulmonary region (i.e. where air exchange occurs at the alveoli). The MPPD v3.01 dosimetry model was used to derive the regional (fractional) deposition of ENM in these regions (Appendix: Chapter 7). The inputs to the MPPD model, including the resulting fate model ENM concentrations, are shown in Appendix: Chapter 7. These values were used to determine the relative deposition of the airborne nano-TiO_2 concentrations that entered the lung and to which parts of the lung. The results of the clearance and ultimate retention of this deposited dose was then calculated by the PBPK model.

Phagocytizing cells (PCS) reside in both the pulmonary region of the lungs and the interstitium of the lungs. The ultimate retention of ENM in the lung was dependent on a number of processes including (i) translocation from the pulmonary region to the interstitium of lungs then to systemic circulation, (ii) sequestration of ENM by PCS, (iii) transfer of loaded-PCS to the tracheobronchial region via mucociliary clearance, and (iv) transfer from the tracheobronchial region to the pharynx via mucociliary clearance. Flow- and diffusion- limited processes, defined by their respective permeability and partition coefficients (Appendix: Chapter 7), governed the exchange of ENM with blood and tissues, while sequestration of ENM by PCS has organ-specific saturation levels and the sequestration rate decreased as the load in PCS approaches saturation. Finally, mucociliary clearance rate was defined by a constant value irrespective of ENM loading in the lung. It has been shown that pulmonary clearance of particulates found in lavages is 10-times faster in rats compared with humans and might be partially explained by the greater mucociliary clearance rate in rats compared with that in humans.[344] Thus, the transport factor governing translocation of loaded-PCS to the tracheobronchial region was changed to 1.44E-6 (min^{-1}), which is one-order of magnitude slower than in the original model of Li et al.[337] Ideally, inhalation rates should fluctuate over time due to differences in metabolic activity.[201] In the current model, an inhalation value of 34.0 L/min was assumed during the work-related activity and a value of 14L/min during non-work activities.[345] Additionally, it was assumed that workers were in the FF during non-work activities. Blood flow was modeled for heavy exercise during the 8-hour workday and 5 workdays per week, while non-working hours and non-workdays reflected blood flow values for people at rest. A complete list of all PBPK parameters and their values of the model can be found in Appendix: Chapter 7. The PBPK model was implemented in Berkeley Madonna™ version 8.3 (Berkeley, CA) and initially ran in iterative durations to determine when, if any, maximal retention in the lung occurred.

Retained-Intake Fraction of Nano-TiO_2 Emissions to Occupational Indoor Air

The results of the fate and exposure model were combined into an overall RiF, which represents the averaged internal wet lung mass of TiO_2 (EXP_{int}) per averaged lifetime emitted mass of TiO_2 (E_{life}). This is different from traditional inhalation iF, which is the inhaled amount per emitted amount.[346] Two different time-horizons were used to represent acute and chronic exposure scenarios. These were defined using a (i) short-term, 1-year of work and (ii) lifetime, 45-years of work periods. The time-weighted average wet lung burden was calculated over an assumed life expectancy of 70 years, defined by periods of (i) non-work between ages 1-20, (ii) work between ages 21-65 and (iii) non-work in their retirement between ages 66-70. Thus, the model assumed emissions that persisted throughout the complete set of working years of 20-65 (E_{life}) irrespective of whether the person was working or not the entire time. Therefore, the 1-year time-weighted lung burden assumed one year of exposure, while the lifetime time-weighted lung burden assumed 45 years of exposure. These wet lung burdens were then divided through by the 70-year life expectancy to obtain a total retained wet lung burden over lifetime. Finally, the 1-year and lifetime ratios of lifetime wet lung dose and lifetime of emissions were scaled by the number of workers (POP) inside of the exposure zones (equation *(7-9)*).

$$RiF = \frac{EXP_{\text{int}}}{E_{\text{life}}} \cdot POP \qquad (7\text{-}9)$$

RiF: Retained intake fraction (*unitless*)
EXP_{int}: Exposure as internal lung dose (µg/g-wet lung)
E_{life}: Lifetime emissions (kg)
POP: Worker population (number of persons)

The number of workers exposed was adapted from Walser et al. and estimated as a lognormal distribution with a geometric mean of 8.7 and geometric standard deviation of 2.8 (Appendix: Chapter 7).[97]

Effect Factors for Nano-TiO_2 in Occupational Indoor Air

The EF describes the human health impact of a substance and is dependent on its underlying dose-response relationship (e.g. chemical, particle).[84] The EF was estimated based on the USEtox approach,[84] defined according to equation (7-10):

$$EF = \frac{0.5}{ED_{50,h,int}} \qquad (7\text{-}10)$$

$ED_{50,h,int}$ is defined as the human-equivalent (h) dose at which 50% of population experiences a carcinogenic or non-carcinogenic impact upon inhaled, internal (int) exposures
0.5: the fraction of the worker population that experiences the adverse human health impact

Thus, when combined with the RiF, equation (7-10) assumes a linear relationship between the exposure and response, up to the point of 50% disease probability in the human population.[84] Unlike USEtox which is concerned with external exposure concentrations, the ED_{50} put forth in this chapter (equation (7-11)) is reported as an internal dose per g of wet-lung since the RiF represented lifetime-averaged internal exposure doses.

$$ED_{50,h,int} = \frac{ED_{50a,t,int}}{AF_a \cdot AF_t} \quad (7\text{-}11)$$

$ED_{50a,t,int}$: animal (a) internal dose (int) of nano-TiO_2 (mg/g-wet lung)
t: duration of the study (e.g. chronic)
AF_a: interspecies extrapolation factor
$AF_{t:}$ study-time conversion factor

Interspecies extrapolation factors are conventionally used to account for anatomical and physiological differences (e.g. metabolic rates) between species, however no such factor was applied in this study as both the exposure and EF were reported as mass of TiO_2 per g-wet lung, under the assumption that effects based on the internal doses and toxic mode of action were equivalent in animals and humans.[347] The $ED_{50a,t,int}$ assumed, a 1:1 correlation of the disease and calculated as *extra risk*. Extra risk being the fraction of animals that respond to a dose, among animals who do not respond, effectively taking into account the background response rate.[310] Time conversion factors are used to account for differences in exposure durations. An AF_t of 2 was used to convert the sub-chronic non-carcinogenic dose-response data to chronic-equivalent values.[347] The dose-response data used to estimate the $ED_{50a,t,int}$ was specific for dry-lung sections. Thus, the dry-lung $ED_{50a,t,int}$ values were converted to a wet-lung value with the conversion factor of 0.11 based on previous results showing that nearly 89% of the lung-weight is lost after drying.[348]

The non-carcinogenic $ED_{50a,t,int}$ was estimated from experimental data found in the literature. Using the PROAST software (Chapter 6), the BMD approach[349] was employed to determine the $ED_{50a,t,inh,NC}$ relationship between internal TiO_2 mass loadings per gram of lung and the corresponding increase in lung inflammation. The BMD approach is an alternative to the NOAEL or LOAEL methods traditionally used to estimate the dose-response relationship (Appendix: Chapter 7). One of the advantages of the BMD approach is that it utilizes all the dose-response data in its estimation, whereas the N(L)OAEL method largely ignores the shape of the dose-response curve.[310,349–353] The BMD is estimated and interpreted from a corresponding BMR, defined as the level of response (i.e. adverse health impact) considered significant. The BMR was defined as the 50% increase in lung-inflammation, according to BAL results of rats and mice

exposed to nano-TiO_2 at concentrations of 0.0 mg/m^3 (control), 0.5 mg/m^3, 2.0 mg/m^3 and 10 mg/m^3 for 6 hours/day, 5 days/week, for 13 weeks.[283] Lung inflammation was interpreted as the percent change in neutrophil count (i.e. neutrophil counts per 200 total cellular samples) and was measured as a function of internal TiO_2 lung burden.[283] Typically a BMR of 10% would be analogous to a corresponding NOAEL value, and thus would require that the resulting BMD is extrapolated to the ED_{50}.[354] Instead, the BMR was set to 50% *extra risk* and assumed to correspond directly to the ED_{50}. While lung inflammation is not a disease in and of itself, it is used here as a general proxy-human health impact, representing a precursor of other non-carcinogenic health effects.

There were no carcinogenic animal studies involving exposure to multiple dosing levels, however in 2011 the U.S. NIOSH conducted a HHRA on nano-TiO_2 by supplementing the lack of ENM-specific dose-response data with using previously published data from both fine- and nano-TiO_2.[355,356] Using this same dataset, a carcinogenic ED_{50} was calculated as the dose where 50% of the exposed animals developed lung tumors. Briefly, two chronic, whole-body, inhalation studies by Lee et al. and Muhle et al. studied the tumor rates of male and female Sprague-Dawley and Fischer-344 rats that were exposed to fine (rutile) particles of TiO_2 with average mass-median-aerodynamic-diameter of 1.6 µm and 1.1 µm, respectively.[355,357] In Lee et al., there were four exposure levels of 0, 10, 50, and 250 mg/m^3. In Muhle et al., there were two exposure levels of 0 and 5 mg/m^3. Heinrich et al. completed a chronic, whole-body, inhalation study on Wistar female rats exposed to 10 mg/m^3 of nano-TiO_2.[284] The dose-response relationships of ENM are known to be more strongly correlated with surface area as opposed to mass-based dose metrics for different diameter particles. Therefore, the doses were converted to surface area based doses using their reported conversion factors of 4.99 m^2/g for the fine- particulate and 48 m^2/g nano-TiO_2. As was done for the non-carcinogenic ED_{50} estimation, the BMR was set to 50% *extra risk* in total lung tumor development.

Classes of Occupational Indoor Air Human Health Characterization Factors for Nano-TiO_2

As discussed previously, both the physico-chemical properties and environmental parameters influence the fate of, exposure to and/or toxicity from ENM. Thus, LCA practitioners, not unlike risk assessors, will be forced to estimate these quantities on a case-by-case basis if the objective is to understand the absolute impacts of a particular exposure scenario. However, as LCA is generally used for comparative purposes, some level of aggregation and generalization of the model and its parameters is warranted. A *Context-dependent Integration* life-cycle impact assessment approach for estimating human health impacts of ENM, as presented in Chapter 5, is used to complete such aggregation. A first approximation

to categorize CF_{NS} was made based on the magnitude of the emission rates, emission frequencies, worker population size and time-frame of exposure.

Results

Emissions of Nano-TiO_2 in the Occupational Indoor Setting

The emission rates for ES1-ES4 were all equal to 6.72E+02 mg/min. These also happened to be the scenarios with the highest emission rates, while emission rates for ES5 was 6.72E+00 mg/min and 6.72E-02 mg/min for ES6. Although the emission rates for ES1-ES4 were the same, their total daily emissions (Table 7-3) were not equal due to changes in the frequency and duration of the emission events.

Table 7-3 Results for emissions and final near-field and far-field concentrations.

No.	**Exposure scenario**	**E_i, [mg/min]**	***Total Daily Emissions (mg)***	**$C‡_{NF}$, [ug m^{-3}]**	**$C‡_{FF}$, [ug m^{-3}]**	**$C^{\dagger}_{NF}$, [ug m^{-3}]**	**$C^{\dagger}_{FF}$, [ug m^{-3}]**
ES1	e-high, *f-short*	6.72E+02	1.08E+05	6.50E+04	3.45E+04	2.49E+04	1.48E+04
ES2	e-high, *f-long*	6.72E+02	1.61E+05	8.15E+04	5.09E+04	4.07E+04	2.54E+04
ES3	e-high, *f-daily*	6.72E+02	3.23E+05	8.15E+04	5.09E+04	8.08E+04	5.02E+04
ES4	e-high, *f-single pulse*	6.72E+02	6.72E+02	3.63E+04	6.01E+03	1.70E+02	1.06E+02
ES5	e-medium, *f-short*	6.72E+00	1.08E+03	6.77E+02	3.71E+02	2.71E+02	1.69E+02
ES6	e-low, *f-short*	6.72E-02	1.08E+01	6.77E+00	3.71E+00	2.71E+00	1.69E+00

C: exposure concentration| † Average daily concentrations during the working hours | ‡ Maximum daily concentration

Total daily emissions for ES1-ES3 differed by less than one-order of magnitude even though emission frequencies and durations were noticeably different. Particularly, ES2 was characterized by 60-minute emission cycles with 60-minute pauses in-between, resulting in a total daily nano-TiO_2 emissions of 1.61E+05 mg. This was only 35% larger than ES1 even though emission events lasted ten minutes long with 20 minute breaks in-between. ES3 had a constant all day emission event that resulted in a total daily nano-TiO2 emission of 3.23E+05 mg, roughly 3-times the daily emission of ES1. ES4 was characterized by a single-pulse emission event that resulted in a total daily nano-TiO_2 emission of 6.72E+02 mg. The total daily emissions for ES5 and ES6 were roughly 2- and 4-orders of magnitude smaller, respectively, than ES1. This was in direct correlation with their 2- and 4-orders of magnitude decrease in emission rate.

Over the course of 1-year total emissions were greatest for ES3, corresponding with its high relative emission rate magnitude and continuous all-day emissions. The total yearly emissions of ES1 and ES2 were only slightly lower than ES3 even though their frequencies were much less often and shorter emission events. However, the single-pulse emission resulted in an over 2-orders of magnitude decrease in yearly emissions compared to ES1, ES2 and ES3 (Figure 7-1).

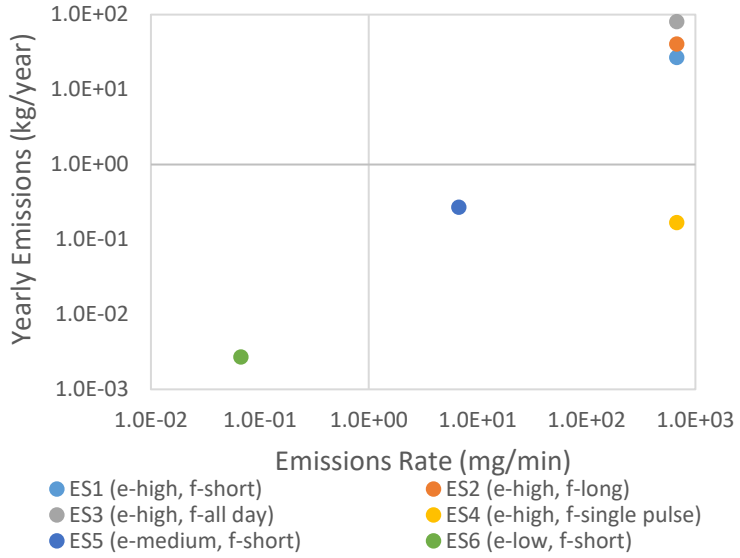

Figure 7-1 Comparison of yearly emissions and emission rate.

As opposed to the change in emission frequency, the most noticeable change in yearly emissions were due to the change in emission rate, whereby the yearly emissions for ES6 were over 4-orders of magnitude smaller than ES1, ES2 and ES3, and over 2-orders of magnitude smaller than ES4 and ES5.

Fate and Transport of Airborne Emissions of Nano-TiO_2 in Occupational Indoor Air

The results of the fate model are reported as two different NF and FF airborne concentrations. Figure 7-2 shows the trends in NF and FF concentrations during the 8-hour workday.

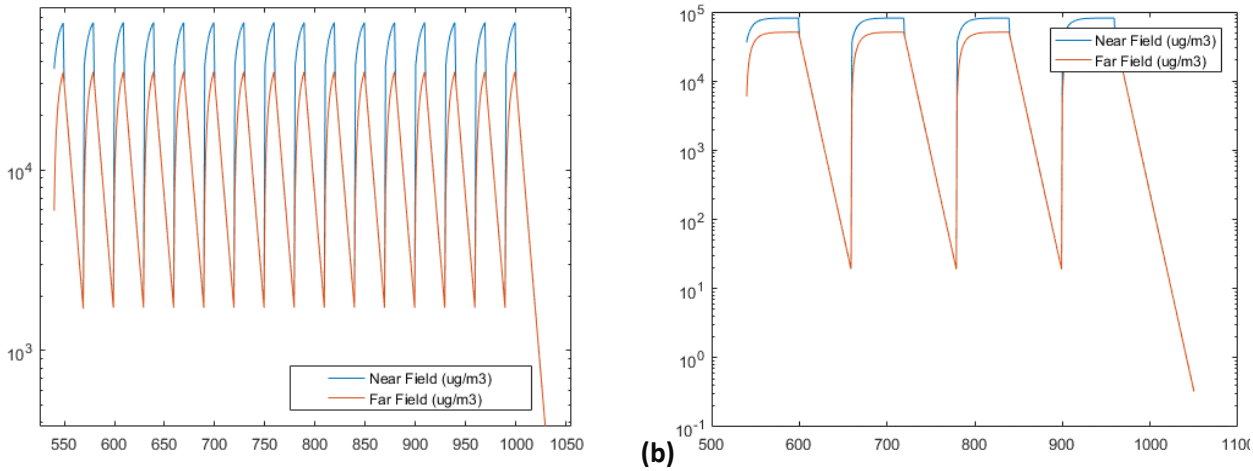

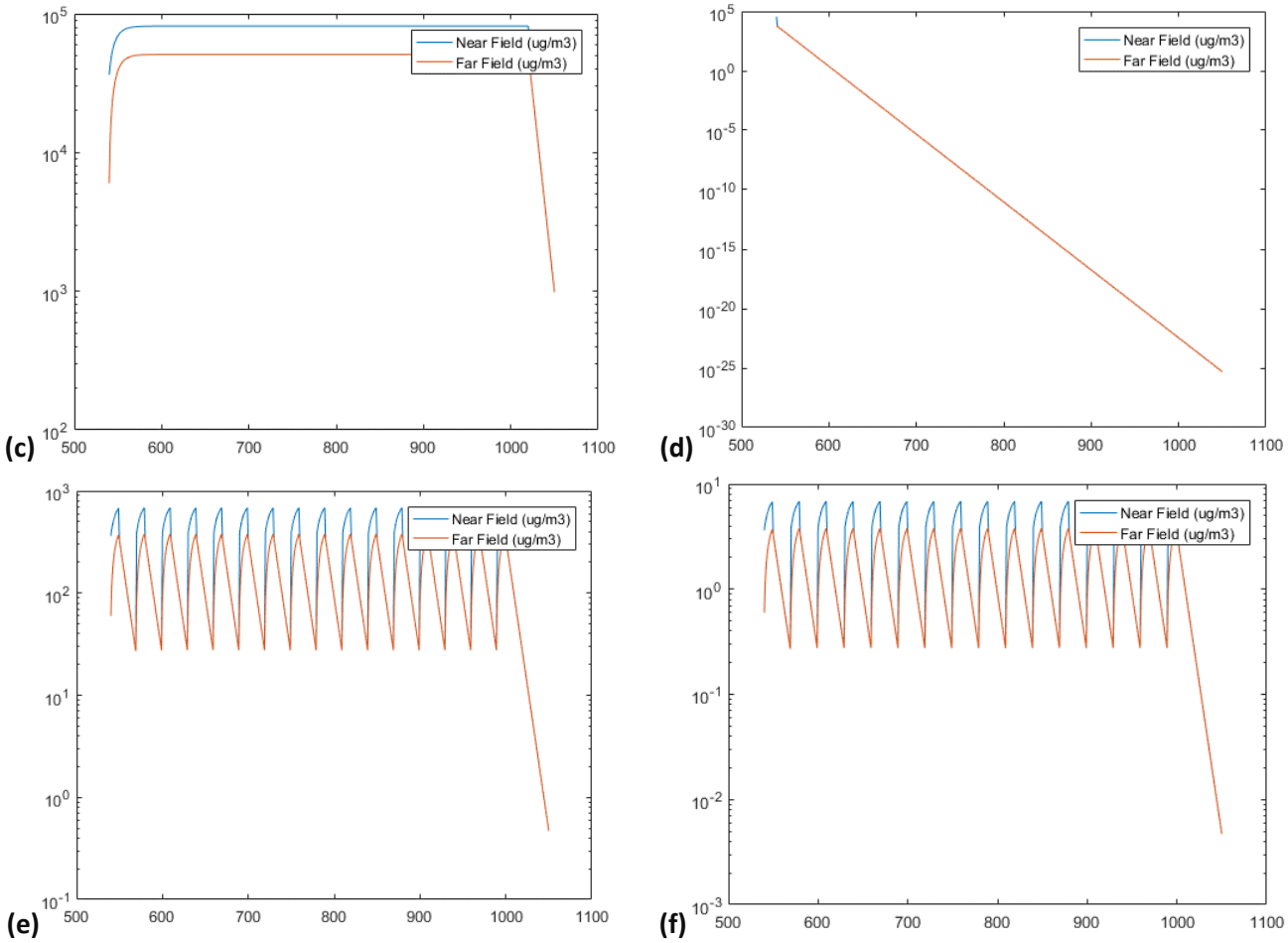

Figure 7-2 Results of the fate and transport model for Exposure Scenario 1 showing near-field (blue) and far-field (orange) nano-TiO2 airborne concentrations during 1 working day of 8 hours. ES1-ES6 are presented in order sequential order (a)-(f). The x-axis reports time in units of minutes and the y-axis reports nano-TiO2 concentration in units of µg/m^3.

ES1 and ES2 reached maximum near-field airborne concentrations of 6.5E+04 µg/m^3 and 8.2E+04 µg/m^3, respectively, shortly after the work-cycles began even though emissions were ongoing throughout the remainder of the workday. Maximum near-field airborne concentrations in ES3, ES5 and ES6 reached 8.2E+04 µg/m^3, 6.8E+02 µg/m^3 and 6.8E+00 µg/m^3, respectively, but were still increasing at the time the work-cycle ended and emissions stopped. The maximum near-field airborne concentration for ES4 of 3.6E+04 µg/m^3 coincided with the exact time it was released, since this was a single-pulse daily emission. The trends in far-field concentrations were similar to the near-field, however these concentrations were on average 50% lower than their respective near-field values.

Average daily airborne concentrations during working hours were on average 45% lower than the maximum daily values. However, this correlation was not linear and was most pronounced for ES1, ES2, and ES4 (Figure 7-3).

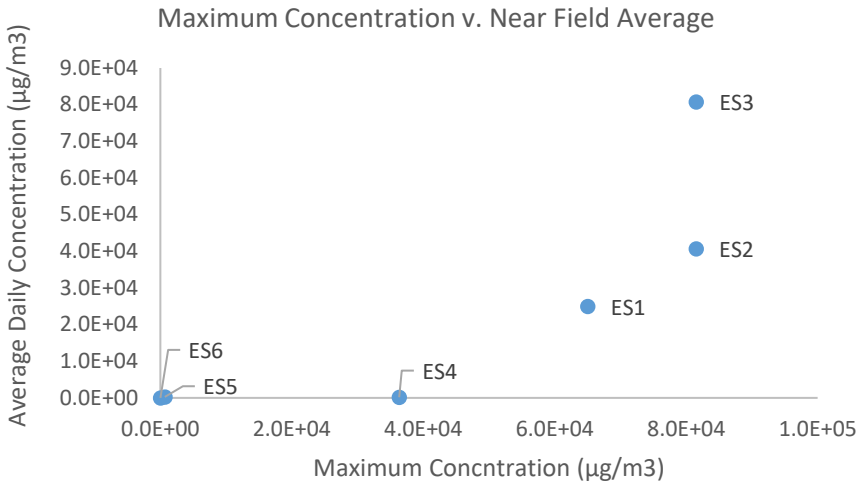

Figure 7-3 Comparison of average and maximum daily airborne nano-TiO2 concentration.

This was particularly true for the single pulse scenario ES4, where the average daily airborne concentration was 99.5% lower than its maximum daily value. In all cases, airborne concentrations effectively reached zero before the next work day, and thus concentrations were not cumulative from day to day. Furthermore, accumulation of nano-TiO2 either plateaued during the work-cycle or was not able to surpass certain work-cycle maximums throughout the day. Thus, regressions of the near-field concentrations were calculated during the time the work-cycle and emissions were active. Regressions of the far-field concentrations were calculated between work-cycles (i.e. pauses) within the 8-hour work day (Appendix: Chapter 7). These regressions describing the work-day airborne concentrations were fed into the PBPK model to estimate the internally-retained lung dose.

The dominant mechanism driving the overall airborne concentration was the air exchange rate between the indoor and outdoor air compartments. In ES1, at the first minute of the first emission event, nearly 94% of the nano-TiO2 remained in the indoor air (i.e. combined near- and far-fields), while 5.7% had been transferred to outside air (Figure 7-4).

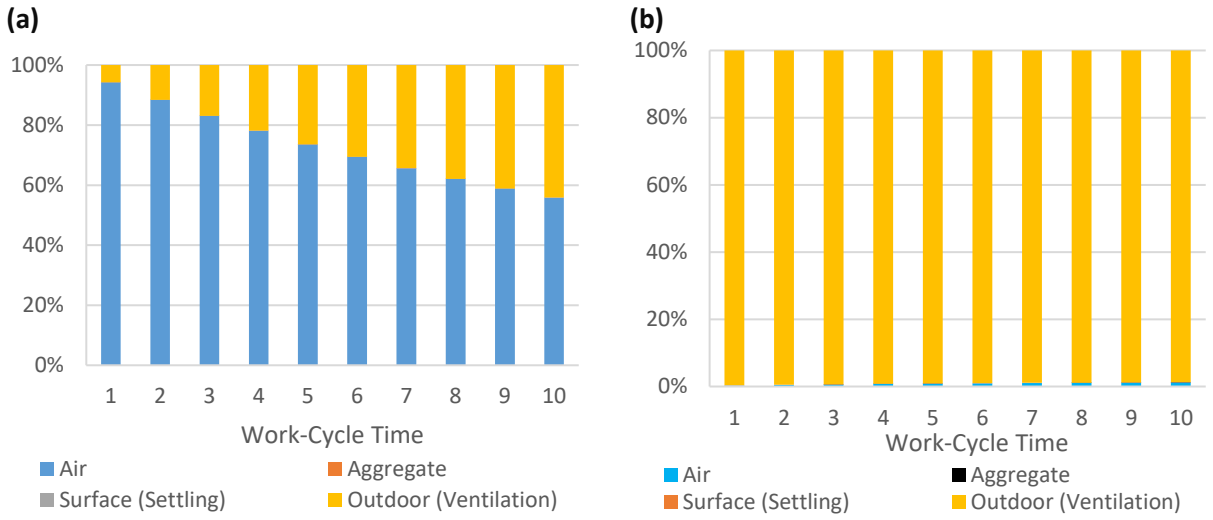

Figure 7-4 Proportional fate and transport of nano-TiO2 per "compartment" during (a) the first 10-minutes of the first emission cycle of ES1 and (b) the final 10-minute emission cycle of ES1 at the end of the work day

An additional 0.0025% of the emissions had been transformed into larger aggregates and 0.0021% had settled to the surface due to gravitational settling. By the end of the first 10-minute emission cycle, the amount of total emissions remaining in the indoor air was only 55.84%, while 44% had been transferred to the outdoor air. The proportion of the emissions that had been removed by homo-aggregation slightly increased to 0.0030% by the second and third minute and then fell back to 0.25% by the end of the emission event. The proportion of emissions removed by gravitational settling onto surfaces increased by over an order of magnitude to 0.03%. These trends continued through the workday whereby the exchange of indoor with outdoor air contributed to nearly 99% removal of the total daily emissions (Figure 7-4). The contributions from gravitational settling and homo-aggregation remained minimal and accounted for roughly 0.07% and 0.00005% of nano-TiO_2 removal from the indoor air. By the end of the final minute of the last emission event of the workday, nearly 1.0% of the emissions remained in the indoor air compartment, as non-agglomerated nano-TiO_2.

In ES2, the overall patterns and trends in removal of nano-TiO_2 from the indoor air by the end of the workday were similar in ES2, ES3 and ES4. However, they differed by the rates at which the indoor air concentrations of nano-TiO_2 decreased. For example, by the end of the 40^{th} minute, the amount of nano-TiO_2 emissions that remained in the indoor air were 25%, 19%, 19% and 0.49% for ES1, ES2, ES3 and ES4, respectively. The relative amount of nano-TiO_2 emissions that remained in the indoor air decreased at the

fastest rate for ES4 since it was only a single pulse event without further addition of nano-TiO_2 over time during the workday. Thus, the clearance mechanisms, mainly driven by the overall air exchange rate of the room, were more effective in this scenario. Although the magnitudes of ES5 and ES6's emission rates were lower than ES1, they had the same relative pattern and trends in removal of nano-TiO_2 from the indoor air.

Exposure to Nano-TiO_2 in Occupational Indoor Air

The fractional percentage of inhaled nano-TiO_2 deposited in the upper airway, tracheobronchial region and the pulmonary (i.e. alveolar) region was 9.8, 24.6 and 40.8, irrespective of the exposure concentration but specific for 21 nm diameter particles. These values were used to determine the relative deposition of the airborne nano-TiO_2 concentrations that entered the lung and to which parts of the lung. The results of the clearance and ultimate retention of this deposited dose was then calculated by the PBPK model and displayed in Table 7-4. The results report the total wet lung burden and retained-intake fraction.

Table 7-4 Results for the internal wet lung burden and the retained-intake fraction, reported as either a lifetime or 1-year value

				Lifetime		**1-Year**	
No.	**Exposure scenario**	**E_i, [mg/min]**	***Total Daily Emissions (mg)***	**Lung Burden**	**RiF**	**Lung Burden**	**RiF**
ES1	e-high, *f-short*	6.72E+02	1.08E+05	2.73E+02	1.25E-09	5.72E+00	2.62E-11
ES2	e-high, *f-long*	6.72E+02	1.61E+05	5.53E+02	1.69E-09	1.16E+01	3.55E-11
ES3	e-high, *f-daily*	6.72E+02	3.23E+05	1.19E+03	1.82E-09	2.50E+01	3.82E-11
ES4	e-high, *f-single pulse*	6.72E+02	6.72E+02	7.04E+00	5.16E-09	1.44E-01	1.05E-10
ES5	e-medium, *f-short*	6.72E+00	1.08E+03	8.10E+00	3.71E-09	1.67E-01	7.64E-11
ES6	e-low, *f-short*	6.72E-02	1.08E+01	3.99E+00	1.83E-07	1.70E-02	7.81E-10

The wet lung is considered as the pulmonary regions of the lung, the interstitial tissue of the lung, and corresponding blood and PCS found in those compartments (i.e. ignoring the upper airways and trachea-bronchial regions of the lung). It was assumed that all exposures during the work cycles occurred within the near-field zone (i.e. all workers were in the near-field), while exposures in-between work-cycles were assumed to take place in the far-field. The final exposure values, therefore, represent the cumulative exposure between both the near- and far-field exposures throughout one 8-hour working day. The results of each exposure scenario are described below.

ES1 e-high, *f-short*

Over the course of 1-work day the wet lung burden increased 16 different times, corresponding with the 16 distinct work-cycles and emission events. Between work cycles, exposures increased very slightly. At the end of the 16-daily work cycles of the first workday, there was a maximum lung burden of 110 µg/g-wet lung. The lung burden did not decrease enough between workdays or workweeks (i.e. over the weekends) to clear the lung of its total nano-TiO_2 load. For example, the maximum exposure by the end of the first work week was 333 µg/g-wet lung, while the remaining lung burden at the beginning of the second work week was 238 µg/g-wet lung. This trend continued until the 5th work week, after which maximum weekly accumulations slowed considerably, having already reached 453 µg/g-wet lung which was 95% of the maximum lung burden of 478 µg/g-wet lung observed at the end of the year (Figure 7-5).

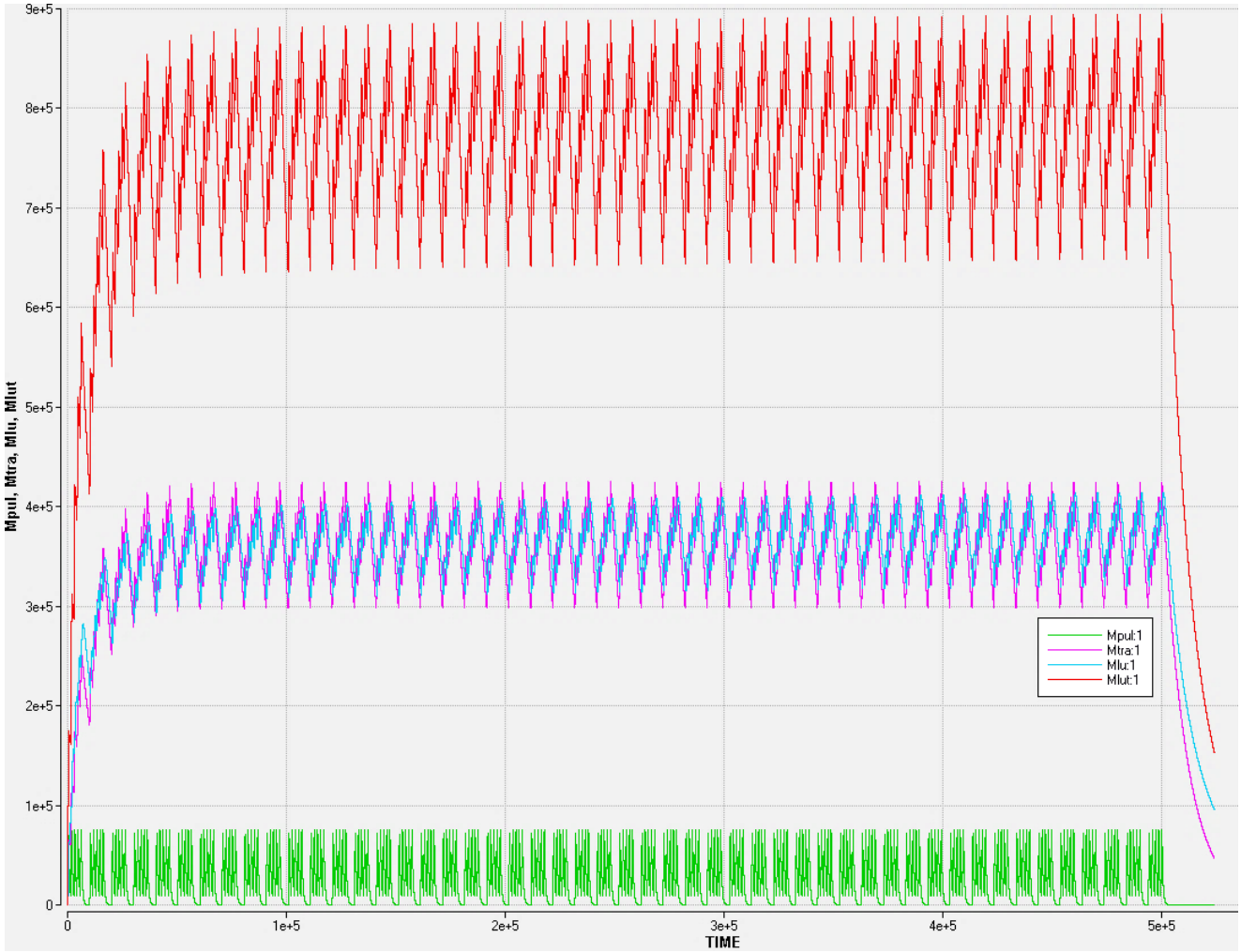

Figure 7-5 Retention of nano-TiO2 in the lung estimated over 1 full work year for ES1. The x-axis represents time in minutes over 1-year and the y-axis represents the mass (µg) of nano-TiO2 in the wet lung. The green trend line represents the change in mass in the air-exchange (pulmonary) regions of the lung, the blue trend line represents the change in mass in the interstitial regions of the lung, the

pink trend line represents the change in mass in the trachea-bronchial regions of the lung, the red trend line represents the total retention in the wet lung including the air-exchange (pulmonary) regions, interstitial regions, trachea-bronchial regions and their macrophages.

A two-week period of non-work activity (i.e. assumed standard holiday) between work years was assumed. The 1-year time-weighted lung burden over a lifetime was 5.72E+00 µg/g-wet lung. Additionally, the lifetime lung-burden was equal to 273 µg/g-wet lung. The corresponding 1-year and lifetime RiF values were 2.62E-11 and 1.25E-09, respectively (Figure 7-6).

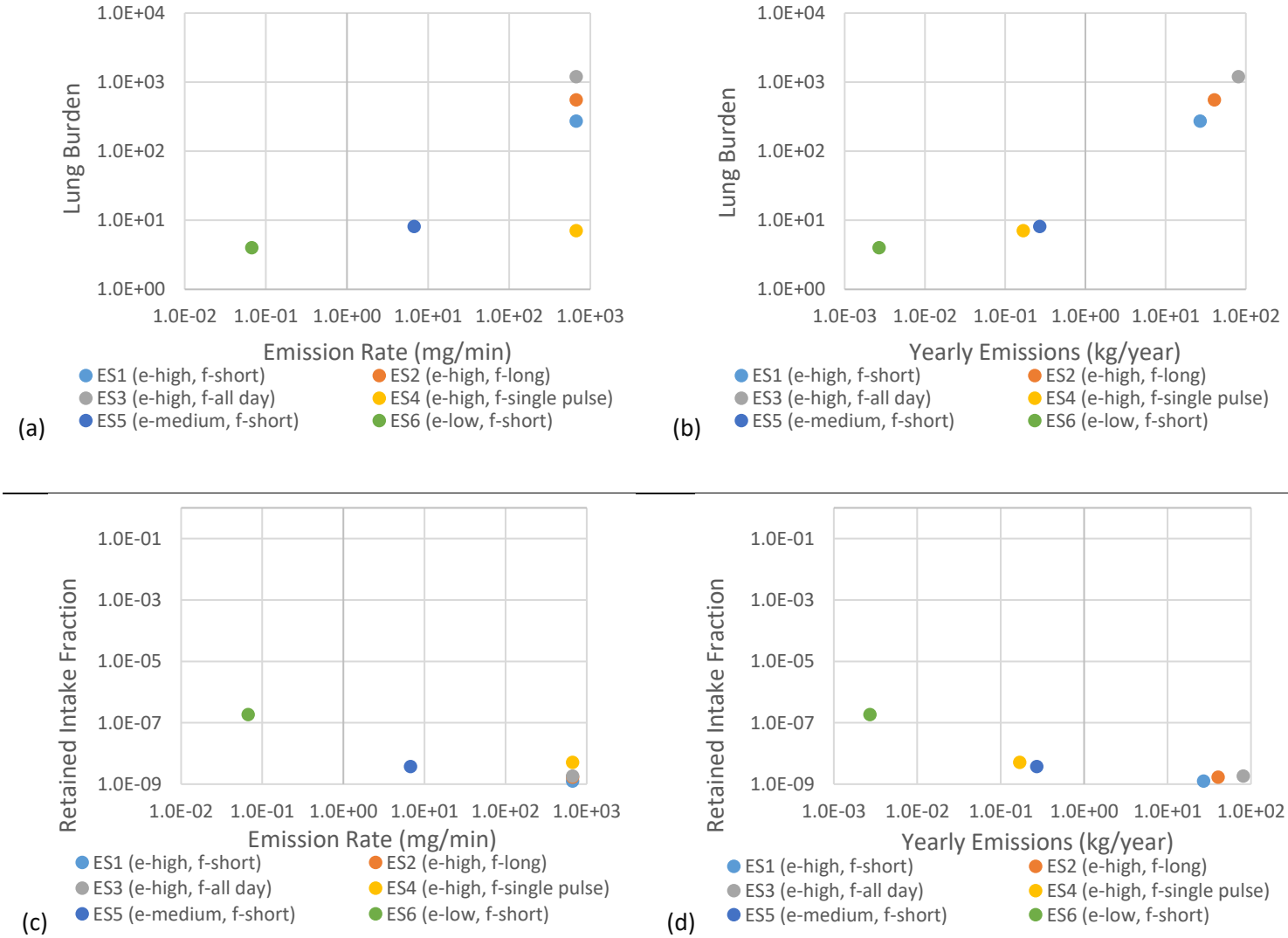

Figure 7-6 Time-weighted retention in the wet lung over lifetime as a function of the (a) emission rate and (b) yearly emissions.as well as the resulting retained intake fraction as a function of (c) the emission rate and (d) the yearly emissions.

Lung burden was mainly influenced by the retention of nanoparticles in the interstitial tissue, where it represented up to 80% of the retained wet lung mass by the end of the first work-year (Figure 7-7).

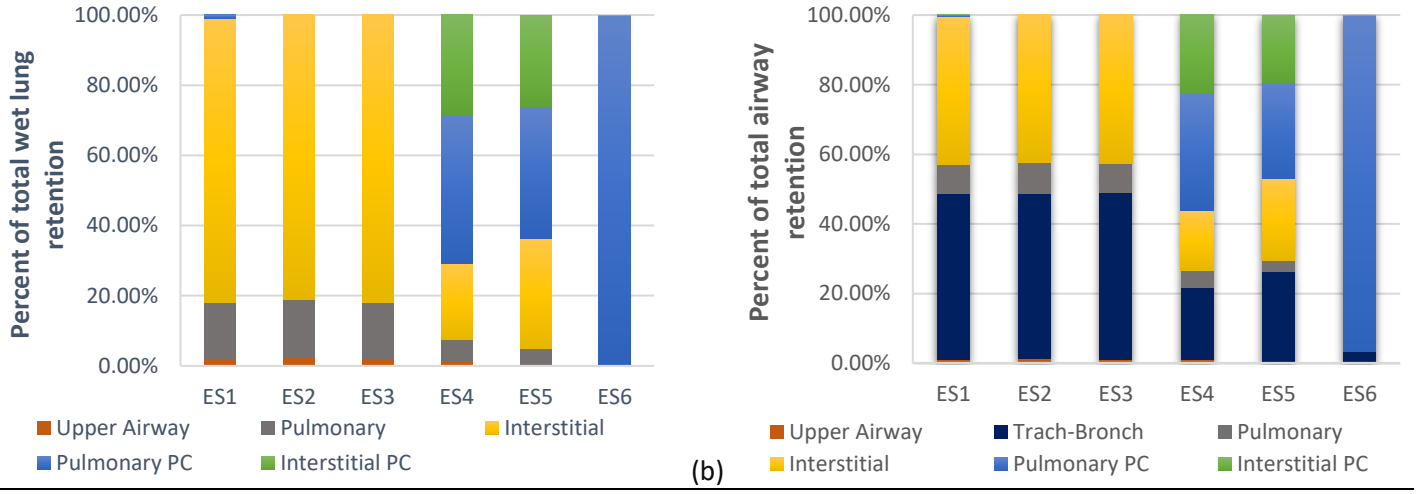

Figure 7-7 Retention of nano-TiO2 in the (a) wet lung and (b) total airway system based on airway regions for all six exposure scenarios.

In contrast, the pulmonary region had cleared itself of all deposited nano-TiO_2 by the beginning of each subsequent work week. Even so, the pulmonary region contributed up to 17% of the total maximum retention observed at the end of the first work-year. The PC located in the interstitial and pulmonary regions reached maximum retentions of 3202 µg and 4644 µg, respectively, very quickly within the first workday. This represented roughly 0.7% and 1.0% of the total lung burden.

The trachea-bronchial region is not defined as part of the wet lung and thus does not directly contribute to the overall lung burden under consideration. However, it is worth noting that retention in this region was similar to the retention pattern in the wet lung, whereby accumulation quickly increased and then leveled off by the 5th work week. Its maximum retention was only 12% lower than the wet lung's value and thus represents an important consideration in the overall exposure since nanoparticles in this region can be transferred to other organ systems such as the gut. Comparatively, accumulation in the upper airway (i.e. head, nasal regions) was less significant (Figure 7-7). The upper airway cleared all nano-TiO2 by each subsequent workday. The maximum retention in this region by the end of the first work-year was 9.80E+03 µg, over 1-order of magnitude smaller than the retention of the wet lung.

ES2 e-high, *f-long*

Over the course of 1-work day the wet lung burden increased 6 different times, corresponding with each of the 6 work-cycles and emission events. Between work cycles, exposures increased very slightly. At the end of the first workday, there was a maximum wet lung burden of 223 μg/g-wet lung. The lung burden did not decrease enough between workdays or workweeks (i.e. over the weekends) to clear the lung of its total nano-TiO_2 load. For example, the maximum exposure by the end of the first work week was 656 μg/g-wet lung, while at the start of the second work week it was 475 μg/g-wet lung. This trend continued until the 6th work week, after which maximum weekly accumulations slowed considerably, having already reached 917 μg/g-wet lung which is 94% of the maximum lung burden of 980 μg/g-wet lung at the end of the year (Appendix: Chapter 7). A two-week period of non-work activity (i.e. assumed standard holiday) between work years was assumed. The 1-year time-weighted lung burden over a lifetime was 1.16E+01 μg/g-wet lung. Additionally, the lifetime lung-burden was equal to 553 μg/g-wet lung. The corresponding 1-year and lifetime RiF values were 3.55E-11 and 1.69E-09, respectively (Figure 7-6).

Lung burden was mainly influenced by the retention of nanoparticles in the interstitial region, where it represented up to 81% of the retained wet lung mass by the end of the first work-year (Figure 7-7). In contrast, the pulmonary region cleared itself of all deposited nano-TiO_2 by the beginning of each subsequent work week. Even so, the pulmonary region contributed up to 17% of the total maximum retention observed at the end of the first work-year. The PCS located in the interstitial and pulmonary regions reached maximum retentions of 3202 μg and 4644 μg, respectively, very quickly within the first workday. This represented roughly 0.3% and 0.5% of the total lung burden.

Retention in the trachea-bronchial region was similar to the retention pattern in the wet lung, whereby accumulation quickly increased and then leveled off by the 6th work week. Its maximum retention was 10% lower than the wet lung's maximum retention value and thus represents an important consideration in the overall exposure as explained previously for ES1. Comparatively, accumulation in the upper airway was less significant. The upper airway cleared all nano-TiO_2 by each subsequent workday. The maximum retention in this region by the end of the first work-year was 2.2E+04 μg, over 1-order of magnitude smaller than retention in the wet lung.

ES3 e-high, *f-daily*

Over the course of 1-work day the wet lung burden increased steadily without pause and correlated with the all-day, constant exposure emissions of this model. At the end of the first workday, the maximum lung

burden was 486 µg/g-wet lung. The lung burden did not decrease enough between workdays or workweeks (i.e. over the weekends) to clear the lung of its total nano-TiO_2 load. For example, the maximum exposure by the end of the first work week was 1.45E+03 µg/g-wet lung, while at the beginning of the second work week it was 1.02E+03 µg/g-wet lung. This trend continued until the 6th work week, after which maximum weekly accumulations slowed considerably, having already reached 1.99E+03 µg/g-wet lung which is 96% of the maximum lung burden of 2.08E+03 µg/g-wet lung at the end of the year (Appendix: Chapter 7). A two-week period of non-work activity (i.e. assumed standard holiday) between work years was assumed. The 1-year time-weighted lung burden over a lifetime was 2.50E+01 µg/g-wet lung. Additionally, the lifetime lung-burden was equal to 1.19E+03 µg/g-wet lung. The corresponding 1-year and lifetime RiF values were 3.82E-11 and 1.82E-09, respectively (Figure 7-6).

Lung burden was mainly influenced by the retention of nanoparticles in the interstitial region, where it represented up to 90% of the retained wet lung mass by the end of the first work-year (Figure 7-7). In contrast, the pulmonary region cleared itself of all deposited nano-TiO_2 by the beginning of each subsequent work week. Even so, the pulmonary region contributed up to 16% of the total maximum retention observed at the end of the first work-year. The PCS located in the interstitial and pulmonary regions reached maximum retentions of 3202 µg and 4644 µg, respectively, very quickly within the first workday. This represented roughly 0.20% and 0.23% of the total lung burden.

Retention in the trachea-bronchial region was similar to the retention pattern in the wet lung, whereby accumulation quickly increased and then leveled off by the 6th work week. Its maximum retention was only 8% lower than the wet lung's maximum retention value and thus represents an important consideration in the overall exposure as explained previously for ES1. Comparatively, accumulation in the upper airway was less significant. The upper airway cleared all nano-TiO2 by each subsequent workday. The maximum retention in this region by the end of the first work-year was 4.1E+04 µg, over 1-order of magnitude smaller than retention in the wet lung.

ES4 e-high, *f-single pulse*

Over the course of 1-work day there was an initial maximum daily lung burden seen within the first hour of exposure, which then slightly decreased by the end of the workday to 0.72 µg/g-wet lung. There were no decreases between workdays nor was there significant decreases between workweeks. This trend continued until the 18th work week when there was a sudden spike in total wet lung retention. The peak

of this increase occurred at week 21, reaching 12.4 µg-wet lung, but then receded to approximately 11.1 µg/g-wet lung by week 25. Thereon, the maximum wet lung retention stayed consistent around 11.1 µg/g-wet lung until the end of the year (Figure 7-8).

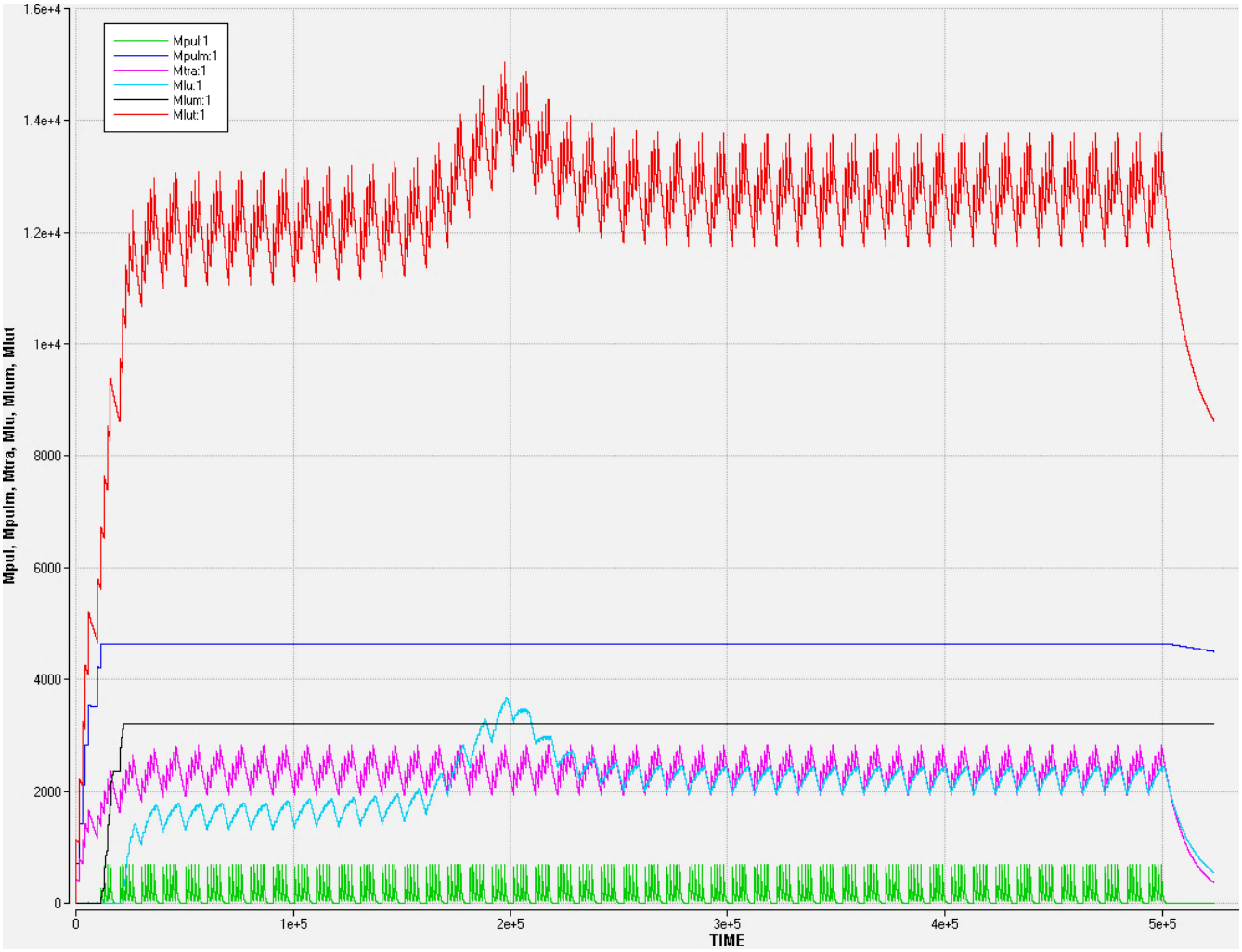

Figure 7-8 Retention of nano-TiO2 in the lung estimated over 1 full work year for ES4. The x-axis represents time in minutes over 1-year and the y-axis represents the mass (µg) of nano-TiO2 in the wet lung. The green trend line represents the change in mass in the air-exchange (pulmonary) regions of the lung, the blue trend line represents the change in mass in the interstitial regions of the lung, the pink trend line represents the change in mass in the trachea-bronchial regions of the lung, the grey trend line represents the change in mass in the lung macrophages, the dark-blue line represents the change in mass in the pulmonary macrophages, the red trend line represents the total retention in the wet lung including the air-exchange (pulmonary) regions, interstitial regions, trachea-bronchial regions and their macrophages.

A two-week period of non-work activity (i.e. assumed standard holiday) between work years was assumed. The 1-year time-weighted lung burden over a lifetime was 1.44E-01 µg/g-wet lung. Additionally,

the lifetime lung-burden was equal to 7.04E+00 µg/g-wet lung. The corresponding 1-year and lifetime RiF values were 1.05E-10 and 5.16E-09, respectively (Figure 7-6).

Lung burden was mainly influenced by the retention of nanoparticles in the interstitial and pulmonary PCS, where they represented 29% and 42%, respectively, of the maximum retained dose seen at the end of the year (Figure 7-7). The interstitium had a maximum retention of 3.20E+03 µg by the end of the work year. This was 22% of the total wet lung retention and is in contrast to ES1-ES3 where the interstitium was the most significant contributor to the total wet lung burden. The pulmonary region cleared itself of all deposited nano-TiO_2 by the beginning of each subsequent work week. This region only contributed up to 6% of the maximum wet lung retention observed at the end of the first work-year.

Retention in the trachea-bronchial region was similar to the retention pattern in the wet lung, however there was no secondary spike in this region's retention, which had leveled off by the 5th work week. Its maximum retention was 74% lower than the wet lung's maximum retention value. Comparatively, accumulation in the upper airway was negligible and only represented 1% of the total wet lung retention by the end of the work-year.

ES5 e-medium, *f-short*

Over the course of 1-work day there were 16 distinct increases in wet lung retention that corresponded with the 16 emission events throughout the day. By the end of the first workday the maximum wet lung retention was 1.15 µg/g-wet lung. There was little decrease between workdays and between work-days. This trend continued until the 11th work week when there was a sudden spike in total wet lung retention. The peak of this increase occurred at week 14, reaching 14 µg-wet lung, but then receding to approximately 12.6 µg/g-wet lung by week 17. Thereon, the maximum wet lung retention stayed consistent around 12.6 µg/g-wet lung until the end of the work-year (Appendix: Chapter 7). The 1-year time-weighted lung burden over a lifetime was 1.67E-01 µg/g-wet lung. Additionally, the lifetime lung-burden was equal to 8.10E+00 µg/g-wet lung. The corresponding 1-year and lifetime RiF values were 7.64E-11 and 3.17E-09, respectively (Figure 7-6).

Lung burden was mainly influenced by the retention of nanoparticles in the pulmonary PCS, where they accounted for 38% of the maximum total retention by the end of the work-year (Figure 7-7). The interstitium accounted for 32% of the maximum total wet lung retention and was also correlated with the

rapid and steep spike in retention seen between weeks 11-17 similar to ES4. The interstitial PC contained 26% of the maximum total wet lung retention. The pulmonary and interstitial PC reached their maximum total retention by the end of the first work-week. The pulmonary region cleared itself of all deposited nano-TiO_2 by the beginning of each subsequent week. This region only contributed up to 4% of the maximum wet lung retention observed at the end of the first year.

Retention in the trachea-bronchial region was similar to the retention pattern in the wet lung, however there was no secondary spike in this region's retention, which had leveled off by the 5^{th} work week. Its maximum retention was 65% lower than the wet lung's maximum retention value. Comparatively, accumulation in the upper airway was negligible and only represented < 1% of the total wet lung retention by the end of the work-year.

ES6 e-low, *f-short*

Over the course of 1-work day there were 16 distinct increases in wet lung retention that corresponded with the 16 emission events. By the end of the first workday the maximum wet lung retention was 1.15E-02 µg/g-wet lung. There was little decrease between workdays and between work-days. Total retention continued largely unabated, reaching a maximum total wet lung retention of 2030 µg/g-wet lung by the end of the first work-year (***Figure 7-9***).

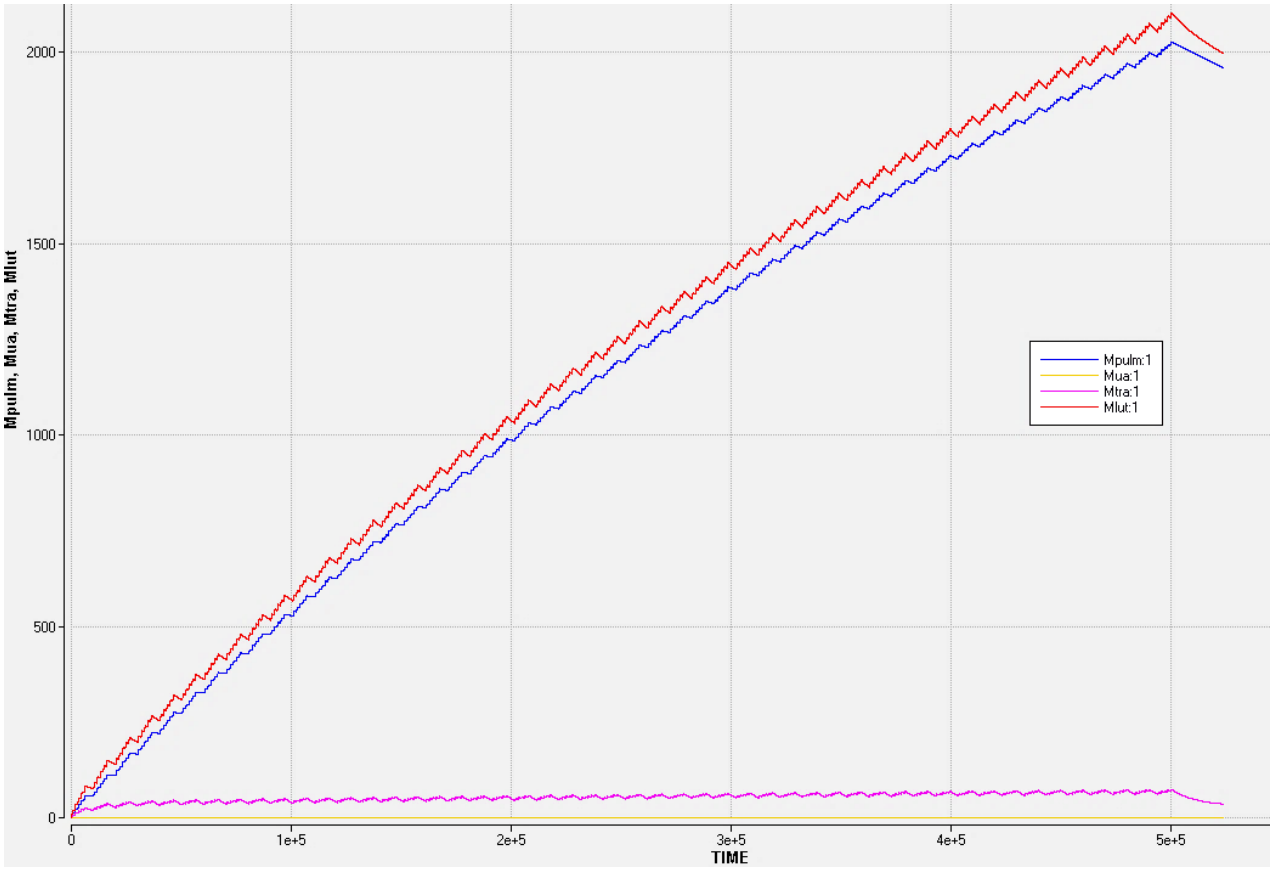

Figure 7-9 Retention of nano-TiO2 in the lung estimated over 1 full work year for ES4. The x-axis represents time in minutes over 1-year and the y-axis represents the mass (µg) of nano-TiO2 in the wet lung. The pink trend line represents the change in mass in the trachea-bronchial regions of the lung, the yellow trend line represents the change in mass in the upper airway, the dark-blue line represents the change in mass in the pulmonary macrophages, the red trend line represents the total retention in the wet lung including the air-exchange (pulmonary) regions, interstitial regions, trachea-bronchial regions and their macrophages.

The 1-year time-weighted lung burden over a lifetime was 1.70E-02 µg/g-wet lung. Additionally, the lifetime lung-burden was equal to 3.99E+00 µg/g-wet lung. The corresponding 1-year and lifetime RiF values were 7.81E-10 and 1.83E-07, respectively (Figure 7-6).

Lung burden was mainly influenced by the retention of nanoparticles in the pulmonary PCS, where they accounted for 99.9% of the maximum total retention by the end of the work-year (Figure 7-7). Retention in the trachea-bronchial region was similar to the retention pattern in the wet lung, which increased largely unabated throughout the work-year. Its maximum retention was 97% lower than the wet lung's maximum retention value. Comparatively, accumulation in the upper airway was negligible and only represented < 0.01% of the total wet lung retention by the end of the work-year.

Influence of Worker Population on the Intake Fraction

The average worker population was estimated from survey-data reported by Walser et al.[97] Based on this dataset, the number of workers in the ENM manufacturing sector was log-normally distributed with a geometric mean of 8.7 and geometric standard deviation of 2.8 (Appendix: Chapter 7). The low- and high-population workforce estimates were defined by the 5th- and 95th-percent confidence intervals, with corresponding values of 1.6 and 47.3 persons. The influence of the worker population on the RiF is shown in Figure 7-10.

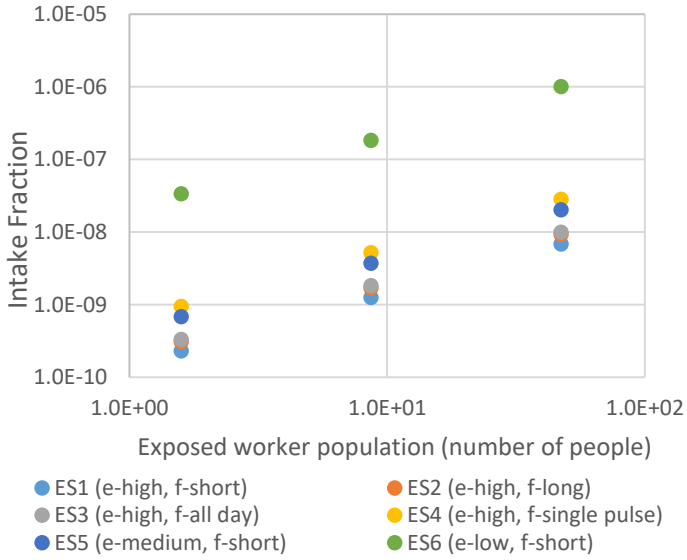

Figure 7-10 Comparison of the intake fraction (shown in log-scale) and number of exposed workers

As expected, the RiF increases linearly with the greater number of workers. Thus, the RiF for the highest worker population was 1.5-orders of magnitude greater than the RiF in the lowest worker population scenario. These results corresponded directly to the 1.5-order of magnitude difference in their respective worker populations.

Effect Factors for Nano-TiO_2 in Occupational Indoor Air

The carcinogenic dose-response data is shown in Figure 7-11.

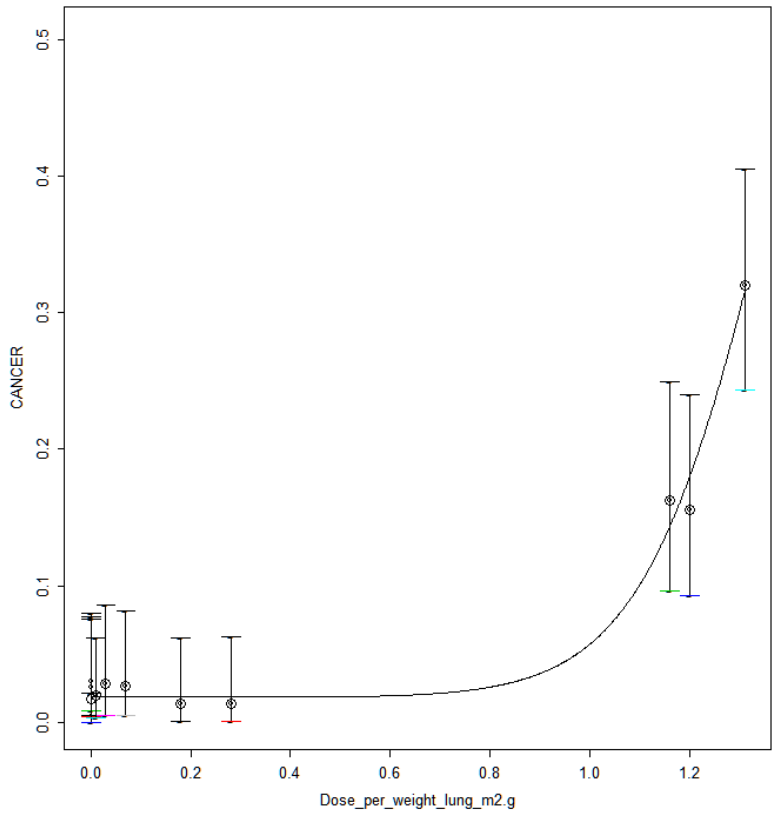

Figure 7-11 Benchmark dose results for cancerous impacts to both mice (black circles) and rats (red triangles). The x-axis represents the internal lung dose reported as surface area of nano-TiO_2 per g-dry lung. The y-axis is reported as the fraction of the animals that result in cases of cancer. The log-likelihood of the fitted Hill model was -208.82. The reported benchmark dose was 1.43 m2/g-dry lung based on the excess risk of 50% over background cancer rates.

The corresponding $ED_{50,a}$ (i.e. BMD) was 1.43 m^2/g-dry lung, with the dose being explicitly expressed as the TiO_2 surface area concentration per gram of dry lung. This was necessary given that both fine- and ultrafine-TiO_2 data were used in the dose-response modeling.[358] After conversion to a mass-based dose-metric, assuming a value of 48 m^2/g-TiO_2, the $ED_{50,a}$ was 2.98E+04 µg/g-dry lung. The original dose-response data was reported for dry-lung measurements, whereby the dry lung was 89.4% of its original wet lung weight. Therefore, the dose metric was converted to its corresponding wet lung $ED_{50,a}$ of 3.16E+03 µg/g-wet lung (Appendix: Chapter 7). After accounting the relevant extrapolation factors, the resulting $ED50_h$ value was 1.58E+03 µg-TiO_2/g-wet lung and the final EF was 3.17E-04 cases/µg nano-TiO_2 /g-wet lung.

The results of the non-carcinogenic dose-response analysis is shown in (Figure 7-12).

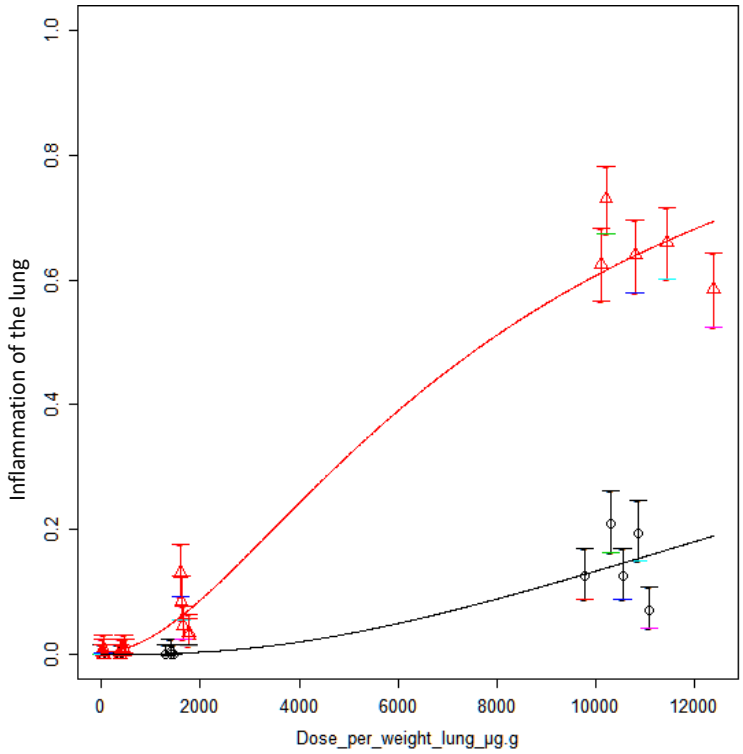

Figure 7-12 Benchmark dose results for non-cancerous impacts to both mice (black circles) and rats (red triangles). The x-axis represents the internal lung dose reported as µg of nano-TiO_2 per g-dry lung. The y-axis is reported as the fraction of the animals that result in inflammation (i.e. the 20% increase in neutrophil count over background rates). The log-likelihood of the fitted Hill model was -1386.37. The reported benchmark doses were 27352 µg/g-dry lung for mice and 7807 µg/g-dry lung for rats based on the excess risk of 50% over background inflammation rates.

BMD values were interpreted from the results of a sub-chronic whole-body inhalation study measuring the changes in BAL fluids upon exposure to nano-TiO_2. Covariation, based on species type, showed that there were distinct dose-response slopes for both mice and rats (Figure 7-12), with rats having lower BMD values (i.e. more sensitive). Based on the approach put forth in USEtox,[84] the BMD for rats was used to estimate the EF because it was the most sensitive species. The original dose-response data was reported for dry lung measurements, whereby the dry lung was 89.4% of its original weight. Therefore, the dose metric was converted to a corresponding wet lung $ED50_a$ of 8.27E+02 µg/g-wet lung. The resulting $ED_{50,h}$ value was 4.14E+02 µg-TiO_2/g-wet lung and the final EF was 1.21E-03 cases/µg (internal) TiO_2 dose.

Classes of Occupational Indoor Air Human Health Characterization Factors for Nano-TiO_2

For each exposure scenario, an acute, 1-year and chronic, lifetime human health CF_{NS} were reported for nano-TiO_2 occupational, airborne emissions (Table 7-5).

Table 7-5 Effect factors (EF), intake fractions (RiF) and ENM-specific characterization factors (CF_{NS}) for six different emission and exposure scenarios that involved differences in emission rates (e) and emission interval frequencies (f)

					Lifetime‡			1-Year‡			Low Population§			High Population§		
Reference	**Emissions per year (kg)**	**Emission Rate (mg/min)**	**EF_C**	**EF_{NC}**	**RiF**	**$CF_{NS,C}$**	**$CF_{NS,NC}$**	**RiF**	**$CF_{NS,C}$**	**$CF_{NS,NC}$**	**RiF**	**$CF_{NS,C}$**	**$CF_{NS,NC}$**	**RiF**	**$CF_{NS,C}$**	**$CF_{NS,NC}$**
ES1 (e-high, *f-short*)	2.70E+01	6.72E+02	3.17E+05	1.21E+06	1.25E-09	3.96E-04	1.51E-03	2.62E-11	8.31E-06	3.17E-05	2.29E-10	7.25E-05	2.77E-04	6.83E-09	2.16E-03	8.25E-03
ES2 (e-high, *f-long*)	4.05E+01	6.72E+02			1.69E-09	5.35E-04	2.04E-03	3.55E-11	1.12E-05	4.29E-05	3.09E-10	9.79E-05	3.74E-04	9.22E-09	2.92E-03	1.11E-02
ES3 (e-high, *f-all day*)	8.10E+01	6.72E+02			1.82E-09	5.75E-04	2.19E-03	3.82E-11	1.21E-05	4.62E-05	3.33E-10	1.05E-04	4.02E-04	9.92E-09	3.14E-03	1.20E-02
ES4 (e-high, *f-single pulse*)	1.69E-01	6.72E+02			5.16E-09	1.63E-03	6.24E-03	1.05E-10	3.34E-05	1.27E-04	9.46E-10	2.99E-04	1.14E-03	2.82E-08	8.92E-03	3.40E-02
ES5 (e-medium, *f-short*)	2.70E-01	6.72E+00			3.71E-09	1.18E-03	4.48E-03	7.64E-11	2.42E-05	9.23E-05	6.80E-10	2.15E-04	8.21E-04	2.03E-08	6.42E-03	2.45E-02
ES6 (e-low, *f-short*)	2.70E-03	6.72E-02			1.83E-07	5.80E-02	2.21E-01	7.81E-10	2.47E-04	9.44E-04	3.36E-08	1.06E-02	4.05E-02	1.00E-06	3.17E-01	1.21E+00
Pini et al.	--	--	4.19E+02	1.72E-02	3.41E-05	1.43E-02	5.85E-07	--	--	--	--	--	--	--	--	--
USEtox	--	--	--	--	1.19E-04†	--	--		--	--	--	--	--	--	--	--

*Reported as an ED4: 4% increase in inflammation rate
†Reported for generic 'organics' and 'inorganics' and not specific for nanoparticles or titanium dioxide
‡Reported for the average number of workers
§Reported for the lifetime exposure scenarios

In this way, the CF_{NS} can be used in a manner that is compatible with life-cycle impact assessment methodologies that contain different "perspectives" based on sources of uncertainty in the modeling choices.[101] In general, the 1-year CF_{NS} were 1-2 orders of magnitude smaller than their corresponding lifetime values (Figure 7-13).

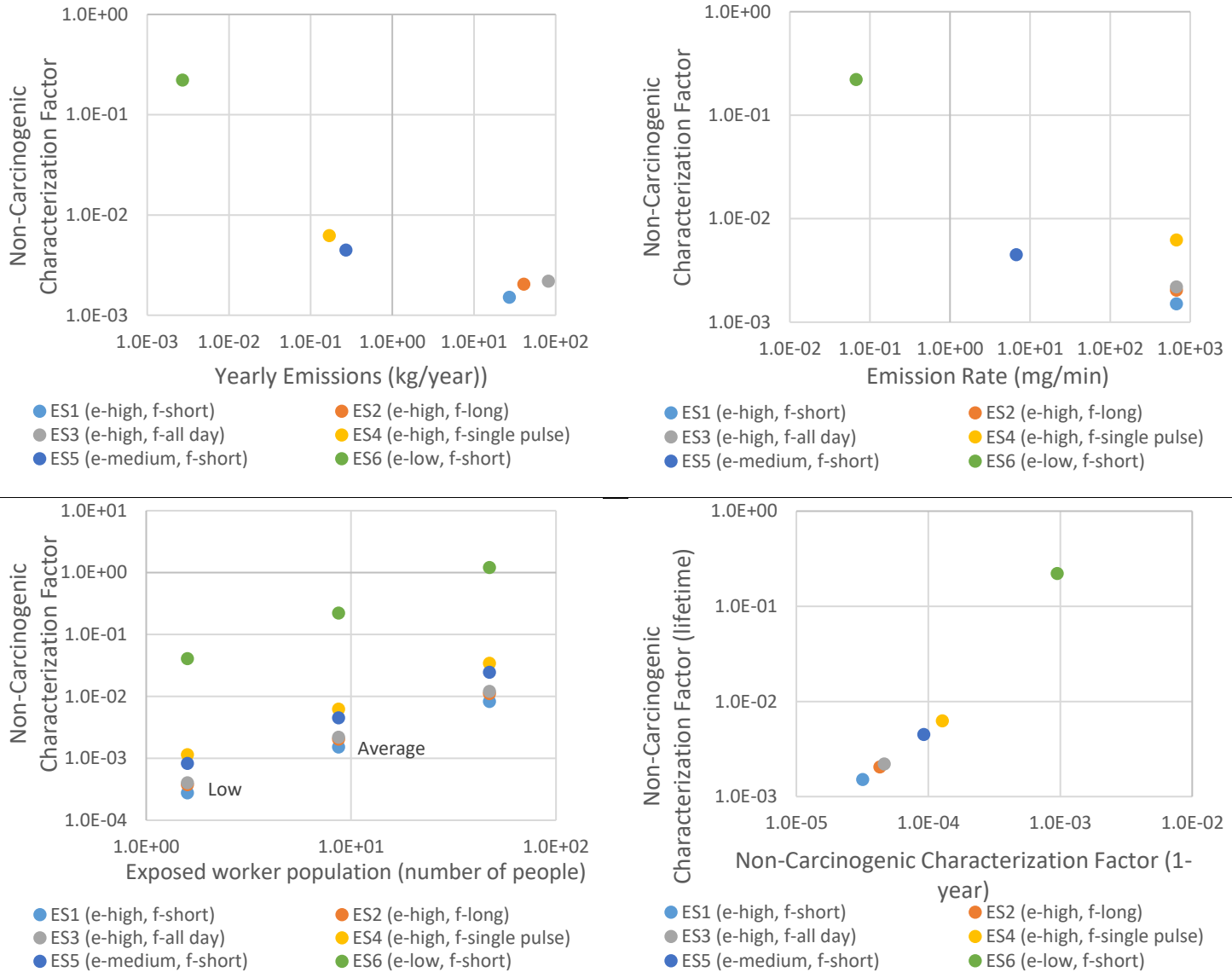

Figure 7-13 Non-carcinogenic characterization factors (lifetime) as a function of the (a) total emissions per year, (b) emission rate in log-scale, (c) exposed population of workers (note: results only displayed for ES1.00 (e-high, *f-short*) scenario), and (d) acute, 1-year versus chronic, lifetime characterization factors.

Because of the non-linear relationship between the emissions (Figure 7-5) and the resulting lung deposition, appropriate use of the CF_{NS} must be considered based on their emission rate and the

frequency of the emission. Emission magnitudes had the greatest influence on the CF_{NS}, particularly at very low emission rates where the CF_{NS} for the lowest emission rate tested was a greater than 1-order of magnitude larger than the medium or high emission rates. CF_{NS} for emissions at the same rate but at different frequencies did not show as much sensitivity, where there was less than 1-order of magnitude difference between the single-pulse (i.e. one short emission per workday) and short-frequent emission scenarios. Thus, when using pre-defined CF_{NS} "classes," these results suggest that assumptions about the emission rates will be more influential than the frequency aspect of the emission. This means that since current life-cycle inventories do not consider temporal dimensions of inventory flows, when deciding on which CF_{NS} to use it is best to associate the emission with the magnitude of the emission (rate) in the inventory.

Discussion

Currently, the estimation of ENM emissions, fate, exposure and human health impacts within LCA have been largely un-addressed in the scientific literature. A main data gap concerns the known life-cycle emissions of ENM-related activities. Using the approaches from Hristozov et al. and Chapter 6 it was possible to make estimations of the emissions in workplaces that handle nano-TiO_2 powders. However, this approach still requires somewhat specific data such as the amount of material handled during a work-cycle and the length of time of a work-cycle. While this information might be too specific or not readily available for most life-cycle inventories, various "groups" or "classes" of these parameters can be estimated and used for sensitivity scoping as was done in this chapter. As was discussed in the results, this led to the findings that the emission magnitude had a stronger influence on the overall CF_{NS} compared with the emission frequency pattern.

Regarding the fate and transport of ENM, recent adaptations to steady-state fate and exposure methodologies[93–96] provide a straightforward first approximation to understanding ENM behavior in the environment. However, such approaches may ultimately use models that are less relevant for ENM as they are for organics and certain metals. Results showed a large difference in the near- and far-field ENM concentrations, with the maximum daily near-field concentrations being twice as large as the far-field. Such conditions were assumed for single, point-source emissions that did not have fugitive emissions. When such conditions are not met, more uniform ENM concentrations might be expected and thus a simpler one-box model may be appropriate.[359] Airborne concentrations were modeled for two indoor air zones, a near-field zone immediately in the sphere of the emission source and a far-field that comprised

the remaining indoor room volume. For example, a steady-state approximation is applied (Appendix: Chapter 7)[311] to ES1, the resulting near-field airborne concentration would be 3.52 mg/m^3. The result is approximately 95% smaller than the maximum near-field concentration predicted by the dynamic model. Indoor occupational emissions are likely to be episodic, leading to non-constant airborne concentrations. This was borne out by the results of the fate model that demonstrated only 2 of the 6 emission scenarios resulted in any pseudo-steady state conditions where airborne concentrations remained constant for at least some portion of the emission event. This only occurred in the two longest emission scenario of 60 minute and all-day emission. Such findings are particularly important since the fate and transport of ENM can be concentration dependent. As has been eluded to by Walser et al., the results of the fate and transport model showed that the overall air exchange rate between the indoor and outdoor air was most influential parameter on airborne nano-TiO_2 concentrations in the workplace.[97] The air exchange rates were high at 8 hr^{-1} but typical for occupational working conditions. This resulted in only minor amounts of removal from homo-aggregation and gravitational settling mechanisms, which might be expected given that the settling velocity of even 1 µm sized particles is circa 12.5 cm/hr.[333] Still, the overall removal from gravitational settling was < 1% in most of the exposure scenarios. These removal mechanisms will likely become much more important when air exchange rates are kept low or particle number concentrations become very high. While it is assumed that conditions in the workplace are likely to be kept high for safety issues, some studies have reported much lower air exchange rates for ENM manufacturing conditions,[359] not to mention other non-industrial workplaces.[360]

In the exposure model applied in this case study, there was a significant departure from currently applied life-cycle impact assessment methods that generally assume inhalation exposures are linearly related to an individual's respiration rate and the concentration of the chemical in air. Walser et al.[97] recently proposed, and Pini et al.[93] implemented, a retention factor based on the outputs from the MPPD model, however this value was actually interpreted from the assumed deposition calculation made by that model and did not consider clearance and ultimate retention of the nano-TiO2. This could be one reason that the lifetime RiF was over 2-orders of magnitude less than what was reported in Pini et al. The results in this chapter show that the retention of nano-TiO_2 in the lung was similar to those from previously reported *in vivo* studies which were on the order of hundreds of days.[202,344,361] This has been shown to be particularly true for deposition in the air-exchange and interstitial regions of the lung, which the results were in agreement with. Of the three main pathways in the model that governed ENM retention in the lung, translocation of loaded-PCS from the pulmonary (i.e. alveolar) to the tracheobronchial region is the

most sensitive parameter and subsequently the limiting factor determining clearance of ENM from the lung. This value was modified to reflect the slower clearance rate of particulates in the human lung compared with the rat lung.[344] In reality, it may be that the difference in retention times is influenced by the rate of phagocytosis by PC and also the penetration of ENM into the alveolar interstitium. However, at the cellular level, it is not clear that such dramatic differences would occur between rat and human rates of phagocytosis nor for the penetration into the interstitium, thus not being to fully explain the retention differences between the species. In the highest exposure scenario, PC were easily saturated and overburdened, leading to accumulation in many of the lung regions. The overall unlimited accumulation found in the air-exchange and interstitial regions for some of the exposure scenarios may be occurring due to mucociliary clearance becoming overburdened, which cannot remove particles at a fast enough rate to reach zero lung burden even at times of low- or no-exposure. However, these results may also be limited by the model's capability to adjust for the increase or decrease of mucociliary clearance activity depending on the mass loading of nanoparticles in the airway. The current version of the model uses a constant transfer factor to describe this mechanism. Additionally, the high concentration of nano-TiO2 found in the tracheobronchial region was expected given the primary particle sizes upon exposure were assumed to be 21 nm. Particles ≤ 100 nm will have a significant amount of deposition in the alveolar region, however particles ≤ 30 nm, particularly those below 10 nm,[344] will show greater deposition and retention in the tracheobronchial region.[202] Additionally, although the density of the particles do not affect deposition of ENM ≤ 100 nm, above this size, lower densities will result in greater deposition in the upper airways such as the tracheobronchial region.[202]

The newly introduced RiF in this study shows an inverse relationship with the emission rate, which is counter-intuitive given that iF values in traditional LCIA are independent of the emission rate. This can be explained by the saturation of PC in the lungs and the relative contribution of PC-sequestered ENM to the overall wet lung burden. Neither of these scales linearly with emission rate, thus bearing the inverse relationship discovered in this study. Further examination on the details of the dynamics of the wet lung burden are shown below. As shown in the results for the exposure, after saturation, the relative contribution of PCS sequestered ENM to the overall wet lung burden decreases as emission rates increases. The amounts in the pulmonary region and interstitium of the lungs scales proportionally with the emission rate after the PCS are saturated. The lifetime wet lung burden increases 3.4 times while emission rate increases 100-fold from low to medium. This is because PCS still play a major role at medium emission rate. But at high emission, which is a 100-fold increase from medium emission, lifetime wet lung

burden increases 31 times, closer to the magnitude of increase in emission rate. This is because the PCS are less important as emission rate goes even higher. This highlights the importance of the emission rate on the "iF" when considering the target organ's physiology.

It should be noted that the RiF and exposure results should be interpreted with caution. Although adaptations were made to the original rat-based model developed by Li et al.[337] to estimate bio-distribution in humans, the results of this model have not been validated by experimental evidence. Li et al. validated their model with empirical data and found good agreement in the measured and estimated amounts of cerium oxide bio-distribution[337]. Also, and in general, reviews of previously used first-order clearance PBPK models tend to under-predict the retention of particulates in the lung when exposure concentrations are either very high or very low[344]. In addition, the model was built based on exposure concentrations that were 2-orders of magnitude lower than the highest exposure scenario presented in this study, which is in effect the worst-case scenario. The results of applying the PBPK-rat model to human exposure scenarios should be considered as potential impacts as opposed to absolute values. The resulting RiF calculated in this chapter did not include the effects and use of personal-protection-equipment in the work environment. At the time of this study, it was not evident which occupational scenarios would require PPE, at what rate PPE would be used and the effectiveness of the PPE to filtering ENM. However, if patterns of PPE usage are known, this could be included in the exposure model.

Additionally, the CF_{NS} presented in this study were calculated for inhalation exposures in the occupational setting, since inhalation is the primary intake route in the workplace scenario.[97] However, the fate and transport model estimates the settling of particles out of the air that could be used for approximating dermal exposures. If there is potential inhalation exposure, there is likely to be potential dermal exposure in the same scenario either from direct settling of ENM onto the skin or settling of ENM onto indoor surfaces that later contact the skin of occupational persons. Dermal exposure and toxicity studies in the literature are much fewer than inhalation studies, potentially being the limiting factor to this approach. As was discussed for fullerenes and titanium dioxide nano-powders in Chapter 6, penetration of such particles into the body through dermal uptake is not anticipated to be as efficient as through inhalation. Furthermore, apart from direct impacts to the lungs and lung-related injuries, ENM that are deposited in the lung may translocate to other regions of the body after inhalation (Oberdorster 2005).[362–364] Although the exposure model presented in this approach allows for the estimation of ENM in 10 other organs of the body, these values were not yet used to address systemic-human health impacts upon inhalation to

nano-TiO2. Future work in this area will address the compounded effects from multi-system organ toxicity.

The EF_C reported in this study was almost 1-order of magnitude smaller than the EF_{NC}. It should be noted that the non-carcinogenic endpoint was pulmonary inflammation, a precursor to the carcinogenic endpoint of pulmonary tumors. Thus, these results intuitively make sense. It would be expected that many more cases of a non-cancerous diseases occur compared with more advanced pathologies such as cancer. This is in contrast to the only other study in the literature that has reported a human health EF for nano-TiO2.[93] Pini et al. report a EF_C that is 4-orders of magnitude greater than their reported EF_{NC}, thus implying that there are many more expected cases of cancer compared with inflammation.[93] However, a likely explanation regarding this discrepancy is the fact that Pini et al. used an inflammation study[283] as a proxy for the carcinogenic endpoint.[93] Therefore, a comparison of their EF_C to the EF_{NC} presented in this chapter is more appropriate. This comparison shows that this work's EF_{NC} was still over 3-orders of magnitude greater than Pini et al.'s EF_C value. Their EF_C value was calculated for as an ED_4 (i.e. a 4% increase over background response) and thus it seems appropriate that they report a lower value compared to ours which was calculated for a 50% increase over the background rate. Thus, while the overall difference in both the non-carcinogenic and carcinogenic CF_{NS} reported in this thesis and what has been previously reported using steady-state models is partially explained by the difference in the fate, exposure and (retained) intake-fractions, a significant difference arises from the selection of toxicological data used to calculate the effect factor (i.e. something that has nothing to do with steady-state versus dynamic models)

Life-Cycle Assessment of Organic Photovoltaics with ENM-Specific Characterization Factors

Life-cycle inventories do not allow for time integrated emission-flows nor are they categorized by time-scale (e.g. kg emissions per hour). If there is exact information regarding the rate of production for the reference-flow (i.e. product), then the reported emissions for that reference-flow could be defined as an emission rate for use in the fate and transport model. Often, this level of life-cycle inventory detail might not be attainable. In such as case, assumptions regarding the emission rate would have to be made. As explained above, the results of the CF_{NS} calculations were most sensitive to the magnitude of the emission rate as opposed to emission frequency. Thus, static inventory flows should be interpreted as the magnitude of an emission rate for best correlation. Based on the previous set of results, it was assumed that the emissions reported in the OPV inventory (Appendix: Chapter 3 and Appendix: Chapter 4)

correspond with the highest emission rate. This is because the highest emission rate was characteristic of an industrial scale scenario, and since the purpose of this thesis is to forecast the potential environmental and human health risks for a prospective, large-scale OPV device, this assumption is warranted. Furthermore, the highest emission rate was correlated with the highest level of risk based on the HHRA in Chapter 6, it was useful to explore whether the LCA results would echo this human health hazard. Therefore, the highest emission rate was used as an initial proof of concept to estimate the human health hazards of nano-TiO_2 use in OPV. Within this category of emission rates, there was a range of half an order of magnitude based on differences in emission frequencies. Since the original frequency was originally described for an actual occupational exposure scenario at the industrial scale, this value was chosen as a proof of concept due to its relevance in forecasting human health impacts at the industrial scale. Both the long-term (lifetime) and the short-term (1-year) CF_{NS} were tested for their influence on the LCA results.

Thus, lifetime CF_{NS} for ES1 was used as a worst-case scenario proof-of-concept for a first approximation of the human health impacts from nano-TiO_2 handled and used at the industrial scale. Emissions across the life-cycle of the OPV panel were considered only during production of the nano-TiO_2 power itself, and during production of the OPV panel. Emissions during nano-TiO_2 production were estimated for the production route outlined by sulfate production route. Hischier et al. assumed there were no emissions to air during production, however this neglects the issues of handling, transferring, and packing the powder once it is created.[193] Thus, emissions were estimated using an average of lower-estimate and higher-estimate emission scenarios as described by the material flow analysis of various ENM reported by Gottschalk and Nowack.[191] This resulted in an estimated 0.25% of the total production rate being emitted to air, and, thus, per kg of nano-TiO_2 produced and handled there were 0.32 mg of this material that ended up as occupational, indoor air emissions. Additionally, there were no known nano-TiO_2 emissions during the production of the OPV panel, and the same modeling assumptions stated above applied for OPV production. It was further assumed that this emission was to indoor occupational air, as opposed to outdoor environmental emissions. The reported emission (e.g. 0.32 mg) was then combined with the both the non-carcinogenic and carcinogenic lifetime CF_{NS} for ES1 to calculate the potential human health impacts. This implicit assumption is that the CF_{NS} for ES1 represents an industrial-scale scenario and the inventory, including the emissions, built for the nano-TiO_2 production and OPV manufacturing represent emissions of a similar magnitude over time at the industrial-scale. This is a significant caveat because there is no relatable time-scale on the inventory.

Preliminary Results

Preliminary cradle-to-gate results show there was no noticeable increase in the carcinogenic and non-carcinogenic human health impacts after including the human health impacts of nano-TiO_2 either using the short-term (1-year) or the lifetime CF_{NS}. The application of the long term (lifetime) CF_{NS} resulted in greater impacts compared to the 1-year CF_{NS}, as was expected given the latter is a one year time-weighted average exposure over an entire lifetime worth of emissions. After applying the lifetime CF_{NS}, the human health impacts only slightly increased at around 1% increase overall (Table 7-6).

Table 7-6 Human health impacts per watt-peak of OPV cell production without a ENM-specific characterization factor for nano-TiO_2 (left columns) and with a ENM-specific characterization factor (right columns)

	No ENM-specific Characterization Factor		**With ENM-specific Characterization Factor (Lifetime average)**	
Percent Contribution by Life-Cycle stage	**Human Health (non-carcinogenic)**	**Human Health (carcinogenic)**	**Human Health (non-carcinogenic)**	**Human Health (carcinogenic)**
Annealing	32.08%	29.55%	31.95%	29.47%
HTL	24.66%	2.46%	24.56%	2.45%
PCBM	14.47%	18.02%	14.41%	17.97%
Lamination	12.31%	14.56%	12.26%	14.51%
FTO Substrate	9.61%	10.44%	9.57%	10.41%
P3HT	0.80%	17.82%	0.80%	17.77%
Printing	3.16%	3.14%	3.14%	3.13%
ETL	1.59%	1.38%	1.58%	1.38%
Aluminum Electrode	0.63%	1.96%	0.62%	1.95%
Nano-TiO2 Spacer	0.05%	0.04%	0.25%	0.18%
Other	0.64%	0.63%	0.86%	0.78%
Total Impacts (CTU)	9.35E-09	3.55E-09	9.38E-09	3.56E-09
Total contribution from nano-TiO_2	N/A	N/A	0.41%	0.28%

These nano-TiO_2 emissions to the indoor, occupational air resulted in a 0.28% and 0.41% contribution to the carcinogenic and non-carcinogenic impacts, respectively. Roughly 50% of these emissions came from handling nano-TiO_2 during OPV-manufacturing and the other half during nano-TiO_2 production. Thus, if a decision maker wanted to reduce the human health impact of OPV, there is not much support for targeting the nano-TiO_2 emissions, for example (Figure 7-14).

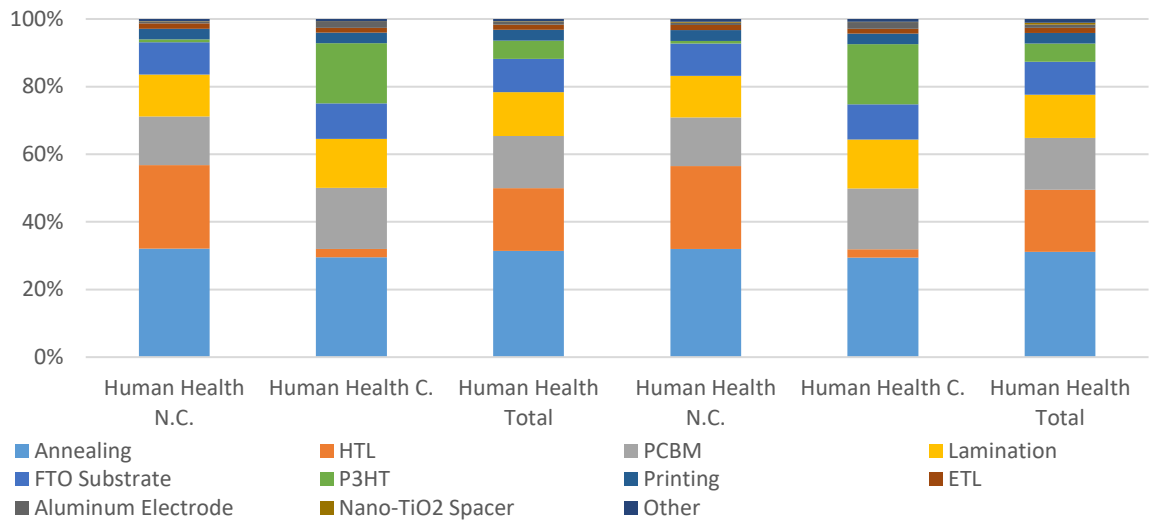

Figure 7-14 Contribution to human health impacts by life-cycle stage

Such results must be met with caution as several assumptions were made in during the calculation. First, emissions from the production route of both the nano-TiO_2 and the OPV panels were not known. These were estimated from generic release distributions previously reported in the literature for the production of ENM-related technologies and thus may not adequately describe the true emissions occurring in these industries.[191] It is likely that emissions to indoor air from powder handling and transfer are not adequately accounted for in these distributions, however this assumption is not clarified in those previous publications.[191]

The nano-TiO_2 CF_{NS} were calculated using models that were emission-specific (i.e. the emission amount changed the resulting CF_{NS}). The CF_{NS} ultimately used to calculate the human health impacts from nano-TiO_2 emissions was an industrial scale emission rate for a representative industrial scale emission scenario and number of workers exposed. While this CF_{NS} might represent a valid industrial scale scenario for handling nano-TiO_2, it is not specific to the actual emissions scenarios represented by the life-cycle inventory for OPV, and thus it was used to forecast impacts at the representative, prospective industrial scale of OPV production.

These preliminary results indicate that the human health impacts from occupational, indoor air emissions of ENM across the OPV life-cycle might be marginal at best. These results are only valid for nano-TiO2 and do not include the human health impacts of fullerenes. The magnitude of fullerene emissions during production, handling and use were not known, however Chapter 6 discussed the relevant fullerene

toxicity data. While some indication of inflammation, for instance, have been demonstrated, fullerenes have also been shown to have anti-inflammatory effects. Thus, its potential to significantly contribute to the human health impacts of OPV due to emissions in occupational indoor air is not anticipated. Furthermore, these are just two material types used in OPV that have been explicitly called-out as ENM. Since OPV are constructed on the order of hundreds of nanometers in thickness, this implies that the all the layers would necessarily have to be composed of materials in the nanometer size range. While this is not usually explicitly stated, this technically implies that the use of ENM comprises the entire panel (less the plastic-substrate). Consequently, the cumulative contribution of ENM emissions along the life-cycle of OPV could potentially be more influential than this preliminary assessment suggests. Lastly, while human health impacts from occupational indoor air emissions seemed to be the most relevant potential impact pathway, emissions during the use phase and end-of-life phase cannot be ruled out. Such emissions will also be important for the determination of potential environmental and ecological impacts.

Chapter 8 Conclusions and Perspectives

The future of energy production and development of sustainable technology options are primed to be, arguably, the most important issues in the 21st-century. In the face of mounting climate change and public health impacts, energy must be evaluated as a sustainability issue addressing not only economic impacts but also impacts on society and the environment. For instance, past experiences with biofuels have demonstrated that when objectives are limited to simply finding alternative or renewable energies, environmental burden shifting can occur.[5–8] The introduction of modern, conventional forms of PV systems in the mid-20th century offered one option of producing electricity from limitless amounts of energy from the sun. Moreover, PV are basically an emission free and environmentally benign technology while it is being used, however there are environmental burdens (e.g. greenhouse gas emissions) that may occur during the production, use or disposal of the PV. Particularly for conventional silicon-based PV, the processing of silicon into semi-conducting wafers and entire panels is a fairly energy intensive process. Consequently, the research and development into alternative PV technologies that are less energy intensive and environmentally preferable is an ongoing endeavor. In this regard, OPV have captured the imaginations of many researchers since it's a very thin, flexible technology requiring much fewer amounts of materials per Wp of power production. However, OPV are also known to have much lower conversion efficiencies and lower lifetimes compared with silicon-based PV. Therefore, the overall objective of this thesis was to demonstrate whether OPV have proven themselves to be an environmentally preferable energy supply option compared with conventional silicon PV.

The Methodological Options Presented in this Thesis

Implicit to the overall objective of the thesis was the question whether existing methodologies commonly used to evaluate the environmental performance of energy supply systems are fully compatible for carrying out such evaluations. In Chapter 1, a review of the literature up to the end of 2013 was made on the environmental performance of OPV. Central to the environmental evaluation of energy-related systems has been the use of LCA because of it facilitates the calculation of the EPBT (i.e. the time it takes to produce the same amount of energy that was consumed in creating the technology). However, LCA also facilitates the calculation of additional environmental and human health impacts of products. Therefore, Chapter 3 and Chapter 4 employed the use of LCA to evaluate prospective OPV devices, their uses and their end-of-life options.

Chapter 5 highlighted the gaps in life-cycle impact assessment methodologies in regards to the human health and ecotoxicity impacts resulting from ENM emissions along the OPV life-cycle. HHRA and ERA are two tools traditionally used for making assessments about the potential human health and environmental risks from regular chemicals. In principal, these tools can also be used to understand the impacts from ENM, although they too can suffer from data and methodological gaps similar to LCA. Chapter 5 expands on these issues and the potential approaches to use LCA and HHRA[3] in separate, complementary or integrated uses for evaluating the environmental and human health benefits of emerging technologies These methodology options were the separate use of LCA, the separate use of HHRA, the combined use of LCA and HHRA (i.e. combining their results together), and three additional approaches to integration of HHRA and LCA at the methodological level. These latter three options were *Global*, *Context-dependent* and *Site-specific* integration. *Global* integration makes use of steady-state models that are less relevant for ENM, *Context-dependent* integration makes use of partially-dynamic models with aggregated environmental and ENM-specific parameters and *Site-specific* integration uses fully-dynamic models with perfect local and material-specific information. Chapter 6 presented the HHRA of the potential ENM-emissions along the OPV life-cycle. Chapter 7 presented the methodology of *Global Integration*, culminating in the production of an occupational, indoor air, human health CF_{NS} for nano-TiO_2.

Overview of the Results of Each Methodological Option

Life-Cycle Assessment of Organic Photovoltaic Systems

The review of existing literature through the end of 2013 demonstrated a general finding that the resource efficiencies and environmental hazards of OPV were lower than that of conventional silicon PV. However, the majority of these studies were limited in their scope, focusing mainly on cradle-to-gate assessments up to the manufacture of the OPV panel as well as limiting their environmental criteria to CED, EPBT and greenhouse gas emissions. For example, CED for the reviewed literature showed values as low as 0.76 MJ/Wp of power production, compared with conventional m-Si which could be as high as 30 MJ/Wp.

Chapter 3 introduced a new, prospective OPV device based on the reviewed literature in terms of their reported material choices, structure and performance of the solar cells as well as other foreseen developments in this area of research. For instance, material choices eliminated the use of resource scarce

[3] This thesis took particular focus on the human health assessment modeling, however the use of ecological risk assessment, its data and methodological gaps, and its synergisms with life-cycle assessment also apply in the environmental (non-human health context)

or cost prohibitive materials such as indium and silver. The results of the CED, for example, ranged from 1.13-2.32 MJ/Wp and were largely in agreement with the prior studies. Looking beyond embodied energy, the environmental and human health impacts decreased across the board compared with conventional silicon-based PV. However, these differences were not uniform across all impact categories. For instance, whereas marine eutrophication impacts for OPV were between 94-97% lower than m-Si, decreases in ionizing radiation were between 77-94% lower. Further results, showed that at a 5% efficiency, OPV would need between 1-9 years of working lifetime such that they achieve environmental parity with silicon-based PV. However, these lifetimes are based on purely hypothetical estimations if there were no other impacts resulting from further use or end-of-life phases.

Chapter 4 expanded the scope of the LCA presented in Chapter 3 to include possible use and end-of-life phases for OPV systems. Two different use phases were considered: a rooftop, solar array and a portable solar charger. Two different end-of-life options were also considered: landfilling and incineration. Whereas cradle-to-gate impacts were, on average, over 90% lower for OPV compared to silicon-based PV, cradle-to-grave impacts of using OPV panels on rooftops were only 60% lower. In one case, metal depletion potential, OPV impacts were in fact greater than m-Si PV. The increases in impacts were due to the need to continually replace the OPV panels every five years over the course of the 25-year rooftop lifetime. The difference between the cradle-to-gate and cradle-to-grave environmental impacts are thus not trivial and demonstrate how significant the use phase can be, even though technically there are no direct emissions during its use. This concept was reinforced by the results of using OPV as a portable charger, which were on average 74% lower than a-Si PV. In contrast to the rooftop scenario, metal depletion remained 87% lower than a-Si for the portable charger scenario.

Consideration of the end-of-life showed only minimal influence on the total cradle-to-grave impacts, however recycling of the panels was not considered. Currently recycling is not applied to solar panels, whereby the majority end up going to landfills. If recycling comes online as a major end-of-life route for silicon cells, there could be a significant reduction in their total impacts. OPV on the other hand do not stand a lot to gain from recycling as their total energy content is minimal given their thinness and low material mass. Thus, eco-design concepts for emerging technologies may stand to benefit by further developing and including prospective use and end-of-life phases to make targeted evaluations of how they can extract the most resource efficiencies and avoid the most environmental hazards.

Emissions of and Human Health Impacts from Engineered Nanomaterials using Risk Assessment

Those aforementioned environmental and human health impacts calculated using LCA did not include the impacts from the ENM used in the OPV technology. ENM-specific emissions had not been estimated either in the prior studies reviewed literature in 0. Main obstacles to including these potential impacts go beyond the reporting of emissions and are limited by current life-cycle impact assessment methodologies that were originally built for understanding the behavior of organic and some metals in the environment, but not ENM. To address this, a more focused HHRA was presented in which potential occupational exposure scenarios during production and use of nano-TiO_2 was presented. The HHRA was conducted for the industrial-scale handling of nano-TiO2 in order to forecast potential human health risks in the OPV life-cycle if this were to reach the industrial level The results showed there was upwards of a 78% lifetime risk of lung inflammation to workers handling nano-TiO_2 during ENM production or OPV panel manufacturing. This estimation of risk was a worst-case scenario, for instance, under the assumption that no personal protective equipment was used and exposure to the individual was 100% of the concentration in the air. The highest probability of risk was particularly relevant when handling and transfer of high volumes of dry nano-TiO_2 powders occurred over 8-hour workdays. The results suggest that risk may exist along the OPV life-cycle if industrial-scale production of this technology is achieved. While these results might be beneficial from a health and safety perspective for laboratory managers, for example, it may ultimately provide little relevance from an eco-design perspective where material choices and occupational workplace conditions at the industrial scale, if reached, may not have the same exposure conditions that were presented in the HHRA. Instead, potential human health impacts calculated within LCA, as opposed to absolute values of risk, might prove more useful for early design and development of emerging technologies such as OPV.

Integrating Life-Cycle Assessment and Risk Assessment for the Evaluation of Organic Photovoltaics

Instead, it would suit decision makers well if there were a tool harmonized at the methodological level to evaluated the human health impacts of occupational, indoor air emissions of ENM. There is one such study in the literature by Pini et al. who published an occupational, indoor air CF_{NS} for nano-TiO_2. Their model can be categorized as a *Global* integrative approach as defined in Chapter 5. In contrast, Chapter 7 introduced a dynamic, mechanistic fate and exposure model based on the approaches and experiences of applying HHRA to the case study of nano-TiO_2. Since the approach to HHRA necessitates very specific exposure conditions, and would mean that *strict* integration of HHRA into LCA would have to be on a case-

by-case basis (see *Site-Specific Integration* in Chapter 5). As an alternative, *Context-Dependent* integration was used to derive different CF_{NS} "classes" based on certain parameters of the model. These classes were based on magnitude of the emission rates, emission frequency patterns (i.e. frequency as well as duration of the emission), workforce population (i.e. number of people exposed), and time-horizon (i.e. short-term versus long-term exposure). The lifetime nor the 1-year CF_{NS} demonstrated any appreciable concern for nano-TiO_2 human health impacts over the cradle-to-gate environmental impacts for producing the OPV panel. Unlike the results of the HHRA, these are results from a tool harmonized at the methodological level, therefore they can be directly interpreted and assessed in the context of all the other human health and life-cycle impact categories presented in the LCA. For example, it was possible to identify how significant the human health impact contributions were for nano-TiO_2 compared to the rest of the human health impacts. Ultimately, nano-TiO_2 emissions to air resulted in a marginal 0.41% and 0.28% contribution to the carcinogenic and non-carcinogenic impacts, respectively. Roughly 50% of these emissions came from OPV panel production and the other half from nano-TiO_2 production. These results provide a clearer indication that efforts to reduce impacts from nano-TiO_2 may not be well justified, in context of other relative human health impact contributors within the OPV life-cycle. All such analyses are either impossible or very difficult when using the *Complementary Use* approach of combing the individual results from LCA and HHRA.

Perspectives on the Environmental Preference of OPV

Presented in this work was a comprehensive set of environmental and human health impacts for a prospective OPV product including its use and end-of-life phases. Compared with conventional silicon, OPV resource efficiencies are greater and their environmental and human health hazards lower, on average. These results are limited by how the PV devices are used and for how long. Uncertainties, mainly associated with the lifetime and efficiencies of OPV, prevent definitive answers in all cases as to whether OPV prove themselves to be an environmentally preferable energy supply option. However, these uncertainties can be marginalized when OPV are limited to products with relatively short lifetimes (e.g. products where the use is typically < 5 years), and the preference for OPV becomes evident for such technology choices and applications. Even so, and based on the results of this thesis, there is still some basis to support the notion that OPV should be employed for such uses as solar rooftop arrays where conventional silicon-based PV has dominated for decades. The human health hazards resulting from the use of ENM in OPV seems marginal at best per the results presented in Chapter 7. It must be noted that these results were specific only to nano-TiO_2 emissions in the occupational indoor air compartment and

their resulting human health impacts. Emissions at other parts of the life-cycle may lead to additional impacts, particularly environmental and ecological toxicity due to emissions at the end-of-life.

Moreover, the resource efficiencies of OPV could be further exploited in other non-conventional and evolving applications and products. One example would be the integration of PV with automobiles and other modes of transportation. This is because the added benefit of producing additional solar power must not come at a price of adding too much additional weight to these application settings. Added weight would have the negative side effect of weighing down the transport device and requiring more energy to overcome inertia. Since OPV are much thinner and lighter than silicon cells or even other 2nd-generation thin-films, the reductions in weight could see the biggest benefits for all-solar powered modes of transport (e.g. www.planetsolar.ch). The obvious assumption here is that OPV would have to have the same efficiency as conventional PV. This is currently not the reality and would require much larger surface areas of the transport system to be covered with the OPV, surface area that might not be feasibly attainable with current efficiencies.

Perspectives on Environmental and Human Health Modeling Options, Development and Data Requirements

LCA stands as the most comprehensive and appropriate methodology for evaluating the resource efficiencies and potential hazards of energy producing technologies such as OPV. Its broad environmental scope and focus on the full extent of a product life-cycle help to ensure that the development or dissemination of a product does not simply just result in the shifting of burdens from one impact category to another. Although, understanding the human health and ecological hazards to ENM is necessary for the evaluation of this technology, which is not achievable using currently existing life-cycle impact assessment methodologies. While ecological risk is also important, the focus of this thesis was on human health modeling of ENM. Even so, the lessons learned in this thesis are applicable to environmental modeling as well. Ultimately, choosing the most appropriate methodological tool for human health evaluation depends on the context of the problem. HHRA is a valid tool for addressing human health risks to ENM and is most appropriate for industrial-scale production of emerging technologies or where human health safety must be ensured. Life-cycle impact assessment can also be adapted to include the human health impacts to ENM, albeit not with the same specificity and determination of risk like in HHRA. This type of approach that integrates the human health impacts of ENM into LCA is an effective tool for early product design and development, or so called eco-design purposes. This is evident by the fact that since

OPV are very much in the early stages of development, other approaches such as *Complementary Use* which involves HHRA, evaluations of absolute risk might be too ambitious since as the technology scales up, the exposure conditions that were specific to the risk assessment are likely to change. Thus, the *Context-Dependent* integrative approach provides a method of evaluating the *relative* human health impacts of ENM that would be more effective at OPV's current scale of development.

Consequential Life-Cycle Assessment of Organic Photovoltaics

A further distinction can be made within LCA between attributional and consequential modeling as was briefly presented in Chapter 2. The LCA work in this thesis employed attributional models, whereby the question being posed was "what is the share of current, total global environmental burden that is attributed to OPV technologies?" While this approach is relevant for hot-spot analysis and a baseline understanding of the environmental burdens associated with OPV, consequential-LCA could be used to better understand what the future and/or long-term effects would be for the large-scale production of and the energy introduced into the market by OPV. This approach would be appropriate for better understanding what, if any, influence energy produced by OPV would replace other technologies, for example.

Data Requirements

Furthermore, models and tools can be extremely useful but only if there is data to accompany it. The latter point represents an unfortunate problem when evaluating emerging technologies such as ENM and OPV. Lab-scale or recently introduced products and processes often mean that good representative data is hard to come by or that it simply doesn't exist. LCA and HHRA require quite comprehensive data and information. Fate and exposure models describing scenarios in which ENM emissions occur and how ENM behave in the environment will require somewhat specific contextual information. The occupational, indoor air environment presented in this thesis represents a much simpler context compared with outdoor fate and transport models that will use several nested and connected media compartments each controlled by their own relative model parameters and ENM-specific parameters. Similar to what was proposed in this thesis, different classes of archetypes or "classes" of environmental conditions should be focused on models with enough detail such that they are both manageable to build and operate yet meaningful in their results. Lastly, as was confronted in this thesis with C60-fullerenes, the existence of relevant toxicological information remains a major barrier to development of relevant LCA and HHRA models. Chronic, multi-dose, *in vivo* toxicological studies are time intensive and expensive to conduct. As

a consequence, there is relatively little published data *in vivo* that can be used to calculate both cancerous and non-cancerous dose-response relationships that are relevant for humans.[97] The resulting set of relatively small amounts of data thus will carry with it greater amounts of uncertainty.

Data Requirements for Emissions of Engineered Nanomaterials from Organic Photovoltaics

In the past few years, models attempting to calculate the emissions from high volume production ENM have been published, however their uncertainty remains high and estimations are limited to certain industries, production routes or use phases, if the latter is included at all.[189–191,199,329,365,366] This thesis was not able to address the question surrounding the ENM emissions during the use and end-of-life phases of the panels, however this remains an ongoing part of the work initiated by this thesis and will subsequently continue. A handful of previous studies have considered the leaching potential of OPV panels but none report the amounts of ENM in the leachates. For instance, Zimmerman et al.[367] found 2.4 ± 0.77 µg Al, 1.3 ± 0.3 µg Ag and 4.4 ± 0.1 µg Zn per gram of PV leached with freshwater, 0.7 ± 0.1 µg Cu^{2+} and 3.9 ± 0.7 µg Zn per gram of PV leached with acidic rainwater, and 0.9 ± 0.2 µg Al and 14.6 ± 1.8 µg Ag per gram of PV leached with seawater[367]. Brun et al.[368] made similar tests finding 63 ± 7 µg Zn^{2+} per liter of mesotrophic water, 14 ± 2 µg Cu^{2+} and 87 ± 7 µg Zn^{2+} per liter of acidic water, and 78 ± 7 µg $AgCl_2^-$ and 17 ± 1 µg Zn^{2+} per liter of seawater[368].

Espinosa et al.[250] assessed the leaching potential over the course of 1-year of both intact rolls of pristine and damaged OPV panels *in situ* while used in a standard solar array (1 kW grid) and in a simulated *unintended* disposal scenario where shredded and intact OPV panels were buried in soil columns. They found that up to 30% of the Ag (14.3 mg per m2 OPV) and 100% of the Zn (79.0 mg per m2 OPV) leached in the case of deliberately damaged panels. Interestingly, there were two sets of pristine panels tested, one in which stayed intact the entire testing period and another that started to de-laminate between days 90 and the end of the testing period (day 182). The intact panel leached no considerable amounts of Ag or Zn while the delaminated panel leached 30% of its total Ag and 54% of its total zinc content[250]. In their soil column experiments, no appreciable Zn leached however up to 15.7% (771.7 mg) and 0.5% (25.6 mg) of the total Ag content leached from the shredded and intact panels, respectively.[250]

These results demonstrate that OPV can in fact leach substances from their individual layers over time, particularly when damaged or they have been physically compromised. However, there is no data showing whether ENM emissions are occurring as well. For reasons discussed in this thesis regarding the current

regulatory environment over ENM, for example, understanding the potential leaching of these materials will likely surface as notable concern. In addition, this information will be of interest in comparison to other 3rd-generation PV such as perovskite solar cells. For example, there are some concerns over the use of heavy metals such as lead used in the perovskite cells, whose related eco- and human-toxicity impacts could potentially be a limiting factor for this technology.

Concluding Statements

The future is bright for OPV technologies. In terms of their resource efficiencies and potential hazards, OPV have proven themselves to be a preferential option compared to conventional silicon-based PV and a sustainable energy supply option for certain applications. The limits of these conclusions rest on the uncertainties OPV possess in terms of their lifetimes and efficiencies. The results presented in this thesis recommend the use and application of OPV for products with short lifetimes as the greater resource efficiencies and lower environmental hazards compared with silicon-based PV were very compelling. Further caveats to these findings involve the assumption that OPV material choices and device structures will continue along the trends pointed to in this thesis. Additionally, LCA, in many ways, was the most appropriate methodology for making these claims, particularly at its current, early-stage development as an emerging technology. HHRA, on the other hand, may be the most powerful methodology for evaluating the human health impacts from the ENM components used in the OPV, although this will be most appropriate at industrial-scales of production. In practice, the general tendency is for different stakeholders to hold on to their tool of choice (e.g. LCA, HHRA, ERA), either out of familiarity or opinion, ultimately excepting the exclusion of a more comprehensive viewpoint.[74,221] An integrated approach, however, that combines the methodologies of LCA and HHRA (as well as ERA) can offer the most flexibility and applicability for OPV given their current level of development while also addressing both the resource efficiencies and hazards of this technology.

Bibliography

1. Robert, K. W., Parris, T. M. & Leiserowitz, A. A. What is Sustainable Development? Goals, Indicators, Values, and Practice. *Environ. Sci. Policy Sustain. Dev.* **47,** 8–21 (2005).
2. Bardi, U. Peak oil: The four stages of a new idea. *Energy* **34,** 323–326 (2009).
3. Carbon accounting. *Nat. Clim. Chang.* (2016). doi:10.1038/nclimate3137
4. Moss, R. H. *et al.* The next generation of scenarios for climate change research and assessment. *Nature* **463,** 747–756 (2010).
5. Fraiture, C. de, Giordano, M. & Liao, Y. Biofuels and implications for agricultural water use: blue impacts of green energy. *Water Policy* **10,** 67 (2008).
6. Escobar, J. C. *et al.* Biofuels: Environment, technology and food security. *Renew. Sustain. Energy Rev.* **13,** 1275–1287 (2009).
7. Howarth, R. W. & Bringezu, S. *Biofuels: Environmental Consequences and Interactions with Changing Land Use - Proceedings of the Scientific Committee on Problems of the Environment (SCOPE) International Biofuels Project Rapid Assessment*. (2008). at <http://cip.cornell.edu/DPubS?service=UI&version=1.0&verb=Display&page=current&handle=scope>
8. Searchinger, T. *et al.* Use of U.S. Croplands for Biofuels Increases Greenhouse Gases Through Emissions from Land-Use Change. *Science (80-.).* **319,** 1238–1240 (2008).
9. Hertwich, E. G. *et al.* Integrated life-cycle assessment of electricity-supply scenarios confirms global environmental benefit of low-carbon technologies. *Proc. Natl. Acad. Sci.* **112,** 6277–6282 (2015).
10. Spanggaard, H. & Krebs, F. C. A brief history of the development of organic and polymeric photovoltaics. *Sol. Energy Mater. Sol. Cells* **83,** 125–146 (2004).
11. Becquerel, A. Recherches sur les effets de la radiation chimique de la lumière solaire, au moyen des courants électriques. *Comptes Rendus L´Academie des Sci.* **9,** 145–149 (1939).
12. Green, M. A. Photovoltaic principles. *Phys. E Low-dimensional Syst. Nanostructures* **14,** 11–17 (2002).
13. Ohl, R. S. Light-sensitive electric device. (1946).
14. Green, M. A. Photovoltaics: coming of age. in *IEEE Conference on Photovoltaic Specialists* 1–8 (IEEE). doi:10.1109/PVSC.1990.111582
15. Green, M. A., Emery, K., Hishikawa, Y., Warta, W. & Dunlop, E. D. Solar cell efficiency tables (version 47). *Prog. Photovoltaics Res. Appl.* **24,** 3–11 (2016).
16. Fraunhofer Institute for Solar Energy Systems ISE. *Photovoltaics Report (2016)*. (2016).
17. Fthenakis, V. & Alsema, E. Photovoltaics energy payback times, greenhouse gas emissions and external costs: 2004–early 2005 status. *Prog. Photovoltaics Res. Appl.* **14,** 275–280 (2006).
18. Barbose, G. *et al.* Tracking US photovoltaic system prices 1998-2012: a rapidly changing market. *Prog. Photovoltaics Res. Appl.* **23,** 692–704 (2015).
19. U.S. Energy Information Agency. *Levelized Cost and Levelized Avoided Cost of New Generation Resources in the Annual Energy Outlook 2016*. (2016). at <http://www.eia.gov/forecasts/aeo/pdf/electricity_generation.pdf>
20. Roselund, C. Demand begins to exceed supply for multicrystalline silicon PV. *PV Magazine* (2015).
21. Kalowekamo, J. & Baker, E. Estimating the manufacturing cost of purely organic solar cells. *Sol. Energy* **83,** 1224–1231 (2009).
22. Laboratory, U. S. N. R. E. Photovoltaic Efficiency Chart. (2016). at <http://www.nrel.gov/ncpv/images/efficiency_chart.jpg>
23. Tang, C. W. Multilayer organic photovoltaic elements. (1979).
24. Espinosa, N., Hösel, M., Jørgensen, M. & Krebs, F. C. Large scale deployment of polymer solar cells on land, on sea and in the air. *Energy Environ. Sci.* **7,** 855 (2014).
25. Krebs, F. C., Tromholt, T. & Jørgensen, M. Upscaling of polymer solar cell fabrication using full roll-to-roll processing. *Nanoscale* **2,** 873 (2010).
26. Jungbluth, N. Life cycle assessment of crystalline photovoltaics in the Swiss ecoinvent database. *Prog. Photovoltaics Res. Appl.* **13,** 429–446 (2005).
27. International Organization for Standardization. *ISO 14044 - Environmental management - Life cycle assessment - Requirements and guidelines*. (2006).
28. International Organization for Standardization. *ISO 14040 - Environmental Management - Life cycle assessment - Principles and framework*. (2006).
29. Roes, A. L., Alsema, E. A., Blok, K. & Patel, M. K. Ex-ante environmental and economic evaluation of polymer photovoltaics. *Prog. Photovoltaics Res. Appl.* **17,** 372–393 (2009).
30. García-Valverde, R., Cherni, J. A. & Urbina, A. Life cycle analysis of organic photovoltaic technologies. *Prog. Photovoltaics Res. Appl.* **18,** 535–558 (2010).
31. Espinosa, N., García-Valverde, R., Urbina, A. & Krebs, F. C. A life cycle analysis of polymer solar cell modules prepared using roll-to-roll methods under ambient conditions. *Sol. Energy Mater. Sol. Cells* **95,** 1293–1302 (2011).
32. US EPA, O. Human Health Risk Assessment.
33. European Union European Environment Agency. Environmental Risk Assessment - Approaches, Experiences and Information Sources — European Environment Agency. (1998). at <http://www.eea.europa.eu/publications/GH-07-97-595-EN-C2>
34. Huber, W. & Kolb, G. Life cycle analysis of silicon-based photovoltaic systems. *Sol. Energy* **54,** 153–163 (1995).
35. Fthenakis, V. *et al. Life Cycle Inventories and Life Cycle Assessments of Photovoltaic Systems*. (2011).
36. Espinosa, N., García-Valverde, R. & Krebs, F. C. Life-cycle analysis of product integrated polymer solar cells. *Energy Environ. Sci.* **4,** 1547 (2011).
37. Espinosa, N. *et al.* Life cycle assessment of ITO-free flexible polymer solar cells prepared by roll-to-roll coating and printing. *Sol. Energy Mater. Sol. Cells* **97,** 3–13 (2012).
38. Espinosa, N., Hösel, M., Angmo, D. & Krebs, F. C. Solar cells with one-day energy payback for the factories of the future. *Energy Environ. Sci.* **5,** 5117–5132 (2012).
39. Yue, D., Khatav, P., You, F. & Darling, S. B. Deciphering the uncertainties in life cycle energy and environmental analysis of organic

photovoltaics. *Energy Environ. Sci.* **5,** 9163 (2012).
40. Emmott, C. J. M., Urbina, A. & Nelson, J. Environmental and economic assessment of ITO-free electrodes for organic solar cells. *Sol. Energy Mater. Sol. Cells* **97,** 14–21 (2012).
41. Espinosa, N. *et al.* OPV for mobile applications: an evaluation of roll-to-roll processed indium and silver free polymer solar cells through analysis of life cycle, cost and layer quality using inline optical and functional inspection tools. *J. Mater. Chem. A* **1,** 7037 (2013).
42. Anctil, A., Babbitt, C. W., Raffaelle, R. P. & Landi, B. J. Cumulative energy demand for small molecule and polymer photovoltaics. *Prog. Photovoltaics Res. Appl.* **21,** 1541–1554 (2013).
43. Krebs, F. C. Fabrication and processing of polymer solar cells: A review of printing and coating techniques. *Sol. Energy Mater. Sol. Cells* **93,** 394–412 (2009).
44. Krebs, F. C. Roll-to-roll fabrication of monolithic large-area polymer solar cells free from indium-tin-oxide. *Sol. Energy Mater. Sol. Cells* **93,** 1636–1641 (2009).
45. Lizin, S. *et al.* Life cycle analyses of organic photovoltaics: a review. *Energy Environ. Sci.* **6,** 3136 (2013).
46. Kumar, A. & Zhou, C. The Race To Replace Tin-Doped Indium Oxide: Which Material Will Win? *ACS Nano* **4,** 11–14 (2010).
47. Samad, W. Z., Yarmo, M. A., Salleh, M. M. & Shafiee, A. Structural, Optical and Electrical Properties of Fluorine Doped Tin Oxide Thin Films Deposited Using Ink jet Printing Technique. *Sains Malaysiana* **40,** 251–257 (2011).
48. Koster, L. J. A. The optimal band gap for plastic photovoltaics. *SPIE Newsroom* (2007). doi:10.1117/2.1200701.0528
49. Krätschmer, W., Lamb, L. D., Fostiropoulos, K. & Huffman, D. R. Solid C60: a new form of carbon. *Nature* **347,** 354–358 (1990).
50. Taylor, R. & Walton, D. R. M. The chemistry of fullerenes. *Nature* **363,** 685–693 (1993).
51. Wudl, F. The chemical properties of buckminsterfullerene (C60) and the birth and infancy of fulleroids. *Acc. Chem. Res.* **25,** 157–161 (1992).
52. Thompson, B. C. & Fréchet, J. M. J. Polymer–Fullerene Composite Solar Cells. *Angew. Chemie Int. Ed.* **47,** 58–77 (2008).
53. Kroon, R., Lenes, M., Hummelen, J. C., Blom, P. W. M. & de Boer, B. Small Bandgap Polymers for Organic Solar Cells (Polymer Material Development in the Last 5 Years). *Polym. Rev.* **48,** 531–582 (2008).
54. Li, C.-Z., Yip, H.-L. & Jen, A. K.-Y. Functional fullerenes for organic photovoltaics. *J. Mater. Chem.* **22,** 4161 (2012).
55. Yan, J. & Saunders, B. R. Third-generation solar cells: a review and comparison of polymer:fullerene, hybrid polymer and perovskite solar cells. *RSC Adv.* **4,** 43286–43314 (2014).
56. Peters, C. H. *et al.* High Efficiency Polymer Solar Cells with Long Operating Lifetimes. *Adv. Energy Mater.* **1,** 491–494 (2011).
57. Anctil, A., Babbitt, C. W., Raffaelle, R. P. & Landi, B. J. Material and Energy Intensity of Fullerene Production. *Environ. Sci. Technol.* **45,** 2353–2359 (2011).
58. Greenland, S. Sensitivity Analysis, Monte Carlo Risk Analysis, and Bayesian Uncertainty Assessment. *Risk Anal.* **21,** 579–584 (2001).
59. Pacca, S., Sivaraman, D. & Keoleian, G. A. Parameters affecting the life cycle performance of PV technologies and systems. *Energy Policy* **35,** 3316–3326 (2007).
60. E, A. & M., W.-S. Environmental impacts of crystalline silicon photovoltaic module production. in *Proceedings 13th CIRP International Conference on Life Cycle Engineering* (2006).
61. DeWild-Scholten, M. & Alsema, E. Environmental Life Cycle Inventory of Crystalline Silicon Photovoltaic Module Production. in *Materials Research Society Conference* (2006).
62. Espinosa, N., Laurent, A. & Krebs, F. C. Ecodesign of organic photovoltaic modules from Danish and Chinese perspectives. *Energy Environ. Sci.* **8,** 2537–2550 (2015).
63. Service, R. F. Outlook Brightens for Plastic Solar Cells. *Science (80-.).* **332,** 293–293 (2011).
64. Larsen, K. End-of-life PV: then what? *Renew. Energy Focus* **10,** 48–53 (2009).
65. Choi, J.-K. & Fthenakis, V. Crystalline silicon photovoltaic recycling planning: macro and micro perspectives. *J. Clean. Prod.* **66,** 443–449 (2014).
66. Manfredi, S., Allacker, K., Chomkhamsri, Kirana Pelletier, N. & Maia de Souza, D. *Product Environmental Footprint (PEF) Guide*. (2012).
67. Chatzisideris, M. D., Espinosa, N., Laurent, A. & Krebs, F. C. Ecodesign perspectives of thin-film photovoltaic technologies: A review of life cycle assessment studies. *Sol. Energy Mater. Sol. Cells* **156,** 2–10 (2016).
68. Guinée, J. B. *et al.* Life Cycle Assessment: Past, Present, and Future †. *Environ. Sci. Technol.* **45,** 90–96 (2011).
69. Battelle and Franklin Associates. *Product Life Cycle Assessment - Guidelines and Principles (Final Report)*. (1992).
70. Fava, J. *et al. A technical framework for life cycle assessment: workshop report*. (1991).
71. R.G. Hunt, Sellers, J. D. & Franklin, W. E. Resource and Environmental Profile Analysis: A Life Cycle Environmental Assessment for Products and Procedures. *Environ. Impact Assess. Rev.* **12,** (1992).
72. (SETAC), S. of E. T. and C. *Guidelines for Life-Cycle Assessment: A Code of Practice*. (1993).
73. Curran, Ma. A. Environmental life-cycle assessment. *Int. J. Life Cycle Assess.* **1,** 179–179 (1996).
74. Steinfeldt, M. & Petschow, U. *Nanotechnologies, Hazards and Resource Efficiency*. (Springer-Verlag, 2007).
75. International Organization for Standardization. *ISO 14025:2006 - Environmental labels and declarations -- Type III environmental declarations -- Principles and procedures*. (2006).
76. Programme, U. N. E. *Global Guidance Principles for Life Cycle Assessment Databases - A Basis for Greener Processes and Products*. (2011).
77. Weidema, B. *Market information in life-cycle assessment*. (2003).
78. US Environmental Protection Agency. *Life Cycle Assessment: Principles and Practice*. (2006).
79. Jungbluth, N., Stucki, M., Frischknecht, R. & Busser, R. *Ecoinvent report No.6 Part XII: Photovoltaics*. (2009).
80. Goedkoop, M. J. *et al. A life cycle impact assessment method which comprises harmonised category indicators at the midpoint and the endpoint level*. (2009).
81. Sustainability, E. C. J. R. C. I. for E. and. *Recommendations for the life cycle impact assessment in the European context*. (2011). doi:10.278/33030
82. Acero, A. P., Rodriguez, C. & Ciroth, A. *LCIA Methods - Impact assessment methods in Life Cycle Assessment and their impact*

categories. (2014).
83. Cucurachi, S., Heijungs, R. & Ohlau, K. Towards a general framework for including noise impacts in LCA. *Int. J. Life Cycle Assess.* **17,** 471–487 (2012).
84. Rosenbaum, R. K. *et al.* USEtox—the UNEP-SETAC toxicity model: recommended characterisation factors for human toxicity and freshwater ecotoxicity in life cycle impact assessment. *Int. J. Life Cycle Assess.* **13,** 532–546 (2008).
85. McKone, T., Bennett, D. & Maddalena, R. *CalTOX 4.0 Technical Support Document*. (2001).
86. Jolliet, O. *et al.* IMPACT 2002+: A new life cycle impact assessment methodology. *Int. J. Life Cycle Assess.* **8,** 324–330 (2003).
87. MacLeod, M. *et al.* BETR North America: A regionally segmented multimedia contaminant fate model for North America. *Environ. Sci. Pollut. Res.* **8,** 156 (2001).
88. Wenzel, H., Hauschild, M. Z. & Alting, L. *Environmental Assessment of Products*. (Springer U.S., 1997).
89. Bachmann, T. M. *Hazardous substances and human health: exposure, impact and external cost assessment at the European scale. Trace metals and other contaminants in the environment*. (Elsevier, 2006).
90. Huijbregts, M. A. J. *et al.* Priority assessment of toxic substances in life cycle assessment. Part I: Calculation of toxicity potentials for 181 substances with the nested multi-media fate, exposure and effects model USES–LCA. *Chemosphere* **41,** 541–573 (2000).
91. European Commission. *ExternE Externalities of Energy ExternE Externalities of Energy*. (2005). at <http://www.externe.info/>
92. Hischier, R. *et al. Implementation of Life Cycle Impact Assessment Methods*. (2010).
93. Pini, M., Salieri, B., Ferrari, A. M., Nowack, B. & Hischier, R. Human health characterization factors of nano-TiO2 for indoor and outdoor environments. *Int. J. Life Cycle Assess.* (2016). doi:10.1007/s11367-016-1115-8
94. Eckelman, M. J., Mauter, M. S., Isaacs, J. a & Elimelech, M. New perspectives on nanomaterial aquatic ecotoxicity: production impacts exceed direct exposure impacts for carbon nanotoubes. *Environ. Sci. Technol.* **46,** 2902–2910 (2012).
95. Salieri, B., Righi, S., Pasteris, A. & Olsen, S. I. Freshwater ecotoxicity characterisation factor for metal oxide nanoparticles: a case study on titanium dioxide nanoparticle. *Sci. Total Environ.* **505,** 494–502 (2015).
96. Miseljic, M. & Olsen, S. I. Life-cycle assessment of engineered nanomaterials: a literature review of assessment status. *J. Nanoparticle Res.* **16,** 1–33 (2014).
97. Walser, T. *et al.* Life-cycle assessment framework for indoor emissions of synthetic nanoparticles. *J. Nanoparticle Res.* **17,** 1–18 (2015).
98. Hofstetter, P., Baumgartner, T. & Scholz, R. W. Modelling the valuesphere and the ecosphere: Integrating the decision makers' perspectives into LCA. *Int. J. Life Cycle Assess.* **5,** 161–175 (2000).
99. Oreskes, N. BEYOND THE IVORY TOWER: The Scientific Consensus on Climate Change. *Science (80-.).* **306,** 1686–1686 (2004).
100. American Chemical Society. Radiative Forcing. (2016). at <https://www.acs.org/content/acs/en/climatescience/atmosphericwarming/radiativeforcing.html>
101. Goedkoop, M. *et al. ReCiPe 2008*. (2008). at <http://www.pre-sustainability.com/download/misc/ReCiPe_main_report_final_27-02-2009_web.pdf>
102. National Geographic. Ozone Depletion Information, Ozone Depletion Facts, Ozone Layer, Ozone Hole. (2016). at <http://environment.nationalgeographic.com/environment/global-warming/ozone-depletion-overview/>
103. *Air Pollution by Photochemical Oxidants*. **52,** (Springer Berlin Heidelberg, 1985).
104. Lippmann, M. HEALTH EFFECTS OF OZONE A Critical Review. *JAPCA* **39,** 672–695 (1989).
105. Rich, S. Ozone Damage to Plants. *Annu. Rev. Phytopathol.* **2,** 253–266 (1964).
106. Frischknecht, R., Heijungs, R. & Hofstetter, P. Einstein'ssons for energy accounting in LCA. *Int. J. Life Cycle Assess.* **3,** 266–272 (1998).
107. Pawłowski, L. Acidification: its impact on the environment and mitigation strategies. *Ecol. Eng.* **8,** 271–288 (1997).
108. US Department of Commerce, N. O. and A. A. NOAA's National Ocean Service Education: Estuaries.
109. WHO. Environmental radiation. *WHO* (2013).
110. Canadian Nuclear Safety Commission. Types and sources of radiation. (2015). at <http://nuclearsafety.gc.ca/eng/resources/radiation/introduction-to-radiation/types-and-sources-of-radiation.cfm>
111. Humbert, S., Fantke, P. & Jolliet, O. in 97–113 (2015). doi:10.1007/978-94-017-9744-3_6
112. WHO | Metrics: Disability-Adjusted Life Year (DALY). *WHO* (2014).
113. Kim, H., Kushto, G. P., Auyeung, R. C. Y. & Piqué, A. Optimization of F-doped SnO2 electrodes for organic photovoltaic devices. *Appl. Phys. A* **93,** (2008).
114. Yu, S., Li, L., Lyu, X. & Zhang, W. Preparation and investigation of nano-thick FTO/Ag/FTO multilayer transparent electrodes with high figure of merit. *Sci. Rep.* **6,** 20399 (2016).
115. Su, H. *et al.* Highly Conductive and Low Cost Ni-PET Flexible Substrate for Efficient Dye-Sensitized Solar Cells. *ACS Appl. Mater. Interfaces* **6,** 5577–5584 (2014).
116. Jiang, C. Y., Sun, X. W., Zhao, D. W., Kyaw, A. K. K. & Li, Y. N. Low work function metal modified ITO as cathode for inverted polymer solar cells. *Sol. Energy Mater. Sol. Cells* **94,** 1618–1621 (2010).
117. Voroshazi, E., Verreet, B., Aernouts, T. & Heremans, P. Long-term operational lifetime and degradation analysis of P3HT:PCBM photovoltaic cells. *Sol. Energy Mater. Sol. Cells* **95,** 1303–1307 (2011).
118. Girotto, C., Voroshazi, E., Cheyns, D., Heremans, P. & Rand, B. P. Solution-Processed MoO 3 Thin Films As a Hole-Injection Layer for Organic Solar Cells. *ACS Appl. Mater. Interfaces* **3,** 3244–3247 (2011).
119. Steim, R., Kogler, F. R. & Brabec, C. J. Interface materials for organic solar cells. *J. Mater. Chem.* **20,** 2499 (2010).
120. Roy, A. *et al.* Titanium suboxide as an optical spacer in polymer solar cells. *Appl. Phys. Lett.* **95,** 13302 (2009).
121. Kim, J. Y. *et al.* New Architecture for High-Efficiency Polymer Photovoltaic Cells Using Solution-Based Titanium Oxide as an Optical Spacer. *Adv. Mater.* **18,** 572–576 (2006).
122. Hayakawa, A., Yoshikawa, O., Fujieda, T., Uehara, K. & Yoshikawa, S. High performance polythiophene/fullerene bulk-heterojunction solar cell with a TiO[sub x] hole blocking layer. *Appl. Phys. Lett.* **90,** 163517 (2007).
123. Apilo, P. *et al.* Roll-to-roll gravure printing of organic photovoltaic modules-insulation of processing defects by an interfacial layer. *Prog. Photovoltaics Res. Appl.* **23,** 918–928 (2015).
124. Brabec, C. J., Shaheen, S. E., Winder, C., Sariciftci, N. S. & Denk, P. Effect of LiF/metal electrodes on the performance of plastic solar

cells. *Appl. Phys. Lett.* **80,** 1288 (2002).
125. Zhou, Y. *et al.* A Universal Method to Produce Low-Work Function Electrodes for Organic Electronics. *Science (80-.).* **336,** 327–332 (2012).
126. Scharber, M. C. & Sariciftci, N. S. Efficiency of bulk-heterojunction organic solar cells. *Prog. Polym. Sci.* **38,** 1929–1940 (2013).
127. Darling, S. B. & You, F. The case for organic photovoltaics. *RSC Adv.* **3,** 17633 (2013).
128. Anctil, A. & Fthenakis, V. in *Third Generation Photovoltaics* (InTech, 2012). doi:10.5772/38977
129. Jung, S. *et al.* All-Inkjet-Printed, All-Air-Processed Solar Cells. *Adv. Energy Mater.* **4,** 1400432 (2014).
130. Swantson, J. in *Ulmann's Encyclopedia of Industrial Chemistry* (2007).
131. Graf, G. in *Ulmann's Encyclopedia of Industrial Chemistry* (2007).
132. Frischknecht, R. *et al. Overview and Methodology; Final Report Ecoinvent Data 2.0*. (2007).
133. Aukkaravittayapun, S. *et al.* Large scale F-doped SnO2 coating on glass by spray pyrolysis. *Thin Solid Films* **496,** 117–120 (2006).
134. Kim, B.-S., Lee, H.-I., Choi, Y.-Y. & Kim, S. Kinetics of the Oxidative Roasting of Low Grade Mongolian Molybdenite Concentrate. *Mater. Trans.* **50,** 2669–2674 (2009).
135. Yang, J. *et al.* Organic photovoltaic modules fabricated by an industrial gravure printing proofer. *Sol. Energy Mater. Sol. Cells* **109,** 47–55 (2013).
136. Kopola, P. *et al.* Gravure printed flexible organic photovoltaic modules. *Sol. Energy Mater. Sol. Cells* **95,** 1344–1347 (2011).
137. Zimmermann, Y.-S. *et al.* Organic photovoltaics: Potential fate and effects in the environment. *Environ. Int.* **49,** 128–140 (2012).
138. Andersson, B. V., Huang, D. M., Moulé, A. J. & Inganäs, O. An optical spacer is no panacea for light collection in organic solar cells. *Appl. Phys. Lett.* **94,** 43302 (2009).
139. Huang, X. *et al.* Preparation of fluorine-doped tin oxide (SnO2:F) film on polyethylene terephthalate (PET) substrate. *Mater. Lett.* **64,** 1701–1703 (2010).
140. Facchetti, A. Polymer donor–polymer acceptor (all-polymer) solar cells. *Mater. Today* **16,** 123–132 (2013).
141. OSA DIRECT. Polyera achieves 6.4% efficiency for all-polymer organic photovoltaic. at <http://www.osadirect.com/news/article/951/polyera-achieves-64-efficiency-for-all-polymer-organic-photovoltaic/>
142. Badgujar, S. *et al.* Highly Efficient and Thermally Stable Fullerene-Free Organic Solar Cells based on Small Molecule Donor and Acceptor. *J. Mater. Chem. A* (2016). doi:10.1039/C6TA06367E
143. Liu, T. *et al.* Ternary Organic Solar Cells Based on Two Compatible Nonfullerene Acceptors with Power Conversion Efficiency >10%. *Adv. Mater.* (2016). doi:10.1002/adma.201602570
144. Holliday, S. *et al.* High-efficiency and air-stable P3HT-based polymer solar cells with a new non-fullerene acceptor. *Nat. Commun.* **7,** 11585 (2016).
145. Jungbluth, N., Tuchschmid, M. & de Wild-Scholten, M. *Life Cycle Assessment of Photovoltaics: update of ecoinvent data V2.0*. (2008). doi:ECN-O--08-025
146. Tsang, M. P., Sonnemann, G. W. & Bassani, D. M. A comparative human health, ecotoxicity, and product environmental assessment on the production of organic and silicon solar cells. *Prog. Photovoltaics Res. Appl.* **24,** 645–655 (2016).
147. Søndergaard, R. R., Espinosa, N., Jørgensen, M. & Krebs, F. C. Efficient decommissioning and recycling of polymer solar cells: justification for use of silver. *Energy Environ. Sci.* **7,** 1006 (2014).
148. Fthenakis, V. M. End-of-life management and recycling of PV modules. *Energy Policy* **28,** 1051–1058 (2000).
149. Goe, M. & Gaustad, G. Strengthening the case for recycling photovoltaics: An energy payback analysis. *Appl. Energy* **120,** 41–48 (2014).
150. Doka, G. *Ecoinvent report No. 13, parts I-V: Life cycle invntories of waste treatment services*. (2009).
151. Fthenakis, V. M. & Kim, H. C. Photovoltaics: Life-cycle analyses. *Sol. Energy* **85,** 1609–1628 (2011).
152. McDonald, N. C. & Pearce, J. M. Producer responsibility and recycling solar photovoltaic modules. *Energy Policy* **38,** 7041–7047 (2010).
153. Šúri, M., Huld, T. A., Dunlop, E. D. & Ossenbrink, H. A. Potential of solar electricity generation in the European Union member states and candidate countries. *Sol. Energy* **81,** 1295–1305 (2007).
154. Müller, A., Wambach, K. & Alsema, E. Life Cycle Analysis of Solar Module Recycling Process. *MRS Proc.* **895,** 895-G03-7 (2005).
155. Espinosa, N. & Krebs, F. C. Life cycle analysis of organic tandem solar cells: When are they warranted? *Sol. Energy Mater. Sol. Cells* **120,** 692–700 (2014).
156. Sandwell, P. *et al.* Off-grid solar photovoltaic systems for rural electrification and emissions mitigation in India. *Sol. Energy Mater. Sol. Cells* **156,** 147–156 (2016).
157. Hengevoss, D., Baumgartner, C., Nisato, G. & Hugi, C. Life Cycle Assessment and eco-efficiency of prospective, flexible, tandem organic photovoltaic module. *Sol. Energy* **137,** 317–327 (2016).
158. Stone, V. *Engineered Nanoparticles : Review of Health and Environmental Safety*. (2009).
159. Aschberger, K. *et al.* Review of carbon nanotubes toxicity and exposure--appraisal of human health risk assessment based on open literature. *Crit. Rev. Toxicol.* **40,** 759–790 (2010).
160. Johnston, H. J. *et al.* A review of the in vivo and in vitro toxicity of silver and gold particulates: Particle attributes and biological mechanisms responsible for the observed toxicity. *Crit. Rev. Toxicol.* **40,** 328–346 (2010).
161. National Institute for Occupational Safety and Health. *Current Intelligence Bulletin 63: Occupational Exposure to Titanium Dioxide*. (2011).
162. Hristozov, D., Ertel, J. & TechnoValuation, M. Nanotechnology and Sustainability: Benefits and Risks of Nanotechnology for Environmental Sustainability. *Forum Forsch* **22,** 161–168 (2009).
163. Som, C. *et al.* The importance of life cycle concepts for the development of safe nanoproducts. *Toxicology* **269,** 160–169 (2010).
164. European Commission. Commission recommendation on the definition of nanomaterial. *Off. J. Eur. Union* **L,** 38–40 (2011).
165. The Project on Emerging Nanotechnologies. The Nanotechnology Consumer Products Inventory. (2015). at <http://www.nanotechproject.org/cpi/>
166. Roco, M. C. Nanotechnology's Future. *Sci. Am.* **295,** 39–39 (2006).

167. European Commission. *Communication from the Commission to the European Parliament, The Council and the European Economic and Social Committee (Second Regulatory Review on Nanomaterials*. (2012).
168. Vance, M. E. *et al.* Nanotechnology in the real world: Redeveloping the nanomaterial consumer products inventory. *Beilstein J. Nanotechnol.* **6,** 1769–1780 (2015).
169. Greßler, S; Nentwich, M. Nano and the environment–Part I: Potential environmental benefits and sustainability effects. *Nano Trust Dossiers* **26,** 1–4 (2012).
170. Royal Society and Royal Academy of Engineering. *Nanoscience and nanotechnologies: opportunities and uncertainties*. *Nanoscience and Nanotechnologies Opportunities and Uncertainties* (Royal Society, 2004).
171. Yokel, R. A. & MacPhail, R. C. Engineered nanomaterials: exposures, hazards, and risk prevention. *J. Occup. Med. Toxicol.* **6,** 7 (2011).
172. European Commission. *Second regulatory review on nanomaterials. Communication from the Commission to the European Parliament, the Council and the European Economic and Social Committee.* (2012).
173. Pietroiusti, A. Health implications of engineered nanomaterials. *Nanoscale* **4,** 1231 (2012).
174. Klaine, S. J. *et al.* Nanomaterials in the environment: behavior, fate, bioavailability, and effects. *Environ. Toxicol. Chem.* **27,** 1825–1851 (2008).
175. Greßler, S; Nentwich, M. Nano and Environment–Part II : Hazard potentials and risks. *Nano Trust Dossiers* **27,** 1–6 (2012).
176. MacPhail, R. C., Grulke, E. A. & Yokel, R. A. Assessing nanoparticle risk poses prodigious challenges. *Wiley Interdiscip. Rev. Nanomedicine Nanobiotechnology* **5,** 374–387 (2013).
177. Chang, X., Zhang, Y., Tang, M. & Wang, B. Health effects of exposure to nano-TiO2: a meta-analysis of experimental studies. *Nanoscale Res. Lett.* **8,** 51 (2013).
178. Griffitt, R. J., Luo, J., Gao, J., Bonzongo, J.-C. & Barber, D. S. Effects of particle composition and species on toxicity of metallic nanomaterials in aquatic organisms. *Environ. Toxicol. Chem.* **27,** 1972–1978 (2008).
179. U.S. Food and Drug Administration. FDA's Approach to Regulation of Nanotechnology Products. (2015).
180. U.S. Environmental Protection Agency. Control of Nanoscale Materials under the Toxic Substances Control Act. (2016).
181. European Chemicals Agency. Nanomaterials. at <http://echa.europa.eu/regulations/nanomaterials>
182. Krug, H. F. Nanosafety Research-Are We on the Right Track? *Angew. Chemie Int. Ed.* n/a-n/a (2014). doi:10.1002/anie.201403367
183. Curran, M. A., Frankl, P., Jeijungs, R., Kohler, A. & Olsen, S. I. *Nanotechnology and life cycle assessment: A systems approach to Nanotechnology and the environment: Synthesis of results obtained at a workshop*. (2007).
184. Hischier, R. & Walser, T. Life cycle assessment of engineered nanomaterials: State of the art and strategies to overcome existing gaps. *Sci. Total Environ.* **425,** 271–282 (2012).
185. Grieger, K. D. *et al.* Analysis of current research addressing complementary use of life-cycle assessment and risk assessment for engineered nanomaterials: have lessons been learned from previous experience with chemicals? *J. Nanoparticle Res.* **14,** 1–23 (2012).
186. Wender, B. A. *et al.* Illustrating anticipatory life cycle assessment for emerging photovoltaic technologies. *Environ. Sci. Technol.* **48,** 10531–10538 (2014).
187. Gavankar, S., Suh, S. & Keller, A. F. Life cycle assessment at nanoscale: review and recommendations. *Int. J. Life Cycle Assess.* **17,** 295–303 (2012).
188. Jolliet, O., Rosenbaum, R. K. & Laurent, A. in *Nanotechnology and Human Health* (eds. Malsch, I. & Emond, C.) 214–265 (CRC Press, 2014).
189. Keller, A. a., McFerran, S., Lazareva, A. & Suh, S. Global life cycle releases of engineered nanomaterials. *J. Nanoparticle Res.* **15,** 1–17 (2013).
190. Sun, T. Y., Gottschalk, F., Hungerbühler, K. & Nowack, B. Comprehensive probabilistic modelling of environmental emissions of engineered nanomaterials. *Environ. Pollut.* **185,** 69–76 (2014).
191. Gottschalk, F. & Nowack, B. The release of engineered nanomaterials to the environment. *J. Environ. Monit.* **13,** 1145 (2011).
192. Keller, A. A., Vosti, W., Wang, H. & Lazareva, A. Release of engineered nanomaterials from personal care products throughout their life cycle. *J. Nanoparticle Res.* **16,** 2489 (2014).
193. Hischier, R. *et al.* Life cycle assessment of façade coating systems containing manufactured nanomaterials. *J. Nanoparticle Res.* **17,** 68 (2015).
194. Walser, T., Demou, E., Lang, D. J. & Hellweg, S. Prospective environmental life cycle assessment of nanosilver T-shirts. *Environ. Sci. Technol.* **45,** 4570–8 (2011).
195. Walser, T. *et al.* Persistence of engineered nanoparticles in a municipal solid-waste incineration plant. *Nat. Nanotechnol.* **7,** 520–524 (2012).
196. Praetorius, A. *et al.* The road to nowhere: equilibrium partition coefficients for nanoparticles. *Environ. Sci. Nano* **1,** 317 (2014).
197. Rosenbaum, R. K. *et al.* USEtox—the UNEP-SETAC toxicity model: recommended characterisation factors for human toxicity and freshwater ecotoxicity in life cycle impact assessment. *Int. J. Life Cycle Assess.* **13,** 532–546 (2008).
198. Meesters, J. A. J., Koelmans, A. A., Quik, J. T. K., Hendriks, A. J. & van de Meent, D. Multimedia Modeling of Engineered Nanoparticles with SimpleBox4nano: Model Definition and Evaluation. *Environ. Sci. Technol.* **48,** 5726–5736 (2014).
199. Koivisto, A. J. *et al.* Industrial worker exposure to airborne particles during the packing of pigment and nanoscale titanium dioxide. *Inhal. Toxicol.* **24,** 839–49 (2012).
200. Nazaroff, W. W. Indoor particle dynamics. *Indoor Air, Suppl.* **14,** 175–183 (2004).
201. Hodas, N. *et al.* Indoor inhalation intake fractions of fine particulate matter: Review of influencing factors. *Indoor Air* n/a-n/a (2015). doi:10.1111/ina.12268
202. Braakhuis, H. M., Park, M. V., Gosens, I., De Jong, W. H. & Cassee, F. R. Physicochemical characteristics of nanomaterials that affect pulmonary inflammation. *Part. Fibre Toxicol.* **11,** 18 (2014).
203. Gottschalk, F., Sun, T. & Nowack, B. Environmental concentrations of engineered nanomaterials: Review of modeling and analytical studies. *Environ. Pollut.* **181,** 287–300 (2013).
204. Gottschalk, F., Sonderer, T., Scholz, R. W. & Nowack, B. Modeled Environmental Concentrations of Engineered Nanomaterials (TiO 2 , ZnO, Ag, CNT, Fullerenes) for Different Regions. *Environ. Sci. Technol.* **43,** 9216–9222 (2009).

205. National Research Council. *Risk Assessment in the Federal Government*. (National Academies Press, 1983). doi:10.17226/366
206. Organization for Economic Cooperation and Development. *Co-operation on risk assessment: Prioritization of important issues on risk assessment of manufactured nanomaterials (Final Report)*. *Development* **33,** (2009).
207. European Food Safety Authority. *The Potential Risks Arising from Nanoscience and Nanotechnologies on Food and Feed Safety*. *The EFSA Journal* **958,** (European Food Safety Authority, 2009).
208. Stone, V. *et al.* ITS-NANO - Prioritising nanosafety research to develop a stakeholder driven intelligent testing strategy. *Part. Fibre Toxicol.* **11,** 9 (2014).
209. US EPA. *Decision document: Conditional registration of HeiQ AGS-20 as a materials preservative in textiles*. (2011).
210. National Institute for Occupational Safety and Health. *Current Intelligence Bulletin 65: Occupational Exposure to Carbon Nanotubes and Nanofibers*. (2013).
211. Lin, D., Tian, X., Wu, F. & Xing, B. Fate and transport of engineered nanomaterials in the environment. *J. Environ. Qual.* **39,** 1896–1908 (2010).
212. Hristozov, D. R., Gottardo, S., Critto, A. & Marcomini, A. Risk assessment of engineered nanomaterials: a review of available data and approaches from a regulatory perspective. *Nanotoxicology* **6,** 1–19 (2012).
213. US EPA. EPA Actions to Reduce Risk for New Chemicals under TSCA (SNUR). (2015). at <http://www.epa.gov/reviewing-new-chemicals-under-toxic-substances-control-act-tsca/epa-actions-reduce-risk-new>
214. Barberio, G., Scalbi, S., Buttol, P., Masoni, P. & Righi, S. Combining life cycle assessment and qualitative risk assessment: the case study of alumina nanofluid production. *Sci. Total Environ.* **496,** 122–31 (2014).
215. Schulte, P. a., Murashov, V., Zumwalde, R., Kuempel, E. D. & Geraci, C. L. Occupational exposure limits for nanomaterials: State of the art. *J. Nanoparticle Res.* **12,** 1971–1987 (2010).
216. Ling, M.-P. *et al.* Risk management strategy to increase the safety of workers in the nanomaterials industry. *J. Hazard. Mater.* **229–230,** 83–93 (2012).
217. Liao, C. M., Chiang, Y. H. & Chio, C. P. Model-based assessment for human inhalation exposure risk to airborne nano/fine titanium dioxide particles. *Sci. Total Environ.* **407,** 165–177 (2008).
218. Brouwer, D. H. Control banding approaches for nanomaterials. *Ann. Occup. Hyg.* **56,** 506–514 (2012).
219. Hristozov, D. *et al.* Demonstration of a modelling-based multi-criteria decision analysis procedure for prioritisation of occupational risks from manufactured nanomaterials. *Nanotoxicology* 1–14 (2016). doi:10.3109/17435390.2016.1144827
220. Jensen, K. A. *et al.* NanoSafer version 1.1: A web-based precautionary risk assessment and management tool for manufactured nanomaterials using first order modeling. unpublished work (2016).
221. Shatkin, J. A. Informing Environmental Decision Making by Combining Life Cycle Assessment and Risk Analysis. *J. Ind. Ecol.* **12,** 278–281 (2008).
222. Linkov, I. & Seager, T. P. Coupling multi-criteria decision analysis, life-cycle assessment, and risk assessment for emerging threats. *Environ. Sci. Technol.* **45,** 5068–74 (2011).
223. Breedveld, L. Combining LCA and RA for the integrated risk management of emerging technologies. *J. Risk Res.* **16,** 459–468 (2013).
224. Meyer, D. E. & Upadhyayula, V. K. K. The use of life cycle tools to support decision making for sustainable nanotechnologies. *Clean Technol. Environ. Policy* **16,** 757–772 (2014).
225. Beaudrie, C. E. H., Kandlikar, M. & Satterfield, T. From cradle-to-grave at the nanoscale: Gaps in U.S. regulatory oversight along the nanomaterial life cycle. *Environ. Sci. Technol.* **47,** 5524–5534 (2013).
226. Kikuchi, Y. & Hirao, M. Practical Method of Assessing Local and Global Impacts for Risk-Based Decision Making: A Case Study of Metal Degreasing Processes. *Environ. Sci. Technol.* **42,** 4527–4533 (2008).
227. Walser, T., Juraske, R., Demou, E. & Hellweg, S. Indoor exposure to toluene from printed matter matters: complementary views from life cycle assessment and risk assessment. *Environ. Sci. Technol.* **48,** 689–97 (2014).
228. Harder, R., Holmquist, H., Molander, S., Svanström, M. & Peters, G. M. Review of Environmental Assessment Case Studies Blending Elements of Risk Assessment and Life Cycle Assessment. *Environ. Sci. Technol.* **49,** 13083–13093 (2015).
229. Ingwersen, W. W. & Subramanian, V. Guidance for product category rule development: process, outcome, and next steps. *Int. J. Life Cycle Assess.* **19,** 532–537 (2013).
230. Darlington, T. K., Neigh, A. M., Spencer, M. T., Nguyen, O. T. & Oldenburg, S. J. Nanoparticle characteristics affecting environmental fate and transport through soil. *Environ. Toxicol. Chem.* **28,** 1191–1199 (2009).
231. Potting, Jose; Hauschild, M. Spatial Differentiation in Life Cycle Impact Assessment: A decade of method development to increase the environmental realism of LCIA. *Int. J. Life Cycle Assess.* **11,** 11–13 (2006).
232. Sonnemann, G. & Schuhmacher, M. *Integrated Life-Cycle and Risk Assessment for Industrial Processes*. (CRC, 2004).
233. Hinds, W. C. *Aerosol Technology: Properties, Behavior, and Measurement of Airborne Particles*. (Wiley-Interscience, 1999).
234. Rosenbaum, R. K. *et al.* Indoor air pollutant exposure for life cycle assessment: regional health impact factors for households. *Environ. Sci. Technol.* **49,** 12823–12831 (2015).
235. Hellweg, S. *et al.* Integrating Human Indoor Air Pollutant Exposure within Life Cycle Impact Assessment. *Environ. Sci. Technol.* **43,** 1670–1679 (2009).
236. Nigge, K.-M. *Life Cycle Assessment of Natural Gas Vehicles - Development and Application of Site-Dependent Impact Indicators*. (Springer Berlin Heidelberg, 2000). doi:10.1007/978-3-642-59775-6
237. Jolliet, O., Ernstoff, A. S., Csiszar, S. A. & Fantke, P. Defining Product Intake Fraction to Quantify and Compare Exposure to Consumer Products. *Environ. Sci. Technol.* **49,** 8924–8931 (2015).
238. Fantke, P. & Jolliet, O. Life cycle human health impacts of 875 pesticides. *Int. J. Life Cycle Assess.* **21,** 722–733 (2016).
239. Kuempel, E. D., Geraci, C. L. & Schulte, P. A. Risk assessment and risk management of nanomaterials in the workplace: translating research to practice. *Ann. Occup. Hyg.* **56,** 491–505 (2012).
240. Schneider, T. & Jensen, K. Relevance of aerosol dynamics and dustiness for personal exposure to manufactured nanoparticles. *J. Nanoparticle Res.* **11,** 1637–1650 (2009).
241. Stebounova, L. V., Morgan, H., Grassian, V. H. & Brenner, S. Health and safety implications of occupational exposure to engineered

nanomaterials. *Wiley Interdiscip. Rev. Nanomedicine Nanobiotechnology* **4,** 310–321 (2012).
242. Schneider, T. & Jensen, K. A. Relevance of aerosol dynamics and dustiness for personal exposure to manufactured nanoparticles. *J. Nanoparticle Res.* **11,** 1637–1650 (2009).
243. Bouillard, J. X. & Vignes, A. Nano-Evaluris: an inhalation and explosion risk evaluation method for nanoparticle use. Part I: description of the methodology. *J. Nanoparticle Res.* **16,** 2149 (2014).
244. Buzea, C., Pacheco, I. I. & Robbie, K. Nanomaterials and nanoparticles: sources and toxicity. *Biointerphases* **2,** 17–71 (2007).
245. Nowack, B. *et al.* Analysis of the occupational, consumer and environmental exposure to engineered nanomaterials used in 10 technology sectors. *Nanotoxicology* **7,** 1–5 (2012).
246. Brouwer, D. H. *et al.* Workplace air measurements and likelihood of exposure to manufactured nano-objects, agglomerates, and aggregates. *J. Nanoparticle Res.* **15,** 2090 (2013).
247. Biswas, P. & Wu, C.-Y. Nanoparticles and the Environment. *J. Air Waste Manage. Assoc.* **55,** 708–746 (2005).
248. Brouwer, D. H. *et al.* Workplace air measurements and likelihood of exposure to manufactured nano-objects, agglomerates, and aggregates. *J. Nanoparticle Res.* **15,** 2090 (2013).
249. Kimberyly-Clark. Alarming Number of Workers Fail to Wear Required Protective Equipment (NYSE:KMB). (2012). at <http://investor.kimberly-clark.com/releasedetail.cfm?ReleaseID=712258>
250. Espinosa, N., Zimmermann, Y.-S., dos Reis Benatto, G. A., Lenz, M. & Krebs, F. C. Outdoor fate and environmental impact of polymer solar cells through leaching and emission to rainwater and soil. *Energy Environ. Sci.* **9,** 1–5 (2016).
251. Hummelen, J. C. *et al.* Preparation and Characterization of Fulleroid and Methanofullerene Derivatives. *J. Org. Chem.* **60,** 532–538 (1995).
252. Johnston, H. J., Hutchison, G. R., Christensen, F. M., Aschberger, K. & Stone, V. The Biological Mechanisms and Physicochemical Characteristics Responsible for Driving Fullerene Toxicity. *Toxicol. Sci.* **114,** 162–182 (2010).
253. Tykhomyrov, A. A., Nedzvetsky, V. S., Klochkov, V. K. & Andrievsky, G. V. Nanostructures of hydrated C60 fullerene (C60HyFn) protect rat brain against alcohol impact and attenuate behavioral impairments of alcoholized animals. *Toxicology* **246,** 158–165 (2008).
254. Lin, A. M.-Y. *et al.* Local carboxyfullerene protects cortical infarction in rat brain. *Neurosci. Res.* **43,** 317–321 (2002).
255. Injac, R. *et al.* Protective effects of fullerenol C60(OH)24 against doxorubicin-induced cardiotoxicity and hepatotoxicity in rats with colorectal cancer. *Biomaterials* **30,** 1184–1196 (2009).
256. Gharbi, N. *et al.* [60]Fullerene is a Powerful Antioxidant in Vivo with No Acute or Subacute Toxicity. *Nano Lett.* **5,** 2578–2585 (2005).
257. BOGDANOVIĆ, V. *et al.* Fullerenol C60(OH)24 Effects on Antioxidative Enzymes Activity in Irradiated Human Erythroleukemia Cell Line. *J. Radiat. Res.* **49,** 321–327 (2008).
258. Huang, S.-T., Liao, J.-S., Fang, H.-W. & Lin, C.-M. Synthesis and anti-inflammation evaluation of new C60 fulleropyrrolidines bearing biologically active xanthine. *Bioorg. Med. Chem. Lett.* **18,** 99–103 (2008).
259. Roursgaard, M. *et al.* Polyhydroxylated C 60 Fullerene (Fullerenol) Attenuates Neutrophilic Lung Inflammation in Mice. *Basic Clin. Pharmacol. Toxicol.* **103,** 386–388 (2008).
260. Liu, Y. *et al.* Immunostimulatory properties and enhanced TNF- α mediated cellular immunity for tumor therapy by C 60 (OH) 20 nanoparticles. *Nanotechnology* **20,** 415102 (2009).
261. Fujita, K. *et al.* Gene expression profiles in rat lung after inhalation exposure to C60 fullerene particles. *Toxicology* **258,** 47–55 (2009).
262. Baker, G. L. *et al.* Inhalation Toxicity and Lung Toxicokinetics of C60 Fullerene Nanoparticles and Microparticles. *Toxicol. Sci.* **101,** 122–131 (2007).
263. Morimoto, Y. *et al.* Inflammogenic effect of well-characterized fullerenes in inhalation and intratracheal instillation studies. *Part. Fibre Toxicol.* **7,** 4 (2010).
264. Sayes, C. M. *et al.* Nano-C60 cytotoxicity is due to lipid peroxidation. *Biomaterials* **26,** 7587–7595 (2005).
265. Kamat, J. Reactive oxygen species mediated membrane damage induced by fullerene derivatives and its possible biological implications. *Toxicology* **155,** 55–61 (2000).
266. Huczko, A., Lange, H. & Calko, E. Short Communication: Fullerenes: Experimental Evidence for a Null Risk of Skin Irritation and Allergy. *Fuller. Sci. Technol.* **7,** 935–939 (1999).
267. Aoshima, H., Saitoh, Y., Ito, S., Yamana, S. & Miwa, N. Safety evaluation of highly purified fullerenes (HPFs): based on screening of eye and skin damage. *J. Toxicol. Sci.* **34,** 555–562 (2009).
268. Yamago, S. *et al.* In vivo biological behavior of a water-miscible fullerene: 14C labeling, absorption, distribution, excretion and acute toxicity. *Chem. Biol.* **2,** 385–389 (1995).
269. Mori, T. *et al.* Preclinical studies on safety of fullerene upon acute oral administration and evaluation for no mutagenesis. *Toxicology* **225,** 48–54 (2006).
270. Chen, H. H. C. *et al.* Acute and Subacute Toxicity Study of Water-Soluble Polyalkylsulfonated C60 in Rats. *Toxicol. Pathol.* **26,** 143–151 (1998).
271. Global and China Titanium Dioxide Industry Report, 2014-2017. (2015). at <http://www.prnewswire.com/news-releases/global-and-china-titanium-dioxide-industry-report-2014-2017-300077141.html>
272. Hext, P. M., Tomenson, J. A. & Thompson, P. Titanium dioxide: inhalation toxicology and epidemiology. *Ann. Occup. Hyg.* **49,** 461–72 (2005).
273. Varner, K. E., Rindfusz, K., Gaglione, A. & Viveiros, E. *Nano Titanium Dioxide Environmental Matters: State of the Science Literature Review*. (2010). at <http://cfpub.epa.gov/si/si_public_file_download.cfm?p_download_id=498019>
274. U.S. Geological Survey. *2012 Minerals Yearbook - Titanium*. (2012). at <http://minerals.usgs.gov/minerals/pubs/commodity/titanium/myb1-2012-titan.pdf>
275. Agrios, A. G. & Pichat, P. State of the art and perspectives on materials and applications of photocatalysis over TiO2. *J. Appl. Electrochem.* **35,** 655–663 (2005).
276. Chen, X. & Mao, S. S. Titanium dioxide nanomaterials: Synthesis, properties, modifications and applications. *Chem. Rev.* **107,** 2891–2959 (2007).
277. Shakeel, M. *et al.* Toxicity of Nano-Titanium Dioxide (TiO2-NP) Through Various Routes of Exposure: a Review. *Biol. Trace Elem. Res.*

172, 1–36 (2016).
278. Noël, A. & Truchon, G. Inhaled Titanium Dioxide Nanoparticles: A Review of Their Pulmonary Responses with Particular Focus on the Agglomeration State. *Nano Life* **5,** 1450008 (2015).
279. Czajka, M. *et al.* Toxicity of titanium dioxide nanoparticles in central nervous system. *Toxicol. Vitr.* **29,** 1042–1052 (2015).
280. Zhang, X., Li, W. & Yang, Z. Toxicology of nanosized titanium dioxide: an update. *Arch. Toxicol.* **89,** 2207–2217 (2015).
281. Shi, H., Magaye, R., Castranova, V. & Zhao, J. Titanium dioxide nanoparticles: a review of current toxicological data. *Part. Fibre Toxicol.* **10,** 15 (2013).
282. Iavicoli, I., Leso, V. & Bergamaschi, A. Toxicological Effects of Titanium Dioxide Nanoparticles: A Review of In Vivo Studies. *J. Nanomater.* **2012,** 1–36 (2012).
283. Bermudez, E. *et al.* Pulmonary responses of mice, rats, and hamsters to subchronic inhalation of ultrafine titanium dioxide particles. *Toxicol. Sci.* **77,** 347–357 (2004).
284. Heinrich, U. *et al.* Chronic Inhalation Exposure of Wistar Rats and two Different Strains of Mice to Diesel Engine Exhaust, Carbon Black, and Titanium Dioxide. *Inhal. Toxicol.* **7,** 533 (1995).
285. Warheit, D. Subchronic inhalation of high concentrations of low toxicity, low solubility participates produces sustained pulmonary inflammation and cellular proliferation. *Toxicol. Lett.* **88,** 249–253 (1996).
286. Chang, X., Zhang, Y., Tang, M. & Wang, B. Health effects of exposure to nano-TiO2: a meta-analysis of experimental studies. *Nanoscale Res. Lett.* **8,** 51 (2013).
287. Newman, M. D., Stotland, M. & Ellis, J. I. The safety of nanosized particles in titanium dioxide– and zinc oxide–based sunscreens. *J. Am. Acad. Dermatol.* **61,** 685–692 (2009).
288. Sadrieh, N. *et al.* Lack of Significant Dermal Penetration of Titanium Dioxide from Sunscreen Formulations Containing Nano- and Submicron-Size TiO2 Particles. *Toxicol. Sci.* **115,** 156–166 (2010).
289. Filipe, P. *et al.* Stratum Corneum Is an Effective Barrier to TiO2 and ZnO Nanoparticle Percutaneous Absorption. *Skin Pharmacol. Physiol.* **22,** 266–275 (2009).
290. Monteiro-Riviere, N. A. *et al.* Safety Evaluation of Sunscreen Formulations Containing Titanium Dioxide and Zinc Oxide Nanoparticles in UVB Sunburned Skin: An In Vitro and In Vivo Study. *Toxicol. Sci.* **123,** 264–280 (2011).
291. Furukawa, F. *et al.* Lack of skin carcinogenicity of topically applied titanium dioxide nanoparticles in the mouse. *Food Chem. Toxicol.* **49,** 744–749 (2011).
292. Wu, J. *et al.* Toxicity and penetration of TiO2 nanoparticles in hairless mice and porcine skin after subchronic dermal exposure. *Toxicol. Lett.* **191,** 1–8 (2009).
293. Senzui, M. *et al.* Study on penetration of titanium dioxide (TiO2) nanoparticles into intact and damaged skin in vitro. *J. Toxicol. Sci.* **35,** 107–113 (2010).
294. Bennat & Müller-Goymann. Skin penetration and stabilization of formulations containing microfine titanium dioxide as physical UV filter. *Int. J. Cosmet. Sci.* **22,** 271–283 (2000).
295. WARHEIT, D. *et al.* Development of a base set of toxicity tests using ultrafine TiO2 particles as a component of nanoparticle risk management. *Toxicol. Lett.* **171,** 99–110 (2007).
296. Unnithan, J., Rehman, M. U., Ahmad, F. J. & Samim, M. Aqueous Synthesis and Concentration-Dependent Dermal Toxicity of TiO2 Nanoparticles in Wistar Rats. *Biol. Trace Elem. Res.* **143,** 1682–1694 (2011).
297. WANG, J. *et al.* Acute toxicity and biodistribution of different sized titanium dioxide particles in mice after oral administration. *Toxicol. Lett.* **168,** 176–185 (2007).
298. Ze, Y. *et al.* TiO2 Nanoparticles Induced Hippocampal Neuroinflammation in Mice. *PLoS One* **9,** e92230 (2014).
299. Shrivastava, R., Raza, S., Yadav, A., Kushwaha, P. & Flora, S. J. S. Effects of sub-acute exposure to TiO 2 , ZnO and Al 2 O 3 nanoparticles on oxidative stress and histological changes in mouse liver and brain. *Drug Chem. Toxicol.* **37,** 336–347 (2014).
300. A. Yakubu, M. Determination of lindane and its metabolites by HPLC-UV-Vis and MALDI-TOF. *J. Clin. Toxicol.* **1,** (2012).
301. European Chemicals Agency. *Chapter R.8: Characterisation of dose[concentration]-response for human health*. *Guidance on information requirements and chemical safety assessment* (2012).
302. Slob, W., Bakker, M. I., Biesebeek, J. D. Te & Bokkers, B. G. H. Exploring the uncertainties in cancer risk assessment using the integrated probabilistic risk assessment (IPRA) approach. *Risk Anal.* **34,** 1401–22 (2014).
303. Limpert, E., Stahel, W. a. & Abbt, M. Log-normal Distributions across the Sciences: Keys and Clues. *Bioscience* **51,** 341 (2001).
304. Slob, W. & Pieters, M. N. A probabilistic approach for deriving acceptable human intake limits and human health risks from toxicological studies: general framework. *Risk Anal.* **18,** 787–98 (1998).
305. Pietroiusti, A. & Magrini, A. Engineered nanoparticles at the workplace: current knowledge about workers' risk. *Occup. Med. (Chic. Ill).* **64,** 319–330 (2014).
306. Brouwer, D. H. *et al.* Occupational dermal exposure to nanoparticles and nano-enabled products: Part 2, exploration of exposure processes and methods of assessment. *Int. J. Hyg. Environ. Health* **219,** 503–512 (2016).
307. Liguori, B., Jensen, A. C. Ø., Hansen, S. F., Baun, A. & Jensen, K. A. Sensitivity Analysis of the exposure assessment module in NanoSafer version 1.1: Ranking of Determining Parameters and Uncertainty. unpublished work (2016).
308. European Committee for Standardization (CEN). *EN 15051 Workplace exposure. Measurement of the dustiness of bulk materials. Requirements and choice of test methods.* (2013).
309. Ramachandran, G. *Occupational Exposure Assessment for Air Contaminants*. (CRC Press, 2005).
310. Crump, K. S. A New Method for Determining Allowable Daily Intakes. *Fondam. Appl. Toxicol.* **871,** 854–871 (1984).
311. Nicas, M. Estimating Exposure Intensity in an Imperfectly Mixed Room. *Am. Ind. Hyg. Assoc. J.* **57,** 542–550 (1996).
312. Koivisto, A. J. *et al.* Range-finding risk assessment of inhalation exposure to nanodiamonds in a laboratory environment. *Int. J. Environ. Res. Public Health* **11,** 5382–5402 (2014).
313. Schneider, T. *et al.* Conceptual model for assessment of inhalation exposure to manufactured nanoparticles. *J. Expo. Sci. Environ. Epidemiol.* **21,** 450–63 (2011).
314. Organization for Economic Cooperation and Development. *Inhalation toxicity testing: expert meeting on potential revisions to OECD*

test guidelines and guidance document. (2012).
315. Levin, M. *et al.* Influence of relative humidity and physical load during storage on dustiness of inorganic nanomaterials: implications for testing and risk assessment. *J. Nanoparticle Res.* **17,** 1–13 (2015).
316. Hinds, W. C. *Aerosol technology: Properties, behavior, and measurement of airborne particles*. (Wiley-Interscience, 1999).
317. Fransman, W. *et al.* Advanced reach tool (ART): Development of the mechanistic model. *Ann. Occup. Hyg.* **55,** 957–979 (2011).
318. Koivisto, A. J. *et al.* Workplace performance of a loose-fitting powered air purifying respirator during nanoparticle synthesis. *J. Nanoparticle Res.* **17,** 177 (2015).
319. Oberdorster, G., Ferin, J. & Lehnert, B. E. Correlation between particle size, in vivo particle persistence, and lung injury. in *Environmental Health Perspectives* **102,** 173–179 (1994).
320. Auffan, M. *et al.* Towards a definition of inorganic nanoparticles from an environmental, health and safety perspective. *Nat. Nanotechnol.* **4,** 634–41 (2009).
321. Donaldson, K. & Poland, C. A. Nanotoxicity: challenging the myth of nano-specific toxicity. *Curr. Opin. Biotechnol.* **24,** 724–734 (2013).
322. Simko, M., Nosske, D. & Kreyling, W. G. Metrics, dose, and dose concept: The need for a proper dose concept in the risk assessment of nanoparticles. *Int. J. Environ. Res. Public Health* **11,** 4026–4048 (2014).
323. Koivisto, A. J. *et al.* Concept To Estimate Regional Inhalation Dose of Industrially Synthesized Nanoparticles. *ACS Nano* **6,** 1195–1203 (2012).
324. Levin, M. *et al.* Limitations in the Use of Unipolar Charging for Electrical Mobility Sizing Instruments: A Study of the Fast Mobility Particle Sizer. *Aerosol Sci. Technol.* **49,** 556–565 (2015).
325. Levin, M. *et al.* Can We Trust Real Time Measurements of Lung Deposited Surface Area Concentrations in Dust from Powder Nanomaterials? *Aerosol Air Qual. Res.* **16,** 1105–1117 (2016).
326. Hellweg, S., Demou, E., Scheringer, M., McKone, T. E. & Hungerbühler, K. Confronting Workplace Exposure to Chemicals with LCA: Examples of Trichloroethylene and Perchloroethylene in Metal Degreasing and Dry Cleaning. *Environ. Sci. Technol.* **39,** 7741–7748 (2005).
327. Meijer, A., Huijbregts, M. & Reijnders, L. Human Health Damages due to Indoor Sources of Organic Compounds and Radioactivity in Life Cycle Impact Assessment of Dwellings - Part 1: Characterisation Factors (8 pp). *Int. J. Life Cycle Assess.* **10,** 309–316 (2005).
328. Kikuchi, E., Kikuchi, Y. & Hirao, M. Monitoring and Analysis of Solvent Emissions from Metal Cleaning Processes for Practical Process Improvement. *Ann. Occup. Hyg.* **56,** 829–842 (2012).
329. Piccinno, F., Gottschalk, F., Seeger, S. & Nowack, B. Industrial production quantities and uses of ten engineered nanomaterials in Europe and the world. *J. Nanoparticle Res.* **14,** 1–11 (2012).
330. Wenger, Y., Li, D. & Jolliet, O. Indoor intake fraction considering surface sorption of air organic compounds for life cycle assessment. *Int. J. Life Cycle Assess.* **17,** 919–931 (2012).
331. Demou, E., Hellweg, S., Wilson, M. P., Hammond, S. K. & McKone, T. E. Evaluating Indoor Exposure Modeling Alternatives for LCA: A Case Study in the Vehicle Repair Industry. *Environ. Sci. Technol.* **43,** 5804–5810 (2009).
332. Jr., E. J. F., Pandian, M. D., Nelson, D. R. & Behar, J. V. Modeling Indoor Air Concentrations Near Emission Sources in Imperfectly Mixed Rooms. *J. Air Waste Manage. Assoc.* **46,** 861–868 (1996).
333. Phalen, R. F. & Phalen, R. N. *Introduction to Air Pollution Science*. (Jones and Bartlett Learning, 2011).
334. BALDWIN, P. E. J. & MAYNARD, A. D. A Survey of Wind Speeds in Indoor Workplaces. *Ann. Occup. Hyg.* **42,** 303–313 (1998).
335. Clift, R., Grace, J. R. & Weber, M. E. *Bubbles, Drops, and Particles*. (Academic Press, 1978).
336. Kleinstreuer, C., Zhang, Z. & Li, Z. Modeling airflow and particle transport/deposition in pulmonary airways. *Respir. Physiol. Neurobiol.* **163,** 128–138 (2008).
337. Li, D. *et al.* In vivo biodistribution and physiologically based pharmacokinetic modeling of inhaled fresh and aged cerium oxide nanoparticles in rats. *Part. Fibre Toxicol.* **13,** 45 (2015).
338. Carlander, U., Li, D., Jolliet, O., Emond, C. & Johanson, G. Toward a general physiologically-based pharmacokinetic model for intravenously injected nanoparticles. *Int. J. Nanomedicine* 625 (2016). doi:10.2147/IJN.S94370
339. Molina, D. K. & DiMaio, V. J. M. Normal Organ Weights in Men. *Am. J. Forensic Med. Pathol.* **33,** 368–372 (2012).
340. Molina, D. K. & DiMaio, V. J. M. Normal Organ Weights in Men. *Am. J. Forensic Med. Pathol.* **33,** 362–367 (2012).
341. Fox, S. *Human Physiology*. (McGraw-Hill, 2010).
342. Salmasi, A.-M. & Iskandrian, A. S. *Cardiac Output and Regional Flow in Health and Disease*. **138,** (Springer Netherlands, 1993).
343. Brown, R. P., Delp, M. D., Lindstedt, S. L., Rhomberg, L. R. & Beliles, R. P. Physiological Parameter Values for Physiologically Based Pharmacokinetic Models. *Toxicol. Ind. Health* **13,** 407–484 (1997).
344. Kuempel, E. D., Sweeney, L. M., Morris, J. B. & Jarabek, A. M. Advances in Inhalation Dosimetry Models and Methods for Occupational Risk Assessment and Exposure Limit Derivation. *J. Occup. Environ. Hyg.* **12,** S18–S40 (2015).
345. EPA., U. S. *Exposure Factors Handbook*. (2011).
346. Bennett, D. H. *et al.* Peer Reviewed: Defining Intake Fraction. *Environ. Sci. Technol.* **36,** 206A–211A (2002).
347. Huijbregts, M. A. J., Rombouts, L. J. A., Ragas, A. M. J. & van de Meent, D. Human-Toxicological Effect and Damage Factors of Carcinogenic and Noncarcinogenic Chemicals for Life Cycle Impact Assessment. *Integr. Environ. Assess. Manag.* **1,** 181 (2005).
348. Levine, K. E., Fernando, R. A., Lang, M., Essader, A. & Wong, B. A. Development and Validation of a High- Throughput Method for the Determination of Titanium Dioxide in Rodent Lung and Lung-Associated Lymph Node Tissues. *Anal. Lett.* **36,** 563–576 (2003).
349. Crump, K. S. Calculation of Benchmark Doses from Continuous Data. *Risk Anal.* **15,** 79–89 (1995).
350. Jager, T., Vermeire, T. G., Rikken, M. G. J. & Van der Poel, P. Opportunities for a probabilistic risk assessment of chemicals in the European Union. *Chemosphere* **43,** 257–264 (2001).
351. Davis, J. A., Gift, J. S. & Zhao, Q. J. Introduction to benchmark dose methods and U.S. EPA's benchmark dose software (BMDS) version 2.1.1. *Toxicol. Appl. Pharmacol.* **254,** 181–191 (2011).
352. Barlow, S. *et al.* Guidance of the scientific committee on a request from EFSA on the use of the benchmark dose approach in risk assessment. *EFSA J.* **1150,** 1–72 (2009).
353. Allen, B. C., Kavlock, R. J., Kimmel, C. a. & Faustman, E. M. Dose-response assessment for developmental toxicity: II. Comparison of

generic benchmark dose estimates with no observed adverse effect levels. *Fundam. Appl. Toxicol.* **23,** 487–495 (1994).
354. *Risk Assessment of Chemicals: An Introduction*. (Springer Netherlands, 2007). doi:10.1007/978-1-4020-6102-8
355. Muhle, H. *et al.* Pulmonary response to toner upon chronic inhalation exposure in rats. *Fundam. Appl. Toxicol.* **17,** 280–299 (1991).
356. Lee, K. P., Trochimowicz, H. J. & Reinhardt, C. F. Pulmonary Response of Rats Exposed to Titanium by Inhalation for Two Years Dioxide (Ti02). *Toxicol. Appl. Pharmacol.* **79,** 179–192 (1985).
357. LEE, K. P., TROCHIMOWICZ, H. J. & REINHARDT, C. F. PULMONARY RESPONSE OF RATS EXPOSED TO TITANIUM-DIOXIDE (TIO2) BY INHALATION FOR 2 YEARS. *Toxicol. Appl. Pharmacol.* **79,** 179–192 (1985).
358. Kuempel, E. D., Tran, C. L., Castranova, V. & Bailer, a J. Lung dosimetry and risk assessment of nanoparticles: evaluating and extending current models in rats and humans. *Inhal. Toxicol.* **18,** 717–24 (2006).
359. Demou, E., Peter, P. & Hellweg, S. Exposure to Manufactured Nanostructured Particles in an Industrial Pilot Plant. *Ann. Occup. Hyg.* **52,** 695–706 (2008).
360. Sundell, J., Levin, H. & Novosel, D. *Ventilation rates and health: report of an interdisciplinary review of the scientific literature*. (2006).
361. Oberdorster, G., Ferin, J. & Lehnert, B. E. Correlation between particle size, in vivo particle persistence, and lung injury. *Environ. Health Perspect.* **102,** 173–179 (1994).
362. Borm, P. J. A. *et al. The potential risks of nanomaterials: a review carried out for ECETOC. Particle and fibre toxicology* **3,** (2006).
363. Geiser, M. *et al.* Ultrafine Particles Cross Cellular Membranes by Nonphagocytic Mechanisms in Lungs and in Cultured Cells. *Environ. Health Perspect.* **113,** 1555–1560 (2005).
364. Fertsch-Gapp, S., Semmler-Behnke, M., Wenk, A. & Kreyling, W. G. Binding of polystyrene and carbon black nanoparticles to blood serum proteins. *Inhal. Toxicol.* **23,** 468–475 (2011).
365. Keller, A. A. & Lazareva, A. Predicted releases of engineered nanomaterials: From global to regional to local. *Environ. Sci. Technol. Lett.* **1,** 65–70 (2013).
366. Fonseca, A. S. *et al.* Characterization of exposure to carbon nanotubes in an industrial setting. *Ann. Occup. Hyg.* **59,** 586–599 (2015).
367. Zimmermann, Y.-S., Schäffer, A., Corvini, P. F.-X. & Lenz, M. Thin-Film Photovoltaic Cells: Long-Term Metal(loid) Leaching at Their End-of-Life. *Environ. Sci. Technol.* **47,** 13151–13159 (2013).
368. Brun, N. R., Wehrli, B. & Fent, K. Ecotoxicological assessment of solar cell leachates: Copper indium gallium selenide (CIGS) cells show higher activity than organic photovoltaic (OPV) cells. *Sci. Total Environ.* **543,** 703–714 (2016).
369. Hudson, K. L., Misra, C., Perrotta, J., Wefers, K. & Williams, F. in *Ulmann's Encyclopedia of Industrial Chemistry* (Wiley-VCH, 2007).
370. Zapp, K. H. *et al.* in *Ullmann's Encyclopedia of Industrial Chemistry* (Wiley-VCH, 2007).
371. Geisler, G., Hofstetter, T. B. & Hungerbühler, K. Production of fine and speciality chemicals: procedure for the estimation of LCIs. *Int. J. Life Cycle Assess.* **9,** 101–113
372. Koponen, I. K., Jensen, K. A. & Schneider, T. Comparison of dust released from sanding conventional and nanoparticle-doped wall and wood coatings. *J. Expo. Sci. Environ. Epidemiol.* **21,** 408–418 (2011).
373. Vorbau, M., Hillemann, L. & Stintz, M. Method for the characterization of the abrasion induced nanoparticle release into air from surface coatings. *J. Aerosol. Sci.* **40,** 209–217 (2009).
374. Aitken, R. A. *et al. Specific Advice on Exposure Assessment and Hazard/Risk Characterisation for Nanomaterials under REACH (RIP-oN 3)*. (2011). at <http://ec.europa.eu/environment/chemicals/nanotech/pdf/report_ripon3.pdf>
375. Cherrie, J. W. The Effect of Room Size and General Ventilation on the Relationship Between Near and Far-Field Concentrations. *Appl. Occup. Environ. Hyg.* **14,** 539–546 (1999).

Appendices

Appendix: Chapter 3

Table A3-1 displays the impact assessment results for each of the OPV embodiments assessed. The *default* solar cell results in the highest impacts, except for human toxicity which was highest for the solar cell using dichlorobenzene during PCBM production instead of toluene.

Table A3-1 Absolute life-cycle impacts for each organic photovoltaic cell considered in this study. Values are reported with their respective reference unit.

Impact category	Reference unit	Default	FTOinkjet	PCBMdcb
Agricultural land occupation	m^2a	8.89E-04	5.89E-04	6.80E-04
Climate change	kg CO_2-Eq	5.22E-02	3.45E-02	3.83E-02
Fossil fuel depletion	kg Oil-Eq	2.09E-02	1.61E-02	1.68E-02
Freshwater ecotoxicity	kg 1,4-DCB-Eq	1.16E-06	1.02E-06	1.06E-06
Freshwater eutrophication	kg P-Eq	2.89E-05	1.39E-05	1.76E-05
Human toxicity	kg 1,4-DCB-Eq	2.08E-03	1.74E-03	2.13E-03
Ionizing radiation	kg U_{235}-Eq	2.12E-02	7.72E-03	1.08E-02
Marine ecotoxicity	kg 1,4-DCB-Eq	3.30E-05	2.84E-05	3.06E-05
Marine eutrophication	kg N-Eq	1.05E-05	6.06E-06	7.19E-06
Mineral resource depletion	kg Fe-Eq	3.52E-02	3.51E-02	3.52E-02
Natural land transformation	m^2	9.64E-06	7.49E-06	8.04E-06
Ozone depletion	kg CFC_{11}-Eq	2.80E-09	2.00E-09	2.20E-09
Particulate matter formation	kg PM_{10}-Eq	6.84E-05	4.59E-05	5.14E-05
Photochemical oxidant formation	kg NMVOC	1.27E-04	9.04E-05	9.87E-05
Terrestrial acidification	kg SO_2-Eq	1.94E-04	1.24E-04	1.41E-04
Terrestrial ecotoxicity	kg 1,4-DCB-Eq	5.48E-06	4.99E-06	5.19E-06
Urban land occupation	m^2a	2.00E-04	1.40E-04	1.59E-04
Water depletion	m^3	2.25E-01	8.89E-02	1.21E-01
Cumulative Energy Demand	MJ-Eq	2.60E+00	8.37E-01	2.30E+00

The foreground inventory data for the default organic photovoltaic cell and all components used across its life-cycle are shown in the following tables. Any background inventory data (i.e. a unit-process from Ecoinvent) are not included.

4-Benzobutyric acid, at plant	Reference Flow Amount: 1kg		Adapted from Anctil et al.[57] using the precursors glutaric acid, benzene, steam and aluminum chloride	
Inventory Item	**Amount**	**Units**	**Other**	**Inventory Flow Source**
Aluminum chloride, at plant	0.83	kg	Original estimate seemed low and was increased to require 6.25 moles	This study
Benzene, at pant, RER	3.15	kg		Ecoinvent
Electricity, medium voltage, production RER, at grid	0.70	MJ		Ecoinvent
Heat, heavy fuel oil, at industrial furnace 1MW, RER	35.03	MJ	Energy for maleic acid recovery and distillation recycling	Ecoinvent
Maleic anhydride, at plant	0.70	kg	Substitute for glutaric acid	Ecoinvent
Steam, for chemical process, at plant, RER	1.18	kg		Ecoinvent
Transportation, freight, rail, RER	0.69	t*km	Based on a distance traveled of 600km by train.	Ecoinvent

Transport, lorry 16-32t, EURO3, RER	0.11	t*km	Based on a distance traveled of 100km by truck.	Ecoinvent
Disposal, hazardous waste, 25% water, to hazardous waste incineration, CH	0.49	kg	Aluminum hydroxide waste reported by Anctil et al.	Ecoinvent

Aluminum chloride, at plant	Reference Flow Amount: 1kg		Estimated from Ullmans Encyclopedia of Industrial Chemistry 2007 for the chlorination of aluminum oxide.[369]	
Inventory Item	**Amount**	**Units**	**Other**	**Inventory Flow Source**
Aluminum, production mix, at plant, RER	0.20	kg		Ecoinvent
Chlorine, liquid, production mix, at plant, RER	0.40	kg		Ecoinvent
Transportation, freight, rail, RER	0.36	t*km	Based on a distance traveled of 600km by train.	Ecoinvent
Transport, lorry 16-32t, EURO3, RER	0.06	t*km	Based on a distance traveled of 100km by truck.	Ecoinvent
Heat, waste	2.25	MJ	This chemical reaction is highly exothermic, producing around 300 kJ/moll of aluminum chloride produced	Ecoinvent

Ammonium fluoride, at plant	Reference Flow Amount: 1kg		Estimated from Ullmans Encyclopedia of Industrial Chemistry 2007 using the feedstocks ammonia and anhydrous fluoride.[370]	
Inventory Item	**Amount**	**Units**	**Other**	**Inventory Flow Source**
Ammonia, liquid, at regional storehouse, RER	0.46	kg		Ecoinvent
Heat, heavy fuel oil, at industrial furnace 1MW, RER	0.57	MJ		Ecoinvent
Hydrogen fluoride, at plant, GLO	0.54	kg		Ecoinvent
Transportation, freight, rail, RER	0.60	t*km	Based on a distance traveled of 600km by train.	Ecoinvent
Transport, lorry 16-32t, EURO3, RER	0.10	t*km	Based on a distance traveled of 100km by truck.	Ecoinvent

Annealing, process	Reference Flow Amount: 1items (i.e. per m^2)		Estimated from Espinosa et al. for their reported measurements of energy consumed during drying the electron-transport layer, active layer, and hole-transporter layer.[38]	
Inventory Item	**Amount**	**Units**	**Other**	**Inventory Flow Source**
Electricity, medium voltage, production RER, at grid	5.07	MJ		Ecoinvent

Bromine, at plant	Reference Flow Amount: 1kg		Adapted from Ecoinvent 3 description but using Ecoinvent 2 data.	
Inventory Item	**Amount**	**Units**	**Other**	**Inventory Flow Source**
Bromine	1.00	kg		Ecoinvent

Chemical plant, organics, RER	4.0E-10	number of items		Ecoinvent
Chlorine, liquid, production mix, at plant, RER	0.60	kg		Ecoinvent
Steam, for chemical processes, at plant, RER	40.07	kg		Ecoinvent
Sulphuric acid, liquid, at plant, RER	0.057	kg		Ecoinvent
Transport, freight, rail, RER	0.99	t*km	Based on a distance traveled of 600km by train.	Ecoinvent
Transport, lorry 16-32t, EURO3, RER	0.17	t*km	Based on a distance traveled of 100km by truck.	Ecoinvent
Water	0.44	m3		Ecoinvent
Sulfate (Emissions to water)	0.055	kg		Ecoinvent
Water vapor (Emissions to air)	0.44	kg		Ecoinvent

C60-fullerenes, at plant	Reference Flow Amount: 1kg		Production C60 C60-fullerenes adapted from Anctil et al.[57] It is based on their pyrolysis production route using toluene as a feedstock. C60 is coproduced with C70 and allocation is applied according to the masses of each produced.	
Inventory Item	**Amount**	**Units**	**Other**	**Inventory Flow Source**
Electricity, medium voltage, production RER, at grid	802.8	MJ		Ecoinvent
Oxygen, liquid, at plant, RER	109.7	kg		Ecoinvent
Solvent Regeneration	456.4	kg		This study
Toluene, liquid, at plant, RER	137.1	kg		Ecoinvent
Transport, freight, rail, RER	228.3	t*km	Based on a distance traveled of 600km by train.	Ecoinvent
Transport, lorry 16-32t, EURO3, RER	38.13	t*km	Based on a distance traveled of 100km by truck.	Ecoinvent
Xylene, at plant, RER	24	kg	The authors assume this value reported by Anctil et al for xylene is a reduced value which has taken into account the regenerated xylene.	Ecoinvent
Carbon dioxide (Emissions to air)	128.11	kg	Estimated waste production.	Ecoinvent
Disposal, hazardous waste, 25% water, to hazardous waste incineration, CH	8.09	kg	Estimated waste production.	Ecoinvent

C60 regeneration	Reference Flow Amount: 1kg		Adapted from the purification step of C60 in Anctil et al.[57] using 1L xylene per 15g of C60. Assumes an 85% recovery rate. This process is used in the PCBM production step.	
Inventory Item	**Amount**	**Units**	**Other**	**Inventory Flow Source**
Electricity, medium voltage, production RER, at grid	52.02	MJ		Ecoinvent

Solvent regeneration	172.8	kg		Ecoinvent
Transport, freight, rail, RER	38.36	t*km	Based on a distance traveled of 600km by train.	Ecoinvent
Transport, lorry 16-32t, EURO3, RER	6.40	t*km	Based on a distance traveled of 100km by truck.	Ecoinvent
Xylene, at plant, RER	63.94	kg	It is assumed that 95% of the xylene is recovered from the solvent regeneration process.	Ecoinvent

Epoxy silica nanocomposite, at plant	Reference Flow Amount: 1kg		Adapted from the production of silica sol used in Roes et al.[29]	
Inventory Item	**Amount**	**Units**	**Other**	**Inventory Flow Source**
Heat, heavy fuel oil, at industrial furnace 1MW, RER	23	MJ		Ecoinvent
Sodium silicate, furnace process, pieces, at plant, RER	3.9	kg		Ecoinvent
Sulphuric acid, liquid, at plant, RER	0.66	kg		Ecoinvent
Water, ultrapure, at plant, GLO	40	kg		Ecoinvent

FTO solution, at plant	Reference Flow Amount: 1kg		Adapted from Aukkaravittayapun et al.[133] for the production of an FTO solution using the precursors SnCl4 and NH4F mixed with 80:20 EtOH:H2O	
Inventory Item	**Amount**	**Units**	**Other**	**Inventory Flow Source**
Ammonium fluoride, at plant	0.014	kg		This study
Ethanol from ethylene, at plant, RER	0.63	kg		Ecoinvent
Heat, heavy fuel oil, at industrial furnace 1MW, RER	298.19	kg		Ecoinvent
Tin tetrachloride pentahydrate, at plant	0.078	kg		This study
Transport, freight, rail, RER	0.43	t*km	Based on a distance traveled of 600km by train.	Ecoinvent
Transport, lorry 16-32t, EURO3, RER	0.072	t*km	Based on a distance traveled of 100km by truck.	Ecoinvent
Water, deionized, at plant, CH	0.20	kg		Ecoinvent

FTO substrate, sputtered, at plant	Reference Flow Amount: 1m^2			
Inventory Item	**Amount**	**Units**	**Other**	**Inventory Flow Source**
Electricity, medium voltage, production RER, at grid	24	MJ		Ecoinvent
FTO solution, at plant	0.034	L	The amount of FTO solution used is calculated using the Sn and F amounts that correspond to the weights of indium and tin in ITO conducting films.	This study

Plastic film, pet, at plant	0.074	kg		This study
Transport, freight, rail, RER	0.018	t*km	Based on a distance traveled of 600km by train.	Ecoinvent
Transport, lorry 16-32t, EURO3, RER	0.0037	t*km	Based on a distance traveled of 100km by truck.	Ecoinvent

Gravure Printing (Energy)	Reference Flow Amount: 1items (i.e. per m2)		Adapted from Roes et al.[29]	
Inventory Item	**Amount**	**Units**	**Other**	**Inventory Flow Source**
Electricity, medium voltage, production RER, at grid	0.46	MJ		Ecoinvent
Heat, heavy fuel oil, at industrial furnace 1MW, RER	1.08	MJ		Ecoinvent
Toluene (emissions), to air	0.022	kg	Emissions from toluene which is used as a solvent in some of the layer applications	Ecoinvent

Hydrazine, at plant	Reference Flow Amount: 1kg		Adapted from Anctil et al.[57] using the feedstocks sodium chlorate and ammonia.	
Inventory Item	**Amount**	**Units**	**Other**	**Inventory Flow Source**
Ammonia, liquid, at regional storehouse, RER	1.07	kg		Ecoinvent
Electricity, medium voltage, production RER, at grid	684	MJ		Ecoinvent
Sodium chlorate, powder, at plant, RER	2.35	kg		Ecoinvent
Steam, for chemical processes, at plant, RER	1.15	kg		Ecoinvent
Transport, freight, rail, RER	2.05	t*km	Based on a distance traveled of 600km by train.	Ecoinvent
Transport, lorry 16-32t, EURO3, RER	0.34	t*km	Based on a distance traveled of 100km by truck.	Ecoinvent
Treatment, sewage, to wastewater treatment, class 3, CH	0.00017		This is estimated to be 5% of the weight for the reactants sodium chlorate and ammonia. By products from the reaction are assumed to be sodium chloride and water with water determining the waste volume.	Ecoinvent

Lamination flexible solar module, at plant	Reference Flow Amount: 1m^2		Adapted from Roes et al.[29]	
Inventory Item	**Amount**	**Units**	**Other**	**Inventory Flow Source**
Electricity, medium voltage, production RER, at grid	0.047	MJ		Ecoinvent
Epoxy resin, liquid, at plant, RER	0.0093	kg		Ecoinvent
Epoxy silica nanocomposite, at plant	0.00099	kg		This study

Heat, natural gas, at industrial furnace > 100kW, RER	0.039	MJ		Ecoinvent
Polyethylene terephthalate, granulate, amorphous, at plant, RER	0.13	kg		Ecoinvent
Silicon product, at plant, RER	0.00044	kg		Ecoinvent
Transport, freight, rail, RER	0.12	t*km	Based on a distance traveled of 600km by train.	Ecoinvent
Transport, lorry 16-32t, EURO3, RER	0.019	t*km	Based on a distance traveled of 100km by truck.	Ecoinvent
Lithium fluoride, layer, application	Reference Flow Amount: 1items (i.e. per m2)		Adapted from Roes et al.[29]	
Inventory Item	**Amount**	**Units**	**Other**	**Inventory Flow Source**
Electricity, medium voltage, production RER, at grid	0.46	MJ		Ecoinvent
Heat, heavy fuel oil, at industrial furnace 1MW, RER	1.08	MJ		Ecoinvent
Lithium fluoride, at plant, CN	6.0E-8	kg		Ecoinvent
Methyl 4-Benzobutyrate, at plant	Reference Flow Amount: 1kg		Production of methyl 4 benzoybutyrate as outlined in Anctil et al.[57] using the precursors 4-benzobutyric acid and methanol. The authors deviate from Anctil et al. by accounting for methanol regeneration.	
Inventory Item	**Amount**	**Units**	**Other**	**Inventory Flow Source**
4-Benzobutyric acid, at plant	1.01	kg		This study
Electricity, medium voltage, production RER, at grid	0.71	MJ		Ecoinvent
Heat, heavy fuel oil, at industrial furnace 1MW, RER	5.54	MJ	Energy needed for distillation of methanol for regeneration. No other inventory data were expected of this regeneration process.	Ecoinvent
Methanol, at regional storage, CH	8.03	kg		Ecoinvent
Steam, for chemical processes, at plant, RER	1.20	kg		Ecoinvent
Transport, freight, rail, RER	0.54	t*km	Based on a distance traveled of 600km by train.	Ecoinvent
Transport, lorry 16-32t, EURO3, RER	0.09	t*km	Based on a distance traveled of 100km by truck.	Ecoinvent
Methanol, at regional storage, CH (avoided product)	7.22	kg	The amount of methanol regenerated	Ecoinvent
Methyl 4-Benzobutyrate p-	Reference Flow Amount: 1kg		Production of methyl 4 benzoybutyrate p-tosylhydrazone as outlined in Anctil et al.[57] using the precursors methyl 4-benzobutyrate and p-toluenesulfonyl hydrazine. The authors	

tosylhydrazone, at plant			deviate from Anctil et al. by accounting for methanol regeneration.	
Inventory Item	**Amount**	**Units**	**Other**	**Inventory Flow Source**
disposal, hazardous waste, 25% water, to waste incineration, CH	0.15	kg		Ecoinvent
Electricity, medium voltage, production RER, at grid	3.38	MJ		Ecoinvent
Heat, heavy fuel oil, at industrial furnace 1MW, RER	1.06	MJ	Energy needed for distillation of methanol for regeneration. No other inventory data were expected of this regeneration process.	Ecoinvent
Methanol, at regional storage, CH	1.39	kg		Ecoinvent
Methyl 4-Benzobutyrate, at plant	0.57	kg		This study
p-toluenesulfonyl hydrazine, at plant	0.62	kg		This study
Transport, freight, rail, RER	1.64	t*km	Based on a distance traveled of 600km by train.	Ecoinvent
Transport, lorry 16-32t, EURO3, RER	0.28	t*km	Based on a distance traveled of 100km by truck.	Ecoinvent
Methanol, at regional storage, CH (avoided product)	7.22	kg	The amount of methanol regenerated	Ecoinvent

Molybdenum(VI) oxide, at plant	Reference Flow Amount: 1kg		Estimation of the production of molybdenum VI oxide based on stoichiometric calculations involving molybdenite and oxygen heated together at 700°C	
Inventory Item	**Amount**	**Units**	**Other**	**Inventory Flow Source**
Heat, heavy fuel oil, at industrial furnace 1MW, RER	0.76	MJ		Ecoinvent
Molybdenite, at plant, GLO	1.11	kg		Ecoinvent
Oxygen, liquid, at plant, RER	0.39	kg		Ecoinvent
Transport, freight, rail, RER	0.9	t*km	Based on a distance traveled of 600km by train.	Ecoinvent
Transport, lorry 16-32t, EURO3, RER	0.15	t*km	Based on a distance traveled of 100km by truck.	Ecoinvent
Sulfur dioxide (emissions), to air	0.89	kg		Ecoinvent

Nano-TiO2, sulphate precipitation, at plant	Reference Flow Amount: 1 kg		Estimation of the production of 1 kg of nano-TiO2 based on the sulphate precipitation route as described in Hischier et al.[193]	
Inventory Item	**Amount**	**Units**	**Other**	**Inventory Flow Source**
Disposal, nano-TiO2, incineration	0.023	kg		Hischier et al. (not modeled)
Electricity, medium voltage, production, RER	0.333	kWh		Ecoinvent

Heat, natural gas, at industrial furnace > 100 kW – RER	1.01	MJ		Ecoinvent
TiOSO4 production, at plant	3.94	kg		Eocinvent
Transport, freight, rail – RER	1.41	tkm		Ecoinvent
Transport, lorry 16-32t, EURO3 – RER	0.235	tkm		Ecoinvent
Urea, as N, at regional storehouse – RER	2.35	kg		Ecoinvent
Water, cooling, unspecified natural origin	0.123	m3		Ecoinvent
Water, ultrapure, at plant – GLO	1.63	kg		Ecoinvent
Ammonia to water	1.4	kg	*Emissions*	Ecoinvent
Carbon dioxide, fossil to air	0.551	kg	*Emissions*	Ecoinvent
Carbonate to water	1.57	kg	*Emissions*	Ecoinvent
Nano-TiO2 to air	4.6E-8	kg	*Emissions*	This study
Nano-TiO2 to water	0.63432	kg	*Emissions*	Hischier et al.
Sulfate to soil	0.0241	kg	*Emissions*	This study
Titanium (IV) oxysulfate to water	0.0634	kg	*Emissions*	Hischier et al. (not modeled)

organic solar cell, 1Wp, at plant	Reference Flow Amount: 1Wp		Estimated based on the assumption that the solar cell is 5% efficient and requires 200cm^2 for each watt-peak of power production	
Inventory Item	**Amount**	**Units**	**Other**	**Inventory Flow Source**
organic solar cell, at plant	200	200cm^2		This study

organic solar cell, at plant	Reference Flow Amount: 1m^2		The amounts of materials used per layer were estimated using well-documented descriptions used in the scientific literature.[29,30,38,128]	
Inventory Item	**Amount**	**Units**	**Other**	**Inventory Flow Source**
Aluminum, primary, at plant, RER	0.001	kg		Ecoinvent
Annealing, process	1	number of items		This study
FTO substrate, sputtered, at plant	1	m^2		This study
Gravure printing	1	number of items		This study
Lamination flexible solar module, at plant	1	m^2		This study
Lithium fluoride, layer, application	1	number of items		This study
Molybdenum(VI) oxide, at plant	0.00024	kg		This study
Monochlorobenzene, at plant, RER	0.0076	kg		Ecoinvent
poly(3-hexylthiophene-2,5-diyl), at plant	0.00024	kg		This study

PCBM, purified 99%, at plant	0.00021	kg		This study
Nano-TiO2, sulphate precipitation, at plant	0.000127	kg		This study
Transport, freight, rail, RER	0.005	t*km	Based on a distance traveled of 600km by train.	Ecoinvent
Transport, lorry 16-32t, EURO3, RER	0.00018	t*km	Based on a distance traveled of 100km by truck.	Ecoinvent
Water, ultrapure, at plant, GLO	0.160	kg		Ecoinvent

poly(3-hexylthiophene-2,5-diyl), at plant	Reference Flow Amount: 1kg		Reaction of thiophene, bromine and hexane. Amounts of inputs and energy adapted from García-Valverde et al.[30]	
Inventory Item	**Amount**	**Units**	**Other**	**Inventory Flow Source**
Bromine, at plant	8.97	kg		This study
Electricity, medium voltage, production RER, at grid	131.07	MJ		Ecoinvent
Heat, heavy fuel oil, at industrial furnace 1MW, RER	1.15	GJ		Ecoinvent
Hexane, at plant, RER	2.58	kg		Ecoinvent
Thiophene, at plant	7.81	kg		This study
Transport, freight, rail, RER	11.61	t*km	Based on a distance traveled of 600km by train.	Ecoinvent
Transport, lorry 16-32t, EURO3, RER	1.94	t*km	Based on a distance traveled of 100km by truck.	Ecoinvent
Water, ultrapure, at plant, GLO	11,136.15	kg		Ecoinvent

PCBM, purified 99%, at plant	Reference Flow Amount: 1kg		Functionalization of C60 into PCBM adapted from the description in Anctil et al.[57]	
Inventory Item	**Amount**	**Units**	**Other**	**Inventory Flow Source**
disposal, hazardous waste, 25% water, to waste incineration, CH	0.05	kg		Ecoinvent
Methanol, at regional storage, CH	11.87	kg		Ecoinvent
PCBM, Unpurified, at plant	1.05	kg		This study
Solvent regeneration	237.5	kg		This study
Transport, freight, rail, RER	7.12	t*km	Based on a distance traveled of 600km by train.	Ecoinvent
Transport, lorry 16-32t, EURO3, RER	1.19	t*km	Based on a distance traveled of 100km by truck.	Ecoinvent
Methanol, at regional storage, CH	8.9	kg		Ecoinvent

PCBM, Unpurified, at plant	Reference Flow Amount: 1kg	Functionalization of C60 into PCBM adapted from the description in Anctil et al.[57] The authors deviate from Anctil et al. by accounting for C60 regeneration. Often large amounts of C60 are not converted to PCBM and this would not be cost effective unless that amount was regenerated.

Inventory Item	Amount	Units	Other	Inventory Flow Source
C60 regeneration	1.21	kg		This study
C60, C60-fullerenes , at plant	2.12	kg		This study
disposal, hazardous waste, 25% water, to waste incineration, CH	54.17	kg	Estimated as: 90% of the methyl 4 benzoybutyrate p-tosylhydrazone; 100% of the pyridine-compounds; 10% of the oDCB; 100% of the sodium hydroxide as sodium chloride; 10% of the toluene; 10% of the monochlorobenzene	Ecoinvent
Electricity, medium voltage, production RER, at grid	159.23	MJ		Ecoinvent
Methyl 4-Benzobutyrate p-tosylhydrazone, at plant	2.01	kg		This study
Monochlorobenzene, at plant, RER	0.087	kg		Ecoinvent
Nitrogen, liquid, at plant, RER	18.90	kg		Ecoinvent
o-Dichlorobenzene, at plant RER	219.63	kg		Ecoinvent
pyridine-compounds, at regional storage, RER	39.50	kg		Ecoinvent
Sodium methoxide, at plant, GLO	0.30	kg		Ecoinvent
Solvent regeneration	347.00	kg		This study
Steam, for chemical processes, at plant, RER	495.34	kg		Ecoinvent
Tap water, at user, RER	26,418.13	kg		Ecoinvent
Toluene, liquid, at plant, RER	0.11	kg		Ecoinvent
Transport, freight, rail, RER	111.84	t*km	Based on a distance traveled of 600km by train.	Ecoinvent
Transport, lorry 16-32t, EURO3, RER	18.64	t*km	Based on a distance traveled of 100km by truck.	Ecoinvent
Plastic film, pet, at plant	Reference Flow Amount: 1kg		The production of extruded plastic film adapted from the Ecoinvent process for extrusion of polyethylene terephthalate.	
Inventory Item	**Amount**	**Units**	**Other**	**Inventory Flow Source**
Extrusion, plastic film, RER	1.0	kg		Ecoinvent
Polyethylene terephthalate, granulate, amorphous, at plant, RER	1.03	kg		Ecoinvent
Transport, freight, rail, RER	0.6	t*km	Based on a distance traveled of 600km by train.	Ecoinvent
Transport, lorry 16-32t, EURO3, RER	0.1	t*km	Based on a distance traveled of 100km by truck.	Ecoinvent
p-toluenesulfonyl chloride (TsCl), at plant	Reference Flow Amount: 1kg		Production of p-toluenesulfonyl chloride adapted from Anctil et al.[57] and with the precursors sulfuryl chloride, toluene	

Inventory Item	Amount	Units	Other	Inventory Flow Source
Electricity, medium voltage, production RER, at grid	0.70	MJ		Ecoinvent
Steam, for chemical processes, at plant, RER	1.20	kg		Ecoinvent
Sulfuryl chloride, at plant	0.74	kg		This study
Toluene, liquid, at plant, RER	0.51	KG		Ecoinvent
Transport, freight, rail, RER	0.75	t*km	Based on a distance traveled of 600km by train.	Ecoinvent
Transport, lorry 16-32t, EURO3, RER	0.13	t*km	Based on a distance traveled of 100km by truck.	Ecoinvent
p-toluenesulfonyl hydrazine, at plant	Reference Flow Amount: 1kg		Production of p-toluenesulfonyl hydrazine adapted from Anctil et al.[57]	
Inventory Item	**Amount**	**Units**	**Other**	**Inventory Flow Source**
Electricity, medium voltage, production RER, at grid	0.69	MJ		Ecoinvent
Hydrazine, at plant	0.62	kg		This study
p-toluenesulfonyl chloride (TsCl), at plant	1.08	kg		This study
Steam, for chemical processes, at plant, RER	1.20	kg		Ecoinvent
Tetrahydrofuran, at plant, RER	0.39	kg		Ecoinvent
Transport, freight, rail, RER	1.25	t*km	Based on a distance traveled of 600km by train.	Ecoinvent
Transport, lorry 16-32t, EURO3, RER	0.21	t*km	Based on a distance traveled of 100km by truck.	Ecoinvent
Solvent regeneration	Reference Flow Amount: 1kg		Adapted from Geisler et al.[371] using steam, nitrogen and cooling water. Assumption that this represents the inventory for a process recovering 95% of solvent.	
Inventory Item	**Amount**	**Units**	**Other**	**Inventory Flow Source**
Electricity, medium voltage, production RER, at grid	0.20	MJ		Ecoinvent
Nitrogen, liquid, at plant, RER	0.01	kg		Ecoinvent
Steam, for chemical processes, at plant, RER	1.50	kg		Ecoinvent
Tap water, at user, RER	80.00	kg		Ecoinvent
Sulfuryl chloride, at plant	Reference Flow Amount: 1kg		Adapted from Anctil et al.[57] using the precursors sulphur dioxide and chlorine.	
Inventory Item	**Amount**	**Units**	**Other**	**Inventory Flow Source**
Chlorine, liquid, production mix, at plant, RER	0.55	kg		Ecoinvent

Electricity, medium voltage, production RER, at grid	0.71	MJ	Q	Ecoinvent
Steam, for chemical processes, at plant, RER	1.21			Ecoinvent
Sulphur dioxide, liquid, at plant, RER	0.50	kg		Ecoinvent
Transport, freight, rail, RER	0.63	t*km	Based on a distance traveled of 600km by train.	Ecoinvent
Transport, lorry 16-32t, EURO3, RER	0.11	t*km	Based on a distance traveled of 100km by truck.	Ecoinvent

Thiophene, at plant	Reference Flow Amount: 1kg		Production of Thiophene (C4H4S) from Butane (C4H10) and sulfur (CS2). The inputs and outputs of production process were adapted from the Patent US 3939179 A [1]and from the Ullmann's Encyclopedia Of Industrial Chemistry.[130]	
Inventory Item	**Amount**	**Units**	**Other**	**Inventory Flow Source**
Aluminium oxide, at plant, RER	0.40	kg		Ecoinvent
Butanes from butenes, at plant, RER	0.69	kg		Ecoinvent
Chromium oxide, flakes, at plant, RER	0.80	kg		Ecoinvent
Heat, heavy fuel oil, at industrial furnace 1MW, RER	1.81	MJ		Ecoinvent
Hydrogen sulfide, H2S, at plant, RER	1.22	kg		Ecoinvent
Secondary Sulphur, at refinery, RER	1.52	kg		Ecoinvent
Transport, freight, rail, RER	1.58	t*km	Based on a distance traveled of 600km by train.	Ecoinvent
Transport, lorry 16-32t, EURO3, RER	0.26	t*km	Based on a distance traveled of 100km by truck.	Ecoinvent

Tin tetrachloride, at plant	Reference Flow Amount: 1kg		Adapted from Ullman's encyclopedia of industrial chemistry following the reaction of tin and chlorine.[131]	
Inventory Item	**Amount**	**Units**	**Other**	**Inventory Flow Source**
Chlorine, liquid, production mix, at plant, RER	0.54	kg		Ecoinvent
Heat, heavy fuel oil, at industrial furnace 1MW, RER	0.13	MJ		Ecoinvent
Tin, at regional storage, RER	0.46	kg		Ecoinvent
Transport, freight, rail, RER	0.6	t*km	Based on a distance traveled of 600km by train.	Ecoinvent
Transport, lorry 16-32t, EURO3, RER	0.1	t*km	Based on a distance traveled of 100km by truck.	Ecoinvent

Tin tetrachloride pentahydrate, at plant	Reference Flow Amount: 1kg	Estimated using stoichiometric calculations following SnCl4 + 5H2O = SnCl4.5H2O.

Inventory Item	Amount	Units	Other	Inventory Flow Source
Tin tetrachloride, at plant	0.74	kg		This study
Water, ultrapure, at plant, GLO	0.26	kg		Ecoinvent

TiOSO4 production, at plant	Reference Flow Amount: 1 kg		Estimation of the production of 1 kg of nano- TiOSO4 based on the digestion of ilmenite (FeTiO3) with sulphuric acid as described in Hischier et al.[193]
Inventory Item	**Amount**	**Units**	**Other**	**Inventory Flow Source**
Chemical plant, organics – RER	4E-10	Items		Ecoinvent
Electricity, medium voltage, production RER	0.333	kWh		Ecoinvent
Heat, unspecific, in chemical plant – RER	2.17	MJ		Ecoinvent
Ilmenite, 54% titanium dioxide, at plant – AU	0.595	kg		Ecoinvent
Sulphuric acid, liquid, at plant – RER	0.0248	kg		Ecoinvent
Transport, freight, rail – RER	0.387	tkm		Ecoinvent
Transport, lorry 16-32t, EURO3 – RER	0.0645	tkm		Ecoinvent
Water, cooling, unspecified natural origin	0.123	m3		Ecoinvent
Disposal, residue from TiO2 production SO4, 30% water, to residual material landfill – CH	0.162	kg		Ecoinvent
Hydrogen sulfide to water	1.58E-6	kg		Ecoinvent
Sulfur dioxide to air	0.00025	kg		Ecoinvent

Average Solar Insolation for European Union Member States

Table A3-2 lists the average solar insolation for EU member state which were used to calculate an average European insolation value.

Table A3-2 Average solar insolation (kWh) for the individual European Union member states and an average[153]

Spain	1659
Cyprus	1902
Greece	1637
Portugal	1632
Italy	1494
Albania	1556
France	1259
Montenegro	1468
Serbia	1472
Croatia	1334
Bulgaria	1406

Bosnia and Herz	1315
Switzerland	1233
Romania	1301
Slovenia	1270
Moldova	1276
Hungary	1266
Austria	1194
Slovakia	1182
Germany	1066
Czech Rep	1109
UK	972
Poland	1071
Netherlands	1025
Belgium	1052
Denmark	987
Ireland	926
Turkey*	1661
Average	**1298.67**

Appendix: Chapter 4

Slanted Roof Mounting Structure Inventory Data

Slanted roof mount construction inventory data is based on a modified Ecoinvent process "slanted-roof construction, mounted, on roof" for which an aluminum backing component was added and defined as: 0.001445 m^3 of aluminum (thickness 2 mm). Given a density of 2.7 g/cm^3 for aluminum, 3.9 kg of aluminum is required for the mounting structure. The previous Ecoinvent inventory entry for aluminum (including aluminum bar extrusion) used as u-profile mounting beams were removed and replaced with the above mention of aluminum backing. It is assumed that the mount would not have to be solid (100% filled) across the area of the backing in order to secure the OPV into place. Instead, holes measuring 12 cm in diameter are evenly spaced through the aluminum-backing leaving 6.7 cm between each hole and the sides. This amounts to 25 circles each measuring 113 cm^2 by area and 0.2 cm in thickness (22.6 cm^3 * 25 = 0.000555 m^3) of aluminum removed from the backing, and thus a total of 0.001445 m^3 of aluminum is used (3.9 kg). The mounting structure is assumed to last 25 years.

Table A4-1 Inventory data for production and disposal of OPV slanted roof mounting structure.

Inventory per 1m^2 of slanted roof mounting and installation for OPV panels			
Flow	**Notes**	**Unit**	**Amount**
aluminium, production mix, wrought alloy, at plant - RER		kg	3.90
corrugated board, mixed fibre, single wall, at plant - RER		kg	0.133
disposal, building, polyethylene/polypropylene products, to final disposal - CH		kg	0.00140
disposal, building, polystyrene isolation, flame-retardant, to final disposal - CH		kg	0.00702
disposal, OPV mounting frame		Item(s)	1
disposal, packaging cardboard, 19.6% water, to municipal incineration - CH		kg	0.133
polyethylene, HDPE, granulate, at plant - RER		kg	0.00140
polystyrene, high impact, HIPS, at plant - RER		kg	0.00702
section bar extrusion, aluminium - RER		kg	0
sheet rolling, aluminium - RER		kg	1.35E-12
sheet rolling, steel - RER		kg	1.49
steel, low-alloyed, at plant - RER		kg	1.49
transport, freight, rail - RER		t*km	1.50
transport, lorry > 16t, fleet average - RER		t*km	0.225
transport, van < 3.5t - RER		t*km	0.434
Inventory for disposal of 1m^2 of OPV mounting structure			
Flow	**Notes**	**Unit**	**Amount**
aluminium, secondary, from old scrap, at plant - RER	Secondary production of recycled aluminum	kg	3.90
dismantling, industrial devices, manually, at plant - CH		kg	5.49
steel, electric, un- and low-alloyed, at plant – RER	Secondary production of recycled steel	kg	1.49
aluminium, primary, at plant - RER	Avoided product	kg	3.78
steel, converter, unalloyed, at plant – RER	Avoided product	kg	1.34

The mounting structure for m-Si was based on the original Ecoinvent process "slanted-roof construction, mounted, on roof" but included the recycling of the main aluminum and steel components via secondary metal production pathways as inputs to and secondary metal products as avoided products from the system.

Table A4-2 Inventory for 1m2 of slanted roof mounting and installation for m-Si panels including disposal (includes disposal of steel and aluminum components)

Flow	Notes	Unit	Amount
aluminium, production mix, wrought alloy, at plant - RER		kg	2.84

aluminium, secondary, from old scrap, at plant - RER	Secondary production of aluminum	kg	5.46
corrugated board, mixed fibre, single wall, at plant - RER		kg	0.133
dismantling, industrial devices, manually, at plant - CH		kg	5.80
dismantling, industrial devices, mechanically, at plant - GLO		kg	5.80
disposal, building, polyethylene/polypropylene products, to final disposal - CH		kg	0.00140
disposal, building, polystyrene isolation, flame-retardant, to final disposal - CH		kg	0.00702
disposal, packaging cardboard, 19.6% water, to municipal incineration - CH		kg	0.133
polyethylene, HDPE, granulate, at plant - RER		kg	0.00140
polystyrene, high impact, HIPS, at plant - RER		kg	7.02E-03
section bar extrusion, aluminium - RER		kg	3.03
sheet rolling, steel - RER		kg	1.50
steel, electric, un- and low-alloyed, at plant - RER	Secondary production of steel	kg	1.50
steel, low-alloyed, at plant - RER		kg	1.50
transport, freight, rail - RER		t*km	1.50
transport, lorry > 16t, fleet average - RER		t*km	0.225
transport, van < 3.5t - RER		t*km	0.434
steel, converter, unalloyed, at plant - RER	Avoided product	kg	1.35
aluminium, primary, at plant - RER	Avoided product	kg	5.30

Recycling Conversion Rates of Secondary Scrap Metal to Primary Metal

Table A4-3 Recycling Conversion Rates of Secondary Scrap Metal to Primary Metal

Alumininum	97%
Copper	76%
Iron (Ferrous Materials)	90%

Inverter

The inventory for the inverter was based on the Ecoinvent process “inverter, 2500W, at plant” defined below. Disposal of the inverter was estimated for the major aluminium, copper and steel components.

Table A4-4 Inventory for 1 inverter (18.5kg) as applied to both the OPVs and m-Si rooftop-installations

Inventory for the production of 1 inverter per functional unit			
Flow	Notes	Unit	Amount
aluminium, production mix, cast alloy, at plant - RER		kg	1.4
capacitor, electrolyte type, > 2cm height, at plant - GLO		kg	0.256
capacitor, film, through-hole mounting, at plant - GLO		kg	0.341
capacitor, Tantalum-, through-hole mounting, at plant - GLO		kg	0.0230
connector, clamp connection, at plant - GLO		kg	0.237
copper, at regional storage - RER		kg	5.51
corrugated board, mixed fibre, single wall, at plant - RER		kg	2.50
diode, glass-, through-hole mounting, at plant - GLO		kg	0.0470
disposal, inverter, to WEEE treatment		Item(s)	1
disposal, packaging cardboard, 19.6% water, to municipal incineration - CH		kg	2.50
disposal, polyethylene, 0.4% water, to municipal incineration - CH		kg	0.0600
disposal, polystyrene, 0.2% water, to municipal incineration - CH		kg	0.310
disposal, treatment of printed wiring boards - GLO		kg	1.703
electricity, medium voltage, production UCTE, at grid - UCTE		kWh	21.2
fleece, polyethylene, at plant - RER		kg	0.0600
inductor, ring core choke type, at plant - GLO		kg	0.351
integrated circuit, IC, logic type, at plant - GLO		kg	0.0280
metal working factory - RER		Item(s)	8.97E-09
polystyrene foam slab, at plant - RER		kg	0.300
polyvinylchloride, at regional storage - RER		kg	0.0100
printed wiring board, through-hole, at plant - GLO		m2	0.225

resistor, metal film type, through-hole mounting, at plant - GLO	kg	0.005
section bar extrusion, aluminium - RER	kg	1.40
sheet rolling, steel - RER	kg	9.80
steel, low-alloyed, at plant - RER	kg	9.80
styrene-acrylonitrile copolymer, SAN, at plant - RER	kg	0.01
transistor, wired, small size, through-hole mounting, at plant - GLO	kg	0.038
transport, freight, rail - RER	t*km	7.11
transport, lorry > 16t, fleet average - RER	t*km	2.30
transport, transoceanic freight ship - OCE	t*km	36.3
wire drawing, copper - RER	kg	5.51

Inventory for disposal of 1 inverter per functional unit			
Flow	Notes	Unit	Amount
aluminium, secondary, from old scrap, at plant - RER	Secondary production of recycled aluminum	kg	1.31
copper, secondary, at refinery - RER	Secondary production of recycled copper	kg	5.50
dismantling, inverter, manual, at plant		kg	4.25
dismantling, inverter, mechanical, at plant		kg	14.3
disposal, residues, mechanical treatment, industrial device, in MSWI - CH		kg	1.13
steel, electric, un- and low-alloyed, at plant - RER	Secondary production of recycled steel	kg	10.6
aluminium, primary, at plant - RER	Avoided product	kg	1.27
copper, at regional storage - RER	Avoided product	kg	4.21
electricity, medium voltage, production RER, at grid - RER	Avoided product from incinerating inverter plastic	MJ	3.35
steel, converter, unalloyed, at plant - RER	Avoided product	kg	9.51

Mechanical and Manual Transfer Coefficients

Table A4-5 Mechanical and Manual Transfer Coefficients

Transfer Coefficients Per Material Per Dismantling Method		
Mechanical		
Metals, outside	50%	scrap, for metal production
Metals, outside	50%	shredder
Metals, inside	100%	shredder
Plastics, inside	100%	shredder
Printed Wiring Board	50%	treatment
Printed Wiring Board	50%	shredder
all else	100%	shredder
Manual		
Metals, outside	100%	scrap, for metal production
Metals, inside	100%	scrap, for metal production
Plastics, inside	100%	incineration
Printed Wiring Board	100%	treatment
all else	100%	shredder

Transfer Coefficients Per Mechanical Dismantling (Shredding)	
Alumininum	82.58%
Copper	78.21%
Iron (Ferrous materials)	95%

Cables

Table A4-6 Inventory for electric cabling as applied to both the OPVs and m-Si rooftop-installations

Inventory during 1m^2 of PV installation			
Flow	Notes	Unit	Amount
acrylonitrile-butadiene-styrene copolymer, ABS, at plant - RER		kg	0.64
copper, at regional storage - RER		kg	0.083
disposal, cabling		m2	1.00
wire drawing, copper - RER		kg	0.083
Inventory for the disposal of cabling per m^2 of PV capacity			
Flow	Notes	Unit	Amount

copper, secondary, at refinery - RER	Secondary production of recycled copper	kg	0.083
disposal, plastic, industry. electronics, 15.3% water, to municipal incineration - CH		kg	0.640
copper, at regional storage - RER	Avoided product	kg	0.0830
electricity, medium voltage, production RER, at grid - RER	Avoided product from incineration of inverter plastics	MJ	2.56

Elemental Composition of the Solar Panels for Use in Ecoinvent's Waste Disposal Tool

Table 7 lists the elemental composition of each solar panel which was used to derive the disposal inventory using Ecoinvent's Waste Disposal Tool.[150] The composition was based on the panel composition at the time of manufacture (i.e. not considering losses or degradation of components over the lifetime of the PV device). See the *Appendix A.1* (available with this article on the publisher's website) to view the final disposal inventory produced by the Ecoinvent Tool.

Table A4-7 PV panel elemental composition that was used to derive the disposal inventory per kg of PV panel considered in the LCA

Component	OPV	a-Si	m-Si
Oxygen (without O from H_2O)	3.56E-01	2.39E-02	4.36E-01
Hydrogen (without H from H_2O)	6.16E-02	8.08E-02	2.29E-02
Carbon	5.36E-01	4.87E-01	8.24E-02
Sulfur	3.42E-04	3.34E-04	1.00E-05
Nitrogen	6.04E-03	2.08E-03	1.62E-03
Phosphor	0.00E+00	0.00E+00	0.00E+00
Boron	0.00E+00	0.00E+00	0.00E+00
Chlorine	1.67E-02	1.32E-03	1.70E-04
Bromium	6.45E-05	5.57E-06	7.01E-07
Fluorine	9.21E-04	1.57E-03	3.13E-03
Iodine	0.00E+00	0.00E+00	0.00E+00
Arsenic	1.75E-06	1.00E-06	1.90E-08
Barium	4.61E-05	1.31E-04	1.87E-06
Cadmium	3.04E-06	1.87E-05	2.61E-08
Cobalt	2.90E-05	1.07E-06	3.16E-07
Chromium	5.07E-06	7.83E-06	2.63E-04
Copper	1.11E-05	2.63E-02	1.13E-02
Mercury	8.30E-08	3.04E-08	8.50E-09
Manganese	1.66E-05	1.68E-05	8.00E-07
Molybdenum	7.18E-04	0.00E+00	0.00E+00
Nickel	3.69E-06	6.25E-07	1.43E-05
Lead	5.16E-06	4.19E-04	3.36E-05
Antimony	1.49E-04	5.70E-06	4.30E-07
Selenium	1.94E-06	1.11E-06	2.10E-08
Tin	5.69E-03	6.11E-04	4.57E-04
Vanadium	1.20E-03	1.20E-03	2.88E-06
Zinc	6.42E-05	6.04E-04	3.96E-06
Beryllium	4.61E-07	2.64E-07	5.00E-09
Scandium	0.00E+00	0.00E+00	0.00E+00
Strontium	8.16E-05	4.66E-05	8.86E-07
Titanium	9.22E-04	5.27E-04	1.00E-05
Thallium	3.69E-07	2.11E-07	4.00E-09
Tungsten	0.00E+00	0.00E+00	0.00E+00
Silicon	4.07E-03	2.20E-03	3.21E-01
Iron	9.22E-05	3.66E-01	3.73E-05
Calcium	2.77E-04	1.61E-03	6.30E-02
Aluminium	4.68E-03	1.60E-03	2.00E-06
Potassium	0.00E+00	0.00E+00	0.00E+00
Magnesium	0.00E+00	4.08E-03	0.00E+00

Sodium	1.35E-03	9.51E-04	5.59E-02

Additional Impact Assessment Results from Chapter 4

Table A8 Absolute life-cycle impacts for S1 (rooftop array)

Impact category	Reference unit	OPV-D (Incineration)	OPV-D (Landfill)	m-Si (Incineration)	m-Si (Landfill)	OPV-D (Incineration, No Mount)	OPV-D (Landfill, No Mount)
Agricultural land occupation	$m^2 \cdot yr$	2.44E+01	2.47E+01	7.23E+01	7.22E+01	1.47E+01	1.50E+01
Climate change potential	kg CO_2-eq	6.94E+02	6.68E+02	1.31E+03	1.31E+03	5.68E+02	5.42E+02
Fossil depletion	kg Oil-eq	2.04E+02	2.08E+02	3.81E+02	3.80E+02	1.67E+02	1.72E+02
Freshwater ecotoxicity	kg 1,4-DCB-eq	2.35E-02	2.37E-02	1.77E-01	1.77E-01	2.03E-02	2.04E-02
Freshwater eutrophication	kg P-eq	5.97E-01	6.12E-01	8.78E-01	8.77E-01	5.33E-01	5.48E-01
Human toxicity	kg 1,4-DCB-eq	1.43E+02	1.43E+02	4.67E+02	4.67E+02	1.06E+02	1.07E+02
Ionizing radiation	kg U_{235}-eq	1.83E+02	1.96E+02	3.64E+02	3.64E+02	1.60E+02	1.73E+02
Marine ecotoxicity	kg 1,4-DCB-eq	2.21E+00	2.22E+00	8.73E+00	8.73E+00	1.72E+00	1.73E+00
Marine eutrophication	kg N-eq	1.60E-01	2.95E-01	7.13E-01	7.07E-01	1.34E-01	2.69E-01
Metal depletion	kg Fe-eq	4.77E+02	4.78E+02	3.77E+02	3.77E+02	4.04E+02	4.05E+02
Natural land transformation	m^2	1.17E-01	1.18E-01	2.57E-01	2.57E-01	8.30E-02	8.41E-02
Ozone depletion	kg CFC_{11}-eq	6.11E-05	6.19E-05	1.15E-04	1.15E-04	2.38E-05	2.46E-05
Particulate matter formation	kg PM_{10}-eq	9.32E-01	9.52E-01	1.59E+00	1.58E+00	7.92E-01	8.12E-01
Photochemical oxidant formation	kg NMVOC	1.82E+00	1.84E+00	4.98E+00	4.94E+00	1.44E+00	1.47E+00
Terrestrial acidification	kg SO_2-eq	2.58E+00	2.64E+00	4.71E+00	4.68E+00	2.16E+00	2.22E+00
Terrestrial ecotoxicity	kg 1,4-DCB-eq	1.16E-01	1.17E-01	3.69E+00	3.69E+00	9.57E-02	9.62E-02
Urban land occupation	$m^2 \cdot yr$	7.26E+00	7.40E+00	1.08E+01	1.09E+01	5.07E+00	5.21E+00
Water depletion	m^3	1.04E+03	1.17E+03	2.62E+04	2.62E+04	1.78E+03	1.91E+03
Cumulative energy demand	MJ-eq	1.16E+04	1.20E+04	2.46E+04	2.46E+04	9.67E+03	1.00E+04

Table A9 Absolute life-cycle impacts for S2 (portable charger)

Impact category	Reference unit	OPV-D (Incineration)	OPV-D (Landfill)	a-Si (Incineration)	a-Si (Landfill)	OPV-NC (Incineration)	OPV-NC (Landfill)	a-Si-NC (Incineration)	a-Si-NC (Landfill)
Agricultural land occupation	$m^2 \cdot yr$	7.53E-02	8.47E-02	2.25E-01	2.33E-01	8.31E-03	8.92E-03	1.72E-01	1.73E-01
Climate change potential	kg CO_2-eq	4.27E+00	3.52E+00	1.06E+01	1.02E+01	5.73E-01	5.22E-01	7.71E+00	7.79E+00
Fossil depletion	kg Oil-eq	1.19E+00	1.34E+00	3.06E+00	3.19E+00	1.97E-01	2.06E-01	2.28E+00	2.30E+00
Freshwater ecotoxicity	kg 1,4-DCB-eq	5.13E-05	5.52E-05	1.08E-04	1.11E-04	1.32E-05	1.35E-05	7.78E-05	7.82E-05
Freshwater eutrophication	kg P-eq	7.25E-04	1.19E-03	4.32E-03	4.72E-03	3.60E-04	3.90E-04	4.03E-03	4.09E-03
Human toxicity	kg 1,4-DCB-eq	2.18E-01	2.24E-01	5.95E-01	6.00E-01	4.99E-02	5.09E-02	4.63E-01	4.64E-01
Ionizing radiation	kg U_{235}-eq	3.09E-01	7.36E-01	2.03E+00	2.41E+00	1.76E-01	2.02E-01	1.93E+00	1.99E+00
Marine ecotoxicity	kg 1,4-DCB-eq	2.60E-03	2.74E-03	7.14E-03	7.26E-03	5.71E-04	5.86E-04	5.55E-03	5.56E-03
Marine eutrophication	kg N-eq	4.09E-04	4.08E-03	2.65E-03	5.32E-03	1.12E-04	3.82E-04	2.42E-03	2.40E-03
Metal depletion	kg Fe-eq	4.02E-01	4.06E-01	2.81E+00	2.81E+00	3.19E-01	3.20E-01	2.74E+00	2.74E+00
Natural land transformation	m^2	3.27E-04	3.67E-04	1.29E-03	1.32E-03	9.23E-05	9.44E-05	1.11E-03	1.11E-03
Ozone depletion	kg CFC_{11}-eq	1.16E-07	1.42E-07	3.11E-07	3.33E-07	2.72E-08	2.87E-08	2.41E-07	2.44E-07
Particulate matter formation	kg PM_{10}-eq	2.71E-03	3.35E-03	1.50E-02	1.55E-02	7.04E-04	7.43E-04	1.34E-02	1.35E-02
Photochemical oxidant formation	kg NMVOC	7.47E-03	8.32E-03	2.65E-02	2.71E-02	1.35E-03	1.40E-03	2.17E-02	2.17E-02
Terrestrial acidification	kg SO_2-eq	7.81E-03	9.84E-03	5.17E-02	5.34E-02	2.01E-03	2.13E-03	4.71E-02	4.73E-02
Terrestrial ecotoxicity	kg 1,4-DCB-eq	2.57E-04	2.71E-04	4.25E-04	4.36E-04	5.91E-05	6.03E-05	2.69E-04	2.71E-04
Urban land occupation	$m^2 \cdot yr$	9.61E-03	1.35E-02	8.96E-02	9.34E-02	2.54E-03	2.81E-03	8.41E-02	8.50E-02
Water depletion	m^3	3.77E+00	8.07E+00	3.05E+01	3.42E+01	1.98E+00	2.24E+00	2.91E+01	2.97E+01
Cumulative energy demand	MJ-eq	5.87E+01	7.09E+01	1.73E+02	1.84E+02	1.12E+01	1.20E+01	1.36E+02	1.37E+02

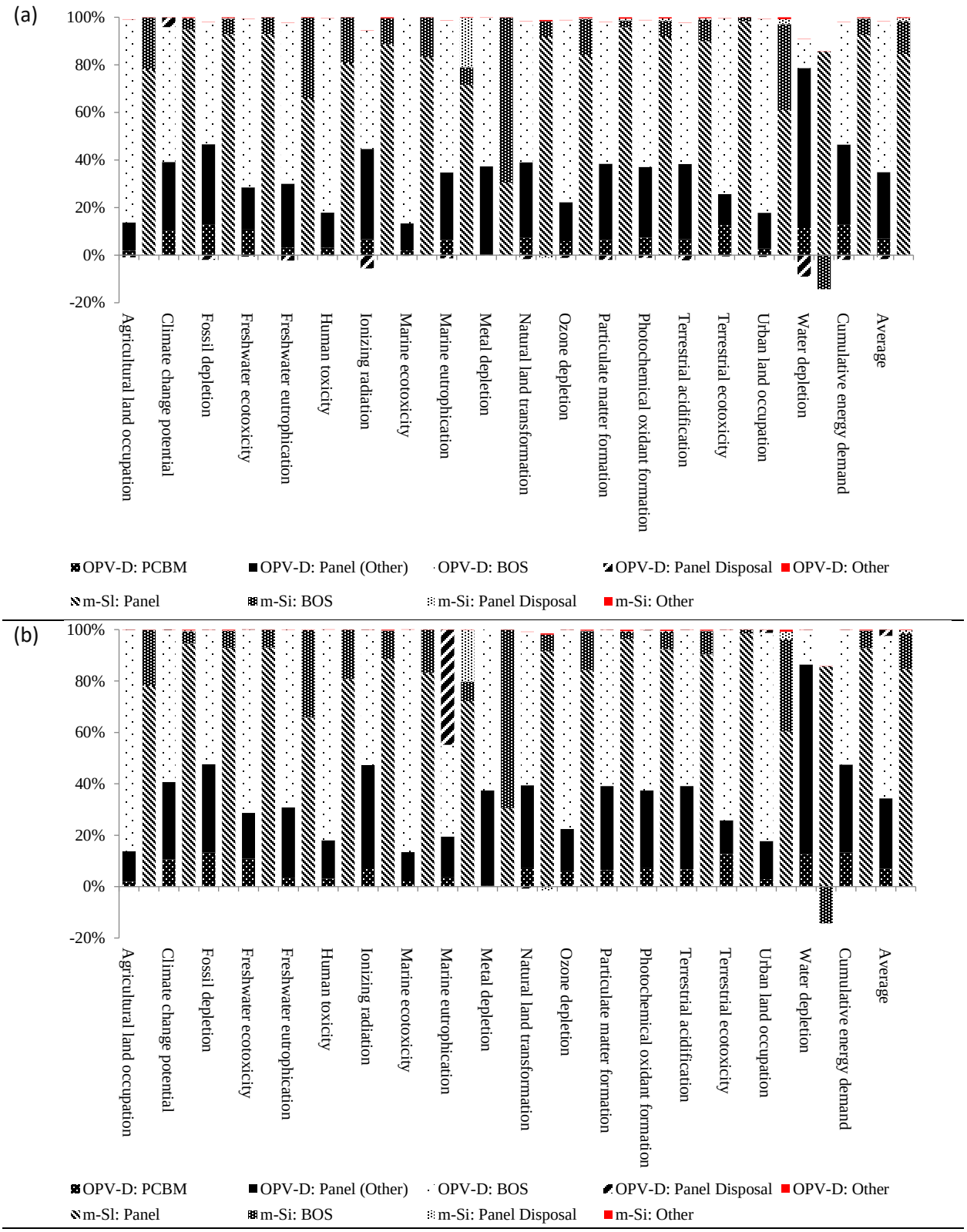

Figure A4-1 Contributions from each life-cycle stage for the OPV-D and m-Si panels when panels were (a) incinerated and (b) landfilled at their end-of-life for S1 (rooftop array).

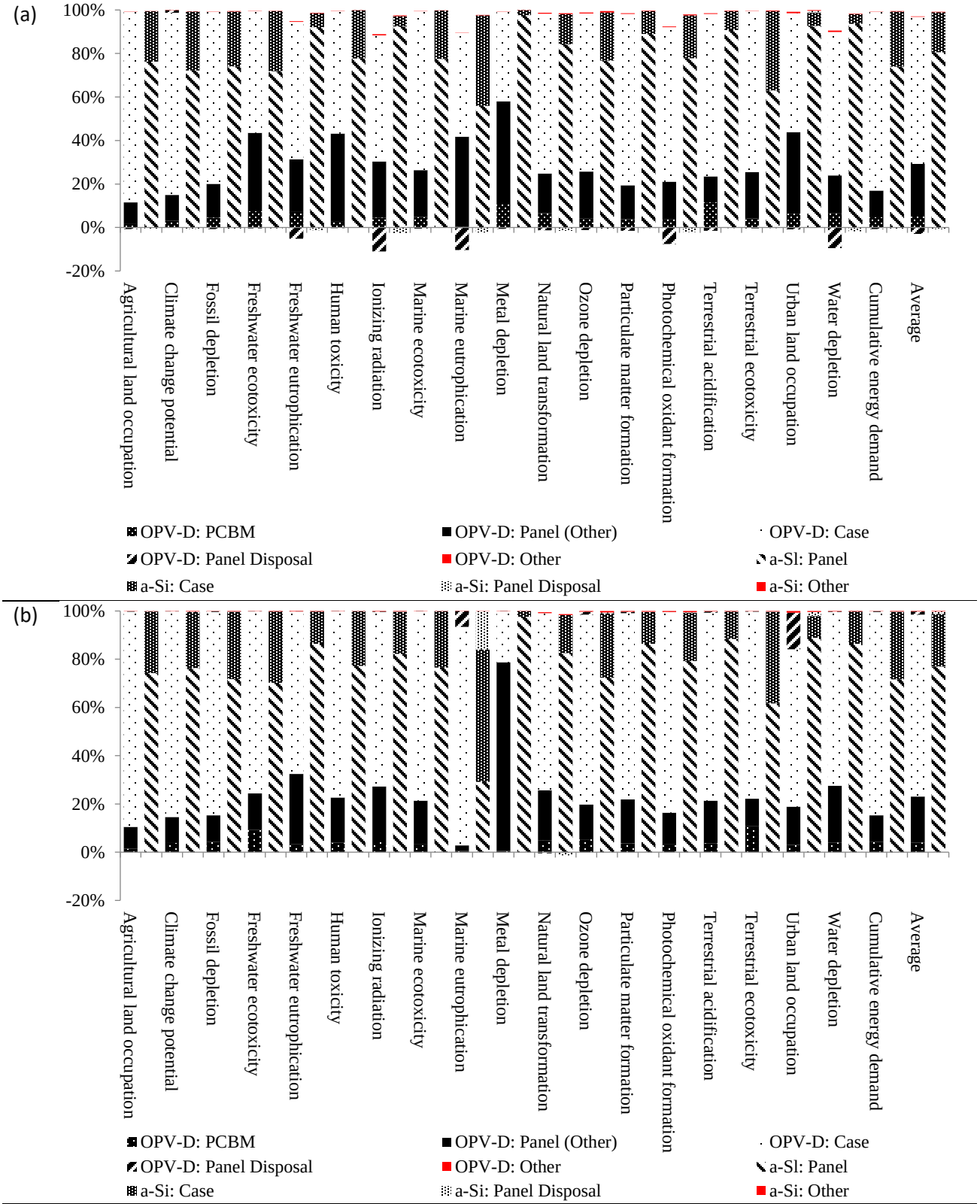

Figure A4-2 Contributions from each life-cycle stage for both the OPV-D and a-Si panels when panels were (a) incinerated and (b) landfilled at their end-of-life for S2 (portable charger).

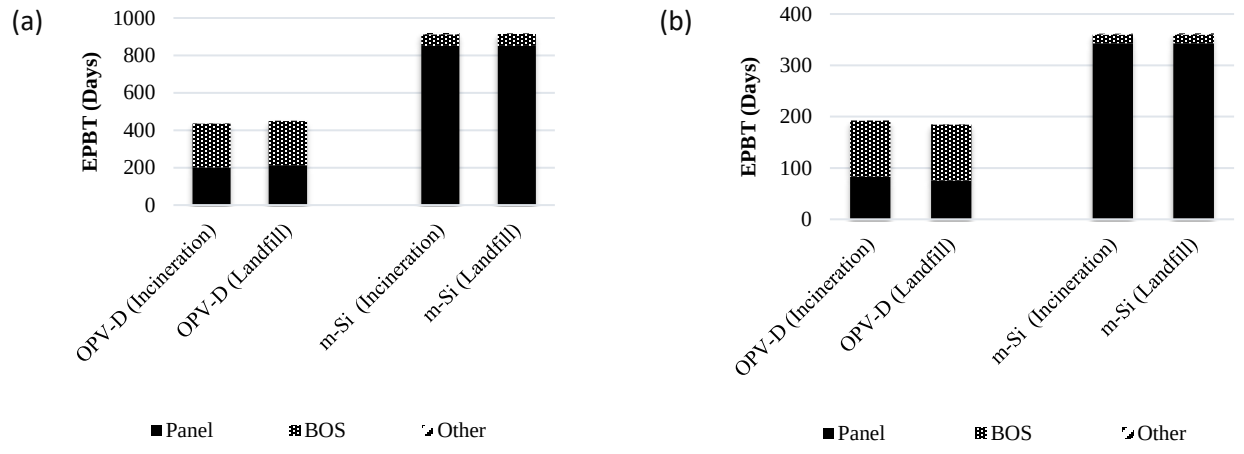

Figure A4-3 Contribution of life-cycle stage to (a) energy payback times and (b) carbon payback times for OPV-D and m-Si panels for S1 (rooftop array).

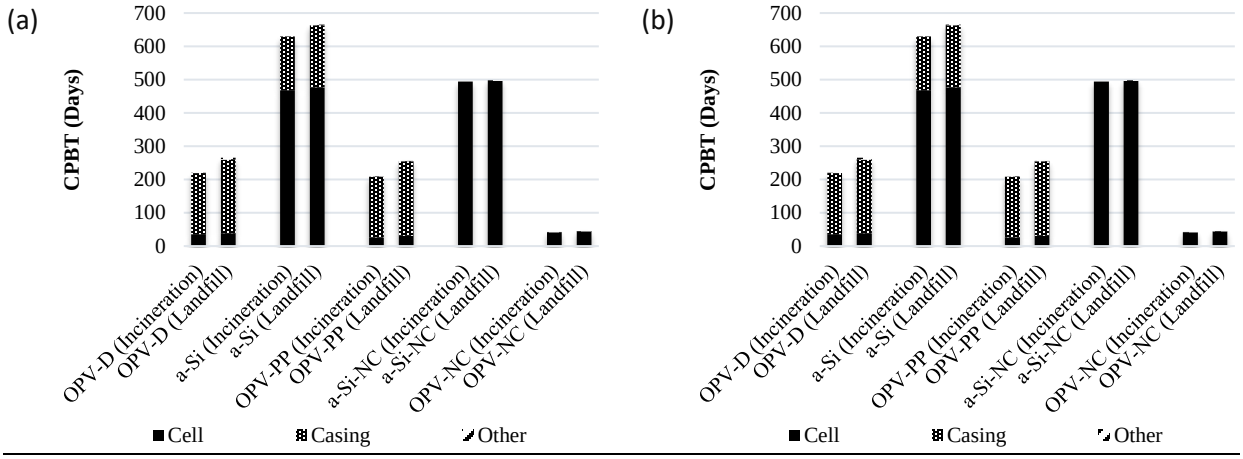

Figure A4-4 Contribution of life-cycle stage to (a) energy payback times and (b) carbon payback times for OPV-D and a-Si panels for S2 (portable charger).

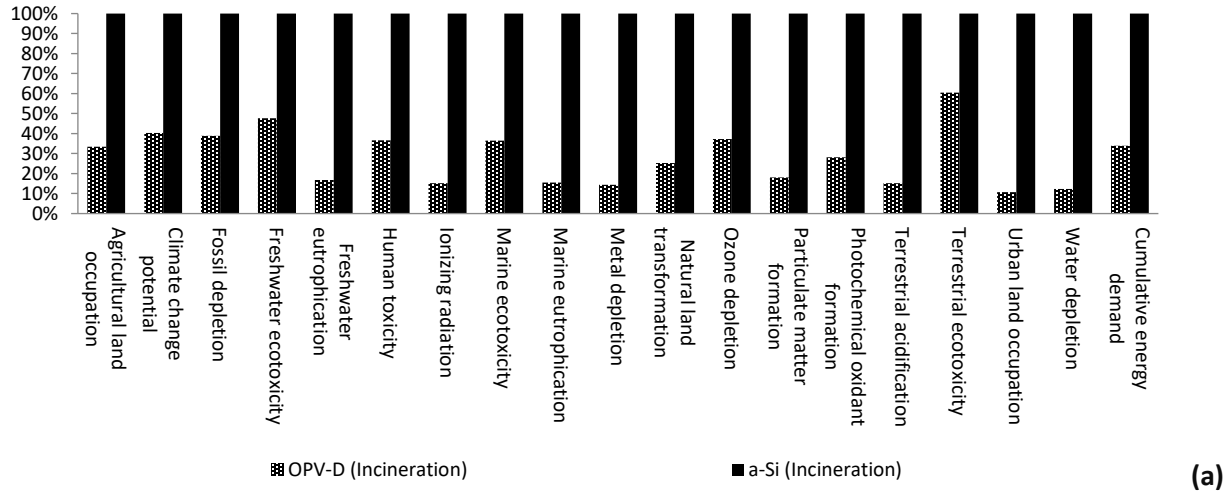

(a)

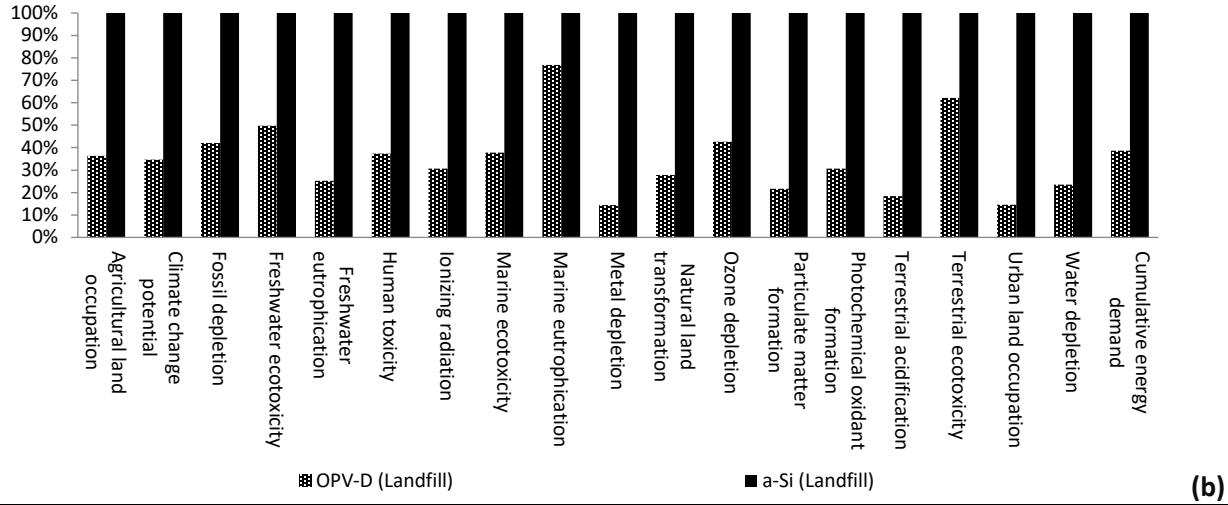

Figure A4-5 Comparison of OPV panels with and without casing for S2 with (a) incineration and (b) landfilling. Results are normalized by the maximum impact values of the two alternatives. In both (a) and (b) the maximum was the silicon panel's impacts.

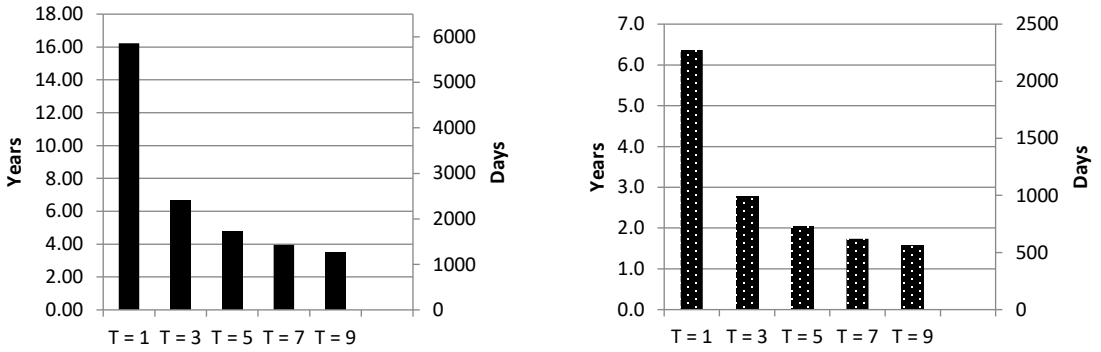

Figure A4-6 EPBTs and CPBTs for S1 based on differences in the assumed lifetimes (T) and while the efficiency was assumed to be 1%.

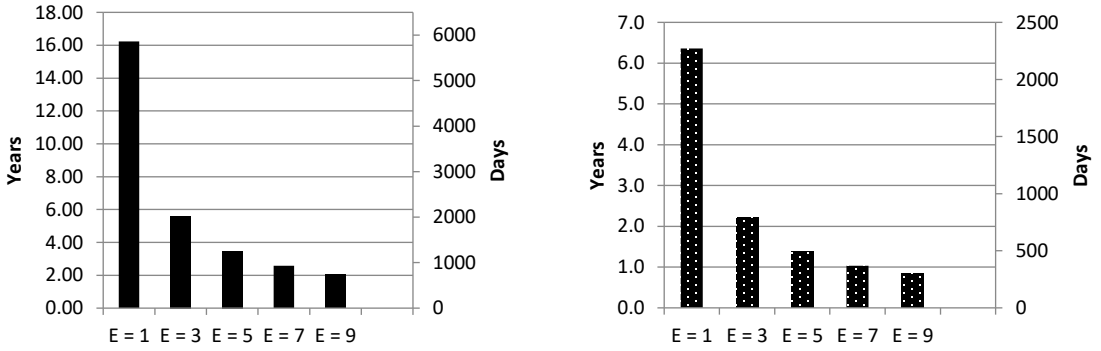

Figure A4-7 EPBTs and CPBTs for S1 based on differences in the assumed efficiencies (E) and while the lifetime of the panel was assumed to be 1-year.

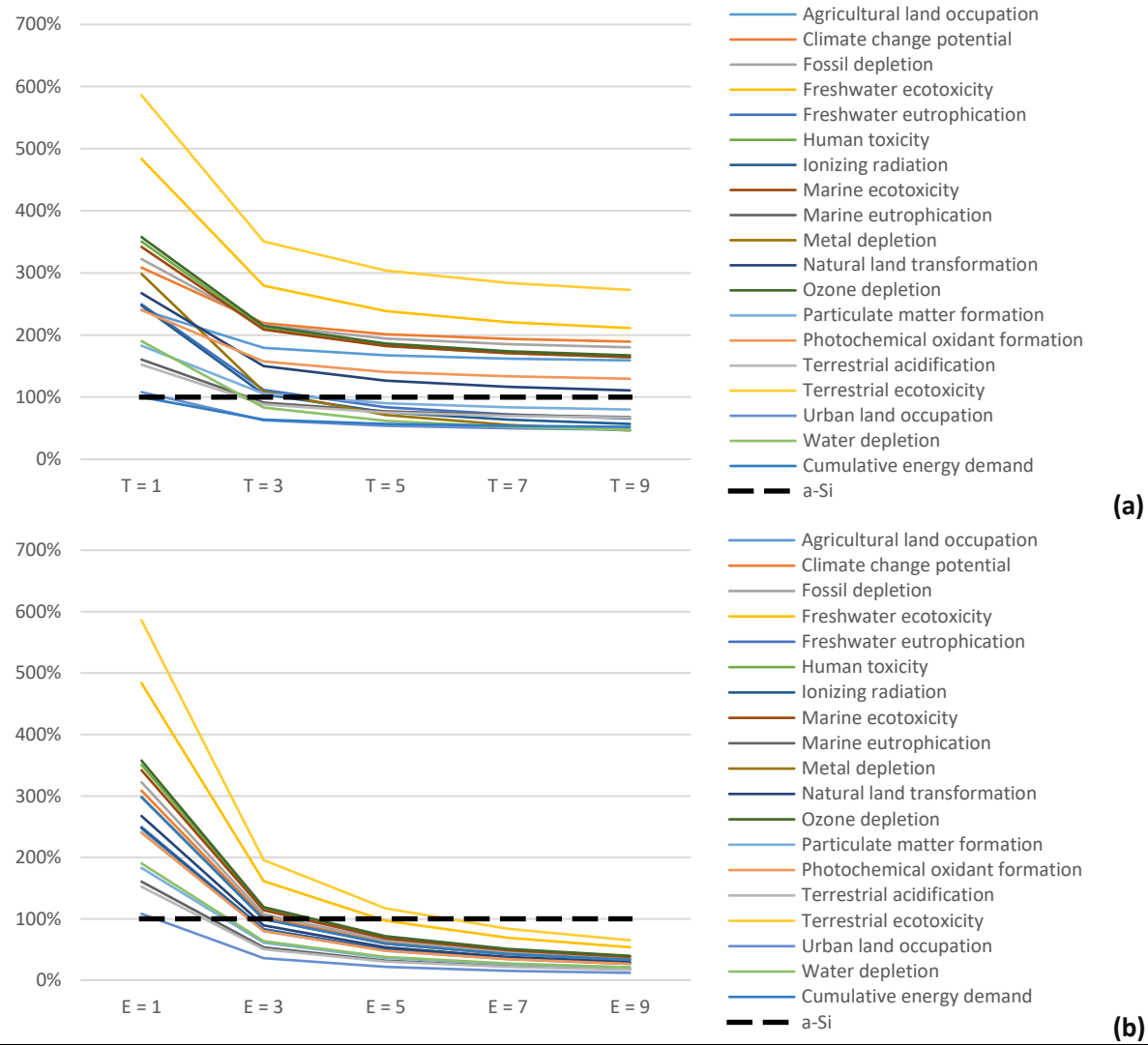

Figure A4-8 Life-cycle impact changes for S2 OPV-D based on differences in the assumed (a) lifetimes (T) of the solar panels and while the efficiency was assumed to be 1% and (b) efficiencies (E) while the lifetime of the solar panels was assumed to be 1-year. The impact results are normalized to the impact values of a-Si (i.e. a-Si's impacts are set at 100%).

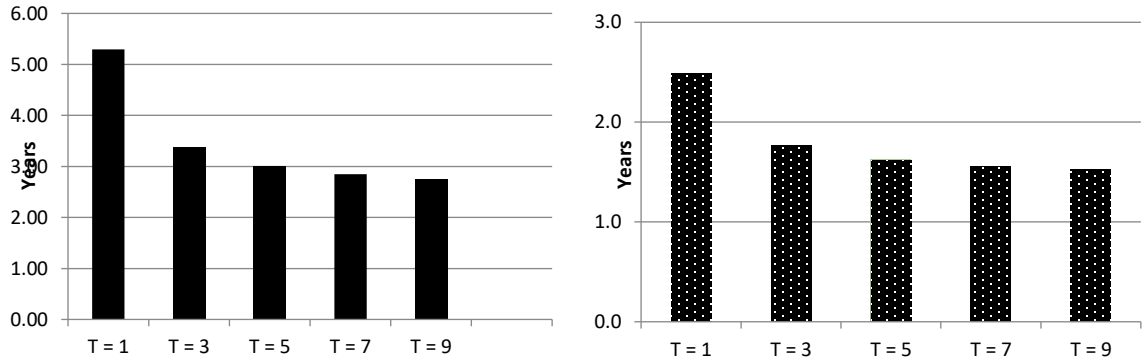

Figure A4-9 EPBTs and CPBTs for S2 based on differences in the assumed lifetimes (T) and while the efficiency was assumed to be 1%.

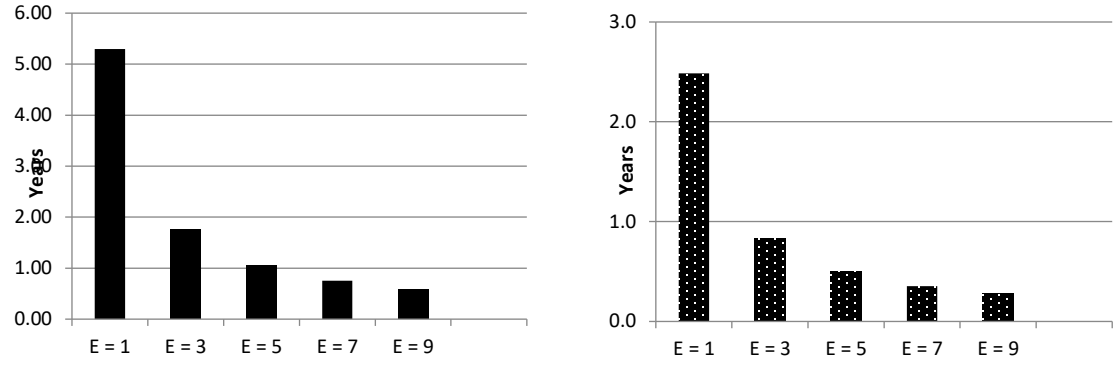

Figure A4-10 EPBTs and CPBTs for S2 based on differences in the assumed efficiencies (E) and while the lifetime of the panel was assumed to be 1-year.

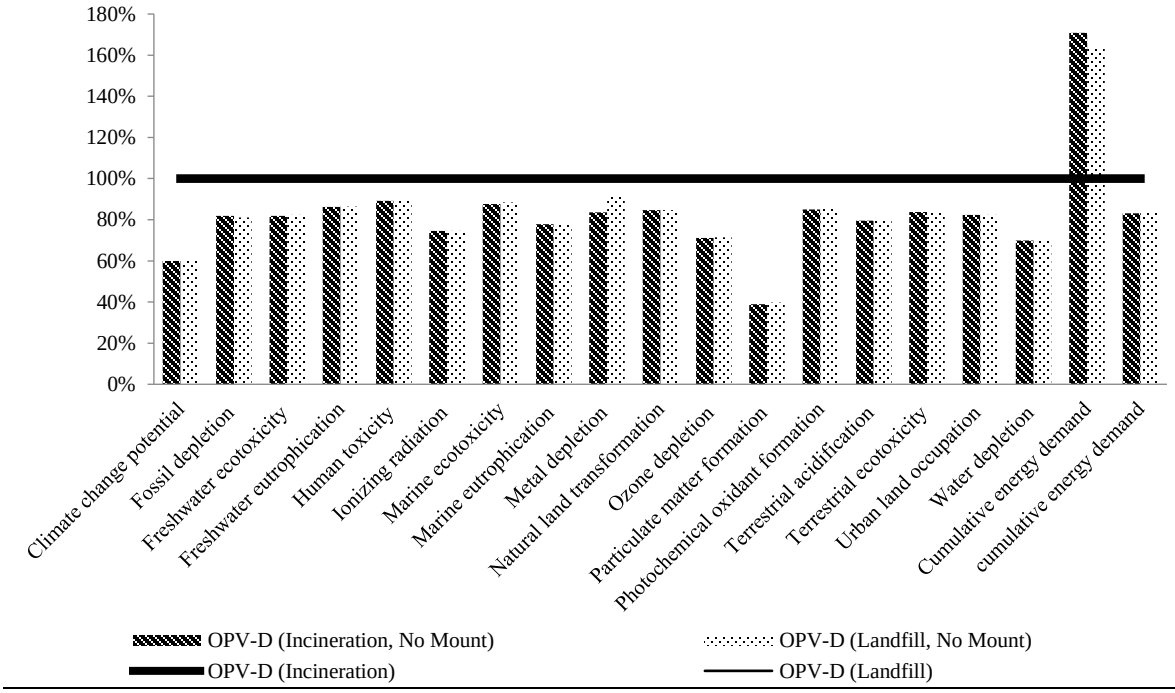

Figure A4-11 Comparison of OPV alternatives for S1 alternatives that involved removing the mounting structure. The impact results are all normalized by OPV-D per end-of-life option.

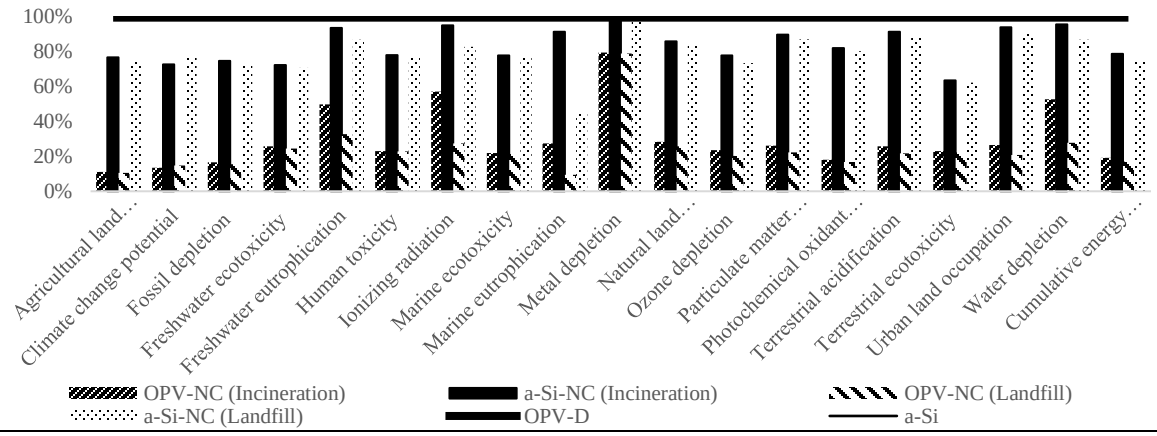

Figure A4-12 Comparison of S2 alternatives based on portable chargers without casing. The impact results in S2 are individually normalized by technology-type (i.e. OPV-NC is normalized by OPV-D and a-Si-NC is normalized by a-SI). NS: no casing materials.

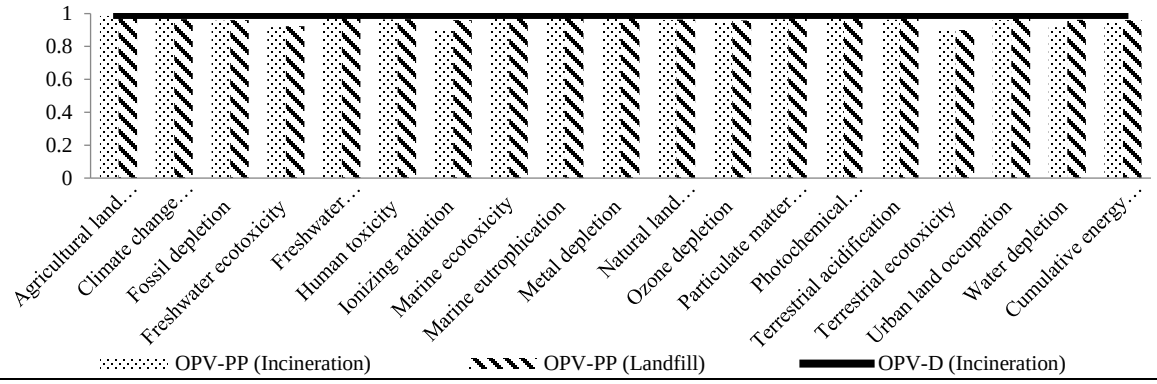

Figure A4-13 Comparison of S2 OPV alternatives based on the use of a copolymer instead of PCBM in the active layer of the solar cell.

Consumer-Adjusted EPBT Calculation for Portable Chargers

EPBTs for portable chargers will largely depend on the usage habits of the consumer (i.e. how frequently they are likely to use a portable charger compared to a fixed electrical outlet). A hypothetical situation is assumed involving a cell phone with charging specifications of 1.2 amp and 5 V. The power drawn from the charger was estimated as 6.00 W (Equation S1):

$$\text{Power} = (\text{Ampere}) \bullet (\text{Voltage}) \qquad \text{Eq. A4-1}$$

Further assumptions were made that the consumer would use the portable charger 5 times a week (i.e. 5 full charging cycles) with each charging cycle lasting 2 hours. This amounts to 520 charging hours per year. The amount of energy generated – analogous to the amount of energy avoided from a conventional charger – was estimated as 11.2 MJ per year (Equation S2):

$$\text{Energy Supplied by Charger} = (\text{Power}) \bullet (\text{Charging time per year})^{\dagger} \qquad \text{Eq. A4-2}$$

†Actual charging times will depend on the technical aspects of the panel. It is assumed that both the OPV and silicon panels have the same wattage and voltage ratings, where Charging Time = (Battery A-h) / (Charging Source Ampere Rating) and Charging Source Ampere = W / V.

The consumer-adjusted EPBTs are calculated using a ratio of the CED per functional unit to the Energy Supplied by Charger (Table 10).

Table A4-10 The consumer-adjusted EPBT, adjusted for consumer charging habits as described in the text.

	CED(MJ) / FU	**Energy Supplied by Charger (**MJ / year)	**Consumer-adjusted EPBT (years)**
OPV-D (Incineration)	58.7	11.2	5.32
OPV-D (Landfill)	70.9	11.2	6.30
a-Si (Incineration)	173	11.2	15.4
a-Si (Landfill)	184	11.2	16.3
a-Si-NC (Incineration)	136	11.2	12.1
a-Si-NC (Landfill)	137	11.2	12.2
OPV-NC (Incineration)	11.2	11.2	1.00
OPV-NC (Landfill)	11.9	11.2	1.03

Similarly, the CPBT should be calculated according to consumer charging patterns. The same assumptions were considered above and the energy generated by the charging unit was assumed to replace carbon emissions generated from a general European medium-voltage electricity mix (RER) as described in the methods of the main text (Table 11).

Table A4-11 The consumer-adjusted CPBT for S2, adjusted for consumer charging habits as described in the text.

	CO_2-eq. / FU	**Energy Supplied by Charger (**kWh / year)	**Avoided Carbon Emissions (kg CO_2-eq. / year)‖**	**Consumer-adjusted CPBT (years)**
OPV-D (Incineration)	4.27	3.11	1.51	2.82
OPV-D (Landfill)	3.52	3.11	1.51	2.32
a-Si (Incineration)	10.6	3.11	1.51	7.02
a-Si (Landfill)	10.2	3.11	1.51	6.68
a-Si-NC (Incineration)	7.71	3.11	1.51	5.08
a-Si-NC (Landfill)	7.79	3.11	1.51	5.16
OPV-NC (Incineration)	0.57	3.11	1.51	0.38
OPV-NC (Landfill)	0.52	3.11	1.51	0.34

‖ Estimated from an avoidance of 0.487 kg CO2-eq. per kWh calculated in Ecoinvent 2.2 for general production of medium-voltage electricity for an average European mix (RER)

Recycling Potential of Silicon PV Panels

Muller et al. previously reported potential reductions of 57% in the energy consumption for silicon wafer production when using recycled silicon wafers as the feedstock.[154] The CED for the production of 1m^2 of a m-Si wafer is 2,800 MJ. There are 7.6 m^2 of m-Si panels used in S1 (rooftop array) for a total of 21,280 MJ of energy consumed (assuming that the panel size is occupied 100% by wafers). Therefore, approximately 12,130 MJ of energy would be saved for the m-Si rooftop solar array if recycled silicon wafers were used. Fthenakis and Kim[151] estimate that it takes 0.34 MJ of energy to dismantle a kg of solar panels. A total of 88.08 kg of m-Si panels were used in S1, amounting in 29.9 MJ needed to dismantle those panels, reducing the potential energy savings to 12,101 MJ. This is a 49% reduction compared to the total CED of 24,621 that was calculated for the m-Si (incinerated) rooftop scenario.

Recycling Potential of OPV Panels

Espinosa et al. estimate that OPV panels could be delaminated using 14.76 MJ of electricity (mechanical delamination) per kg of panel processed.[62] This would amount to nearly 325 MJ consumed for the recovery of the PET. The assumption can be made that this is directly consumed in a secondary PET production process and that this process consumes only half of the energy (1066 MJ) of primary production for the 13 kg of PET consumed in the functional unit, just for illustration, then a total 858 MJ (208 MJ savings) of energy would be consumed in order to recycle the PET.

Appendix: Chapter 6

Table A6-1 Toxicological data used to calculate the non-carcinogenic dose-response data

Dose mg/m3	Diameter (nm)	Species	BAL Cell Sample Size	Macrophages (%)	Macrophages (Count)	Neutrophil (%)	Neutrophil (Count)
0	21	M	200	0.99	198	0	0
0	21	M	200	1	200	0	0
0	21	M	200	0.99	198	0	0
0	21	M	200	1	200	0	0
0	21	M	200	1	200	0	0
0.5	21	M	200	0.995	199	0	0
0.5	21	M	200	1	200	0	0
0.5	21	M	200	0.995	199	0	0
0.5	21	M	200	0.99	198	0	0
0.5	21	M	200	1	200	0	0
2	21	M	200	0.995	199	0.005	1
2	21	M	200	1	200	0	0
2	21	M	200	1	200	0	0
2	21	M	200	0.995	199	0.005	1
2	21	M	200	1	200	0	0
10	21	M	200	0.8	160	0.195	39
10	21	M	200	0.865	173	0.125	25
10	21	M	200	0.915	183	0.07	14
10	21	M	200	0.775	155	0.21	42
10	21	M	200	0.875	175	0.125	25
0	21	R	200	1	200	0	0
0	21	R	200	0.995	199	0.005	1
0	21	R	200	1	200	0	0
0	21	R	200	0.99	198	0.01	2
0	21	R	200	0.99	198	0.005	1
0.5	21	R	200	0.995	199	0.005	1
0.5	21	R	200	0.985	197	0.01	2
0.5	21	R	200	0.99	198	0.005	1
0.5	21	R	200	0.99	198	0.005	1
0.5	21	R	200	1	200	0	0
2	21	R	200	0.91	182	0.085	17
2	21	R	200	0.97	194	0.03	6
2	21	R	200	0.96	192	0.035	7
2	21	R	200	0.87	174	0.13	26
2	21	R	200	0.95	190	0.045	9
10	21	R	200	0.235	47	0.73	146
10	21	R	200	0.4	80	0.585	117
10	21	R	200	0.365	73	0.625	125
10	21	R	200	0.315	63	0.66	132
10	21	R	200	0.35	70	0.64	128
0	21	H	200	0.965	193	0.02	4
0	21	H	200	0.955	191	0.025	5
0	21	H	200	0.995	199	0.005	1
0	21	H	200	0.965	193	0.03	6
0	21	H	200	0.93	186	0.035	7
0.5	21	H	200	0.945	189	0.015	3
0.5	21	H	200	0.975	195	0.015	3
0.5	21	H	200	0.955	191	0.005	1
0.5	21	H	200	0.99	198	0.005	1
0.5	21	H	200	0.905	181	0.025	5
2	21	H	200	0.985	197	0.005	1

2	21	H	200	0.98	196	0	0
2	21	H	200	0.97	194	0.015	3
2	21	H	200	0.85	170	0.02	4
2	21	H	200	0.97	194	0.01	2
10	21	H	200	0.88	176	0.06	12
10	21	H	200	0.92	184	0.065	13
10	21	H	200	0.965	193	0.02	4
10	21	H	200	0.635	127	0.36	72
10	21	H	200	0.985	197	0.005	1

Extrapolation factors used in dose-response modeling

Deterministic risk assessment procedures generally utilize single-point uncertainty factors such as interspecies extrapolation factors of 10. These values are meant to provide conservative and strongly protective regulatory exposure limits. To translate this stochastically, distributions for both an interspecies and intraspecies extrapolation factor were defined. Assumptions were made that these values would be log-normally distributed such that values of 10 were one-order of magnitude greater than the mean and occur at the 99th-percentile. In this way, the protective yet conservative nature of these factors was conserved in the approach.

Results of the dose-response modeling of macrophage percent cell changes[283] using PROAST software

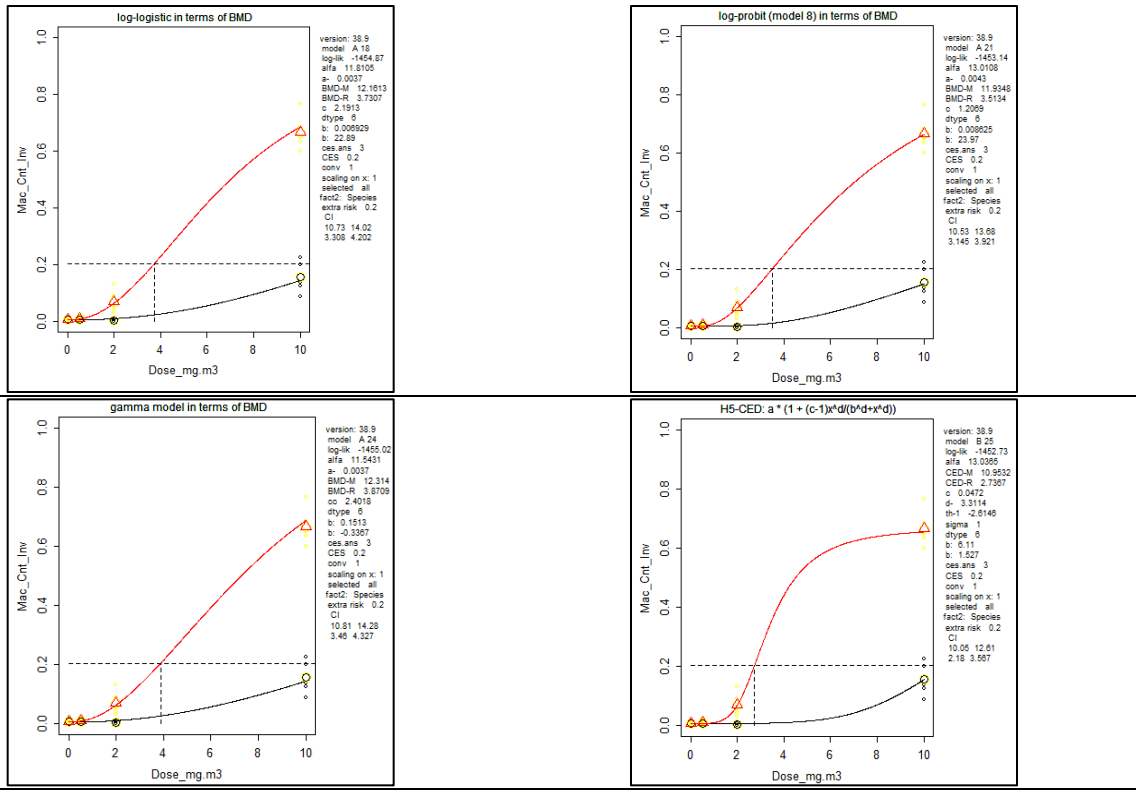

Figure A6-1 Results for quantal analysis of percent change in macrophages for mice and rats as a potential covariate to the y-intercept (variable "a") and slope (variable "b"). Note that the response is an inverse of the actual change (i.e. macrophage counts actually decreased, and the inverse was necessary to calculate the dose-response curves in PROAST. The benchmark response was set at 20% and analysis based on species covariation.

Table A6-2 Fitted models to the dose-response macrophage data[283] with rats and mice as a possible covariate

Model	Covariation	npar	Log-likelihood	Accept	BMC	BMCL	BMCU

null	NA	2	-1501.87	--	NA	NA	NA
full	NA	9	-1450.83	--	NA	NA	NA
two-stage	b	5	-1457.2	no	4.22	NA	NA
log-logist	b	5	-1454.87	yes	3.73	3.31	4.2
Weibull	b	5	-1456.78	no	4.15	NA	NA
log-prob	b	5	-1453.14	yes	3.51	3.14	3.92
gamma	b	5	-1455.02	yes	3.87	3.46	4.33
LVM: E3-	a	5	-1465.47	no	4.44	NA	NA
LVM: H5-	b	6	-1452.73	yes	2.74	2.18	3.57

BMR: 0.2 Extra Risk
P-value (goodness-of-fit): 0.05

Neutrophil Data

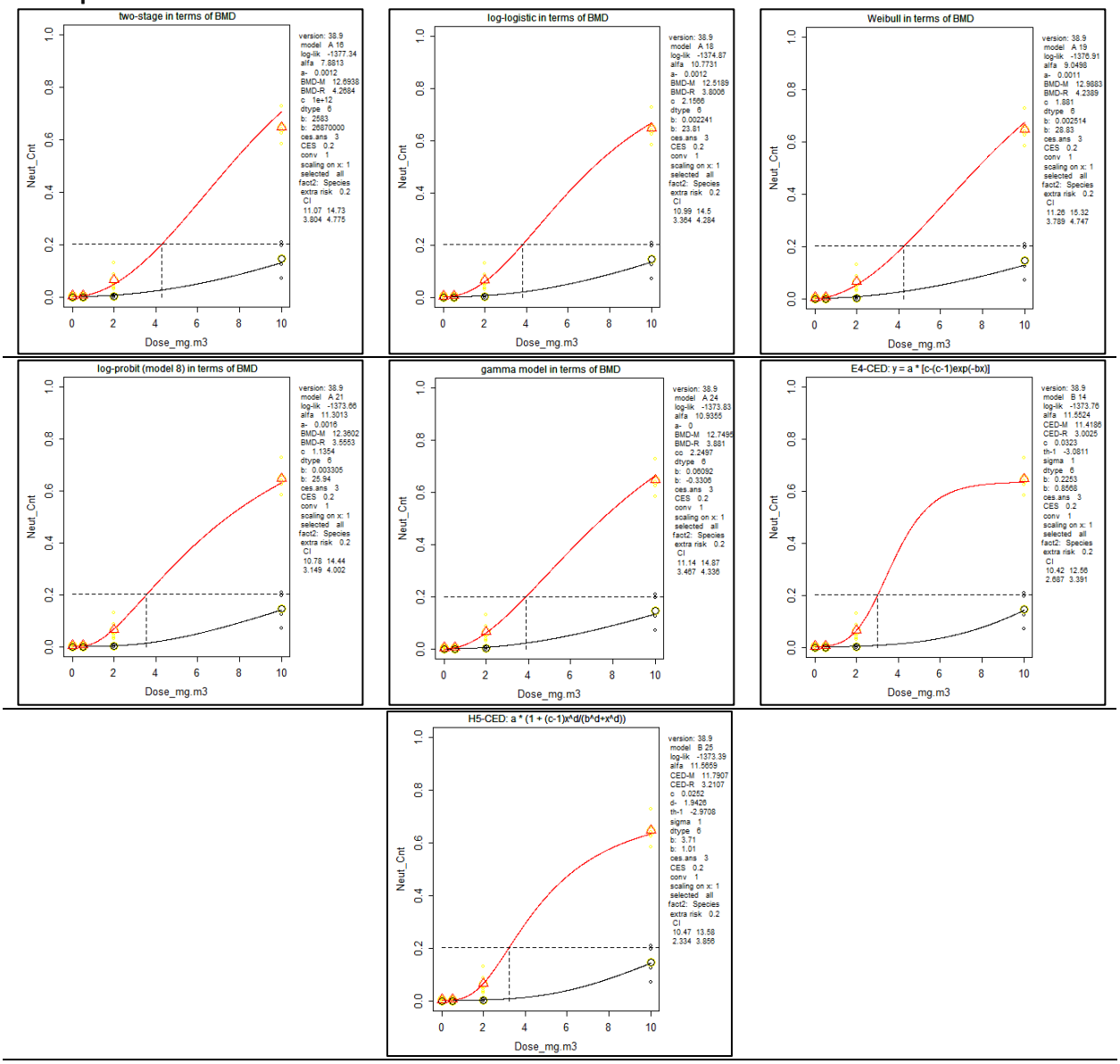

Figure A6-2 Results for quantal analysis of percent change in neutrophil for mice and rats as a potential covariate to the y-intercep (variable "a") and slope (variable "b"). Note that the response is an inverse of the actual change (i.e. macrophage counts actually decreased, and the inverse was necessary to calculate the dose-response curves in PROAST. The benchmark response was set at 20% and analysis based on species covariation.

Table A6-3 Fitted models to the dose-response neutrophil data[283] with rats and mice as a possible covariate

Model	Covariation	npar	Log-likelihood	Accept	BMC	BMCL	BMCU
null	NA	2	-1420.53	--	NA	NA	NA
full	NA	9	-1370.09	--	NA	NA	NA
two-stage	ab	6	-1373.14	yes	4.37	4	4.9
log-logist	ab	6	-1370.87	yes	3.89	3	4.39
Weibull	ab	6	-1373.02	yes	4.34	4	4.87
log-prob	ab	6	-1368.35	yes	3.64	3	4.05
gamma	ab	6	-1370.84	yes	4.02	4	4.51
LVM: E4-	a	5	-1371.54	yes	3.48	NA	NA
LVM: H5-	a	6	-1369.86	yes	3.21	3	3.39

BMR: 0.2 Extra Risk
P-value (goodness-of-fit): 0.05

Summary Statistics of the Mice Data

Four valid mathematical models were fit to the mice macrophage dose-response data whose bootstrap summary statistics are listed in Table ##. The four distributions were aggregated into a single description of the BMC_a that was normally distributed with a mean and standard deviation of 11.9 mg/m^3 and 1.1, respectively. For mice, there were 7 valid mathematical models that fit neutrophil dose-response data (Table ##). The summary statistics for the bootstrap results of each model are displayed in Table ##. The distributions for each model were aggregated into a single normal distribution defined by a mean and standard deviation of 12.44 mg/m^3 and 1.2, respectively.

Table A6-4 BMC_a results (**mg/m3)** and models fit for a 20% increase in neutrophil count in mice dose-response data.

Model	Two-Stage	Log-logistic	Weibull	Log-probabilistic	Gamma	EXP4	Hill5	Aggregation of Models
Median	4.26	3.81	4.25	3.56	3.89	3.00	3.17	**3.76**
Mean	4.28	3.82	4.26	3.57	3.90	3.02	3.11	**3.71**
Standard Deviation	0.29	0.27	0.29	0.24	0.25	0.21	0.49	**0.56**
Minimum	3.26	2.99	3.38	2.84	3.03	2.42	2.11	**2.11**
Maximum	5.48	5.17	5.54	4.69	5.08	4.24	4.58	**5.54**

Table A6-5 BMC_a results (**mg/m3)** and models fit for a 20% change in macrophage count in mice dose-response data.

Model	Log-Log	Log-probabilistic	Gamma	Hill5	Aggregation of Models
Median	4.26	3.81	4.25	3.56	3.89
Mean	4.28	3.82	4.26	3.57	3.90
Standard Deviation	0.29	0.27	0.29	0.24	0.25
Minimum	3.26	2.99	3.38	2.84	3.03
Maximum	5.48	5.17	5.54	4.69	5.08

Summary Results of the Rat Macrophage Data

Four valid mathematical models were (Table ##) fit to the rat macrophage data with a BMC_a that was normally distributed with a mean and standard deviation of 3.47 mg/m^3 and 0.56.

Table A6-6 BMC_a results (**mg/m^3)** and models fit for a 20% change in macrophage count in rat dose-response data.

Model	Log-Log	Log-probabilistic	Gamma	Hill5	Aggregation of Models
Median	3.73	3.52	3.87	2.66	**3.60**
Mean	3.74	3.53	3.89	2.73	**3.47**
Standard Deviation	0.26	0.23	0.25	0.50	**0.56**
Minimum	2.94	2.74	3.06	2.12	**2.12**
Maximum	4.88	4.62	5.01	4.48	**5.01**

Exposure Section

Currently, monitoring data on ENM-emission characteristics and/or source strengths are slowly emerging for some nano-TiO_2 occupational ES, such as powder handling[199,242,323] and simulated sanding[372,373]. However, most current measurement devices are unable to distinguish ENMs from background natural or incidental nano aerosols[374]. Although there are powerful instruments available to measure actual workplace concentrations to ENMs[199,312,366], such options are not always available due to technical and logistical challenges. When this is the case, risk assessors can use models. To demonstrate the feasilbilty of using models to estimate workplace exposure to ENMs, the exposure assessment was completed using an interim, un-released update to the NanoSafer 1.0 control banding exposure algorithm, titled NanoSafer v1.1_β. Version 1.1_β uses a two-box aerosol model to assess near-field (NF) and far-field (FF) maximum potential exposure without taking into account localized or personal exposure controls[375] (Table ##). For each exposure scenario, a total work-room volume equal to the combined volume of the NF (V_{NF}) and FF (V_{FF}) was defined, where the NF was always defined as 12.17 m^3 and the minimum value of V_{total} has been set to 38 m^3. The emission source, E_i (mg/min) is described as

Regression Analysis: LOG(SD) versus LOG(DI)$_{resp}$

The results of 59 particulate powder case tests used to determine the correlation between their dustiness index and standard deviations. Note that 3 cases contained missing values.

Table A6-7 Statistical Parameters and Least Squares Summary

Predictor	Coefficient	Standard Error (SE) of the Coefficient	T-statistic	P-value
Constant	-0.625	0.211	-2.96	0.004
LOG(DI)resp	0.8714	0.0822	10.61	0.000

Standard Deviation of the Error Terms = 0.511187 R^2 = 66.4% R^2(adjusted) = 65.8%

Table A6-8 Analysis of variance parameters and results for the hypothesis that beta = 0

Source	Degrees of Freedom (*df*)	Sum of Squares (SS)	Mean Squared Value (MS)	F-statistic	P-value
Regression	1	29.40	29.40	112.49	0.000
Residual Error	57	14.90	0.26		
Total	58	44.29			

Table A6-9 Unusual observations found in the regression

Observation	LOG(DI)resp	LOG(SD)	Fit	SE Fit	Residual	St Resid
56	3.74	14.91	26.34	0.126	-11.43	-2.31 R
57	3.78	11.76	26.66	0.129	-14.90	-3.01 R
59	3.78	14.15	26.71	0.129	-12.56	-2.54 R
62	4.84	37.22	35.89	0.208	0.132	0.28 X

R denotes an observation with a large standardized residual.
X denotes an observation whose X value gives it large leverage.

Results of the Emissions Distributions

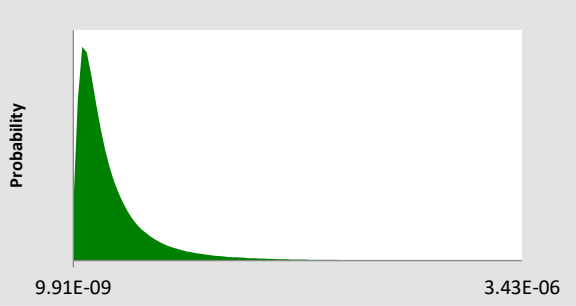

ES1

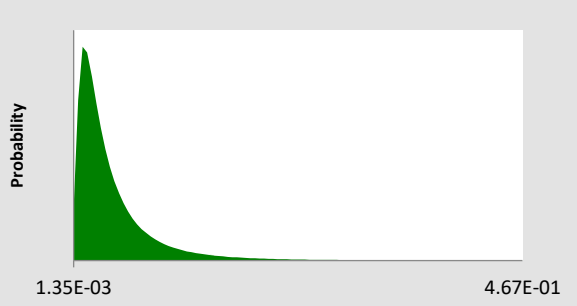

ES2

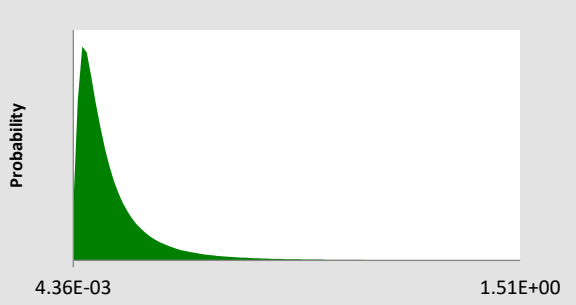

ES3

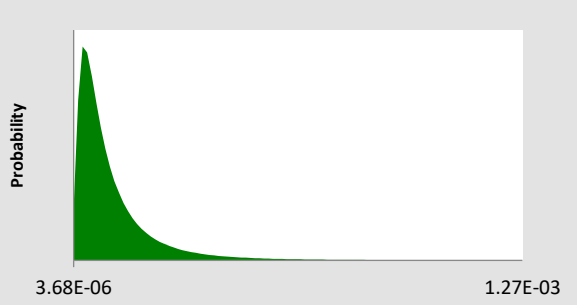

ES4

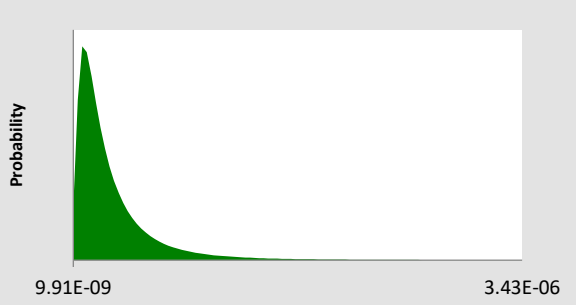

ES5

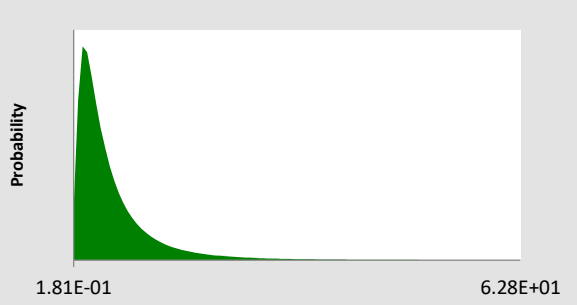

ES6

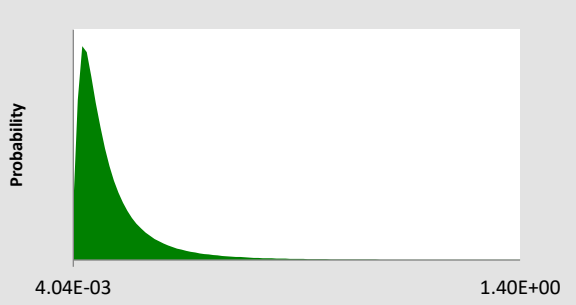

ES7

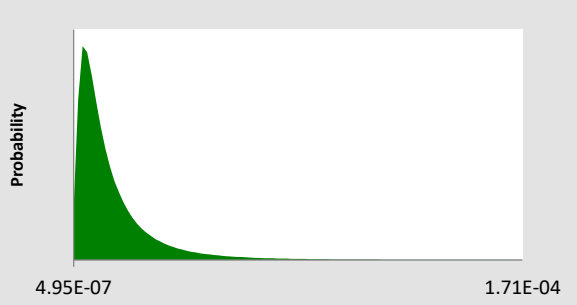

ES8

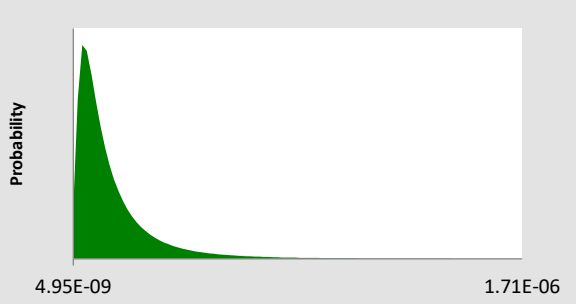

ES9

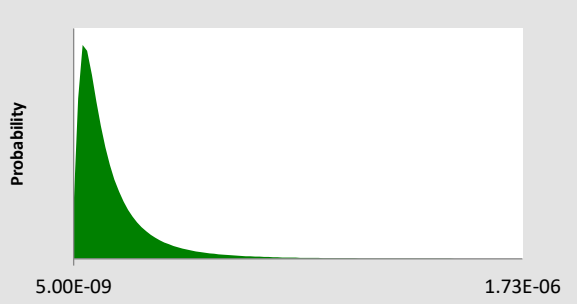

ES10

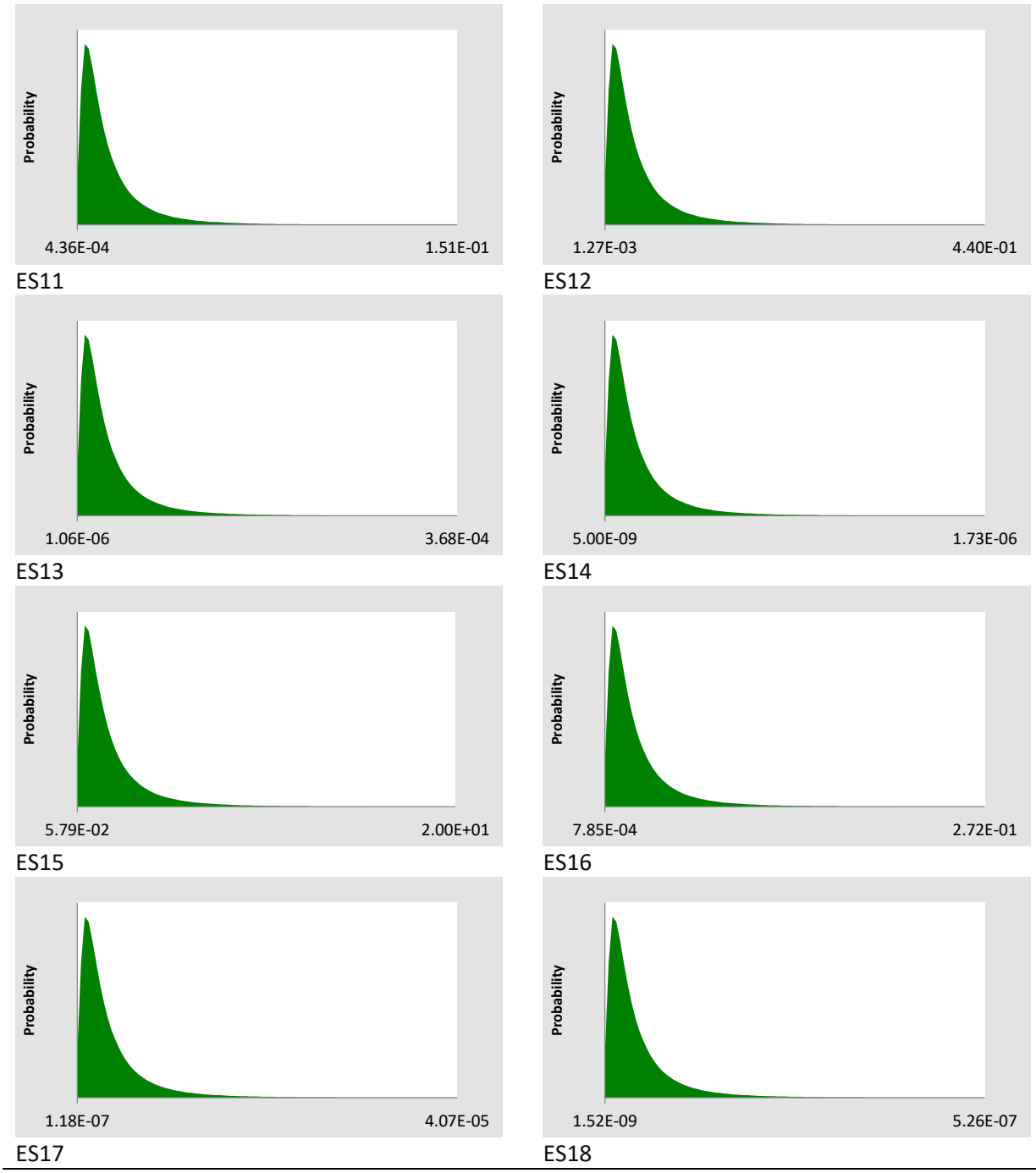

Figure A6-3 Distributions of the exposure concentrations (mg/m^3) per exposure scenario

Results: Monte Carlo simulations for the risk characterization ratios

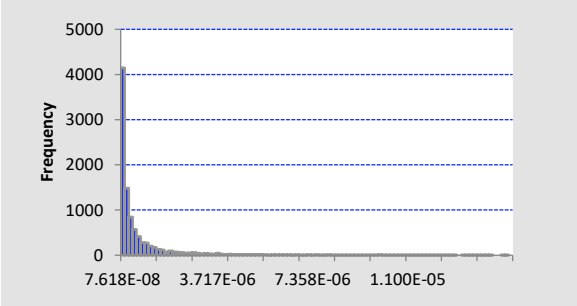

ES1

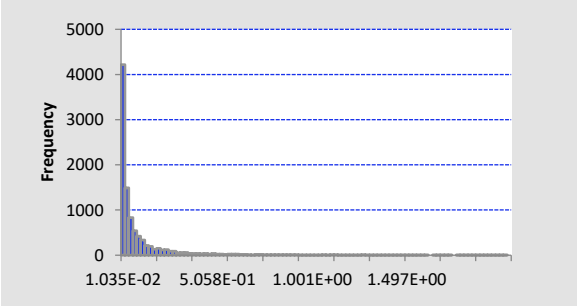

ES2

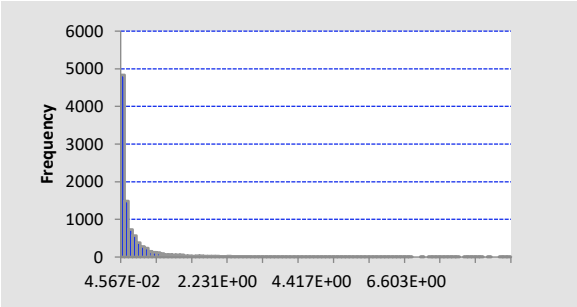

ES3

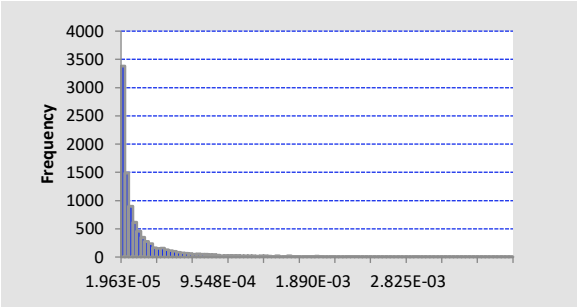

ES4

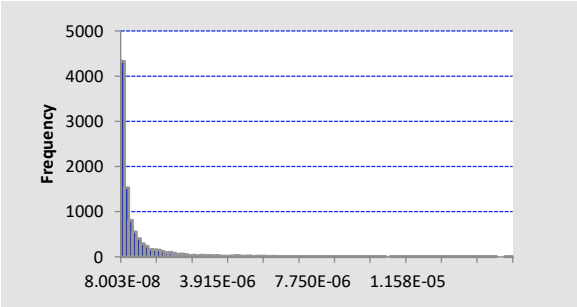

ES5

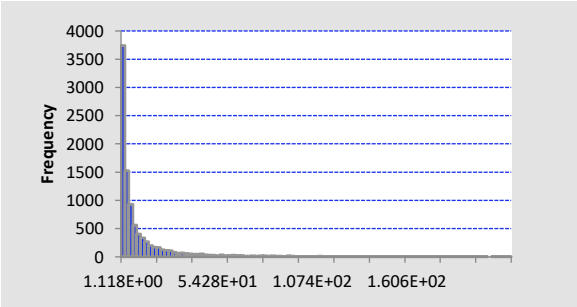

ES6

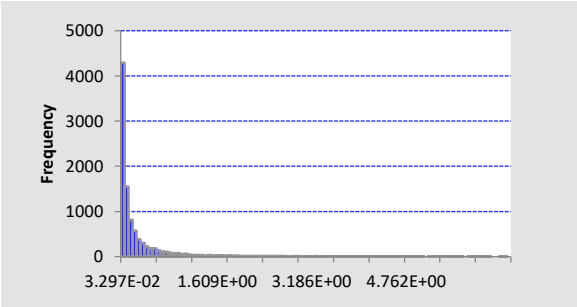

ES7

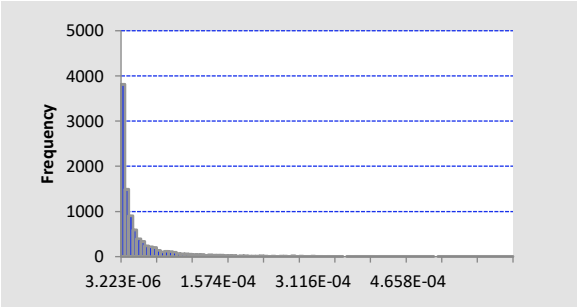

ES8

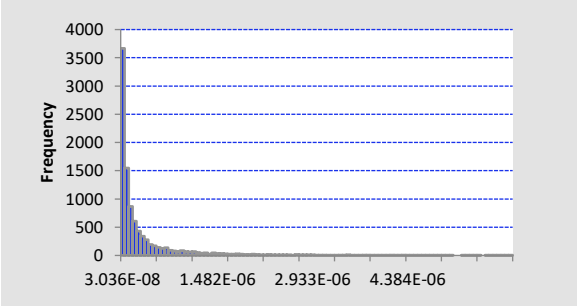

ES9

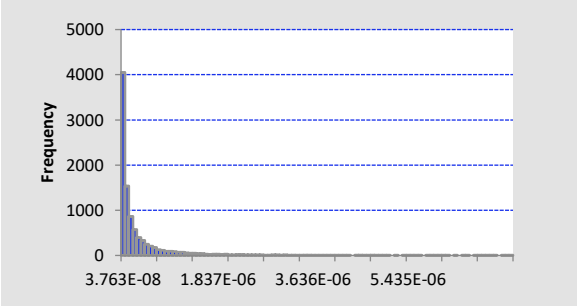

ES10

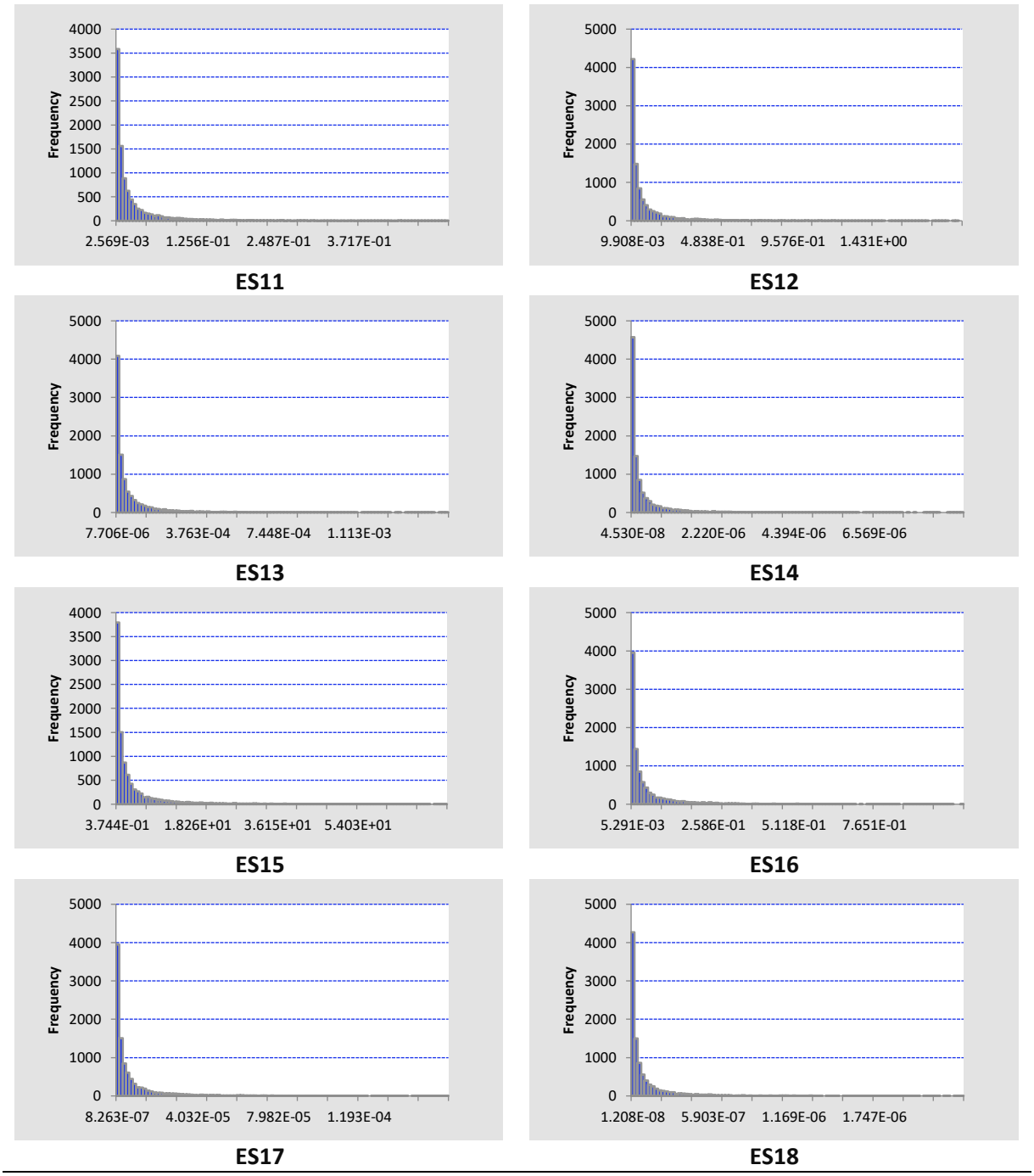

Figure A6-4 Results of the monte carlo simulations for estimating the benchmark dose response in humans (BMC_h). The y-axis represents the number of monte-carlo simulations and the x-axis is a unitless dimension of risk, whereby the existence of risk is any value ≥ to 1.

Global Sensitivity Analysis: Risk Characterization Results

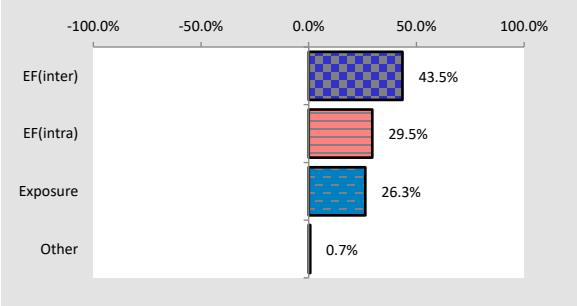

ES1

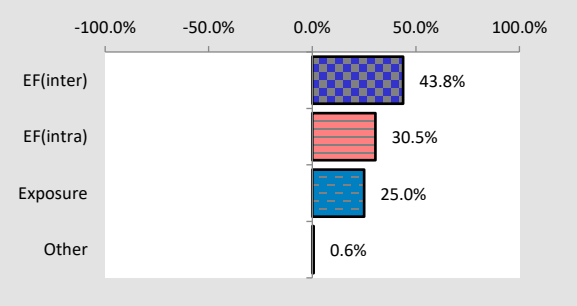

ES2

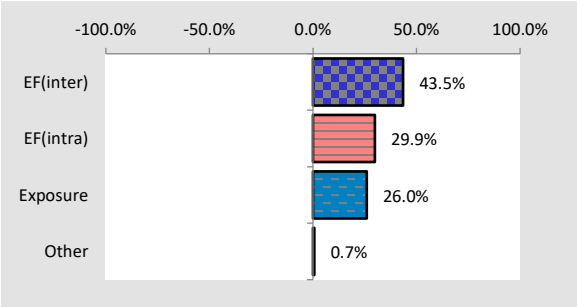

ES3

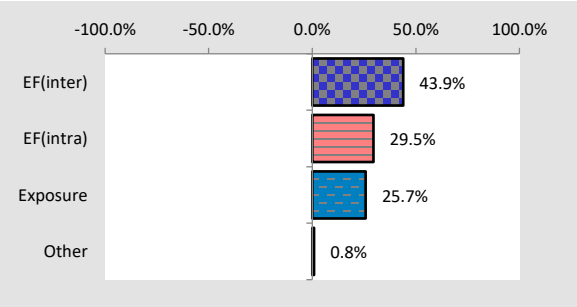

ES4

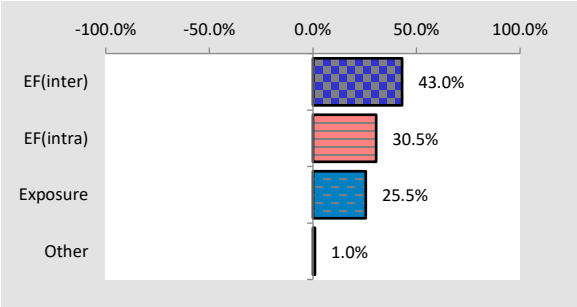

ES5

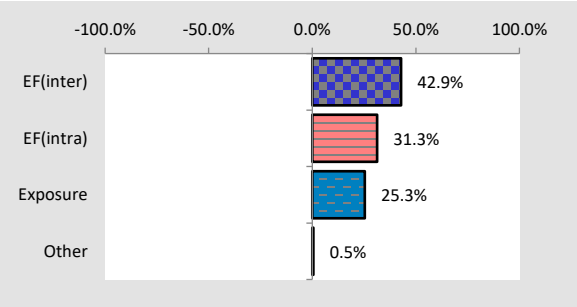

ES6

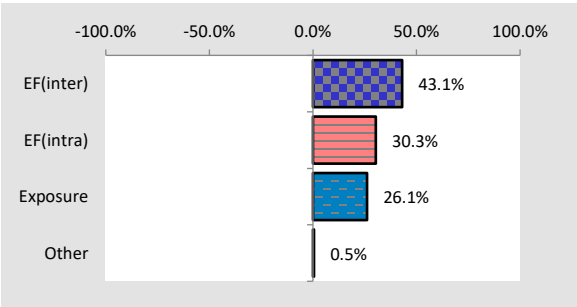

ES7

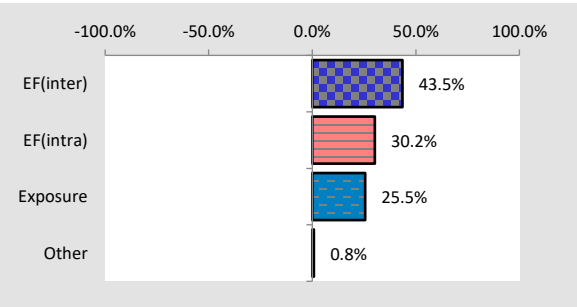

ES8

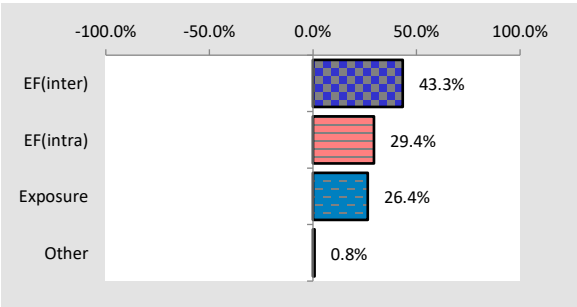

ES9

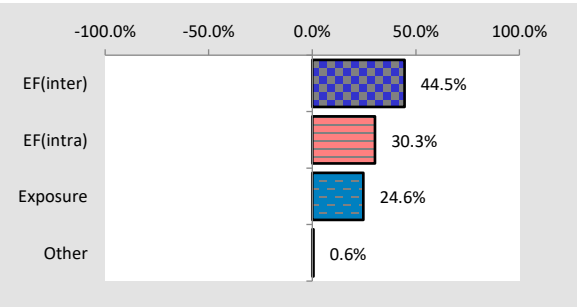

ES10

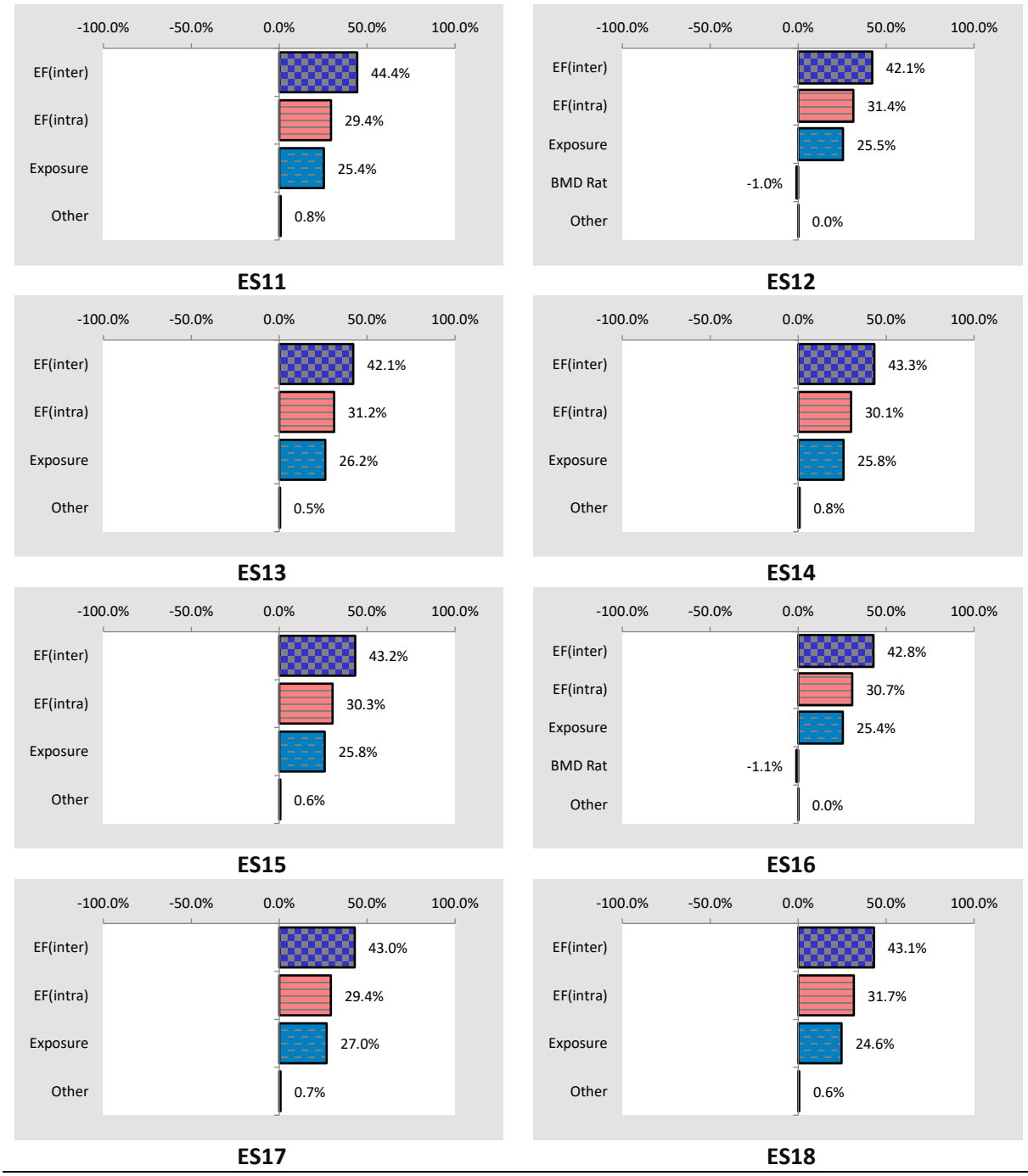

Figure A6-5 Results of the global sensitivity analysis that provide the percent contribution (x-axis) of each parameter that was used in estimating the risk characterization ratio. EF(inter): extrapolation factor used to extrapolate the BMCanimal to BMChuman. EF(intra): extrapolation factor used to extrapolate between different persons in the human population. Exposure: the resulting nano-TiO_2 concentrations per exposure scenario.

Appendix: Chapter 7

Results for the fate and transport models in terms of their regression during periods of emission and non-emission cycles for each exposure scenario are displayed in Figure A7-1.

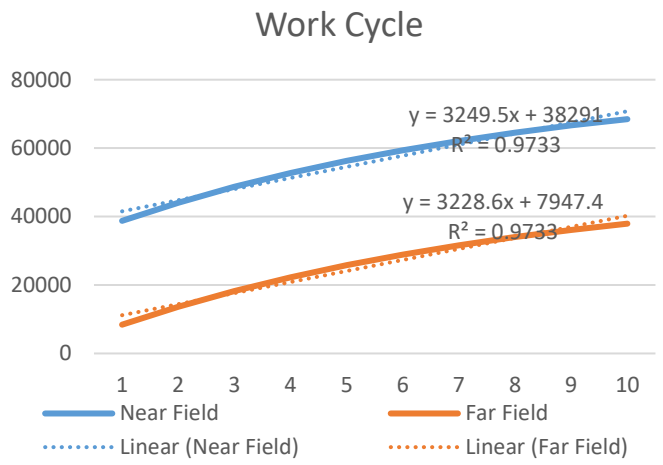

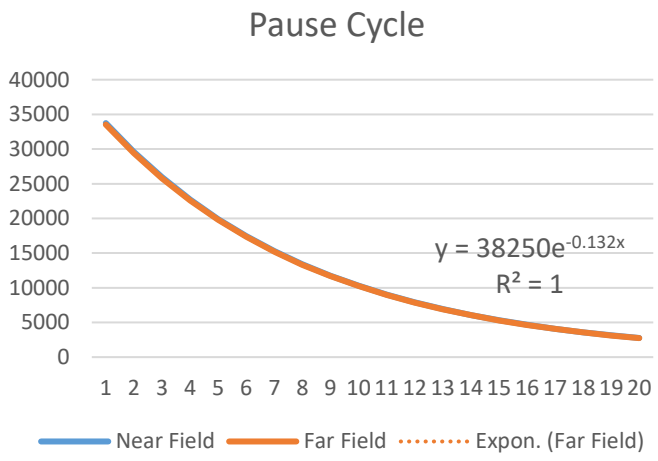

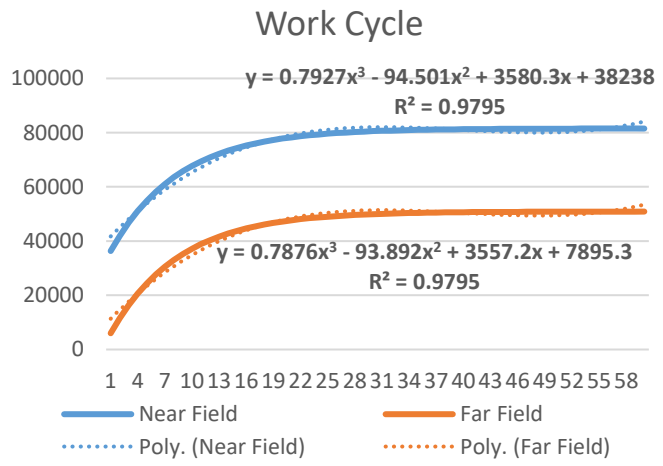

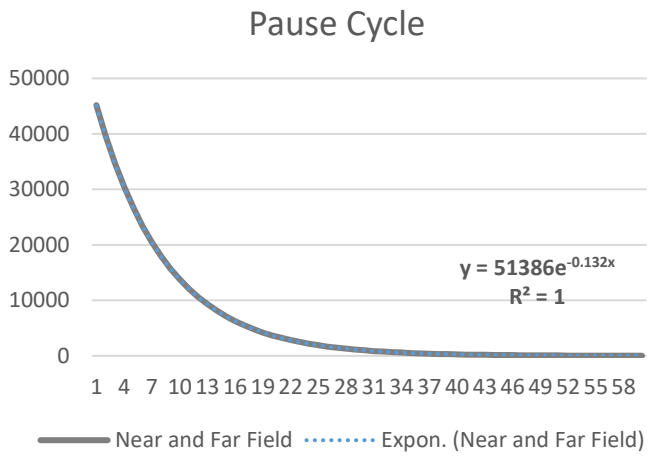

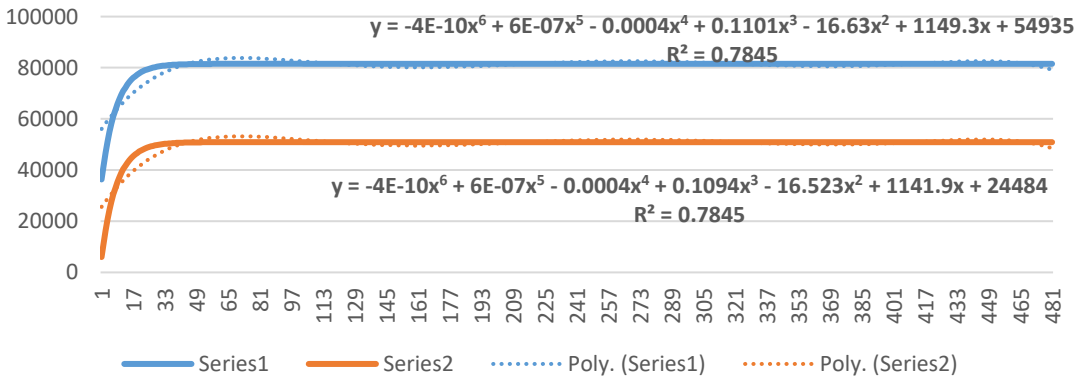

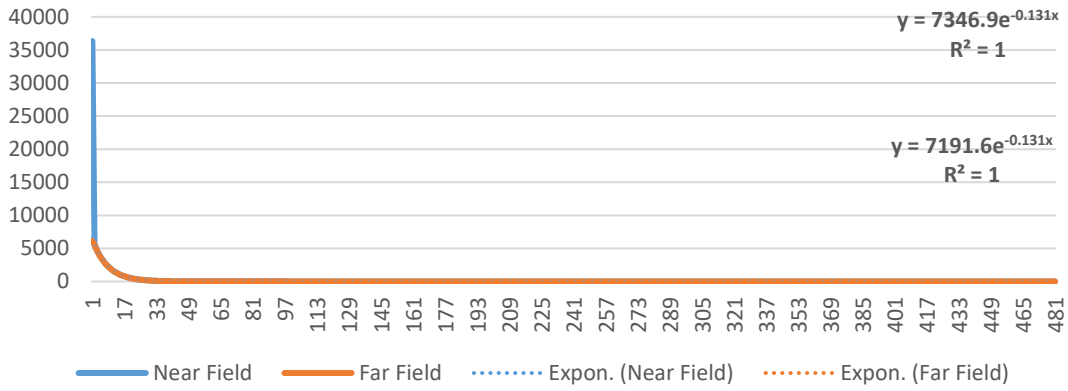

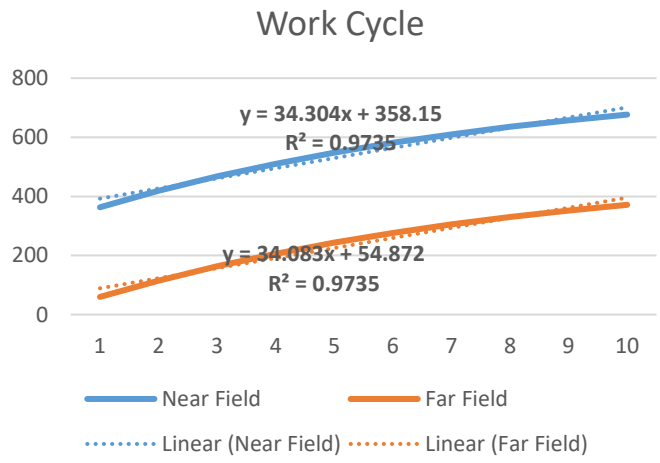

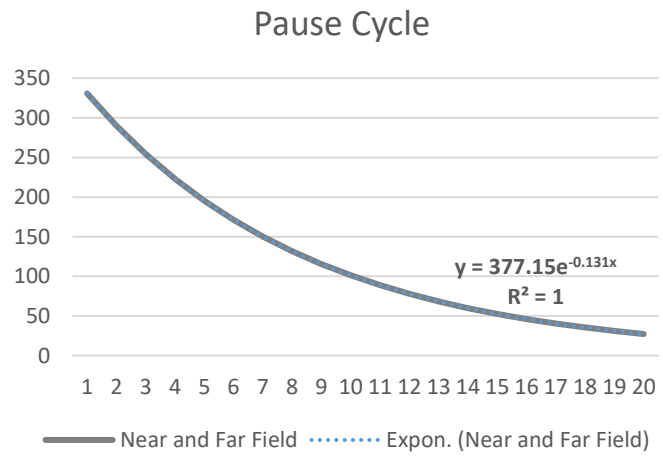

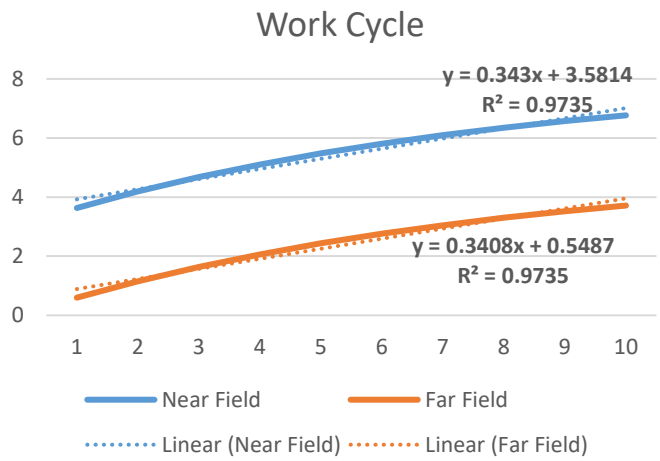

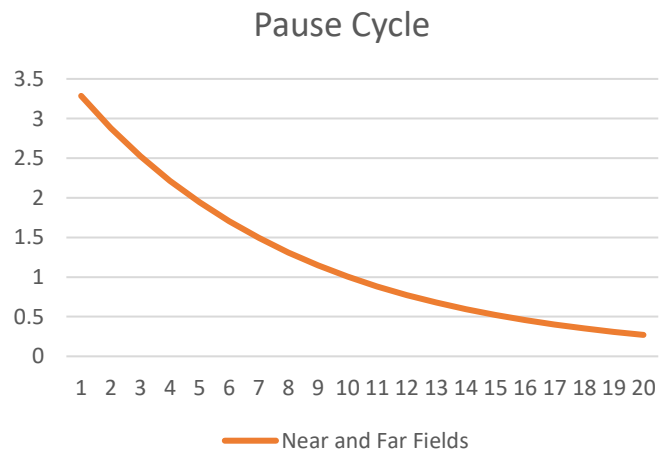

Figure A7-1 Trends in the airborne nano-TiO2 concentrations during emission events and non-emission events for ES1-ES6 corresponding with rows 1-6. Results are specific for the default scenarios involving 21 nm nano-TiO2.

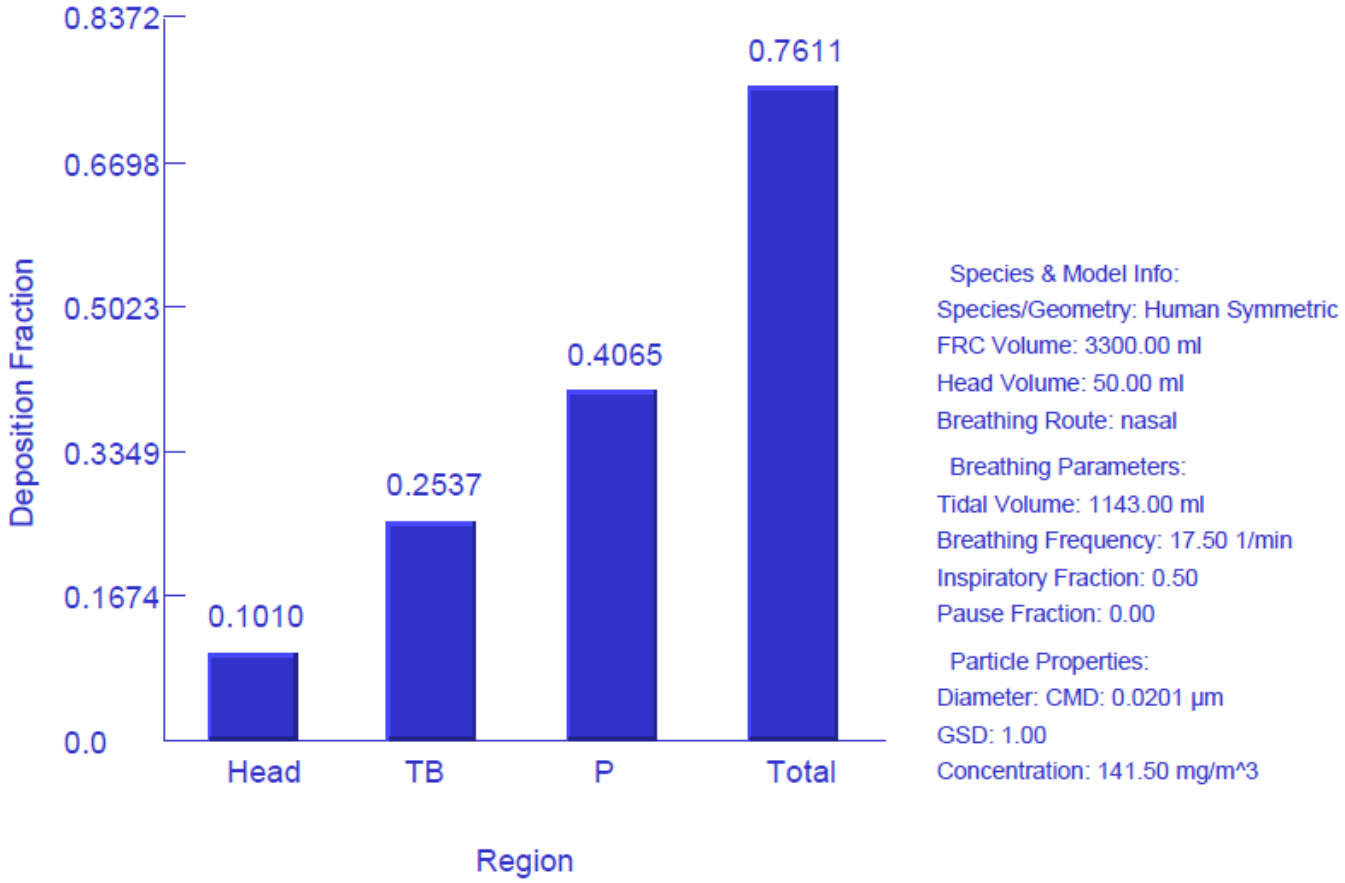

Figure A7-2 Deposition of the 21 nm nano-TiO2 in the human lung as calculated using the MPPD model

Table A7-1 Parameters and their values for operating the PBPK exposure model. These parameters are part of a larger model and set of code that is available upon request.

ENM-specific Parameters	
CLEu = 0.0543	clearance rate to urine from blood in kidneys, Li et al., 2016 - 1/min
CLEfl = 2.53e-4	clearance rate to feces from liver, Li et al., 2016 - 1/min
CLEfgi = 2.35e-3	clearance rate to feces from GI tract, Li et al., 2016 - 1/min
kuagi = 5.58e-3	clearance rate from upper airway region, Li et al., 2016 - 1/min
kab0 = 18.8	maximum uptake rate by phagocytizing cells, Carlander et al., 2016 - 1/min
ksab0 = 0.126	maximum uptake rate by phagocytizing cells in spleen, Carlander et al., 2016 - 1/min
kde = 8.83e-21	desorption rate by phagocytizing cells, Li et al., 2016 - 1/min
kuabr = 1.39e-6	transport factor from upper airway region to brain via the olfactory bulb, Li et al., 2016 - 1/min
kpulmtra = 1.44e-6	transport factor from inactive pulmonary phagocytizing cells to tracheobronchial region, Li et al., 2016 - 1/min
ktragi = 9.2e-5	transport factor from tracheobronchial region to GI tract, Li et al., 2016 - 1/min
kgiab = 9.02e-5	absorption rate of GI tract, Li et al., 2016 - 1/min
kluip =1.87e-8	transfer rate from interstitium of lungs to pulmonary region, Li et al., 2016 - 1/min
klupi = 2.1e-3	transfer rate from pulmonary region to interstitium of lungs, Li et al., 2016 - 1/min
Mcap = 1.21e-6	maximum uptake capacity in individual phagocytizing cells, Carlander et al., 2016 - ug
Nbloodcap = 0.185*1e+4	number of phagocytizing cells per gram blood weight, Carlander et al., 2016 - 1/g
Nscap = 2.08*1e+8	number of phagocytizing cells per gram immunology organs weight, Carlander et al., 2016 - 1/g
Nlcap = 2.72*1e+7	number of phagocytizing cells per gram liver weight, Carlander et al., 2016 - 1/g
Nlucap = 2.69*1e+6	number of phagocytizing cells per gram lungs weight, Carlander et al., 2016 - 1/g
Nbrcap = 3.06*1e+5	number of phagocytizing cells per gram brain weight, Carlander et al., 2016 - 1/g

Nhcap = 0.076*1e+6	number of phagocytizing cells per gram heart weight, Carlander et al., 2016 - 1/g
Nkcap = 0.99*1e+5	number of phagocytizing cells per gram kidneys weight, Carlander et al., 2016 - 1/g
Nrestcap = 8.11*1e+6	number of phagocytizing cells per slowly perfused tissue weight, Carlander et al., 2016 - 1/g
Npulcap = 3.90*1e+6	number of phagocytizing cells per pulmonary weight, Li et al., 2016 - 1/g
Ngicap = 0.506*1e+6	number of phagocytizing cells per GIT weight, Li et al., 2016 - 1/g
Mbloodcap=Mcap * Nbloodcap	maximum uptake capacity in phagocytic cells per blood weight - ug/g
Mscap=Mcap * Nscap	maximum uptake capacity in phagocytic cells per spleen weight - ug/g
Mlcap=Mcap * Nlcap	maximum uptake capacity in phagocytic cells per liver weight - ug/g
Mlucap=Mcap * Nlucap	maximum uptake capacity in phagocytic cells per lung weight - ug/g
Mbrcap=Mcap * Nbrcap	maximum uptake capacity in phagocytic cells per brain weight - ug/g
Mhcap=Mcap * Nhcap	maximum uptake capacity in phagocytic cells per heart weight - ug/g
Mkcap=Mcap * Nkcap	maximum uptake capacity in phagocytic cells per kidney weight - ug/g
Mrestcap=Mcap * Nrestcap	maximum uptake capacity in phagocytic cells per carcass weight - ug/g
Mpulcap =Mcap * Npulcap	maximum uptake capacity in phagocytic cells per pulmonary weight - ug/g
Mgicap = Mcap * Ngicap	maximum uptake capacity in phagocytic cells per GIT weight - ug/g
P = 0.974	partition coefficient tissue:blood, Carlander et al., 2016 - unitless
Xrich = 0.126	permeability coefficient from blood to richly perfused tissue, Carlander et al., 2016 - unitless
Xbr = 1.92e-6	permeability coefficient from blood to brain tissue, Carlander et al., 2016 - unitless
Xrest = 2.13e-5	permeability coefficient from blood to rest of the body, Carlander et al., 2016 - unitless
frbr=0.371	fraction of capillary blood remained in brain when measured, Li et al., 2016 - unitless
fro=0.144	fraction of capillary blood remained in other organs when measured, Li et al., 2016 - unitless
delaygi = 112.8	time delay for nanoparticles to travel from respiratory system to GI tract, Li et al., 2016 - min
delayf = 474	time delay for nanoparticles in feces be excreted out, Li et al., 2016 - min
Human physiologic parameters	
BW = 75000	body weight for workers, assumption of higher % of male in this specific workforce - g
Qtot = IF work=1 THEN 25000 ELSE 5000	cardiac output, heavy excercise, literature - mL/min
Ws = 169.25	weight of spleen, literature - g
Wgi = 2265	weight of GI tract, literature - g
Wl = 1463.5	weight of liver, literature - g
Wlu = 984	weight of lungs, literature - g
Wbr = 1342.9	weight of brain, literature - g
Wh = 288.6	weight of heart, literature - g
Wk = 314.375	weight of kidneys, - g
Wblood = Wbloodt-Wsb-Wgib-Wlb	weight of arterial and venous blood, literature - g
Wbloodt = 0.07*BW	weight of total blood, literature - g
Wrest = BW-Ws-Wgi-Wl-Wlu-Wbr-Wh-Wk-Wbloodt	weight of rest of the body, literature - g
Wsb = 0.22*Ws	weight of blood in spleen, from literatures for rat - g
Wgib = 0.1*Wgi	weight of blood in GI tract, estimated - g
Wlb = 0.21*Wl	weight of blood in liver, from literatures for rat - g
Wlub = 0.36*Wlu	weight of blood in lungs, estimated - g
Wbrb = 0.03*Wbr	weight of blood in brain, values from literatures for rat - g
Whb = 0.26*Wh	weight of blood in heart, values from literatures for rat - g
Wkb = 0.16*Wk	weight of blood in kidneys, values from literatures for rat - g
Wrestb = 0.017*Wrest	weight of blood in rest of the body, values from literatures for rat - g
fQs = 0.03	fraction of cardiac output to spleen, literature - unitless
fQgi = IF workingday*workinghour=1 THEN 0.05 ELSE 0.2	fraction of cardiac output to GI tract, leterature - unitless
fQl = IF workingday*workinghour=1 THEN 0.11 ELSE 0.25	fraction of cardiac output to liver, literature - unitless
fQbr = IF workingday*workinghour=1 THEN 0.04 ELSE 0.15	fraction of cardiac output to brain, literature - unitless
fQh = 0.05	fraction of cardiac output to heart, literature - unitless
fQk = IF workingday*workinghour=1 THEN 0.04 ELSE 0.20	fraction of cardiac output to kidneys, literature - unitless
fQrest = 1-fQs-fQgi-fQl-fQbr-fQh-fQk	fraction of cardiac output to rest of the body, literature - unitless
Qs = fQs*Qtot	blood flow to spleen - mL/min
Qgi = fQgi*Qtot	blood flow to GI tract - mL/min

Ql = fQl*Qtot	blood flow to liver - mL/min
Qbr = fQbr*Qtot	blood flow to brain - mL/min
Qh = fQh*Qtot	blood flow to heart - mL/min
Qk = fQk*Qtot	blood flow to kidneys - mL/min
Qrest = fQrest*Qtot	blood flow to rest of the body - mL/min

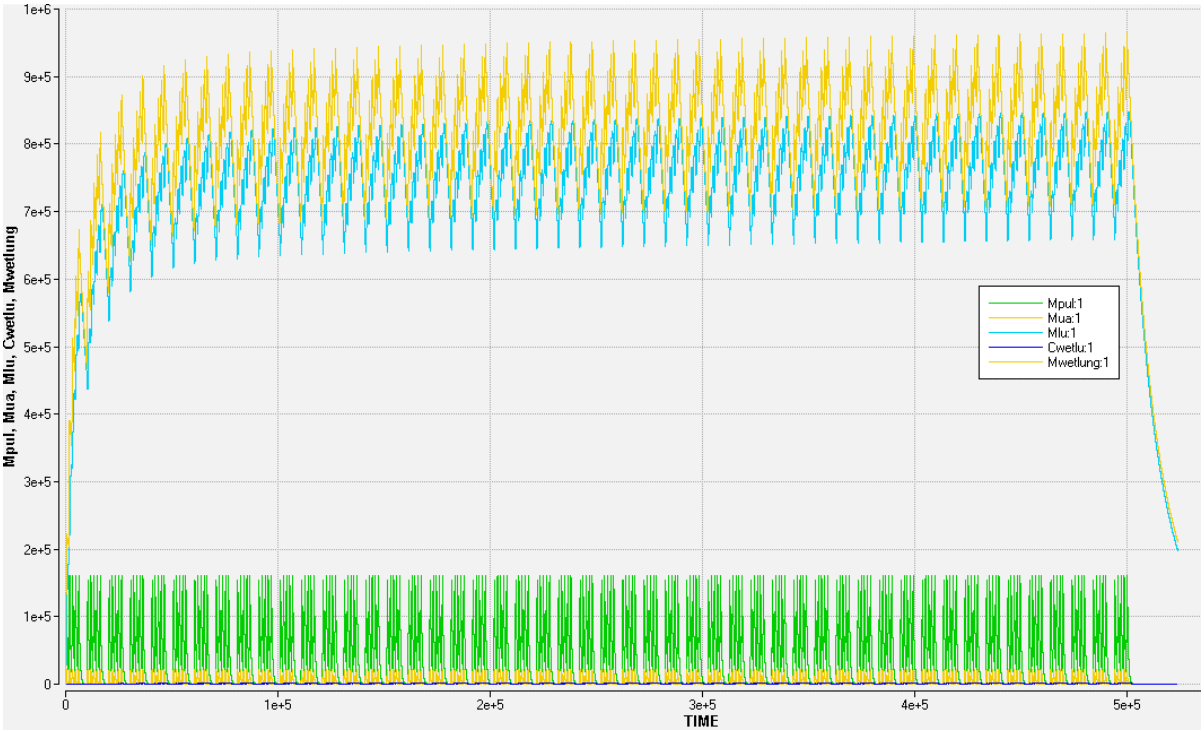

Figure A7-2 Retention of nano-TiO2 in the lung estimated over 1 full work year for ES2. The x-axis represents time in minutes over 1-year and the y-axis represents the mass (µg) of nano-TiO2 in the wet lung. The green trend line represents the change in mass in the air-exchange (pulmonary) regions of the lung, the blue trend line represents the change in mass in the interstitial regions of the lung, the pink trend line represents the change in mass in the trachea-bronchial regions of the lung, the red trend line represents the total retention in the wet lung including the air-exchange (pulmonary) regions, interstitial regions, trachea-bronchial regions and their macrophages.

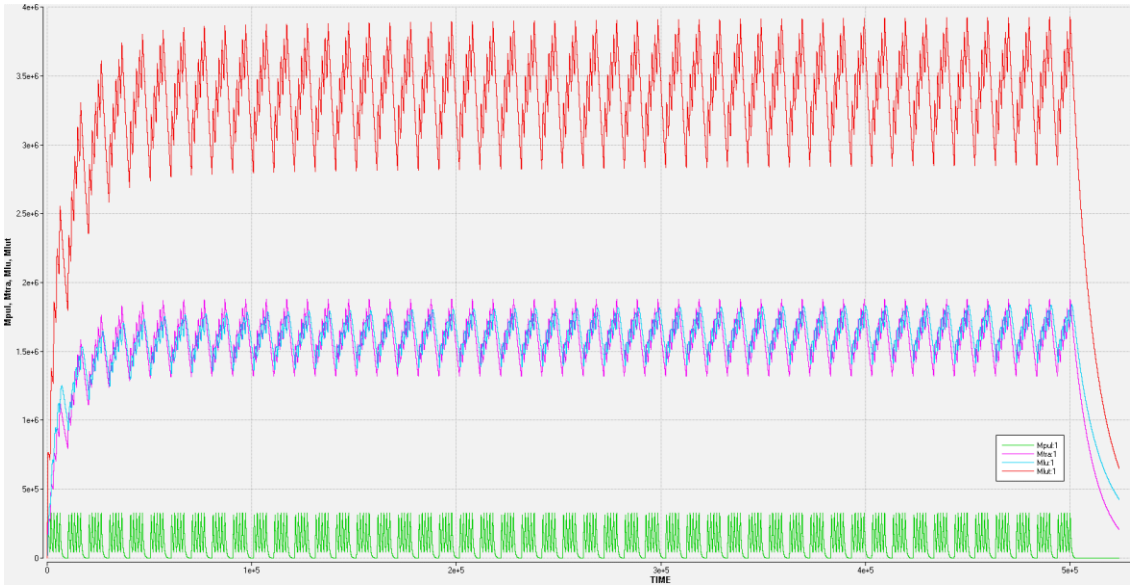

Figure A7-3 Retention of nano-TiO2 in the lung estimated over 1 full work year for ES3. The x-axis represents time in minutes over 1-year and the y-axis represents the mass (µg) of nano-TiO2 in the wet lung. The green trend line represents the change in mass in the air-exchange (pulmonary) regions of the lung, the blue trend line represents the change in mass in the interstitial regions of the lung, the pink trend line represents the change in mass in the trachea-bronchial regions of the lung, the red trend line represents the total retention in the wet lung including the air-exchange (pulmonary) regions, interstitial regions, trachea-bronchial regions and their macrophages.

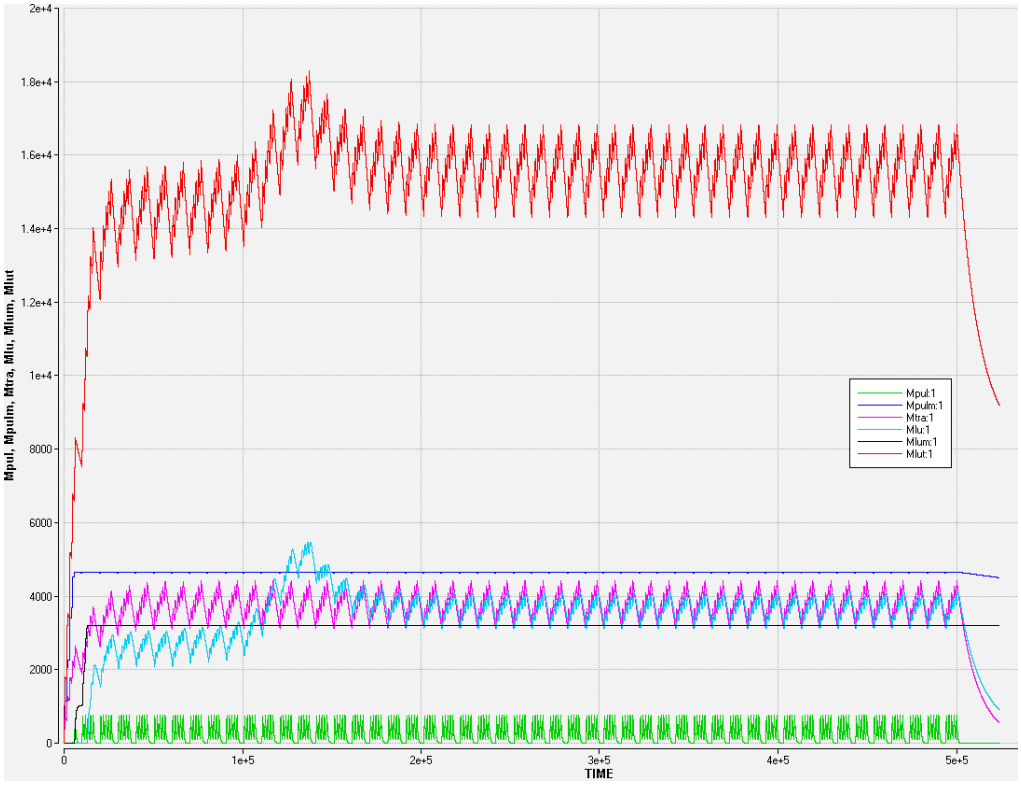

Figure A7-4 Retention of nano-TiO2 in the lung estimated over 1 full work year for ES4. The x-axis represents time in minutes over 1-year and the y-axis represents the mass (µg) of nano-TiO2 in the wet lung. The green trend line represents the change in mass in the air-exchange (pulmonary) regions of the lung, the blue trend line represents the change in mass in the interstitial regions of the lung, the pink trend line represents the change in mass in the trachea-bronchial regions of the lung, the grey trend line represents the change in mass in the lung macrophages, the dark-blue line represents the change in mass in the pulmonary macrophages, the red trend line represents the total retention in the wet lung including the air-exchange (pulmonary) regions, interstitial regions, trachea-bronchial regions and their macrophages.

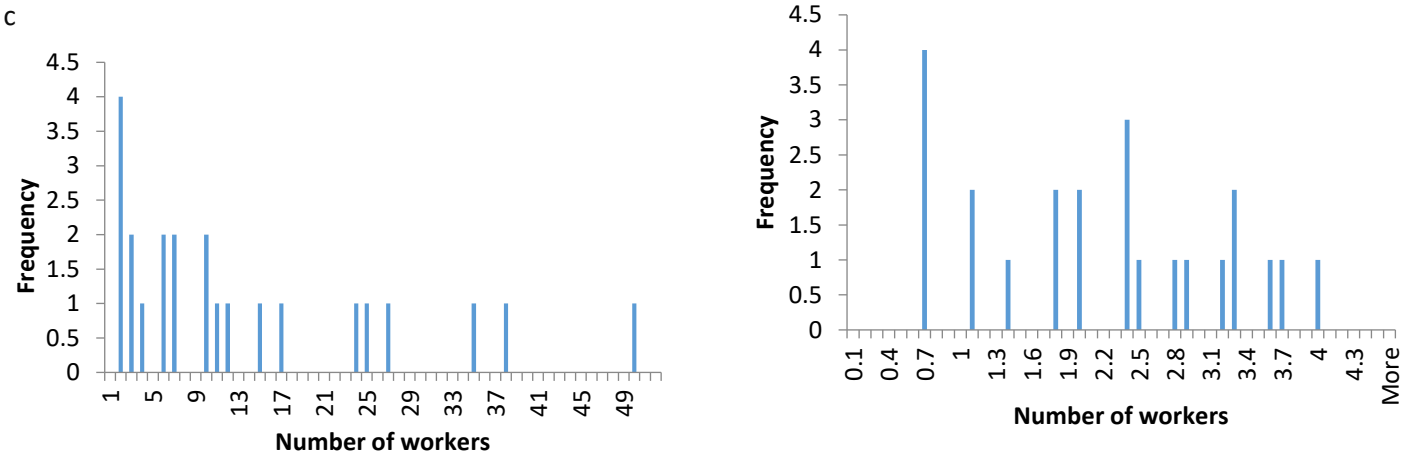

Figure A7-5 Number of workers along the x-axis and their frequency according to (a) original data and (b) log-transformed data presented by Walser et al.[97]

Table A7-2 Toxicological data used to calculate the carcinogenic dose-response relationship

Concentration mg/m3	Dose mg/g-dry lung	Dose m²/dry lung	Dose m²/g-dry lung	Animal Gender	Animal Sample Size	Species	Cancer Cases
0	0.00	0.00	0.00	F	77	R	2
10	32.30	0.16	0.07	F	75	R	2
50	130.00	0.65	0.28	F	74	R	1
250	545.80	2.72	1.16	F	74	R	12
0	0.00	0.00	0.00	M	79	R	2
10	20.70	0.10	0.03	M	71	R	2
50	118.30	0.59	0.18	M	75	R	1
250	784.80	3.92	1.20	M	77	R	12
0	0	0.00	0.00	MF	100	R	3
5	2.72	0.01	0.01	MF	100	R	2
0	0	0.00	0.00	F	217	R	1
10	39.29	1.89	1.31	F	100	R	32

Table A7-3 Toxicological data used to calculate the non-carcinogenic dose-response data

Dose mg/m3	Dose µg/g-dry lung	Diameter (nm)	Species	BAL Cell Sample Size	Macrophages (%)	Macrophages (Count)	Neutrophil (%)	Neutrophil (Count)
0	5.71	21	M	200	0.99	198	0	0
0	21.0	21	M	200	1	200	0	0
0	14.1	21	M	200	0.99	198	0	0

0	32.7	21	M	200	1	200	0	0
0	15.5	21	M	200	1	200	0	0
0.5	381	21	M	200	0.995	199	0	0
0.5	335	21	M	200	1	200	0	0
0.5	349	21	M	200	0.995	199	0	0
0.5	361	21	M	200	0.99	198	0	0
0.5	365	21	M	200	1	200	0	0
2	1411	21	M	200	0.995	199	0.005	1
2	1458	21	M	200	1	200	0	0
2	1411	21	M	200	1	200	0	0
2	1400	21	M	200	0.995	199	0.005	1
2	1299	21	M	200	1	200	0	0
10	10860	21	M	200	0.8	160	0.195	39
10	9776	21	M	200	0.865	173	0.125	25
10	11080	21	M	200	0.915	183	0.07	14
10	10306	21	M	200	0.775	155	0.21	42
10	10540	21	M	200	0.875	175	0.125	25
0	42.4	21	R	200	1	200	0	0
0	35.3	21	R	200	0.995	199	0.005	1
0	35.5	21	R	200	1	200	0	0
0	38.6	21	R	200	0.99	198	0.01	2
0	31.4	21	R	200	0.99	198	0.005	1
0.5	423	21	R	200	0.995	199	0.005	1
0.5	454	21	R	200	0.985	197	0.01	2
0.5	483	21	R	200	0.99	198	0.005	1
0.5	382	21	R	200	0.99	198	0.005	1
0.5	380	21	R	200	1	200	0	0
2	1620	21	R	200	0.91	182	0.085	17
2	1769	21	R	200	0.97	194	0.03	6
2	1772	21	R	200	0.96	192	0.035	7
2	1605	21	R	200	0.87	174	0.13	26
2	1660	21	R	200	0.95	190	0.045	9
10	10211	21	R	200	0.235	47	0.73	146
10	12383	21	R	200	0.4	80	0.585	117
10	10110	21	R	200	0.365	73	0.625	125
10	11440	21	R	200	0.315	63	0.66	132
10	10793	21	R	200	0.35	70	0.64	128

List of Publications

Much of the methods, results and other content contained in Chapter 3 was previously published in Progress in Photovoltaics: Research and Applications and can be found online at. The full citation of this publication is: Tsang, M. P., Sonnemann, G. W. & Bassani, D. M. A comparative human health, ecotoxicity, and product environmental assessment on the production of organic and silicon solar cells. Prog. Photovoltaics Res. Appl. 24, 645–655 (2016). [http://onlinelibrary.wiley.com/doi/10.1002/pip.2704/full].

Most of the methods, results and other content contained in Chapter 4 was published in Solar Energy Materials and Solar Cells. The full citation of this publication is: Tsang, M. P., Sonnemann, G. W. & Bassani, D. M. Life-cycle assessment of cradle-to-grave opportunities and environmental impacts of organic photovoltaic solar panels compared to conventional technologies. Sol. Energy Mater. Sol. Cells 156, 37–48 (2016). [http://dx.doi.org/10.1016/j.solmat.2016.04.024].

Portions of Chapter 5 were submitted as a single manuscript in 2015 and is currently still under peer-review.

Chapter 6 was submitted in 2016 and is currently under peer-review.

Chapter 7 is currently being prepared for submission in late 2016.

Résumé Détaillé

Introduction

L'énergie est une problématique fondamentale de la société au 21ème siècle, et au centre des enjeux de durabilité. Au cours des deux derniers siècles, l'énergie a été le facteur le plus influent sur la modification de la société. Le développement et l'utilisation des combustibles fossiles ont stimulé une importante croissance de l'industrie et de la population mondiale ainsi que des réalisations technologiques à une échelle jamais vue avant la révolution industrielle. Cependant, cela s'est fait au détriment d'importants coûts environnementaux et de santé publique. Le monde est à présent entré dans une ère de pic pétrolier et les émissions de gaz à effet de serre d'origines anthropiques produisent des modifications environnementales majeures et problématiques telles que le changement climatique. [4]

Dans ce contexte, la durabilité n'est pas simplement une question d'énergie, mais aussi une question d'environnement et de santé publique. Le coût réel d'une source d'énergie ne peut pas être quantifié uniquement en fonction de ses coûts d'extraction, de raffinage et de distribution, mais il doit également tenir compte des « externalités » ou des coûts indirects liés à ses dommages environnementaux. Ce point de vue global est nécessaire pour éviter un transfert d'impacts, comme cela peut être le cas avec les biocarburants (qui génèrent une utilisation des terres et une consommation d'eau douce accrues)[5-7] ou pour l'utilisation de l'énergie solaire avec des panneaux photovoltaïques (PV) qui génèrent une augmentation de l'utilisation de métaux. [9]

Par conséquent, la recherche et le développement de nouvelles sources durables pour répondre aux demandes énergétiques actuelles et futures est un enjeu majeur du 21eme siècle. Face à la nécessité urgente de diminuer les émissions de gaz à effet de serre, les sources d'énergie renouvelable comme le PV ont un rôle important dans la stratégie mondiale d'approvisionnement en énergie.

D'abord coûteuses et de faible efficacité, les cellules PV à base de silicium [10] ont rapidement mûri pour atteindre des rendements de 20% au milieu des années 1980. A l'échelle du laboratoire, le rendement a été augmenté au - delà de 25% pour la plupart des cellules à base de silicium. [11] Des records de rendement en laboratoire ont été atteint avec plus de 45 % de conversion de la lumière en électricité en utilisant par exemple des cellules de gallium, d'indium et d'arsenic. Les cellules à base de silicium sont encore la technologie photovoltaïque la plus largement utilisée dans le monde, en particulier à grande échelle et pour les systèmes placés sur les toits. Elle

représente plus de 90% de la production mondiale de PV par an. [12] L'utilisation du PV à base de silicium engendre des bénéfices environnementaux important et une meilleure gestion des ressources par rapport aux systèmes de production électriques classiques. Des études antérieures ont montré, par exemple, que les émissions de gaz à effet de serre par kWh d'électricité produit à l'aide de PV à base de silicium sont cinq fois plus faibles que la production à base de charbon et plus de deux fois plus faibles que la production à base de gaz naturel [13]. En outre, les quatre dernières décennies de développement du PV sont marquées par la recherche et le développement d'une large gamme de technologies viables, allant du PV classique à base de silicium monocristallin et multi-cristallin (m-Si) aux technologies de deuxième génération, telles que le silicium amorphe (a-Si), le cadmium-tellurure et le cadmium-indium-gallium-sélénium. Depuis la fin des années 1990, les financements de R&D ont permis de développer les technologies dites de troisième génération. Cette génération de PV est beaucoup plus diversifiée par rapport aux générations précédentes et comprend notamment des cellules photovoltaïques sensibilisées par colorant, avec de la perovskite, des points quantiques ou bien des cellules photovoltaïques organiques (PVO).

L'objectif de cette thèse repose sur les technologies de 3ème génération qui utilisent des matériaux organiques dans leurs couches actives au lieu de composés inorganiques tels que le silicium. La première technologie PVO a été développée par CW Tang en 1979 avec un dispositif organique d'hétérojonction [14]. Ce premier dispositif utilisait une couche active de phtalocyanine de cuivre et d'un dérivé de pérylène, un carbone polycyclique. Cette technologie est restée principalement une technologie de laboratoire, avec de petits projets pilotes (www.infinitypv.com) en ligne seulement depuis 2015 et le déploiement à grande échelle de panneaux solaires PVO déployés sur le terrain à des fins de recherche et de démonstration[15]. Conceptuellement, les cellules PVO ne sont pas très différentes des technologies photovoltaïques classiques dans le sens où elles sont composées des mêmes composants principaux comme deux électrodes et une couche active (i.e. où la séparation de charge se produit). Contrairement à d'autres technologies photovoltaïques, la couche active d'une cellule PVO est composée de couches de matériaux organiques donneurs d'électrons (semi-conducteur n) et accepteur d'électrons (semi-conducteur p), d'où le nom de cette technologie. De plus, pour atteindre leur extrême finesse, les dispositifs PVO utilisent généralement des nanomatériaux fabriqués (NMF) comme composants principaux des couches actives et additionnelles. Les cellules PVO peuvent nécessiter des composants supplémentaires tels qu'un substrat sur lequel tous les autres composants sont déposés ainsi que des couches pour améliorer l'efficacité et la séparation des charges, telles que le transport d'électrons et les

couches de transport de trous, et des couches de revêtement barrière pour la protection. Cependant, il n'y a pas de géométrie PVO ni de composition "standard" les PVO étant encore une technologie en plein développement.

Objectif de cette thèse

Bien que les technologies photovoltaïques captent le rayonnement solaire disponible et le transforment en une forme d'énergie plus utile (c.-à-d. l'électricité), des charges environnementales (des émissions de gaz à effet de serre par exemple) peuvent survenir pendant la production, l'utilisation ou l'élimination du panneau PV. Ceci étant dit, le PVO a de nombreuses caractéristiques qui en font un choix convaincant pour un développement ultérieur dans le domaine de l'énergie solaire. Ainsi, les cellules photovoltaïques sont extrêmement minces, flexibles, nécessitent de faibles quantités de matériaux et des processus de production à faible consommation énergétique [16]. L'objectif général de cette thèse est de vérifier si le PVO est préférable pour l'approvisionnement en énergie par rapport au PV classique à base de silicium d'un point de vue environnemental et de santé humaine. Un objectif sous-jacent de la thèse est de vérifier que les méthodologies existantes, couramment utilisées pour évaluer la performance environnementale des systèmes d'approvisionnement en énergie, comme l'analyse du cycle de vie (ACV), sont appropriées. Cette thèse aborde également les questions concernant les limites actuelles de l'utilisation de l'ACV pour évaluer les impacts associés au PVO, tels que les impacts potentiels sur la santé humaine associés à l'utilisation de nanomatériaux, et de quelle façon et avec quels outils cette question peut-elle être traitée pour informer de manière constructive le développement de cette technologie.

Questions abordées dans cette thèse:

1) Quelle est la gamme complète des impacts environnementaux du berceau à la tombe des technologies photovoltaïques organiques potentielles ?
2) Comment les impacts environnementaux des technologies photovoltaïques organiques se comparent-ils aux photovoltaïques traditionnels à base de silicium ?
3) Quelles sont les limites actuelles de l'utilisation de l'évaluation du cycle de vie pour évaluer les technologies photovoltaïques organiques et autres technologies émergentes ?
4) Quels sont les outils disponibles pour traiter les risques pour la santé humaine et les risques pour les nanomatériaux fabriqués ?
5) Comment ces impacts sur la santé humaine des nanomatériaux artificiels peuvent-ils être intégrés dans les méthodologies d'évaluation du cycle de vie ?

Analyse du cycle de vie

L'utilisation de l'ACV est l'élément central de l'évaluation environnementale des systèmes liés à l'énergie. L'ACV est un outil de gestion de l'environnement décrit par la norme ISO 14040:2006 et 14044:2006. [18,19] Une très brève introduction est fournie ici, une explication plus détaillée de son utilisation et des méthodes se trouvant dans le chapitre 2. L'ACV est considérée comme un outil essentiel d'évaluation en raison de sa capacité à suivre l'ensemble de l'énergie utilisée à chaque étape du cycle de vie du système. Cette information peut être utilisée pour déterminer combien de temps il faudra au système, pendant son utilisation, pour générer l'énergie qui a été consommée pendant la production de ce même système. Ceci est connu comme le temps de retour énergétique (TRE) [20-22]. Des mesures similaires telles que le temps de retour carbone (TRC) peuvent également être calculées puisque l'ACV permet le suivi de flux de matières non énergétiques tels que l'émission de gaz à effet de serre tout au long du cycle de vie. Le TRE et le TRC sont des paramètres essentiels auxquels tous les systèmes de production d'énergie sont discriminés. L'ACV se compose de (1) l'objectif et la définition du champ d'application, (2) l'inventaire du cycle de vie, (3) l'évaluation d'impact du cycle de vie et (4) les étapes d'interprétation.

Le but et le champ d'étude définissent ce qui est étudié dans l'ACV et incluent la définition de l'unité fonctionnelle et des limites du système. L'unité fonctionnelle décrit une fonction remplie, telle qu'un processus (une régénération de solvant), un produit (un panneau solaire) ou un événement (une restauration environnementale). L'unité fonctionnelle est directement liée aux limites du système, ce qui clarifie davantage les aspects de l'unité fonctionnelle qui sont ou non inclus dans l'évaluation. Un aspect important des limites du système est l'identification des phases du cycle de vie contenues dans l'étude. Par exemple, une étude peut être définie de porte à porte (gate-to-gate) si l'évaluation ne comprend qu'une étape du cycle de vie (par exemple, la fabrication d'un produit), du berceau à la porte de l'usine si l'évaluation inclut l'extraction de la matière première jusqu'à la fabrication du produit, et du berceau à la tombe si l'évaluation comprend chaque étape du cycle de vie. De plus, l'identification et le choix des critères d'évaluation de l'impact sur l'environnement et la santé humaine doivent être réalisés dans le cadre de la définition de l'objectif et du cadre de l'étude.

La deuxième étape d'une ACV, l'inventaire du cycle de vie, consiste à identifier, quantifier et regrouper tous les flux de matières, d'énergie et de déchets contenus dans l'unité fonctionnelle dans les limites des

frontières du système. De nombreuses fois, les données d'inventaire peuvent être obtenues à partir de bases de données d'inventaire de cycle de vie préexistantes telles que Ecoinvent qui est la base de données la plus utilisée pour les études d'ACV. L'évaluation de l'impact du cycle de vie implique la conversion des données d'inventaire du cycle de vie en impacts sur l'environnement et la santé humaine, parfois appelées impacts sur le cycle de vie. Ces effets peuvent comprendre l'acidification de la terre et de l'eau, le potentiel de changement climatique, le potentiel d'épuisement des ressources, l'écotoxicité, l'eutrophisation des cours d'eau, la toxicité humaine, le potentiel de rayonnement ionisant, les changements d'affectation des terres, le potentiel d'appauvrissement de la couche d'ozone, la formation de particules, et le potentiel de formation d'oxydant photochimique (smog). L'étape finale d'une ACV est l'interprétation utilisée pour (a) comprendre et établir les liens logiques entre les résultats de l'analyse d'impact du cycle de vie, l'inventaire du cycle de vie et la définition de l'objectif / du champ d'application, mais aussi (b) identifier les anomalies et erreurs qui peuvent se présenter dans chacune de ces étapes. Enfin, l'ACV ne quantifie pas les impacts absolus sur l'environnement ou la santé humaine. Au lieu de cela, l'ACV utilise des modèles généralisés qui fournissent un impact potentiel, relatif. Ceci est en contraste avec certaines autres analyses d'impact telles que l'évaluation des risques pour la santé humaine (ERSA) [23] et de l'évaluation des risques environnementaux (ERA). [24] Dans ces approches, les substances individuelles contenues dans un produit sont identifiées et évaluées par leur probabilité d'exposition dans une population dans des conditions environnementales distinctes et spécifiquement définies.

La technologie photovoltaïque organique étudiée dans cette thèse

Les ACV des études de cas présentées dans cette thèse concernent spécifiquement l'évaluation des dispositifs de PVO qui utilisent dans la couche active le [6,6]-phényl-C61-butanoate de méthyle (PCBM, un fullerène C_{60} modifié) et le poly(3-hexylthiophène) (P3HT). Le fullerène C_{60} a suscité le plus d'intérêt dans la recherche PVO comme semi-conducteur organique de "type n" (i.e. accepteur d'électrons) en raison de sa forte électronégativité et de sa mobilité électronique élevée. Plus précisément, le PCBM est largement utilisé, souvent en conjonction avec le polymère P3HT de "type p" (i.e. donneur d'électron) [25-28]. Pendant la séparation de charge dans la couche active, il y a création d'un porteur de charges à la fois positive et négative, ce dernier étant appelé "trou" ou absence d'un électron dans un atome. Le courant est créé lorsque la charge négative est autorisée à se déplacer à travers le PCBM et à travers la cathode (arrière) tandis que les trous se propagent simultanément à travers le P3HT jusqu'à l'anode transparente [29].

Les substrats des premiers dispositifs PVO étaient des structures initialement rigides telles que le verre, mais il est devenu commun et technologiquement possible d'imprimer les composants d'une cellule de PVO directement sur un substrat flexible [16,26]. Le substrat utilisé dans ce travail était du polyéthylène téréphtalate (PET), qui est réputé pour être un matériau particulièrement efficace pour les gros volumes d'impression roll-to-roll de panneaux de PVO [26]. Immédiatement adjacente au substrat se situe la couche (avant) transparente d'anode, vers laquelle les porteurs de charge positifs (i.e. les trous) voyagent.

Les anodes transparentes couramment utilisés sont constituées d'ITO (oxyde d'indium et d'étain), compte tenu de leur niveau élevé de transparence optique et de leur conductivité électrique [30]. Toutefois, en raison d'un coût plus faible, d'une plus grande abondance et à un degré moindre de sa toxicité, [31-33] l'oxyde d'étain dopé au fluor (FTO) a été utilisé. Le FTO était un remplacement convenable en raison de qualités favorables telles que sa grande disponibilité, des prix du marché inférieurs et son efficacité relative comme un oxyde conducteur transparent par rapport au ITO [30,34,35]. Le FTO a également le potentiel d'être imprimé [33] sur un substrat flexible. [36]

Comme indiqué précédemment, la couche active de cellules PVO est constituée de matériaux organiques donneurs et accepteurs. L'hétérojonction en vrac est une morphologie d'entrelacement des matériaux donneurs et accepteurs qui maximise l'opportunité de séparer les charges. Pour éviter la recombinaison des porteurs de charge mobiles dans la couche active et augmenter l'efficacité, les cellules PVO reçoivent souvent une couche de transport de trous et une couche de transport d'électrons. PEDOT:PSS est une couche de transport de trous couramment utilisée dans les cellules PVO, mais il a été démontré que ce matériau a une faible stabilité dans des conditions ambiantes [37,38]. Au lieu de cela, le matériau MoO_3 a été choisi pour la couche de transport de trous en raison de sa bonne stabilité, de son absence d'interférence avec le profil d'absorption de la lumière de la couche active (i.e. pas d'interférence avec le profil 350-700 nm d'absorption de la lumière de la couche active) et la compatibilité avec le dépôt et le traitement à base de solution [39].

Une couche supplémentaire de nano-TiO_2 a été ajoutée entre la couche active et la cathode, pour augmenter l'absorption de lumière. Dans de nombreux cas, la réflexion de la lumière à partir de la cathode (arrière) redirige la lumière vers la couche active pour une deuxième passe, et en fonction de l'épaisseur

de la cellule, cela peut interférer avec l'absorption. Cela est particulièrement vrai lorsque l'épaisseur de la couche active est de l'ordre des dizaines de nanomètres [40,41]. Les espaceurs optiques peuvent éviter ce problème et augmenter le spectre de la lumière absorbée.

L'espaceur optique a l'avantage supplémentaire d'agir comme une couche bloquant les trous mais également comme une couche transportant les électrons [42]. Toutefois, une couche de fluorure de lithium a été modélisée pour accroître l'efficacité et la mobilité des porteurs de charge négative à la cathode (retour) [43,44]. En plus d'être une couche de transport d'électrons efficace, le fluorure de lithium peut aussi protéger contre les dommages au cours des processus « roll-to-roll », ce qui conduit à des dégradations de l'appareil. [43]

Enfin, une cathode (arrière) est nécessaire pour la collecte des porteurs de charge négative. [45] Une couche d'aluminium a été intégrée en tant que cathode. Des métaux de faibles fonctions de travail peuvent être relativement réactifs, conduisant à une oxydation potentielle et à la dégradation de l'appareil [45]. Ainsi, pour résoudre ces problèmes, la cellule PVO a été conçu avec des couches supplémentaires de stratification (i.e. encapsulation et des couches de protection).

Analyse du cycle de vie du berceau à la porte de l'usine

Une ACV du berceau à la porte de l'usine sur la production de cellules PVO par rapport à des technologies classiques telles que le silicium est présenté. L'unité fonctionnelle considérée est 1 'Wp' (i.e. 'watt-peak'). La cellule PVO requiert 200 cm² par Wp produit pour un rendement hypothétique de 5% [20]. Des rendements de l'ordre de 2-3 % ont été rapportés pour les cellules à base de PCBM en laboratoire[21,46,47]. Cependant, un déploiement à grande échelle de cellules PVO ont déjà montré des rendements de près de 2% [15]. En outre, des rendements à l'échelle du laboratoire de l'ordre de 15% ont été rapportés dans la littérature pour les dispositifs à base de PCBM semblables à ceux qui sont considérés dans cette thèse [48]. En règle générale, au fur et à mesure que les technologies photovoltaïques se développent, le passage d'une échelle laboratoire à une échelle industrielle pourrait faire diminuer le rendement de 20% à 50% [49]. Ainsi, l'hypothèse de travail concernant le rendement représente un objectif à court terme optimiste mais réaliste.

Les cellules PVO ont ensuite été comparées avec des cellules PV m-Si classique et des cellules PV a-Si. Pour chaque option technologique, les flux environnementaux ont été définis pour l'extraction des matières

premières, le traitement des matériaux, la fabrication et le transport pour chaque conception de cellules solaires. L'ACV a été conduite dans openLCA v1.4.2 (GreenDelta, Berlin). L'analyse d'impact a été réalisée en utilisant les catégories d'impact de ReCiPe (H) v1.0.5 [50], USEtox (www.usetox.org) pour les indicateurs de santé humaine et d'écotoxicité de l'eau douce et enfin la demande cumulée d'énergie (CED) [51].

La plus grande contribution à l'impact global sur la santé humaine et l'environnement des cellules PVO *standard* provient de la production et du dépôt (i.e. la pulvérisation) de l'anode FTO sur le substrat. La production de substrats FTO a une contribution moyenne de 62 % pour toutes les catégories d'impact, avec un maximum de 95% pour la déplétion des métaux et de 57% pour l'épuisement des combustibles fossiles. La forte contribution de la production moyenne de FTO-substrat est due au procédé de pulvérisation cathodique, dont l'influence avait déjà été soulignée dans de précédentes études ACV sur les substrats à base d'ITO [31]. Les contributions de la fabrication de PCBM, le recuit de la couche active, et le laminage de la cellule solaire ont des contributions moyennes de 11%, 11% et 6%, respectivement. Les contributions de la production de PCBM varient considérablement (allant de 13% pour l'appauvrissement de l'ozone à un minimum de 4% pour la privation d'eau). Pour la production de PCBM, les impacts ont été fortement influencés à la fois par la production de C_{60}-fullerène et sa purification en PCBM. Cela est dû en partie aux effets en amont de la production de toluène, de dichlorobenzène *ortho* et des composés de pyridine. Les estimations de la littérature pour la demande en énergie cumulée par kg de PCBM varient entre 64 et 125 GJ. Les impacts de la production de l'espaceur optique en nano-TiO_2 varient de 10% pour l'eutrophisation marine à 0,01% pour la privation d'eau. Sa contribution globale à tous les impacts sur l'environnement et la santé humaine (en moyenne de 0,55%).

La contribution du recuit de 11% est plus élevée par rapport à la littérature qui estiment des contributions entre 0,2 et 10 % [21,52]. Cependant, dans certaines études, l'énergie consommée au cours du recuit de la couche active n'est pas explicitée [53], ou elle est tout simplement omise de l'évaluation [20]. Pour la stratification, les influences majeures sont dues à la production de PET et de la résine époxy. Dans la littérature, la contribution de la stratification dans l'indicateur CED par exemple, varie considérablement : de 0,1 % à 37 % [20,21,46]. En ce qui concerne le copolymère P3HT, une contribution plus faible de 2 % en moyenne est observée pour toutes les catégories d'impact. Des études antérieures ont démontré que le P3HT peut contribuer entre 0,1 et 0,8% pour l'indicateur CED, ce qui est en accord avec les résultats de cette thèse. Bien que ce soit une contribution assez modérée par rapport à l'impact

global, la littérature fait état d'une tendance à remplacer le P3HT par de nouveaux polymères. [54] Bien que ceux - ci ont le potentiel d'accroître l'efficacité des cellules PVO, ils pourraient générer une augmentation des impacts [54].

Une autre modélisation a été réalisée pour substituer la pulvérisation de l'électrode FTO par l'impression par jet d'encre de l'électrode. La pulvérisation a déjà été identifiée comme étant un processus énergivore et, lorsqu'il est évité, diminue l'ensemble de l'indicateur CED [20,46,53]. Les résultats de cette thèse ont confirmé cela, mais aussi démontré que les autres catégories d'impact ne répondent pas nécessairement à la même tendance que la CED. Par exemple, alors que la CED présente une diminution d'impact d'environ 56 %, les réductions d'impact variaient de 2 % pour l'épuisement des métaux à 72 % pour les rayonnements ionisants. En outre, une évaluation pour un dispositif remplaçant le PCBM avec un copolymère dans la couche active a été effectuée. Il en résulte une diminution moyenne de 10 % pour toutes les catégories d'impact. Considérant que le PCBM a déjà été identifié comme un facteur ayant une influence de faible à modérée dans les impacts de la production de la cellule PVO sur la santé humaine et l'environnement [20,31,53,55], des réductions relativement importantes du au remplacement du polymère ont été observées pour l'écotoxicité, où les impacts ont été réduits de 20 %. En général, les polymères tels que le P3HT ont montré des contributions beaucoup plus faibles aux impacts environnementaux de la production de PVO, mais les polymères sont très hétérogènes et leur CED, par exemple, peut varier d'un ordre de grandeur[54].

Par rapport à des cellules m-Si et a-Si, les impacts du PVO *par défaut* étaient en moyenne 93% plus faibles. Le TRE (c'est-à-dire le temps qu'il faudra au système pour générer l'énergie consommée pendant la production de ce même système) a été évalué à 0,27 ans (97 jours) pour la cellule PVO par défaut. Les cellules m-Si et a-Si ont un TRE de respectivement 3,6 et 2,8 ans. Pour les variantes du PVO, le TRE est de 0,12 ans (42 jours) et de 0,24 ans (87 jours) respectivement pour le dispositif à jet d'encre et pour toutes les cellules en polymère.

Analyse du cycle de vie du berceau à la tombe

Les résultats de cette ACV sont largement en faveur des cellules PVO, puisque tous les résultats d'impact sont plus faibles que pour les cellules de silicium classiques à unité fonctionnelle identique. Cependant, les résultats de cette ACV initiale du berceau à la porte de l'usine ne tiennent pas compte des phases d'utilisation et de fin de vie du dispositif PVO et étant donné les faibles rendements et la durée de vie du

PVO, cela pourrait avoir une influence importante sur la comparaison des deux types de système. Ainsi, l'ACV est étendue du berceau à la tombe en incluant les phases d'utilisation et de fin de vie. Les cellules photovoltaïques organiques ne sont actuellement pas produites à l'échelle industrielle ou utilisées à des fins commerciales. Par conséquent, deux systèmes différents (deux utilisations du PV) ont été pris en compte afin de mieux éclairer le rôle que le PVO pourrait jouer pour les secteurs de la production d'énergie et des produits de consommation. Le système 1 (S1) est défini par une unité fonctionnelle d'une production d'un kWh moyen d'électricité durant 25 ans sur un toit (Figure 4 -2), tandis que le système 2 (S2) est défini par une unité fonctionnelle d'une production moyenne de 10 Wh d'électricité sur cinq ans via un dispositif de chargeur de portable. Pour S1, en plus de l'installation sur le toit des panneaux PVO et silicium, la structure de montage, un onduleur et des câbles pour l'installation électrique ont été également pris en compte. Pour S2, on a supposé que les chargeurs portatifs nécessitent un étui de protection en PET-polyester d'un mm d'épaisseur.

Deux scénarios de fin de vie ont été envisagés : (a) incinération et (b) mise en décharge. À l'heure actuelle, les infrastructures, l'économie, la législation et la taille du flux de déchets montrent que la plupart des panneaux PV finissent dans ces filières d'élimination classiques, par opposition au recyclage [56-58]. Ces deux processus de gestion de fin de vie ont été calculés en utilisant les outils de modélisation de la fin de vie dans Ecoinvent [59]. L'outil a été utilisé pour créer un inventaire basé en partie sur la composition élémentaire des déchets. La composition des déchets pour chaque panneau est basée sur la composition du panneau au moment de la fabrication (c'est-à-dire sans tenir compte des pertes ou de la dégradation des composants pendant la durée de vie du dispositif photovoltaïque). Pour l'incinération, le pouvoir calorifique inférieur (PCI) des principaux composants ont été utilisées pour déterminer la récupération d'énergie potentielle du système. Comme la plupart des panneaux PVO sont en PET, leur PCI de 22,9 MJ/kg a été utilisée. Ainsi, 4,95 MJ d'énergie sont produits par kg de panneau PVO incinéré. Les cellules m-Si sont composées presque entièrement de matériaux qui ont des PCI très faibles et on a donc supposé que l'incinération des panneaux m-Si ne produisait pas d'énergie. Les panneaux PVO pèsent 0,22 kg par $m^{2,}$ ce qui entraîne l'élimination de 22 kg de panneaux de PVO. Les panneaux m-Si pèsent 12 kg / $m^{2,}$ ce qui entraîne une élimination totale de 88 kg de panneaux en silicium.

Les systèmes PVO S1 et S2 ont moins d'impact que leurs homologues à base de silicium. Pour S1, les impacts du panneau PVO-D (avec incinération) sont plus faibles de 96% pour l'épuisement de l'eau à 40% pour l'eutrophisation d'eau douce. Par contre l'appauvrissement des métaux était d'environ 21% plus

élevé pour le système PVO-D que pour le système à base de silicium à cause de la production de l'électrode FTO.

L'impact du système PVO-D S2 est plus faible que pour le système a-Si : on remarque une diminution de 92% pour l'eutrophisation marine à 56% pour l'écotoxicité en eau douce. Pour les systèmes S2, la diminution relative entre le PVO et le PV à base de silicium est plus prononcée que pour les systèmes S1. La raison des différences entre les impacts relatifs entre le S1 et le S2 s'explique en partie par les différentes phases d'utilisation. La phase d'utilisation de S1 est 5 fois plus longue que pour S2 (respectivement 25 ans et 5 ans). Par conséquent, compte tenu de la durée de vie du PVO supposée de 5 ans, il a été nécessaire de remplacer les panneaux PVO " plusieurs fois au cours de la phase d'utilisation du système S1. Pour le système S2 il n'y a pas besoin de remplacements car la phase d'utilisation est de 5 ans. Ce résultat est similaire à ceux d'Espinosa et al. où, en moyenne, la majorité des impacts générés sur l'ensemble du cycle de vie de leur parc solaire (d'une durée de 35 ans) est due à la production et à l' élimination des panneaux eux - mêmes. [60]

Pour le système S1, le TRE (tableau 4 -5) des panneaux PVO-D est de 436 jours (incinération) et 449 jours (décharge). Ces TRE sont d'environ 53% et 51% plus courts que pour les panneaux à base de silicium. Pour le système S2, le TRE pour les panneaux PVO-D était plus court : 220 jours (incinération) et 265 jours (mise en décharge). Comme il a été expliqué précédemment, il est probable que le TRE pour S1 soit beaucoup plus élevé en raison de l'obligation de remplacer les panneaux PVO-D tous les cinq ans. De plus, le TRE plus faible pour le scénario « incinération » par rapport au scénario « mise en décharge » est une conséquence de la production d'énergie lors de l'incinération. Cet effet est légèrement plus influent pour S2 en raison de la quantité ajoutée de plastique incinéré. Bien que les résultats démontrent que les panneaux PVO-D par défaut ont abouti à une réduction de 50% à 65% de TRE par rapport aux panneaux de silicium, les TRE sont plus élevés que ceux précédemment observés de l'ordre de quelques jours ou semaines (chapitre 3). [20,46,53,55,61]

Les résultats de ce chapitre sont uniformes quel que soit le mode de gestion de fin de vie (c'est-à-dire l'incinération par rapport à la décharge). Cela est particulièrement vrai pour S1 mais pas pour S2, qui avait des réductions d'impact plus marquées pour l'incinération en raison de la valeur ajoutée apporté par l'incinération du boîtier en plastique avec le panneau PVO. Il convient de noter que les impacts du changement climatique pour le VPO-D sont supérieurs de 3 % (S1) et de 16 % (S2) lorsqu'ils sont incinérés

plutôt qu'enfouis. Ceci est une conséquence nécessaire de la combustion des composants en plastique qui ont été convertis entièrement en CO_2 au cours du processus. Bien que les options de fin de vie testées dans cette ACV n'aient eu qu'une influence marginale sur les impacts sur l'environnement et la santé humaine, cette analyse n'a pas inclus les effets potentiels du recyclage des panneaux photovoltaïques. Le PV à base de silicium peut tirer le meilleur parti du recyclage puisque la production de plaquettes de silicium et de panneaux a une contribution majeure sur les impacts globaux pour le m-Si et l'a-Si. Müller et al., ont fait état d'une réduction de près de 57 % de la consommation d'énergie pour les modules m-Si fabriqués avec des plaques de silicium recyclé [62]. Dans le cadre du S1, dans l'approche du berceau à la porte de l'usine, la diminution du besoin énergétique rapportée par Müller et al. pourrait conduire à des réductions potentielles de la CED de 49 % pour les panneaux m-Si, ce qui donne une CED de 12 520 MJ. Cette estimation est légèrement supérieure à l'estimation de la CED de 11 634 MJ pour le VPO-D, soulignant ainsi l'importance de cette option en fin de vie. Bien que la CED n'ait pas une relation linéaire avec les autres catégories d'impact, [55] une hypothèse raisonnable serait que la plupart des autres catégories d'impact diminueront également, mais avec une amplitude différente. Cela entraîne une certaine incertitude entourant les avantages environnementaux du PVO sur les panneaux conventionnels. Contrairement aux m-Si, aucune information pertinente sur les options de recyclage possibles pour les a-Si ne se trouve dans la littérature, et en raison de sa teneur en silicium beaucoup plus faible, la faisabilité du recyclage des a-Si est incertaine. [58]

Ces résultats reposent sur les hypothèses que les PVO ont une durée de vie de 5 ans et une efficacité de conversion de 5%. Afin de tester l'influence de ces hypothèses sur les résultats globaux, différentes analyses de sensibilité ont été réalisées : dans un premier temps des panneaux ayant un rendement de 1 % et une durée de vie allant de 1 à 9 ans ont été testés puis dans un second temps, leur durée de vie a été fixée à 1 an et les rendements ont varié de 1 à 9 %. Pour S1, l'augmentation de la durée de vie d'un à trois ans a entraîné une forte baisse initiale des impacts sur la santé humaine et l'environnement, qui ensuite se stabilise après ces trois ans. Lorsqu'une durée de vie maximale de neuf ans est considérée, 9 des 17 impacts pour l'OPD-D, y compris le potentiel de changement climatique et la CED sont restés proportionnellement plus élevés que les panneaux m-Si. En conséquence, le TRE et le TRC ne sont jamais inférieurs aux m-Si. Le TRE varie d'un maximum de 16 ans pour une durée de vie d'1 an pour un minimum de 3,5 ans pour une durée de vie de 9 ans, alors que le TRC va d'un maximum de 6,4 ans à un minimum de 1,6 ans, respectivement. Une tendance similaire a été observée pour l'analyse de sensibilité sur le rendement du panneau : une augmentation de 1-3 % du rendement induit également une forte baisse

initiale des impacts sur la santé humaine et l'environnement (Figure 4 -4). Au - delà de 3 %, les réductions d'impact ont commencé à se stabiliser, mais pas aussi fortement que dans le cas de la sensibilité sur la durée de vie. Ainsi, avec une efficacité de 9% seulement l'épuisement des métaux est resté proportionnellement plus élevé que m-Si. En particulier, le potentiel de DEC et le changement climatique étaient de 18% et 16% inférieure à m-Si, avec un TRE et TRC de 2,1 ans et 305 jours, respectivement.

Pour S2, l'augmentation de la durée de vie d'un à trois ans a également entraîné une forte baisse initiale qui s'est ensuite stabilisée au - delà de 3 ans. Pour une durée de vie maximale de 9 ans, 7 des 17 impacts, y compris la CED et le potentiel de changement climatique sont restés plus élevés que pour l'a-Si. Cela a abouti à des TRE et TRC de 2,8 ans et 1,5 ans, respectivement, qui restent supérieurs à l'a-Si. En revanche, les effets de l'augmentation de l'efficacité a entraîné une diminution plus nette et légèrement plus soutenue lors de la variation de 1 à 9% d'efficacité (figure 4 -5). Pour 3% d'efficacité, plus de la moitié des impacts sur la santé humaine et l'environnement des PVO-D étaient inférieurs à l'a-Si et à 5 % de rendement tous les impacts étaient inférieurs à ceux du a-Si. Cela signifie que pour un rendement de 5% le TRE et le TRC étaient inférieurs à ceux de l'a-Si. Avec un rendement de 9 %, le TRE et le TRC sont de 215 jours et 101 jours, respectivement.

Ces résultats indiquent qu'il faudrait privilégier l'augmentation du rendement de la cellule PV plutôt que l'augmentation de sa durée de vie. En effet, avec une plus grande efficacité, les panneaux photovoltaïques sont plus petits pour une puissance de sortie similaire : de plus petites quantités de matériaux sont donc nécessaires pour la production de la structure de trame (S1), ou les matériaux d'enveloppe (S2). L'augmentation de la durée de vie, quant à elle, n'influe pas sur la quantité de matériaux nécessaire.

Limitations de l'approche de l'évaluation actuelle du cycle de vie

Les résultats actuels des études de cas en ACV suggèrent que les PVO sont une technologie de production d'énergie préférable par rapport à des panneaux PV à base de silicium, d'un point de vue de la santé humaine et de l'environnement, en particulier pour les utilisations où la durée de vie du produit sont relativement courtes (<5 ans) ou lorsque les systèmes de produits sont extrêmement simplifiés. Un élément manquant dans les précédentes études était une estimation des émissions des NM et le calcul de leurs impacts sur la santé humaine et / ou éco-toxicologiques. Globalement une cellule PVO se compose d'une anode, d'une cathode, d'une couche active et d'un substrat. Des composants supplémentaires peuvent inclure une couche de transport de trous, une couche de transport d'électrons,

des bloqueurs d'UV, des revêtements, des barrières et / ou des espaceurs optiques, par exemple. Pour parvenir à la finesse caractéristique du PVO, ces couches doivent contenir peu de matériaux et ceux-ci doivent avoir une taille allant d'une dizaine à quelques centaines de nanomètres. Par conséquent, les matières utilisées seront souvent de taille nanométrique.

Les NM sont vaguement définis comme des matériaux ayant une seule dimension égale ou inférieure à 100 nanomètres (nm) et généralement dans la gamme de 1-100 nm[63].A l'échelle nanométrique, il y a de nouvelles applications possibles allant de l'utilisation dans les produits pharmaceutiques jusqu'au secteur de l'énergie en passant par l'industrie textile et l'agriculture [64]. Il est également prévu que l'utilisation et la production de NM aident à la protection de l'environnement, à la création d'emplois et à l'augmentation de la croissance économique [65,66]. En plus d'être fabriqués dans des gammes de taille qui sont beaucoup plus petites que leurs homologues en vrac, les NM peuvent prendre différentes formes (par exemple des fibres) et différents modes de réalisation (matériaux enrobés, par exemple). Les NM ne sont pas seulement définis physiquement, mais aussi par leurs propriétés et comportements distincts. Par exemple, lorsque les matériaux diminuent en taille, le rapport entre la surface et le volume augmente jusqu'au point où de nouvelles propriétés physico-chimiques apparaissent par rapport aux matériaux à l'échelle micro [67]. Toutefois, ces mêmes caractéristiques physico-chimiques menant à l'amélioration des propriétés des matériaux, aux progrès technologiques et à un meilleur rendement des ressources peuvent également présenter des risques pour la santé humaine et l'environnement [68-71] résultant de rejets intentionnels et/ou non intentionnels de NM à travers le cycle de vie du PVO. [72,73]

L'ACV, en théorie, peut être appliquée à des NM. La première utilisation formelle de l'ACV pour les technologies NM est venue au cours d'un atelier datant de 2006 et intitulé *Nanotechnology and life cycle assessment* [74], où il a été reconnu que «[L'ACV] est tout à fait adaptée aux nanomatériaux et aux produits liés aux NM». Dans la pratique, cependant, peu d'études ACV complètes sur les NM ont été publiées, en particulier celles dont les limites du système sont du berceau à la tombe [75]. Cette lacune dans la littérature est due à un manque de bases de données qui contiennent des inventaires de cycle de vie spécifiques aux NM pour décrire les inputs de matière et d'énergie et la production de déchets lors de la production, mais aussi en raison de l'absence de méthodes d'évaluation des impacts capable de caractériser le devenir des NM, leur exposition et leurs impacts sur la santé humaine [75-78].

En ce qui concerne les émissions, il y a eu quelques tentatives de modéliser et de calculer les principaux flux de NM provenant de la production [79-81] mais aussi de l'utilisation [82-84] et de l'élimination de ces matériaux [85]. Ces approches et ces modèles peuvent être utilisés pour estimer les émissions moyennes mondiales de NM qui pourraient être utilisées pour créer des inventaires d'émissions directes des produits et des processus liés aux NM. Pour être utile dans l'ACV, chaque émission de NM doit contenir un facteur de caractérisation (FC_{NS}) qui convertit son émission en un impact potentiel sur la santé humaine ou l'environnement.

Il y a une poignée d'articles publiés qui ont fait une première approximation pour modéliser le devenir des NM, leur exposition et leur toxicité dans les ACV [86-89]. Ces premières approximations comprennent 1 FC pour la santé humaine [89] et 3 FC [1] pour l'écotoxicité des nanomatériaux [86-88]. Dans chaque cas, les auteurs modifiaient les FC existant dans USEtox pour les rendre propres au NM. Les méthodes d'évaluation de l'impact du cycle de vie actuelles, telles que USEtox, tirent parti d'un certain nombre d'hypothèses qui décrivent commodément le sort et le transport des petites molécules organiques et des métaux, mais ces méthodes ne sont pas appropriées pour les NM ou décrivent de manière similaire les matières colloïdales[90]. Les principales hypothèses utilisées dans les méthodes d'évaluation de l'impact supposent que les conditions sont à l'état d'équilibre et que les systèmes ont atteint l'équilibre thermodynamique [91,92]. Par conséquent, ces modèles supposent qu'il n'y a aucun changement dans la concentration du polluant dans le temps et que le sort de ces polluants peut être estimé à l'aide de coefficients (d'équilibre), de partition (par exemple, le coefficient de partition de l'octanol-eau, K_{ow}). Ces coefficients sont définis par le rapport de la concentration de la pollution restante dans un milieu par rapport à un autre milieu (par exemple l'octanol par rapport à l'eau), une fois que le système impliquant les 2 milieux a atteint l'équilibre.

Toutefois, lorsqu'ils sont libérés dans un milieu spécifique, les NM existent dans leur propre phase et ne forment pas de phases uniformes avec le milieu environnant contrairement aux matériaux organiques. Par conséquent, et par définition, les NM ne sont pas thermodynamiquement stables, même si certains NM peuvent être *cinétiquement* stables pendant de longues périodes de temps [90]. En d'autres termes, un rapport de concentration de NM entre deux milieux ne peut pas être prédit à partir d'un coefficient de partage précédemment mesuré si les conditions n'étaient pas exactement les mêmes entre les deux scénarios[90]. Cela s'explique par le fait que le comportement du NM dans l'environnement est fortement dépendant de la concentration (selon les conditions initiales, la quantité de NM, et le moment

où le système est mesuré, les résultats seront différents) [87,90]. Ainsi, à la place des coefficients de partage d'équilibre, les NM doivent être décrits en utilisant des modèles cinétiques dynamiques utilisant le devenir et l'exposition. Par exemple, ces modèles peuvent employer l'utilisation des constantes de vitesse du premier ordre pour décrire la dissolution du NM en ions dans la colonne d'eau [93]. En outre, les modèles à l'état d'équilibre ne sont également pas en accord avec le fait que les taux d'émissions du NM ne sont généralement pas des événements réguliers. Cela est particulièrement vrai pour les scénarios en intérieur et d'occupation[94,95]où les émissions de NM sont susceptibles d'être épisodiques. Enfin, l'exposition au NM, et plus particulièrement l'inhalation du NM, présentera des mécanismes dépendant de sa concentration elle-même influencée par les échanges avec les poumons (dégagement et rétention notamment). Autrement dit, l'inhalation du NM ne dépend pas seulement du degré d'inhalation de l'individu qui est exposé[96]. Elle dépend également des caractéristiques du NM, des mécanismes et des temps biologiques au cours desquels l'exposition est mesurée[97]. Il a été proposé d'utiliser un facteur de rétention spécifique au NM, appelé *R*, calculé en utilisant des modèles de dépôt et de dégagement des voies respiratoires des poumons tels que le modelé 'Multi-Pathway Particle Dosimetry' (MPPD) [98]. Le modèle MPPD est un outil généralement utilisé dans l'Evaluation Quantitative des Risques Sanitaires (EQRS), équivalent du Human Health Risk Assessment (EQRS), pour déterminer la dose intra-pulmonaire venant de l'exposition à des concentrations dans l'air de produits chimiques et de particules. Cependant, le modèle MPPD actuel ne permet pas d'estimer le dépôt ou le dégagement tout en considérant des conditions d'exposition qui changent au fil du temps.

En alternative à l'ACV, l'Evaluation des risques environnementaux (ERE) [24] et l'EQRS [23] pourraient être utilisées sur une base au cas par cas pour déterminer si les NM posent également des risques écologiques ou de santé humaine, semblables à ce qui est fait pour des produits chimiques réguliers (Figure 5 -4)[99]. Cependant, l'EQRS est sujet aux mêmes problèmes de manque de données et de lacunes méthodologiques que l'ACV, et donc l'EQRS ne peut pas servir nécessairement comme une panacée à la question des impacts sur la santé humaine des produits contenant des NM tels que le PVO. Par exemple, les efforts actuels sur l'EQRS des NM ne sont pas suffisants pour suivre le rythme de leur production et de leur utilisation dans l'industrie. À ce jour, l'Environmental Protection Agency des États - Unis (US EPA) a publié un seul EQRS des NM [100] tandis que l'Institut national de la santé et de la sécurité au travail (US NIOSH) a publié deux niveaux d'exposition spécifiques aux NM[101,102]. Les lacunes de données dans l'évaluation de la toxicité et de l'exposition entravent le processus d'EQRS [72103104]. Alors que les États - Unis [105] et l'UE [106], par exemple, peuvent demander et recueillir des données pour aider à la procédure

d'EQRS pour les NM, une évaluation de tous les NM enregistrés n'a pas été réalisée. Bien que certaines données et certains efforts de modélisation puissent être contournés avec une EQRS, par exemple, en mesurant directement les doses d'exposition ou les concentrations auxquelles on est soumis. Plus communément, cependant, des approches *qualitatives* d'EQRS[107-110] ont été mises en avant pour *prioriser* les efforts de recherche, la gestion de l'environnement et les activités de réglementation dans le cas des NM. Néanmoins, de nombreux modèles spécifiques aux NM, des approches qualitatives par niveaux de contrôle jusqu'à des approches dynamiques plus sophistiquées[112.113]ont été élaborées ou sont en cours d'élaboration pour les NM. Ces outils sont donc une option pour lutter contre les effets sur la santé humaine des NM utilisés dans le PVO.

Par conséquent, l'ACV permettant le calcul des impacts potentiels sur la santé humaine de nombreuses sources d'émissions tout au long du cycle de vie, les décideurs pourraient trouver utile d'employer cet outil à tous les stades de développement de la technologie et à des fins d'écoconception. Toutefois, pour les technologies contenant des NM, si l'évaluation des NM n'est pas possible, les décideurs peuvent choisir d'utiliser simplement une EQRS, en particulier une fois la fabrication d'un produit atteint des volumes relativement importants. Le développement à grande échelle ou l'adoption d'un produit par la société exige que les risques sur la santé humaine soient évités. Le développement à grande échelle implique un enregistrement auprès des organismes de réglementation appropriés qui peuvent avoir besoin d'une EQRS dans le cadre de l'enregistrement ou de la conformité d'un produit. Tout en ayant la capacité de fournir des estimations définitives des risques des NM pour la santé humaine, un inconvénient critique de cette option est le niveau de détail induit, qui n'est pas nécessaire dans le cas du développement à un stade précoce. Par conséquent, ces outils sont souvent utilisés séparément par différents types de parties prenantes qui ont différents besoins.

Cependant, *une utilisation complémentaire*, en utilisant les deux outils séparément, puis en combinant leurs résultats, est une approche évidente lorsque l'évaluation à la fois de l'efficacité des ressources et des effets sur la santé du NM doit être envisagée. Cette option implique donc nécessairement une évaluation détaillée de l'exposition au risque et du NM. Par conséquent, *une utilisation complémentaire* sera la plus appropriée au cours du développement de la technologie à grande échelle ou quand il sera nécessaire d'assurer la protection de la santé humaine[107114115]. *Cette utilisation complémentaire* exige également que les différents champs d'application ou les résultats des deux outils soient conciliés. Pour clarifier, l'ACV échelonne ses résultats à un service ou à une unité «

fonctionnelle » (par exemple, la production d'un kWh d'énergie moyenne), tandis que l'ERE est définie par un scénario d'exposition pertinent (par exemple, le risque pour la santé humaine posé par des émissions de TiO_2 à l'échelle nano dans une installation industrielle). Ainsi, leurs résultats demandent une conversion à réaliser avec prudence (i.e. normaliser les résultats de chaque outil de telle sorte qu'ils puissent être comparés sur des unités relatives, telles que la conversion en dommages) avant que les comparaisons des résultats puissent être faites [116]. Même dans ce cas-là, ces 2 méthodes peuvent ne pas être comparables, à moins que les champs d'application de chaque outil aient été définis de façon stratégique. Autrement dit, l'*utilisation complémentaire* ne sera probablement pas en mesure d'exprimer la façon proportionnelle l'ENM-risque qui en résulte dans le contexte des risques toxicologiques définies par LCA.

Par opposition à l'*utilisation complémentaire*, l'*intégration* se réfère ici à la combinaison des méthodes de chaque outil au lieu de combiner leurs résultats. [117] Cette approche utilise des méthodes généralement attribuées à l'ERSA pour estimer le sort et les effets dus à l'exposition aux NM. Parce que l'intégration permet (a) l'interprétation des risques toxicologiques des NM dans un produit (unité fonctionnelle) et (b) la comparaison directe des risques des NM à tous les autres risques chimiques estimés pendant le cycle de vie, cette approche permet de veiller à ce que le transfert d'impacts ne se produise pas. [86] L'intégration peut donc être utilisé comme une alternative à des utilisations existantes d'utilisation *complémentaire* ou *séparée*, mais il peut être aussi utilisé uniquement pour l'évaluation du développement d'un produit dans sa phase de conception, pour de l'écoconception, ou pour des déclarations environnementales de produit par exemple. [118]

Santé humaine et évaluation des risques : Étude de cas du dioxyde de titane

L'ERE est utilisée comme un outil préliminaire pour évaluer les risques pour la santé humaine des NM utilisés dans les dispositifs de PVO, puis les principaux aspects méthodologiques des EQRS sont identifiés afin d'être intégrés dans les méthodes d'évaluation de l'impact du cycle de vie. Alors que les émissions de NM peuvent conduire à des impacts sur l'environnement et la santé humaine, cette thèse a choisi de se concentrer sur les aspects de la santé humaine. Pour commencer à déterminer ces impacts potentiels, l'EQRS a été appliquée aux études de cas sur le PVO utilisées dans cette thèse. L'EQRS est un moyen d'identifier les dangers d'une substance, de quantifier la relation « dose-effet » de la substance avec les dommages toxicologiques, d'estimer l'exposition à la substance et de quantifier la probabilité du risque basée sur la comparaison du niveau d'exposition avec la relation « dose-effet ». Dans le cadre de thèse,

seul l'aspect *qualitatif* des risques posés par les émissions de NM durant les étapes du cycle de vie du PVO sera abordé. Ainsi, une EQRS *qualitative* a été utilisée pour identifier les étapes du cycle de vie et les scénarios d'exposition qui justifieraient une analyse plus approfondie par une EQRS quantitative. En utilisant un ensemble de critères qualitatifs, il a été évalué (i) l'existence d'une interaction directe avec le NM, (ii) le volume de NM impliqués, (iii) l'utilisation d'équipements de protection individuelle, (iv) la probabilité que les émissions de NM se produisent, et (v) la voie d'exposition potentielle. Sur la base de ces critères, il a été constaté que les émissions et l'exposition finale au NM étaient plus susceptibles de se produire lors de la production du NM, ainsi que lors la fabrication des panneaux PVO. Alors que les émissions et l'exposition lors de l'utilisation et des phases de fin de vie ne pouvaient pas être exclues, il était attendu que les émissions seraient beaucoup plus faibles au cours de ces étapes du cycle de vie puisque les NM sont encapsulés dans une matrice polymère, au lieu d'être traités comme des poudres sèches et volatiles pendant les étapes de production et de fabrication. Dans ces scénarios de travail, les émissions seraient limitées à l'air intérieur environnant, conduisant potentiellement à deux voies d'exposition : par inhalation et par voie cutanée.

Cette thèse se concentre sur un NM représentatif de ce qui est utilisé en quantités industrielles et dont les données toxicologiques et physico-chimiques seraient suffisamment fournies pour établir le devenir, l'exposition et la modélisation de l'effet pour l'EQRS quantitative. Par conséquent, le TiO_2 (dioxyde de titane) nanométrique utilisé comme espaceur optique du PVO est utilisé comme étude de cas dans cette thèse pour étudier et déterminer les impacts potentiels sur la santé humaine induits par l'utilisation des technologies NM dans le PVO. En ce qui concerne les études *in vivo* d'inhalation des animaux, le nano-TiO_2 a été relié à plusieurs impacts négatifs tels que l'inflammation, l'histopathologie, la cytotoxicité, le stress oxydant, les effets oncogènes et les impacts géno-toxiques. Par rapport à son homologue dispersé, ces effets se sont révélés être plus prononcés. En ce qui concerne les effets néfastes de l'exposition cutanée, les études *in vivo* sur animaux démontrent un certain niveau de pénétration, principalement dans les couches épidermiques superficielles de la peau. Dans certains cas, du stress oxydant ou des lésions sur les organes peuvent se produire alors que peu ou pas d'irritation de la peau est observée. L'EQRS a modélisé les émissions pour plusieurs volumes (de faible à élevé) d'utilisation de nano-TiO_2 qui ont inclus la manipulation de ces matériaux en opposition aux émissions lors de la production des matériaux. Le devenir et le transport des nano-TiO_2 ont été modélisés dans un modèle d'atmosphère intérieur à deux zones où l'émission est supposée venir d'une seule source située dans une zone de champ proche qui a ensuite été reliée à une zone de champ lointain au sein de cette même

pièce. L'exposition a été supposée se produire complètement à l'intérieur de la zone de champ proche et a été estimée comme étant la concentration dans l'air sans prendre en compte du dépôt et / ou de la rétention des particules dans les poumons. Cette corrélation avec les données *in vivo* de toxicité a été prise à partir d'un modèle d'exposition par inhalation chronique pour mesurer les effets de l'inflammation pulmonaire chez la souris et le rat. Les résultats de l'EQRS ont démontré que le risque d'inflammation due à l'inhalation de nano-TiO_2 était très probable dans les cas où de grands volumes de nano-poudre sont manipulés et jetés dans de grands conteneurs ouverts. Plus précisément, ce fut le cas pour lequel des sacs de 10 kg de nano-TiO_2 ont été transférés sur une période de 10 minutes dans de grands réservoirs de mélange tout au long d'une journée de travail de 8 heures. De tels scénarios peuvent se présenter à la fois lors de la production de nano-TiO_2 ainsi que lors de la fabrication du panneau PVO, dans l'hypothèse où cette technologie atteint des volumes de production industrielle à grande échelle.

Les résultats de l'EQRS démontrent que l'inquiétude suscitée par les risques toxicologiques potentiels pour la santé humaine lors de l'utilisation de NM dans le PVO peut être justifiée, même dans les cas où de grands volumes de NM sont utilisés dans des configurations à l'échelle industrielle. Ces résultats sont importants et signalent que les technologies PV émergentes telles que le PVO peuvent engendrer des risques éventuels sur la santé humaine et l'environnement. Bien que cette information soit particulièrement importante pour les gestionnaires de risques professionnels qui veulent identifier et diminuer l'importance des impacts sur la santé humaine sur un lieu de travail, les résultats de tels cas EQRS ne permettent de savoir si le PVO sont un choix de production d'énergie préférable par rapport au silicium photovoltaïque. Pour ce faire, l'estimation du devenir, de l'exposition et de l'effet devrait être en corrélation avec l'unité fonctionnelle dans une ACV pour permettre des comparaisons directes avec les impacts sur la santé humaine du silicium PV.

Intégration des impacts 'nano-spécifiques' sur la santé humaine via la méthodologie ACV : Application au photovoltaïque organique

L'EQRS a été intégrée à l'évaluation de l'impact du cycle de vie. De cette façon, les résultats de l'ACV ont été mis à jour pour inclure les contributions des nano-TiO_2 comme une première indication de la façon dont les impacts sur la santé humaine pourraient évoluer suite à la prise en compte des émissions liées au NM au long du cycle de vie du PVO. Ce travail a abouti à la création d'un facteur de caractérisation spécifique aux nano particules (CF_{NS}) pour une utilisation dans l'ACV. Plus précisément, la plupart des éléments de la modélisation EQRS utilisés pour estimer les quantités émises, le devenir et les effets

associés à ces substances ont été adaptés pour une utilisation dans l'étape d'évaluation des impacts. L'objectif de cette thèse étant une analyse prospective, le scénario d'émission à l'échelle industrielle a été utilisé pour suivre les conditions et les rejets de nano-TiO2 du fait des volumes élevés sur le lieu de travail. En raison de la nature non-équilibrée du comportement des NM dans l'environnement, le devenir et l'exposition des résultats sont directement dépendant de l'intensité de la source d'émission et des concentrations dans l'air en nano-TiO_2. Ainsi, diverses sources d'émission et ainsi que les fréquences d'émission associées ont été évaluées afin de déterminer leur influence sur le devenir et l'exposition des particules nano-TiO2. Le modèle présente deux compartiments, champ proche et champ lointain, ce dernier ayant été modifié pour tenir compte des autres sources (hors ventilation) de l'élimination des particules du compartiment de l'air intérieur. Ces mécanismes d'élimination incluent l'homo-agrégation et la sédimentation gravitationnelle des particules sur des surfaces intérieures. L'exposition au nano-TiO_2 a été évaluée à l'aide d'un modèle pharmacocinétique basé sur la physiologie (PBPK) pour déterminer le dépôt, le dégagement et la rétention de ces particules dans les poumons au cours du temps. Le modèle PBPK a calculé la dose pulmonaire interne de nano-TiO_2 conduisant à une série de réactions impliquant la translocation due aux particules dans la région pulmonaire et l'interstitium des poumons, mais également à la circulation systémique, la séquestration de particules par les cellules phagocytaires, et le transfert de particules et / ou de cellules vers la zone trachéo-bronchique via la clairance muco-ciliaire. Le facteur de caractérisation final CF_{NS} a été défini pour deux catégories d'impact sur la santé humaine : les impacts cancérigènes et non cancérigènes sur la base de données *in vivo* pertinentes reposant sur des mécanismes toxicologiques de dose-effet conduisant à la croissance de tumeurs pulmonaires et à l'inflammation du poumon chez les animaux.

Les résultats de la modélisation du CF_{NS} pour les particules nano-TiO_2 démontrent qu'il existe une sensibilité significative en fonction de la puissance de la source d'émission ainsi que des durées pendant lesquelles la population des travailleurs est exposée sur le site industriel. Cependant, pour le cas où des travailleurs étaient exposés régulièrement dans une production à l'échelle industrielle, il y avait très peu de changements dans les impacts sur la santé humaine de l'étude ACV-PVO après réévaluation du cycle de vie selon l'approche « Berceau à la porte de l'usine » avec la prise en compte du CF_{NS} nouvellement défini. La contribution totale s'élève à moins de 1% des impacts sur la santé humaine provoqués par les émissions de nano-TiO_2 au cours de la production de NM ou la fabrication de PVO. Ces résultats suggèrent que les émissions de NM à travers le cycle de vie peuvent être considérées comme marginales dans la majorité des cas. Cependant, ces résultats doivent être considérés avec prudence car

ils ne tiennent en compte que des impacts liés aux émissions de nano-TiO_2 pendant seulement une partie du cycle de vie complet du PVO. D'autres émissions peuvent se produire pendant la phase d'utilisation, mais plus probablement pendant les phases de fin de vie, surtout lors d'une mise en décharge avec des émissions au fil du temps. En outre, les panneaux PVO sont fabriqués avec des couches de matériaux qui sont toutes déposées à des niveaux d'épaisseur de l'ordre du nanomètre. Par conséquent, le PVO peut présenter beaucoup plus d'émissions de NM le long du cycle de vie que seulement les particules nano-TiO_2. Néanmoins, tous ces matériaux ne peuvent être préparés et manipulés de la même manière, ils auront donc probablement des niveaux différents de toxicité. Ainsi, leur contribution ultime pour les impacts sur la santé humaine à travers le cycle de vie du PVO variera.

Conclusions et perspectives

Les résultats de l'étude de cas ACV-PVO et l'évaluation ultérieure des impacts sur la santé humaine due à l'utilisation de certains NM dans le PVO conduisent à penser que la technologie PVO est une option de production d'énergie préférable par rapport au PV silicium pour les critères de santé humaine et d'impacts sur l'environnement. Ces résultats sont fortement dépendants de la manière dont les dispositifs photovoltaïques sont utilisés et de leurs durées de vie. Les incertitudes, principalement liées à la durée de vie et l'efficacité du PVO, empêchent de se prononcer définitivement afin de savoir si le PVO se révèle être une option d'approvisionnement en énergie écologiquement préférable. Cependant, ces incertitudes peuvent être marginalisées lorsque les technologies PVO sont limitées à des produits ayant des durées de vie relativement courtes (par exemple les produits où l'utilisation est typiquement <5 ans), pour lesquelles la préférence pour le PVO devient manifeste. Les résultats de cette thèse ont cependant montré que le PVO avait vocation à être utilisé pour des panneaux solaires sur les toits, là où le PV à base de silicium a dominé pendant des décennies.

En terme d'approche la plus appropriée pour évaluer les technologies émergentes, l'ACV se présente comme la méthode la plus complète pour évaluer l'efficacité des ressources et les dangers potentiels des technologies de production d'énergie telles que le PVO. Sa large prise en compte des différentes variables environnementales sur toute l'étendue du cycle de vie d'un produit contribue à assurer que le développement ou la diffusion d'un produit ne se traduisent pas par un transfert de pollution d'une catégorie d'impact à l'autre. La compréhension de la santé humaine et des risques écologiques des NM est nécessaire pour l'évaluation de cette technologie, mais n'est pas totalement possible par les méthodologies d'évaluation d'impact actuelles. Alors que l'EQRS a permis une évaluation plus détaillée

des risques absolus de l'utilisation de NM à une étape du cycle de vie spécifique, les évaluations de risque absolu sont peut-être trop ambitieuses depuis que la technologie PVO se développe. Au lieu de cela, une approche intégrée dans l'évaluation des impacts du cycle de vie permet d'évaluer à des stades de développement antérieures du PVO de telle façon que les résultats des impacts des NM sur la santé humaine puissent être directement interprétés et évalués dans le cadre de toutes les autres catégories d'impact sur la santé humaine présentes dans l'ACV. Cette approche permet des analyses sur les points sensibles, l'identification et l'évitement de transferts de pollution et le soutien pour les concepts d'éco-conception, nécessaires pour le développement durable d'une source d'énergie renouvelable émergente.

Les travaux de cette thèse visent à combler les lacunes de données et les choix de modélisation. En particulier, la probabilité et la quantification des émissions de NM à travers le cycle de vie demeurent largement inconnues. Bien que certains travaux ont démontré que le PVO peut émettre des lixiviats provenant des différentes couches au fil du temps, [119-121] en particulier lorsqu'elles sont endommagées, il n'y a pas de données montrant quelle fraction de ces substances sont dans leur nano-forme (i.e. par opposition à ionique). En ce qui concerne la modélisation, une autre distinction peut être faite dans l'ACV entre attributionnel et conséquentiel. Ce travail de thèse a utilisé des ACV attributionnelles pour répondre à la question « Quelle est la part de charge environnementale globale, qui peut être attribuée aux technologies PVO ?» Bien que cette approche soit pertinente pour l'analyse des points sensibles et une compréhension basique des charges environnementales associées au PVO, une ACV conséquentielle pourrait être utilisée pour mieux comprendre ce que les effets futurs et / ou à long terme seraient dans le secteur de l'énergie avec l'émergence des panneaux PVO. Cette approche serait appropriée pour une meilleure compréhension, le cas échéant, des conséquences liées à une substitution partielle d'une technologie classique par du PVO.

Mots clés : l'analyse du cycle de vie, photovoltaïques organiques, nanomatériaux fabriqués, l'evaluation des risques, l'exposition, énergie renouvelable

Bibliographie du Résumé Détaillé

1. Robert, K. W., Parris, T. M. & Leiserowitz, A. A. What is Sustainable Development? Goals, Indicators, Values, and Practice. *Environ. Sci. Policy Sustain. Dev.* **47,** 8–21 (2005).
2. Bardi, U. Peak oil: The four stages of a new idea. *Energy* **34,** 323–326 (2009).
3. Carbon accounting. *Nat. Clim. Chang.* (2016). doi:10.1038/nclimate3137
4. Moss, R. H. *et al.* The next generation of scenarios for climate change research and assessment. *Nature* **463,** 747–756 (2010).
5. Fraiture, C. de, Giordano, M. & Liao, Y. Biofuels and implications for agricultural water use: blue impacts of green energy. *Water Policy*

10, 67 (2008).

6. Escobar, J. C. *et al.* Biofuels: Environment, technology and food security. *Renew. Sustain. Energy Rev.* **13,** 1275–1287 (2009).
7. Howarth, R. W. & Bringezu, S. *Biofuels: Environmental Consequences and Interactions with Changing Land Use - Proceedings of the Scientific Committee on Problems of the Environment (SCOPE) International Biofuels Project Rapid Assessment*. (2008). at <http://cip.cornell.edu/DPubS?service=UI&version=1.0&verb=Display&page=current&handle=scope>
8. Searchinger, T. *et al.* Use of U.S. Croplands for Biofuels Increases Greenhouse Gases Through Emissions from Land-Use Change. *Science (80-.).* **319,** 1238–1240 (2008).
9. Hertwich, E. G. *et al.* Integrated life-cycle assessment of electricity-supply scenarios confirms global environmental benefit of low-carbon technologies. *Proc. Natl. Acad. Sci.* **112,** 6277–6282 (2015).
10. Green, M. A. Photovoltaics: coming of age. in *IEEE Conference on Photovoltaic Specialists* 1–8 (IEEE). doi:10.1109/PVSC.1990.111582
11. Green, M. A., Emery, K., Hishikawa, Y., Warta, W. & Dunlop, E. D. Solar cell efficiency tables (version 47). *Prog. Photovoltaics Res. Appl.* **24,** 3–11 (2016).
12. Fraunhofer Institute for Solar Energy Systems ISE. *Photovoltaics Report (2016)*. (2016).
13. Fthenakis, V. & Alsema, E. Photovoltaics energy payback times, greenhouse gas emissions and external costs: 2004–early 2005 status. *Prog. Photovoltaics Res. Appl.* **14,** 275–280 (2006).
14. Tang, C. W. Multilayer organic photovoltaic elements. (1979).
15. Espinosa, N., Hösel, M., Jørgensen, M. & Krebs, F. C. Large scale deployment of polymer solar cells on land, on sea and in the air. *Energy Environ. Sci.* **7,** 855 (2014).
16. Krebs, F. C., Tromholt, T. & Jørgensen, M. Upscaling of polymer solar cell fabrication using full roll-to-roll processing. *Nanoscale* **2,** 873 (2010).
17. Jungbluth, N. Life cycle assessment of crystalline photovoltaics in the Swiss ecoinvent database. *Prog. Photovoltaics Res. Appl.* **13,** 429–446 (2005).
18. International Organization for Standardization. *ISO 14044 - Environmental management - Life cycle assessment - Requirements and guidelines*. (2006).
19. International Organization for Standardization. *ISO 14040 - Environmental Management - Life cycle assessment - Principles and framework*. (2006).
20. Roes, A. L., Alsema, E. A., Blok, K. & Patel, M. K. Ex-ante environmental and economic evaluation of polymer photovoltaics. *Prog. Photovoltaics Res. Appl.* **17,** 372–393 (2009).
21. García-Valverde, R., Cherni, J. A. & Urbina, A. Life cycle analysis of organic photovoltaic technologies. *Prog. Photovoltaics Res. Appl.* **18,** 535–558 (2010).
22. Espinosa, N., García-Valverde, R., Urbina, A. & Krebs, F. C. A life cycle analysis of polymer solar cell modules prepared using roll-to-roll methods under ambient conditions. *Sol. Energy Mater. Sol. Cells* **95,** 1293–1302 (2011).
23. US EPA, O. Human Health Risk Assessment.
24. European Union European Environment Agency. Environmental Risk Assessment - Approaches, Experiences and Information Sources — European Environment Agency. (1998). at <http://www.eea.europa.eu/publications/GH-07-97-595-EN-C2>
25. Thompson, B. C. & Fréchet, J. M. J. Polymer–Fullerene Composite Solar Cells. *Angew. Chemie Int. Ed.* **47,** 58–77 (2008).
26. Krebs, F. C. Fabrication and processing of polymer solar cells: A review of printing and coating techniques. *Sol. Energy Mater. Sol. Cells* **93,** 394–412 (2009).
27. Kroon, R., Lenes, M., Hummelen, J. C., Blom, P. W. M. & de Boer, B. Small Bandgap Polymers for Organic Solar Cells (Polymer Material Development in the Last 5 Years). *Polym. Rev.* **48,** 531–582 (2008).
28. Li, C.-Z., Yip, H.-L. & Jen, A. K.-Y. Functional fullerenes for organic photovoltaics. *J. Mater. Chem.* **22,** 4161 (2012).
29. Koster, L. J. A. The optimal band gap for plastic photovoltaics. *SPIE Newsroom* (2007). doi:10.1117/2.1200701.0528
30. Krebs, F. C. Roll-to-roll fabrication of monolithic large-area polymer solar cells free from indium-tin-oxide. *Sol. Energy Mater. Sol. Cells* **93,** 1636–1641 (2009).

31. Lizin, S. *et al.* Life cycle analyses of organic photovoltaics: a review. *Energy Environ. Sci.* **6,** 3136 (2013).
32. Kumar, A. & Zhou, C. The Race To Replace Tin-Doped Indium Oxide: Which Material Will Win? *ACS Nano* **4,** 11–14 (2010).
33. Samad, W. Z., Yarmo, M. A., Salleh, M. M. & Shafiee, A. Structural, Optical and Electrical Properties of Fluorine Doped Tin Oxide Thin Films Deposited Using Ink jet Printing Technique. *Sains Malaysiana* **40,** 251–257 (2011).
34. Kim, H., Kushto, G. P., Auyeung, R. C. Y. & Piqué, A. Optimization of F-doped SnO2 electrodes for organic photovoltaic devices. *Appl. Phys. A* **93,** (2008).
35. Yu, S., Li, L., Lyu, X. & Zhang, W. Preparation and investigation of nano-thick FTO/Ag/FTO multilayer transparent electrodes with high figure of merit. *Sci. Rep.* **6,** 20399 (2016).
36. Su, H. *et al.* Highly Conductive and Low Cost Ni-PET Flexible Substrate for Efficient Dye-Sensitized Solar Cells. *ACS Appl. Mater. Interfaces* **6,** 5577–5584 (2014).
37. Jiang, C. Y., Sun, X. W., Zhao, D. W., Kyaw, A. K. K. & Li, Y. N. Low work function metal modified ITO as cathode for inverted polymer solar cells. *Sol. Energy Mater. Sol. Cells* **94,** 1618–1621 (2010).
38. Voroshazi, E., Verreet, B., Aernouts, T. & Heremans, P. Long-term operational lifetime and degradation analysis of P3HT:PCBM photovoltaic cells. *Sol. Energy Mater. Sol. Cells* **95,** 1303–1307 (2011).
39. Girotto, C., Voroshazi, E., Cheyns, D., Heremans, P. & Rand, B. P. Solution-Processed MoO 3 Thin Films As a Hole-Injection Layer for Organic Solar Cells. *ACS Appl. Mater. Interfaces* **3,** 3244–3247 (2011).
40. Steim, R., Kogler, F. R. & Brabec, C. J. Interface materials for organic solar cells. *J. Mater. Chem.* **20,** 2499 (2010).
41. Roy, A. *et al.* Titanium suboxide as an optical spacer in polymer solar cells. *Appl. Phys. Lett.* **95,** 13302 (2009).
42. Hayakawa, A., Yoshikawa, O., Fujieda, T., Uehara, K. & Yoshikawa, S. High performance polythiophene/fullerene bulk-heterojunction solar cell with a TiO[sub x] hole blocking layer. *Appl. Phys. Lett.* **90,** 163517 (2007).
43. Apilo, P. *et al.* Roll-to-roll gravure printing of organic photovoltaic modules-insulation of processing defects by an interfacial layer. *Prog. Photovoltaics Res. Appl.* **23,** 918–928 (2015).
44. Brabec, C. J., Shaheen, S. E., Winder, C., Sariciftci, N. S. & Denk, P. Effect of LiF/metal electrodes on the performance of plastic solar cells. *Appl. Phys. Lett.* **80,** 1288 (2002).
45. Zhou, Y. *et al.* A Universal Method to Produce Low-Work Function Electrodes for Organic Electronics. *Science (80-.).* **336,** 327–332 (2012).
46. Espinosa, N., Hösel, M., Angmo, D. & Krebs, F. C. Solar cells with one-day energy payback for the factories of the future. *Energy Environ. Sci.* **5,** 5117–5132 (2012).
47. Service, R. F. Outlook Brightens for Plastic Solar Cells. *Science (80-.).* **332,** 293–293 (2011).
48. Scharber, M. C. & Sariciftci, N. S. Efficiency of bulk-heterojunction organic solar cells. *Prog. Polym. Sci.* **38,** 1929–1940 (2013).
49. Darling, S. B. & You, F. The case for organic photovoltaics. *RSC Adv.* **3,** 17633 (2013).
50. Goedkoop, M. J. *et al. A life cycle impact assessment method which comprises harmonised category indicators at the midpoint and the endpoint level*. (2009).
51. Hischier, R. *et al. Implementation of Life Cycle Impact Assessment Methods*. (2010).
52. Espinosa, N. *et al.* Life cycle assessment of ITO-free flexible polymer solar cells prepared by roll-to-roll coating and printing. *Sol. Energy Mater. Sol. Cells* **97,** 3–13 (2012).
53. Anctil, A. & Fthenakis, V. in *Third Generation Photovoltaics* (InTech, 2012). doi:10.5772/38977
54. Anctil, A., Babbitt, C. W., Raffaelle, R. P. & Landi, B. J. Cumulative energy demand for small molecule and polymer photovoltaics. *Prog. Photovoltaics Res. Appl.* **21,** 1541–1554 (2013).
55. Tsang, M. P., Sonnemann, G. W. & Bassani, D. M. A comparative human health, ecotoxicity, and product environmental assessment on the production of organic and silicon solar cells. *Prog. Photovoltaics Res. Appl.* **24,** 645–655 (2016).
56. Choi, J.-K. & Fthenakis, V. Crystalline silicon photovoltaic recycling planning: macro and micro perspectives. *J. Clean. Prod.* **66,** 443–449 (2014).
57. Larsen, K. End-of-life PV: then what? *Renew. Energy Focus* **10,** 48–53 (2009).

58. McDonald, N. C. & Pearce, J. M. Producer responsibility and recycling solar photovoltaic modules. *Energy Policy* **38,** 7041–7047 (2010).
59. Doka, G. *Ecoinvent report No. 13, parts I-V: Life cycle invntories of waste treatment services*. (2009).
60. Espinosa, N., Laurent, A. & Krebs, F. C. Ecodesign of organic photovoltaic modules from Danish and Chinese perspectives. *Energy Environ. Sci.* **8,** 2537–2550 (2015).
61. Goe, M. & Gaustad, G. Strengthening the case for recycling photovoltaics: An energy payback analysis. *Appl. Energy* **120,** 41–48 (2014).
62. Müller, A., Wambach, K. & Alsema, E. Life Cycle Analysis of Solar Module Recycling Process. *MRS Proc.* **895,** 895-G03-7 (2005).
63. Som, C. *et al.* The importance of life cycle concepts for the development of safe nanoproducts. *Toxicology* **269,** 160–169 (2010).
64. The Project on Emerging Nanotechnologies. The Nanotechnology Consumer Products Inventory. (2015). at <http://www.nanotechproject.org/cpi/>
65. Roco, M. C. Nanotechnology's Future. *Sci. Am.* **295,** 39–39 (2006).
66. European Commission. *Communication from the Commission to the European Parliament, The Council and the European Economic and Social Committee (Second Regulatory Review on Nanomaterials*. (2012).
67. Vance, M. E. *et al.* Nanotechnology in the real world: Redeveloping the nanomaterial consumer products inventory. *Beilstein J. Nanotechnol.* **6,** 1769–1780 (2015).
68. Royal Society and Royal Academy of Engineering. *Nanoscience and nanotechnologies: opportunities and uncertainties*. *Nanoscience and Nanotechnologies Opportunities and Uncertainties* (Royal Society, 2004).
69. Yokel, R. A. & MacPhail, R. C. Engineered nanomaterials: exposures, hazards, and risk prevention. *J. Occup. Med. Toxicol.* **6,** 7 (2011).
70. European Commission. *Second regulatory review on nanomaterials. Communication from the Commission to the European Parliament, the Council and the European Economic and Social Committee.* (2012).
71. Pietroiusti, A. Health implications of engineered nanomaterials. *Nanoscale* **4,** 1231 (2012).
72. Klaine, S. J. *et al.* Nanomaterials in the environment: behavior, fate, bioavailability, and effects. *Environ. Toxicol. Chem.* **27,** 1825–1851 (2008).
73. Greßler, S; Nentwich, M. Nano and Environment–Part II : Hazard potentials and risks. *Nano Trust Dossiers* **27,** 1–6 (2012).
74. Curran, M. A., Frankl, P., Jeijungs, R., Kohler, A. & Olsen, S. I. *Nanotechnology and life cycle assessment: A systems approach to Nanotechnology and the environment: Synthesis of results obtained at a workshop*. (2007).
75. Hischier, R. & Walser, T. Life cycle assessment of engineered nanomaterials: State of the art and strategies to overcome existing gaps. *Sci. Total Environ.* **425,** 271–282 (2012).
76. Grieger, K. D. *et al.* Analysis of current research addressing complementary use of life-cycle assessment and risk assessment for engineered nanomaterials: have lessons been learned from previous experience with chemicals? *J. Nanoparticle Res.* **14,** 1–23 (2012).
77. Wender, B. A. *et al.* Illustrating anticipatory life cycle assessment for emerging photovoltaic technologies. *Environ. Sci. Technol.* **48,** 10531–10538 (2014).
78. Gavankar, S., Suh, S. & Keller, A. F. Life cycle assessment at nanoscale: review and recommendations. *Int. J. Life Cycle Assess.* **17,** 295–303 (2012).
79. Keller, A. a., McFerran, S., Lazareva, A. & Suh, S. Global life cycle releases of engineered nanomaterials. *J. Nanoparticle Res.* **15,** 1–17 (2013).
80. Sun, T. Y., Gottschalk, F., Hungerbühler, K. & Nowack, B. Comprehensive probabilistic modelling of environmental emissions of engineered nanomaterials. *Environ. Pollut.* **185,** 69–76 (2014).
81. Gottschalk, F. & Nowack, B. The release of engineered nanomaterials to the environment. *J. Environ. Monit.* **13,** 1145 (2011).
82. Keller, A. A., Vosti, W., Wang, H. & Lazareva, A. Release of engineered nanomaterials from personal care products throughout their life cycle. *J. Nanoparticle Res.* **16,** 2489 (2014).
83. Hischier, R. *et al.* Life cycle assessment of façade coating systems containing manufactured nanomaterials. *J. Nanoparticle Res.* **17,** 68 (2015).

84. Walser, T., Demou, E., Lang, D. J. & Hellweg, S. Prospective environmental life cycle assessment of nanosilver T-shirts. *Environ. Sci. Technol.* **45,** 4570–8 (2011).
85. Walser, T. *et al.* Persistence of engineered nanoparticles in a municipal solid-waste incineration plant. *Nat. Nanotechnol.* **7,** 520–524 (2012).
86. Eckelman, M. J., Mauter, M. S., Isaacs, J. a & Elimelech, M. New perspectives on nanomaterial aquatic ecotoxicity: production impacts exceed direct exposure impacts for carbon nanotoubes. *Environ. Sci. Technol.* **46,** 2902–2910 (2012).
87. Salieri, B., Righi, S., Pasteris, A. & Olsen, S. I. Freshwater ecotoxicity characterisation factor for metal oxide nanoparticles: a case study on titanium dioxide nanoparticle. *Sci. Total Environ.* **505,** 494–502 (2015).
88. Miseljic, M. & Olsen, S. I. Life-cycle assessment of engineered nanomaterials: a literature review of assessment status. *J. Nanoparticle Res.* **16,** 1–33 (2014).
89. Pini, M., Salieri, B., Ferrari, A. M., Nowack, B. & Hischier, R. Human health characterization factors of nano-TiO2 for indoor and outdoor environments. *Int. J. Life Cycle Assess.* (2016). doi:10.1007/s11367-016-1115-8
90. Praetorius, A. *et al.* The road to nowhere: equilibrium partition coefficients for nanoparticles. *Environ. Sci. Nano* **1,** 317 (2014).
91. Rosenbaum, R. K. *et al.* USEtox—the UNEP-SETAC toxicity model: recommended characterisation factors for human toxicity and freshwater ecotoxicity in life cycle impact assessment. *Int. J. Life Cycle Assess.* **13,** 532–546 (2008).
92. Goedkoop, M. *et al. ReCiPe 2008*. (2008). at <http://www.pre-sustainability.com/download/misc/ReCiPe_main_report_final_27-02-2009_web.pdf>
93. Meesters, J. A. J., Koelmans, A. A., Quik, J. T. K., Hendriks, A. J. & van de Meent, D. Multimedia Modeling of Engineered Nanoparticles with SimpleBox4nano: Model Definition and Evaluation. *Environ. Sci. Technol.* **48,** 5726–5736 (2014).
94. Koivisto, A. J. *et al.* Industrial worker exposure to airborne particles during the packing of pigment and nanoscale titanium dioxide. *Inhal. Toxicol.* **24,** 839–49 (2012).
95. Nazaroff, W. W. Indoor particle dynamics. *Indoor Air, Suppl.* **14,** 175–183 (2004).
96. Hodas, N. *et al.* Indoor inhalation intake fractions of fine particulate matter: Review of influencing factors. *Indoor Air* n/a-n/a (2015). doi:10.1111/ina.12268
97. Braakhuis, H. M., Park, M. V., Gosens, I., De Jong, W. H. & Cassee, F. R. Physicochemical characteristics of nanomaterials that affect pulmonary inflammation. *Part. Fibre Toxicol.* **11,** 18 (2014).
98. Walser, T. *et al.* Life-cycle assessment framework for indoor emissions of synthetic nanoparticles. *J. Nanoparticle Res.* **17,** 1–18 (2015).
99. MacPhail, R. C., Grulke, E. A. & Yokel, R. A. Assessing nanoparticle risk poses prodigious challenges. *Wiley Interdiscip. Rev. Nanomedicine Nanobiotechnology* **5,** 374–387 (2013).
100. US EPA. *Decision document: Conditional registration of HeiQ AGS-20 as a materials preservative in textiles*. (2011).
101. National Institute for Occupational Safety and Health. *Current Intelligence Bulletin 63: Occupational Exposure to Titanium Dioxide*. (2011).
102. National Institute for Occupational Safety and Health. *Current Intelligence Bulletin 65: Occupational Exposure to Carbon Nanotubes and Nanofibers*. (2013).
103. Lin, D., Tian, X., Wu, F. & Xing, B. Fate and transport of engineered nanomaterials in the environment. *J. Environ. Qual.* **39,** 1896–1908 (2010).
104. Hristozov, D. R., Gottardo, S., Critto, A. & Marcomini, A. Risk assessment of engineered nanomaterials: a review of available data and approaches from a regulatory perspective. *Nanotoxicology* **6,** 1–19 (2012).
105. US EPA. EPA Actions to Reduce Risk for New Chemicals under TSCA (SNUR). (2015). at <http://www.epa.gov/reviewing-new-chemicals-under-toxic-substances-control-act-tsca/epa-actions-reduce-risk-new>
106. European Chemicals Agency. Nanomaterials. at <http://echa.europa.eu/regulations/nanomaterials>
107. Barberio, G., Scalbi, S., Buttol, P., Masoni, P. & Righi, S. Combining life cycle assessment and qualitative risk assessment: the case study of alumina nanofluid production. *Sci. Total Environ.* **496,** 122–31 (2014).
108. Schulte, P. a., Murashov, V., Zumwalde, R., Kuempel, E. D. & Geraci, C. L. Occupational exposure limits for nanomaterials: State of the

art. *J. Nanoparticle Res.* **12,** 1971–1987 (2010).

109. Ling, M.-P. *et al.* Risk management strategy to increase the safety of workers in the nanomaterials industry. *J. Hazard. Mater.* **229–230,** 83–93 (2012).
110. Liao, C. M., Chiang, Y. H. & Chio, C. P. Model-based assessment for human inhalation exposure risk to airborne nano/fine titanium dioxide particles. *Sci. Total Environ.* **407,** 165–177 (2008).
111. Brouwer, D. H. Control banding approaches for nanomaterials. *Ann. Occup. Hyg.* **56,** 506–514 (2012).
112. Hristozov, D. *et al.* Demonstration of a modelling-based multi-criteria decision analysis procedure for prioritisation of occupational risks from manufactured nanomaterials. *Nanotoxicology* 1–14 (2016). doi:10.3109/17435390.2016.1144827
113. Jensen, K. A. *et al.* NanoSafer version 1.1: A web-based precautionary risk assessment and management tool for manufactured nanomaterials using first order modeling. unpublished work (2016).
114. Kikuchi, Y. & Hirao, M. Practical Method of Assessing Local and Global Impacts for Risk-Based Decision Making: A Case Study of Metal Degreasing Processes. *Environ. Sci. Technol.* **42,** 4527–4533 (2008).
115. Walser, T., Juraske, R., Demou, E. & Hellweg, S. Indoor exposure to toluene from printed matter matters: complementary views from life cycle assessment and risk assessment. *Environ. Sci. Technol.* **48,** 689–97 (2014).
116. Linkov, I. & Seager, T. P. Coupling multi-criteria decision analysis, life-cycle assessment, and risk assessment for emerging threats. *Environ. Sci. Technol.* **45,** 5068–74 (2011).
117. Harder, R., Holmquist, H., Molander, S., Svanström, M. & Peters, G. M. Review of Environmental Assessment Case Studies Blending Elements of Risk Assessment and Life Cycle Assessment. *Environ. Sci. Technol.* **49,** 13083–13093 (2015).
118. Ingwersen, W. W. & Subramanian, V. Guidance for product category rule development: process, outcome, and next steps. *Int. J. Life Cycle Assess.* **19,** 532–537 (2013).
119. Brun, N. R., Wehrli, B. & Fent, K. Ecotoxicological assessment of solar cell leachates: Copper indium gallium selenide (CIGS) cells show higher activity than organic photovoltaic (OPV) cells. *Sci. Total Environ.* **543,** 703–714 (2016).
120. Zimmermann, Y.-S., Schäffer, A., Corvini, P. F.-X. & Lenz, M. Thin-Film Photovoltaic Cells: Long-Term Metal(loid) Leaching at Their End-of-Life. *Environ. Sci. Technol.* **47,** 13151–13159 (2013).
121. Espinosa, N., Zimmermann, Y.-S., dos Reis Benatto, G. A., Lenz, M. & Krebs, F. C. Outdoor fate and environmental impact of polymer solar cells through leaching and emission to rainwater and soil. *Energy Environ. Sci.* **9,** 1–5 (2016).

(Intentionally Blank Page)